European Commission

Horizon 2020
European Union funding
for Research & Innovation

REDUCTION OF RADIOLOGICAL ACCIDENT CONSEQUENCES

Action	Research and Innovation Action NFRP-2018-1
Grant Agreement #	847656
Project name	**R**eduction of **R**adiological **C**onsequences of design basis and design extension **A**ccidents
Project Acronym	R2CA
Project start date	01.09.2019
Deliverable #	D3.4
Title	**Rod cladding failure during LOCA- Final report on experimental database reassessment and model/code improvements**
Author(s)	Tatiana Taurines, Sébastien Belon (IRSN), Brahim Dif, Asko Arkoma (VTT), Tadas Kaliatka (LEI), Katalin Kulacsy (EK), Matthias Jobst (HZDR), Iurii Ovdiienko (SSTC), Paul Van Uffelen (JRC), Jan Klouzal (UJV), Rolando Calabrese (ENEA),
Version	01
Related WP	WP3 LOCA
Related Task	T3.2. Evaluation of the failed rod number (IRSN)
Lead organization	IRSN
Submission date	28.02.2023
Dissemination level	PU

This project has received funding from the Euratom research and training programme 2014-2018 under the grant agreement n° 847656

History

Date	Submitted by	Reviewed by	Version (Notes)
28.02.2023	T. Taurines (IRSN),	S. Belon (IRSN) N. Girault (IRSN)	01

Contents

List of figures

List of tables

Abbreviations

AME	Absolute mean error
ATHLET	Analysis of thermal-hydraulics of leaks and transients
ATHLET-CD	ATHLET with core degradation modules
BOC	Beginning of cycle
CCO	Cross-connection object
CL	Cold Leg
CV	Control volume
BU	Burn-Up
BWR	Boiling Water Reactor
CT	Computer Tomography
DBA	Design Basis Accident
DCH	Decay Heat
DEC-A	Design Extension Accident
DNB	Departure for Nucleate Boiling
ECCS	Emergency core cooling system
EFPD	Equivalent full power days
EOC	End Of Cycle
EPR	European Pressurized Reactor
FA	Fuel Assembly
FP	Fission Products
FRAPTRAN	Fuel Rod Analysis Program Transient
LB	Large Break
HL	Hot Leg
HPIS	High pressure injection system (Safety injection pumps)
KWU	Kraftwerk Union (former German joint subsidiary of Siemens and AEG for construction of nuclear power plants)
LOCA	Loss Of Coolant Accident
LOOP	Loss of offsite power
LP	Low pressure
LPIS	Low pressure injection system
MA	Maintenance
PCMI	Pellet/cladding mechanical interaction
PCT	Peak Cladding Temperature
PRZ	Pressurizer
PWR	Pressurized Water Reactor
RCS	Reactor coolant system
RHR	Residual heat removal
RIP	Rod Internal Pressure
RPF	Rod power factor
RPV	Reactor pressure vessel
RSK	German Reaktorsicherheitskommission (Reactor safety commission)
SF	Single Failure
SFP	Spent Fuel Pool
SG	Steam generator
TC	Cladding temperature
TFO	Thermofluid object
TH	Thermal-Hydraulics
VVER	Vodo-Vodianoi Enyergeticheskiy Reaktor
WP	Work Package

1. Introduction

To have a more realistic evaluation of the radiological consequences into environment following a LOCA within DBA or DEC-A conditions, the work carried out within the R2CA project aimed at improving :

- The global release rates of radionuclides and their transport from the core to the environment through the primary circuit and the containment
- The evaluation of the number of rod failures at core scale
- The complex fuel pellet behaviour.

In Task 3.2 to which this report is dedicated, the focus was on the prediction of number of failed fuel rods during A LOCA within DBA and DEC-A conditions. Indeed, various methods, approaches and assumptions are currently used for existing reactors in different countries for the LOCA source term evaluation in their safety analyses, as shown in the methodology review performed at the very beginning of the project. These methodologies often used for DBA analyses, conservative assumptions and often dealt with decoupled approaches to predict the FP releases into the environment. In particular, assumptions on a fixed amount of failed rods are often used. A first review was performed in 2016 and was summarized in the OECD FFRD report [1] (cf. Table 1).

Country	Failed rod rate for radiological assessment
Belgium	100%
Czech Republic	100%
Finland	10%
France	EPR 10% (proposed) Other PWRs 33%
Germany	SB LOCA 1% LB LOCA 10%
Hungary	SB and MB LOCA 1% (changing) LB LOCA 100% (changing)
Japan	100%
Republic of Korea	No explicit limit
Slovakia	No explicit limit
Spain	100% for American design NPPs 10% for the German design NPP
Sweden	No explicit limit
Switzerland	No explicit limit
U.K.	100%
U.S.A.	100%

Table 1 : Fuel failure rate considered in radiological assessment in safety analyses from [1].

As a consequence, most LOCA radiological consequences are assessed with an assumed proportion of failed fuel rods ranging from 1 to 100%. Very few methodologies are suited to evaluate the number of failed rods due to several limitations:

- Predicting clad ballooning and burst during a LOCA is complex and dedicated models are needed to better evaluate the number of failed fuel rods. In particular, new burst criteria are needed since most of available ones were developed to predict flow blockage for reflooding evaluations
- Modelling a full core pin by pin is very computational-time consuming and original methodologies have to be developed to propose adapted nodalizations.

The main objective of task 3.2 was than to better estimate the number of failed rods during a LOCA transient within DBA/DEC-A conditions by developing/updating models and methods. It included:

- Improvement of the clad failure models and elaboration of a new clad failure criterion,
- Whole core modelling by model extrapolation or statistical approach

The work consisted in first revisiting the existing experimental databases for Zr-based alloy clad bursts and the existing associated models in the different simulation tools used within the project in order to identify gaps where improvements could be made. Main part of the work then consisted in developing and or improving the clad burst models as well as in refining the calculation methodologies that will allow to perform updated reactor calculations with an improved prediction of the radiological consequences of LOCA within DBA and DEC-A conditions.

Nine organizations were involved in this task using different simulation tools and methodologies. As a results, the update and improvements made by each of them also differs a lot. However, the outcome on failed rod number prediction was generally associated to the improvement of the initial methodology and associated codes.

Both clad failure models and whole core modelling are addressed in this report. More specifically, section 2 is dedicated to thermomechanical database and model reassessments and code developments. EK, VTT, IRSN and ENEA/JRC contributed to this section. A review of methods with TRANSURANUS (by JRC) and new full core methodologies are presented in Section 3. SSTC and UJV proposed approaches based on a fuel performance code using data provided by a system thermohydraulic code. LEI, IRSN and HZDR proposed integrated methodologies with one code.

2. Cladding thermo-mechanical models reassessment

During the project, several partners worked on reassessing thermomechanical models, in particular burst criteria and creep models.

IRSN work was dedicated to several topics:

- burst database reassessment and comparison with existing criteria,
- new burst criteria development,
- test/validation on DRACCAR validation test cases.

The work performed at EK with respect to the cladding thermo-mechanical models consisted of the following steps:

- reassess part of the LOCA strain database used to establish the burst strain criterion to see the effect of the inclusion of the burst opening into the strain values,
- assess the importance of the local vs. average cladding thicknesses,
- establish a best-estimate burst strain limit,
- make a best-estimate fitting of the parameters of the plastic deformation of the code FRAPTRAN,
- establish a conservative burst strain limit.

The result of this activity is a best-estimate code that can simulate the burst tests with the minimum error, but when used with the conservative burst strain limit for safety analyses, it gives reliably conservative predictions.
The cladding material studied in the project is the Russian Zr1%Nb called E110.

Work performed by VTT consisted in implementing models in the FRAPTRAN code :

- new cladding creep models
- new phase transition models
- burst criteria from literature and developed by IRSN during the project.

Validation tests were then analysed to assess new models performances.

ENEA and JRC contributed to the review and the analysis of existing creep and phase transformation models for M5™ and Zy-4 alloys relevant for the TRANSURANUS code.

Burst database reassessment

IRSN contribution

A large burst test database was built with the aim of collecting the test controlling parameters, listed hereafter:

- Cladding state: alloy, internal/external oxide thickness, hydrogen content, burn-up, outside diameter, as-received thickness, corrosion layer thickness;
- Test conditions: heating method, conditioning temperature and duration, heating rate close to burst, azimuthal temperature gradient, free volumes.

Unfortunately, only a few datasets with all parameters are available and, for most of the datasets, a lot of parameters are missing.

General characteristics

About 1440 LOCA burst tests were collected from literature and IRSN data with more than twenty experimental programs.
Currently 1409 burst tests were selected for burst criteria definition. Almost 80% of tests were performed on Zy-4 samples under temperature ramps (rate controlled or semi-integral tests) (cf. Table 2). Main characteristics of collected tests are gathered in Table 3.

Alloy / Test type	Zy-4	M5/E110/Zr-1%Nb	Zirlo/Opt Zirlo	Zy-2
Creep	78	12	0	0
T ramp	1093	55	79	12
P ramp	31	49	0	0
Total	1202	116	79	12

Table 2: General overview (cladding alloy, test type and number of tests) of complete collected burst tests.

Detailed characteristics of burst tests performed on Zy-4 are gathered in Table 4. About 90 % of the tests were temperature ramp tests mainly directly heated by Joule Effect (46.4 %) or by internal electrical heaters (39.1 %). Most of the tested claddings were as-received ones (~90 %), about 10 % of the tests were performed on pre-hydrided and/or pre-oxidized claddings and only 3% of the tested claddings were irradiated.

Heating Mode	**Joule Effect**	**Internal Electrical Heater**	**External Electrical Heater**	**External Infrared Heater**	**Nuclear**
	585/41.5 %	509/36.1 %	104/7.4 %	126/8.9 %	85/6.1 %
Alloy	Zy-4	M5/E110/Zr-1%Nb	Zirlo/Opt Zirlo	Zy-2	
	1202/85.3 %	116/8.2 %	79/5.6 %	12/0.9%	
Test Type	T ramp	Creep	P ramp		
	1239/87.9 %	90/6.4 %	80/5.7 %		
Cladding state	As-Received	Pre-hydrided or/and pre-oxidized	Irradiated		
	1197/85 %	161/11.4 %	51/3.6 %		
Rod configuration	Single	Bundle			
	1013/71.9 %	396/28.1 %			
Environment	Steam	Inert			
	1160/82.3 %	249/17.3 %			

Table 3: Main Burst Database characteristics described with independent lines (for each testing characteristic, the number of tests, fraction of the overall database and constitutive cladding material are provided – In green more than 50% of the test database, in orange more than 25%, in blue other tests).

Number of tests		**Joule Effect**	**Internal Electrical Heater**	**External Electrical Heater**	**External Infrared Heater**	**Nuclear**	**Total number of tests**
Test type	T_{ramp}	507	427	0	80	79	1093/90.9 %
	Creep	78	0	0	0	0	78/6.5%
	P_{ramp}	0	0	31	0	0	31/2.6%
Cladding State	As-Received	487	427	31	57	49	1051/87.4 %
	Pre-hyd. or/and pre-ox.	98	0	0	17	0	115/9.6 %
	Irradiated	0	0	0	6	30	36/3 %
Configuration	Single	568	166	31	80	43	888/73.9 %
	Bundle	17	261	0	0	36	314/26.1%
Environment	Steam	454	412	0	80	79	1025/85.3%
	Inert	131	15	31	0	0	177/14.7 %
Total number of tests		585/48.7 %	427/35.5 %	31/2.6%	80/6.7 %	79/6.6 %	

Table 4: Main Burst Database characteristics of burst tests performed on Zy-4.

Burst parameters

The minimum mandatory set of burst parameters to select a test to build burst criteria is composed of:

- Cladding geometrical data (outer diameter, as-received thickness);
- Heating rate;
- Burst temperature;
- External and internal burst pressures;
- Circumferential strain at burst opening mid-height (usually maximum circumferential strain).

Uncertainties on burst parameters are often unavailable and may be significant since both temperature and pressure are never measured at burst location. After most of the tests, burst temperatures were estimated using thermal axial profiles and/or TC measurements but very few details are usually available. Concerning the heating rate, given values are usually mean values that may be far lower close to burst time in particular when burst occurs just before the device reflooding in semi-integral tests.

Burst pressure is a complicated concept, in particular for irradiated fuel rods when axial gas communication is impaired by fuel/cladding bonding in areas where cladding strain is small. It is usually measured in plena (lower and/or upper) and could be very different from the pressure in the balloon at burst in some cases. For some tests, burst pressures were unfortunately not reported in available references, therefore correlations between filling pressure, maximum pressure and measured pressure at burst were built when data are available. These correlations were then used to deduce burst pressures for some experiments (less than 10% of the tests). Of course, these correlations can only be used when the test conditions and tested rods are similar in particular concerning plena characteristics (location, volume, temperature). For most of the tests having a sufficiently opened gap between pellets and cladding, and using internal pressure regulation or with a cold large plenum, internal pressure variation during burst tests (from ballooning onset to burst) is quite limited.

Finally, strain is sometimes measured by approximated techniques using diameters without opening corrections; this issue is very important when establishing models on true stress or circumferential strain.

Histograms on main burst parameters are given in Figure 1 and percentiles are given in Table 5. Engineering burst stress (σ_e) and true burst stress (σ_T) were calculated as:

$$\sigma_e = \frac{P_i(r_e - t_0) - P_e r_e}{t_0} \text{ and } \sigma_T = \sigma_e.(1+\varepsilon_e)^2$$

$$\text{with } \varepsilon_e = \frac{C_e - C_e^0}{C_e^0}$$

Where P_i is the internal pressure at burst time, P_e is the external pressure at burst time, r_e the cladding external radius, t_0 the cladding thickness for as-received geometry[11] and ε_e circumferential strain at mid-burst height (generally maximum circumferential strain). C_e is the maximum cladding external circumference at burst and C_e^0 is the initial maximum cladding external circumference.

In some references [2] [3] ,the engineering stress is approximated by $\sigma_{e\,approx} = \frac{(P_i - P_e)(r_e - t_0/2)}{t_0}$. This approximation leads to an overestimation of the engineering burst stresses by $(P_i - P_e)/2$ compared to eq. (1). In the following, when data or criteria from this work are compared to literature references using this approximation, engineering stresses are corrected to allow comparison.

[11] For irradiated or pre-oxidized claddings, zirconia layers influence on burst stress and strain is not well described in literature. In this study, as-received geometry was used for true burst stress evaluations.

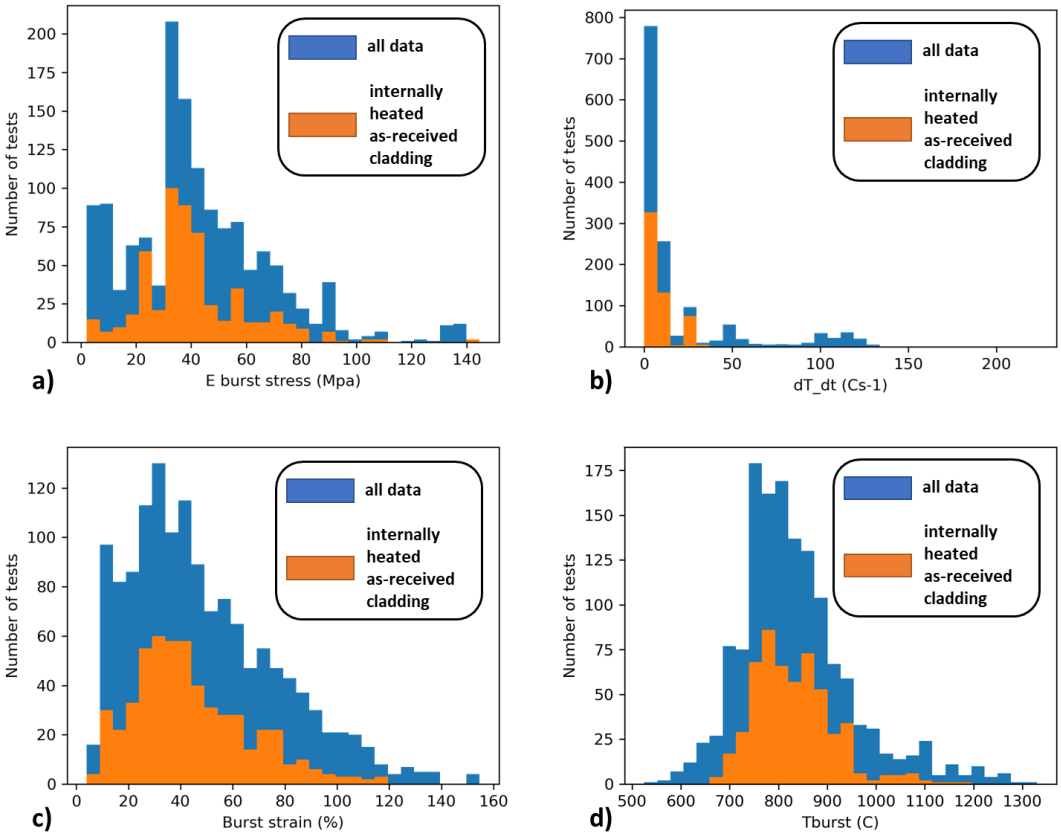

Figure 1: Histograms of selected parameters. a) Engineering burst stress (MPa), b) Heating rate (°C/s), c) Circumferential burst strain (%), d) Burst temperature (°C). Blue all data base, orange tests on AR received cladding internally heated.

75% of burst tests were performed at heating rates (around burst) lower than about 20°C/s. 80% of bursts in the database occurred at temperatures higher than 710° and lower than 1000°C with a median value around 810°C. In some tests, very large circumferential strains were reached (maximum value 155%), the median value is 43% and 10% of the tests led to strains lower than 16%.

Percentile / Parameter	0 (min)	0.1	0.25	0.5 (median)	0.75	0.9	1 (max)
Burst temperature (°C)	525	710	757	813	889	993	1330
Heating rate (°C/s)	0	0	1	6	19	71,4	223
Engineering Burst Stress (MPa)	2.1	8.9	26.9	38.2	56.3	75.4	144.7
Engineering Circumferential Burst Strain (%)	4	16	28	43	66	89	155
True Burst Stress (MPa)	3.8	21.7	42.8	80.7	144.1	204.5	436.9

Table 5: Some statistics about main burst parameters.

Comparison with existing LOCA burst criteria

Maximum circumferential strains at burst are plotted in Figure 2 for all heating modes or only for internal heating modes with two heating rate ranges (between 1 and 10°C/s and above 10°C/s). The NUREG-0630 envelope is also plotted for comparison [2]. These figures illustrate the following statements:

- Maximum circumferential strains for burst tests with similar heating rate and pressure difference are significantly scattered;
- The higher the burst pressure difference is the lower the burst temperature is;
- Maximum strain reached with internal heating methods are lower than the ones reached by external heating methods;
- Highest burst temperatures (above 1100°C) only occur for heating rates higher than 10°C/s;
- For bursts at temperatures higher than ~1000°C, higher strains are reached with high heating rates;
- NUREG-0630 strain envelopes could be considered as upper envelopes in particular for bursts at temperatures higher than about 1000°C and with internal heating modes, since several tests lead to higher burst strains. This criterion cannot be considered for predicting burst.

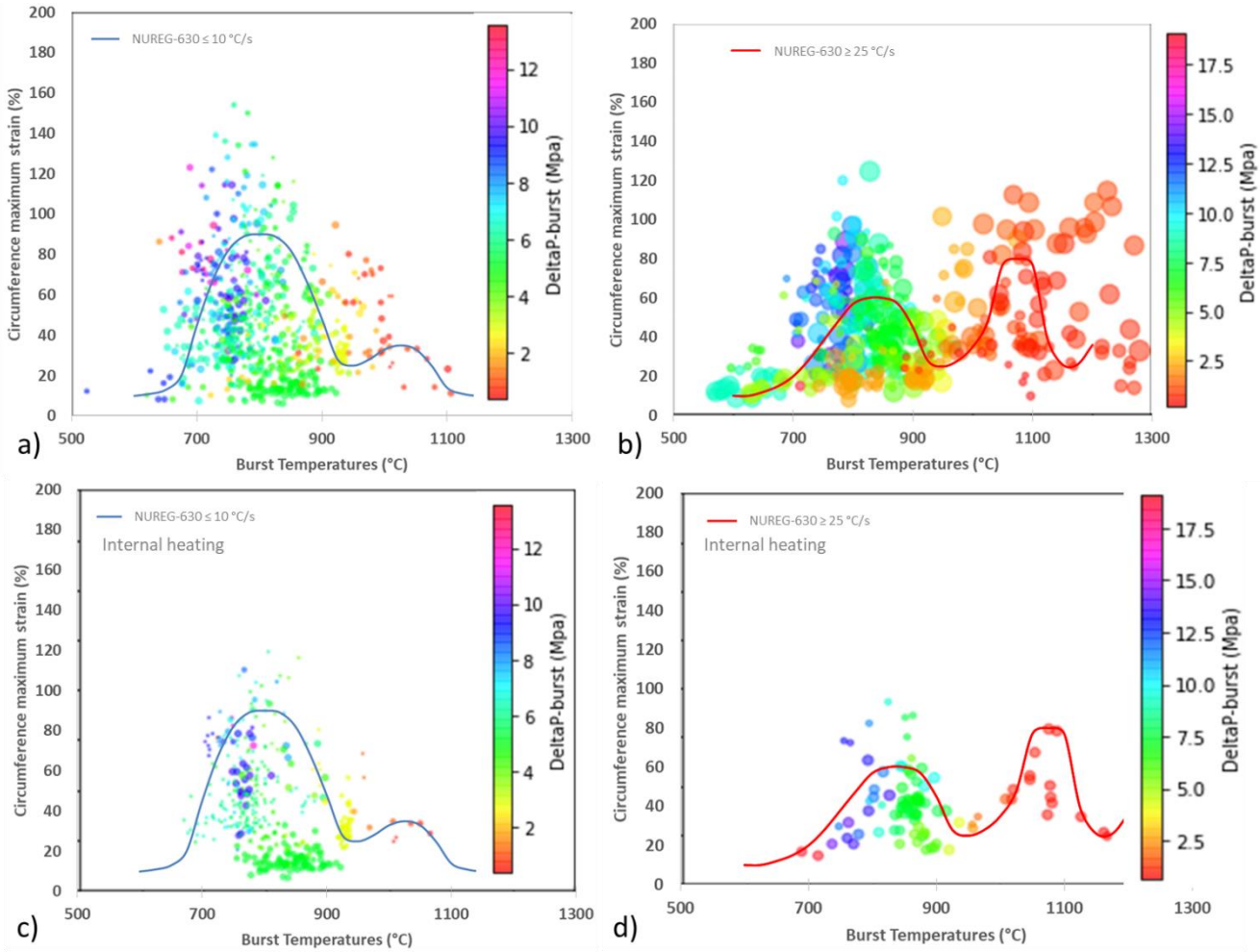

Figure 2: Maximum circumferential burst strain versus burst temperature compared to NUREG-0630 strain envelopes. a) All heating modes, heating rates between 1 and 10°C/s, b) All heating modes, heating rates higher than 25°C/s, c) Internal heating modes, heating rates between 1 and 10°C/s and d) Internal heating modes, heating rates higher than 25°C/s Marker size is proportional to the heating rate.

The same kind of analysis was performed on engineering stress to compare burst data with the Chapman criteria [2]. These figures (cf. Figure 3 a) to d)) illustrates the following statements:

- The higher the burst pressure difference is the lower the burst temperature is;
- Generally, the higher the heating-rate is the higher burst temperature is;
- The Chapman criteria seems to be in agreement with some data points however some burst stresses are clearly over-predicted.

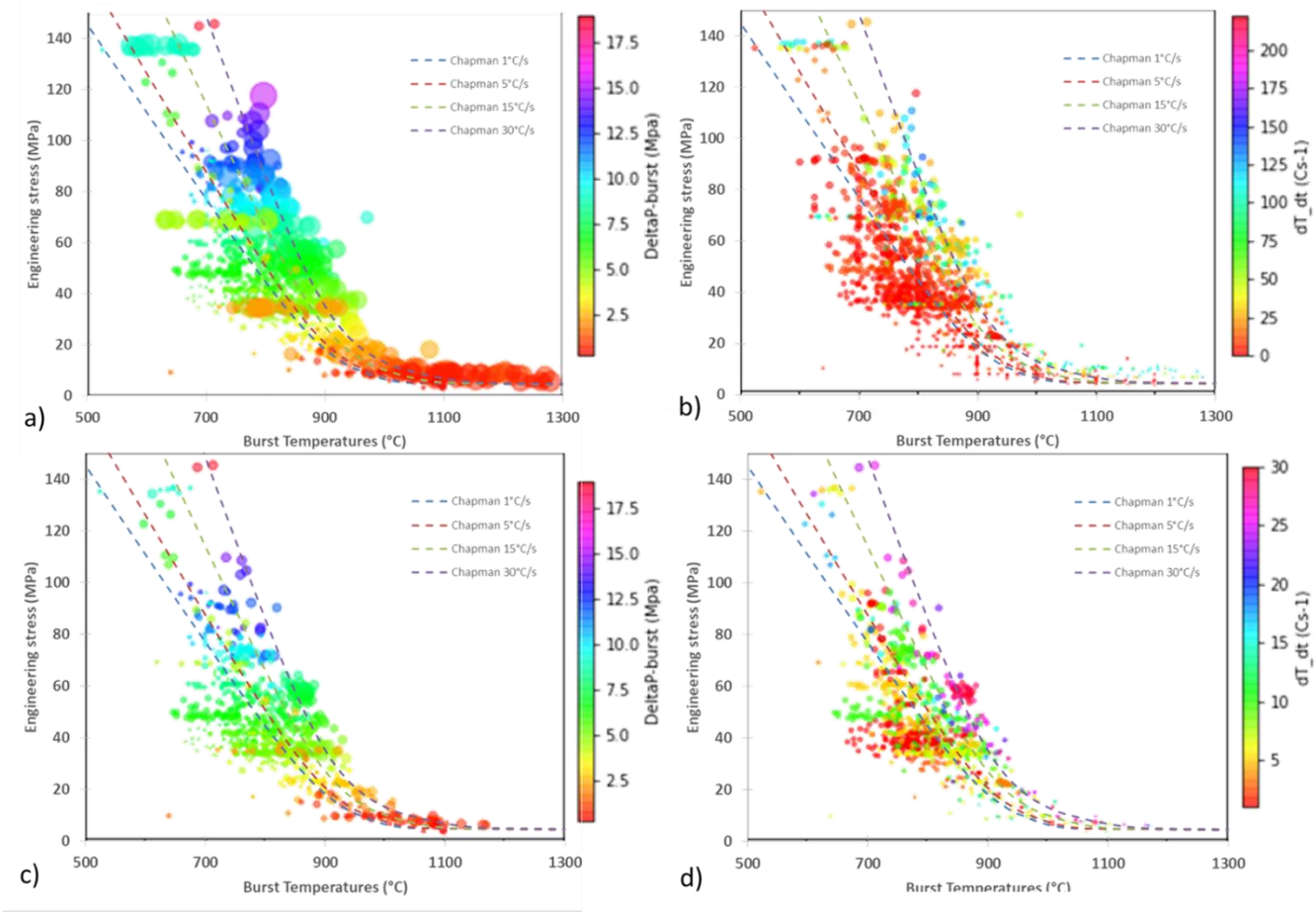

Figure 3: Engineering burst stress versus burst temperature compared to Chapman criteria. a) All data with colour map on pressure difference, b) All data with colour map on heating rate, c) Heating rates in the range 1-30°C/s with colour map on pressure difference, d) Heating rates in the range 1-30°C/s with colour map on heating rate.

True burst stress was also analysed to look for trends and to help building a new burst criterion. The data are compared with the EDGAR criterion proposed in [4] from creep tests performed on Zy-4 (cf. Figure 4). The EDGAR criterion is fairly consistent with collected data. Data dispersion is very strong with burst stresses differences varying within a decade.

To evaluate the impact of the heating rate on true burst stress, data were plotted for several heating rate ranges (cf. Figure 5). As for burst engineering stress, the higher the heating rate is, the higher burst stress is. However, for heating rates lower than 10°C/s, the impact of the heating rate is limited and the trend is exponential in the range 700-1000°C.

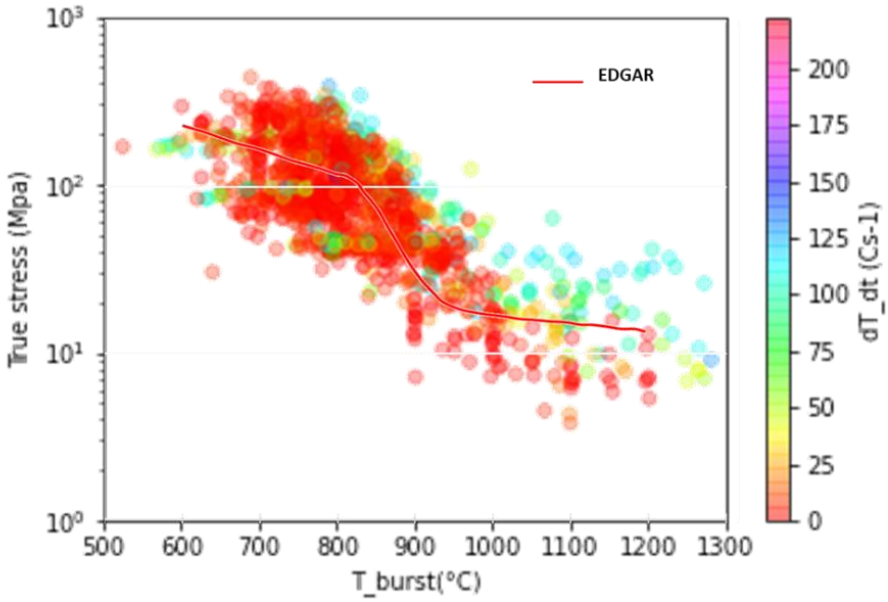

Figure 4: True burst stress versus burst temperature with colour map on heating rate and EDGAR criteria built from creep tests[2].

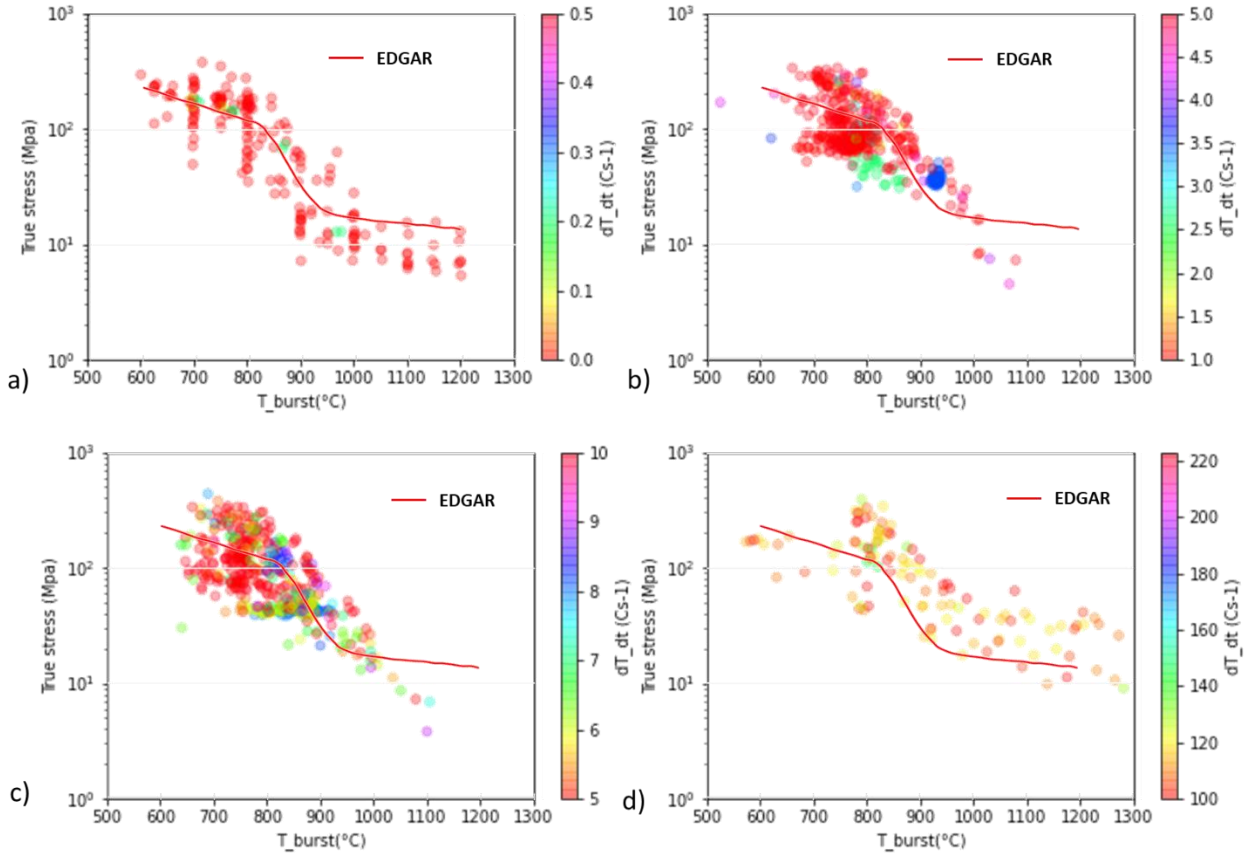

Figure 5: True burst stress versus burst temperature with colour map on heating rate and EDGAR criteria built from creep tests [2] a) For heating rates in the range 0-0.5°C/s, b) For heating rates in the range 1-5°C/s, c) For heating rates in the range 5-10°C/s and d) For heating rates in the range 100-223°C/s.

EK contribution

The code FRAPTRAN used by EK for LOCA simulations has two LOCA-specific burst failure criteria: engineering hoop strain and true hoop stress. Due to the nature of high-temperature clad ballooning, even samples tested in similar conditions may suffer significantly different total strains at burst, which gives rise to a large scatter in the experimental data. This scatter makes it extremely difficult to define the burst strain limit, which in turn increases the uncertainty of code calculations. In order to overcome this difficulty, in the framework of the R2CA project the geometry of ballooned and burst samples (produced outside of the project) was studied to investigate whether the local ballooning can be isolated and the burst parameters can be set up based on the remaining, uniformly expanded part of the cladding, or some other convenient method can be found. The samples were made of the Russian cladding alloy E110 containing 1% of niobium.

Since the behaviour of the cladding depends on the temperature, pressure increase rate, material, thickness, the following matrix was set up in order to see the geometries of samples of two different variants of the Russian alloy (denoted as E110 and E110G or E110opt) tested at the largest possible temperature range and at two very different and LOCA-relevant pressure increase rates – taking into account the availability of samples. The ballooning-and-burst tests had been performed at constant temperature and constant pressure increase rate.

	dp/dt ≈ 0.5 bar/s	**dp/dt ≈ 1.5-2.6 bar/s**
T ≈ 700 °C	E110G slim	E110G
T ≈ 800 °C	3xE110G, E110G slim, E110	E110G, E110
T ≈ 900 °C	E110G, E110G slim	2xE110G
T ≈ 1000 °C	E110G	E110G
T ≈ 1200 °C	E110G	E110G

Table 6 : Matrix of samples for the detailed geometrical assessment

Here the basic geometry of the cladding is: inner radius: 3.88 mm, outer radius: 4.55 mm (these are the present day fuel rods), whereas 'slim' denotes the new fuel rods (under testing in lead test assemblies) with inner radius: 3.88 mm, outer radius: 4.45 mm.

Two types of geometry data were used in the project that in the following will be called engineering-level data and local data. At the engineering level the geometry in a certain axial position is typically given by the total strain, from which the average thickness can be calculated, whereas the local data contain local thicknesses.

The total strain is typically provided in the experimental datasets, but it is not always clear what it really refers to and how it was determined. Some experimentalists [5] [6] define burst strain as the strain at the tip of the crack, whereas most others [7] [8] as the strain at mid-burst. Here crack tip means the end of the crack in the axial direction. For the crack tip the total strain is unambiguous, but for the middle of the burst it is not. In the cases studied within the framework of R2CA the following types of total strain measurement were identified (here the edge of the crack means the edge of the crack lip):

- $\frac{\text{outer circumference of the sample measured from one edge of the crack to the other edge of the crack}}{\text{initial outer circumference}}$, i.e. not including the gap between the crack lips
- $\frac{\text{total outer circumference of the sample}}{\text{initial outer circumference}}$, i.e. including the gap between the crack lips
- other complicated definitions, e.g. involving the cross-sectional area at mid-burst and a radius defined based on this area, compared to the initial radius

Obviously from the standpoint of strains and strain limits only the circumference of the metal counts, so all the strains that include the gap between the crack lips are wrong. In the framework of the R2CA project an effort was made to reassess at least some of the available burst measurements.

The other part of the work performed in the project was to compare local strains to average strains at a given position, and strains measured at several special points along the sample: outside of the balloon, at the edge of the balloon, at the burst crack tip and at the middle of the burst crack.

Measurements made on the samples and data processing

Two series of measurements were made:

1. One to assess the effect of the inclusion of the burst opening into the cladding strain at mid-burst position.
2. The second one to map the strains at different axial positions along the samples.

In the first series twelve samples from the second part of the experimental series BALL from the database [8] were reassessed. All of them had been cast in resin and cut at mid-burst earlier. Now a high-resolution picture was taken from each sample and points were determined along the inner and the outer circumference, opposite each other. The coordinates were recorded and the thickness was determined in each point. This was done manually.

In the second series nineteen samples from previous ballooning-and-burst experiments (not done in the framework of R2CA) were subjected to a computer tomography (CT) scan. The resulting gigabytes of points were then processed for each sample:

- The axis of the sample was determined manually. The parts above and below the burst were often tilted with respect to each other, in these cases two axes were determined.
- The points were distributed into 0.1 mm thick axial discs, and within each disc into 0.5° azimuthal angle, practically triangular segments. Most points were naturally at the rim of these segments (where the inner and outer surfaces of the cladding were), but due to reflexions some were seen inside the segments as well. The coordinates of the points close to the surface were averaged, so that one point was obtained as the inner surface of the cladding and one as the outer, in the given volume of 0.1 mm x 0.5°.
- As the resulting points were still rather scattered, a 20-point axial moving average was applied to them for each azimuthal angle.
- Straight lines were fitted at each azimuthal angle to the inner and the outer cladding surface and the distance between these was determined as the thickness of the cladding.

As a result the cladding thickness was obtained at intervals of 0.1 mm (axially) and 0.5° (azimuthally). This was all done using scripts and programs written specifically for the R2CA project.
In the last step the axial positions of interest (non-ballooned, edge of the balloon, edge of the burst, middle of the burst) were determined manually and the cladding thickness data pertaining to these positions were collected into separate files, also by a program written specifically for the R2CA project.

Effect of the inclusion of the burst opening on total strains:

The choice of the samples (the second part of the experimental series BALL from the database [8] was made for several reasons:

- they were from an earlier batch of cladding material than the other samples used in the present work, so they added to the variety of the data;
- they had been cast in resin and cut at mid-burst, so they were ready for these measurements and unsuited for many others;
- these experiments were carried out at constant temperatures ranging from 800 to 1200 °C and pressure increase rates between 0.6 bars and 6.6 bars, which covers the ranges of interest to this work.

Figure 6 shows an example (sample No. 13). In this specific case the circumferencial strain given in the database was 58%, whereas 37% was measured.

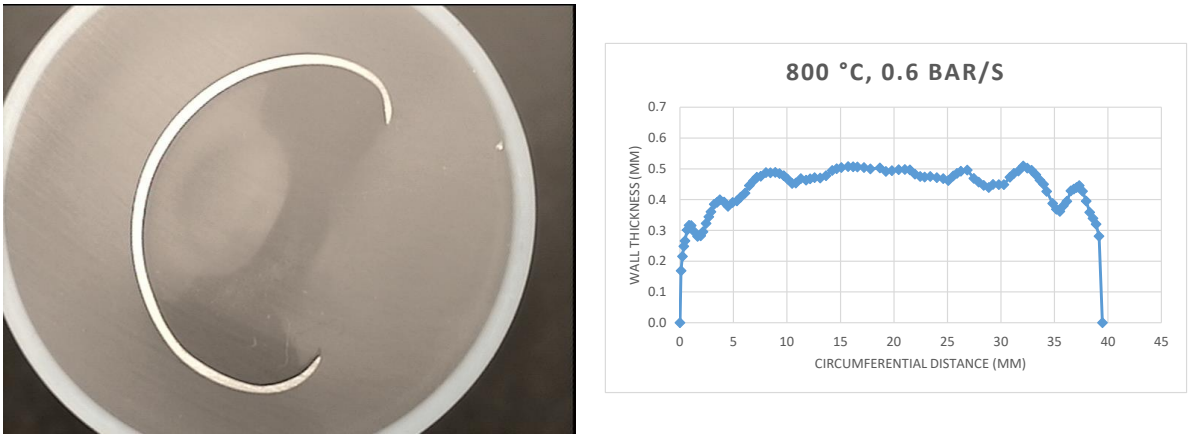

Figure 6. Left: sample No. 13 [8], right: the local cladding wall thickness along the circumference

Table 7 shows the strains given in the database and measured within the R2CA project. These corrections were applied when establishing the new burst criteria.

Sample number	Strain from [8] (–)	New strain (–)	New strain / strain from [8]
13	0.58	0.37	0.64
14	0.18	0.15	0.83
15	0.49	0.21	0.43
16	0.36	0.26	0.72
17	0.34	0.18	0.53
18	0.15	0.14	0.93
19	0.26	0.11	0.42
20	0.66	0.58	0.88
21	0.46	0.41	0.89
22	0.41	0.37	0.90
23	0.41	0.28	0.68
24	0.43	0.43	1.00

Table 7 : Previous and new circumferential strains in the 2nd part of the BALL dataset

Effect of the local vs. average thicknesses

Classically the total circumferential elongation at mid-burst (or at the burst edge) is measured and the average strain is calculated from this. Considering how variable the shapes of the bursts and the burst lips are, there was a hope that excluding the local balloon or only the burst lips from the measurements would reduce the scatter in the burst strain data. This exclusion would mean e.g. in the graph already shown in Fig. 6 but complemented with the delimiting lines in Figure 7 that only the part between the dotted lines would be kept if only the burst lips were to be omitted, or the part between the dashed lines would be kept if the whole part that could be tentatively identified as the local balloon were omitted.

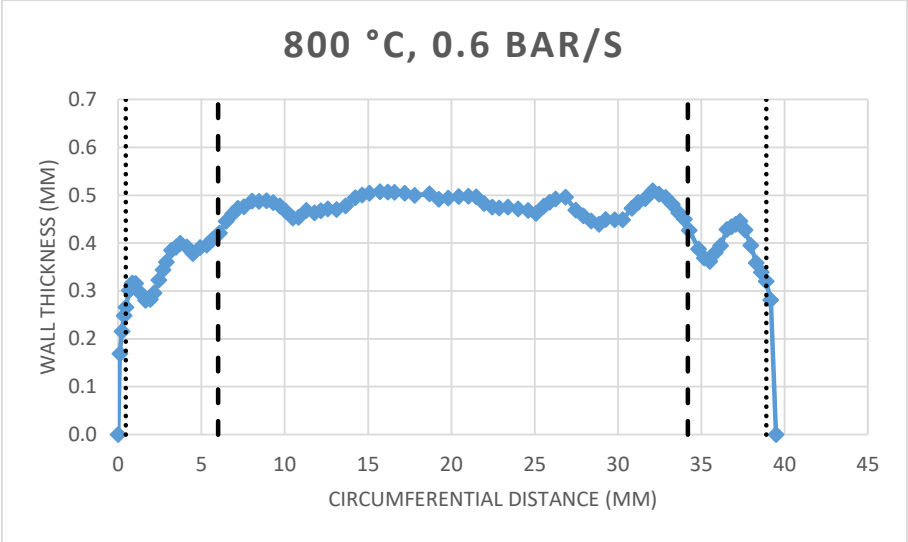

Figure 7. Delimiting lines between burst lips, local balloon and remaining ('thick') part

Figure 8 shows the strains obtained taking into account the whole cross-section (left) and only the part without the local balloon (right). The results are not dramatically different, and, contrary to expectations, the scatter is not significantly smaller. Considering the amount of extra work necessary to obtain the local data for the reduced azimuthal length and how arbitrary it often is to determine what could be considered as the local balloon, it is not worth processing and reassessing masses of samples with this method.

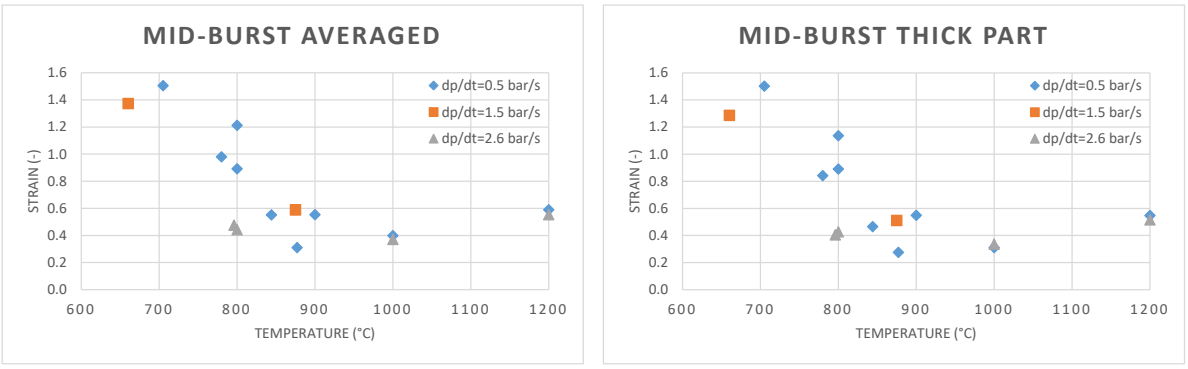

Figure 8. Left: average strains at mid-burst, right: strains omitting the balloon

Effect of the position where the burst strain is defined

Moving from the unballooned part of a sample towards the middle of the burst, the strain increases. The samples subjected to CT were analysed from this point of view as well. For further usability only the average strains were compared in all axial positions, so that the results can be used without massive CT scans and data processing. Figure 9 shows the results.

The edge of the burst represents the area where local instability starts, therefore it has been decided to use it as an alternative to the middle of the burst.The scatter of the data is not reduced by using the strain at the edge of the burst instead of the middle. Only the absolute values are, as summarised in Figure 10. If the edge of the burst is considered instead of the middle, the reduction in strain is in almost all the cases above 60%. This value will be used conservatively in the following.

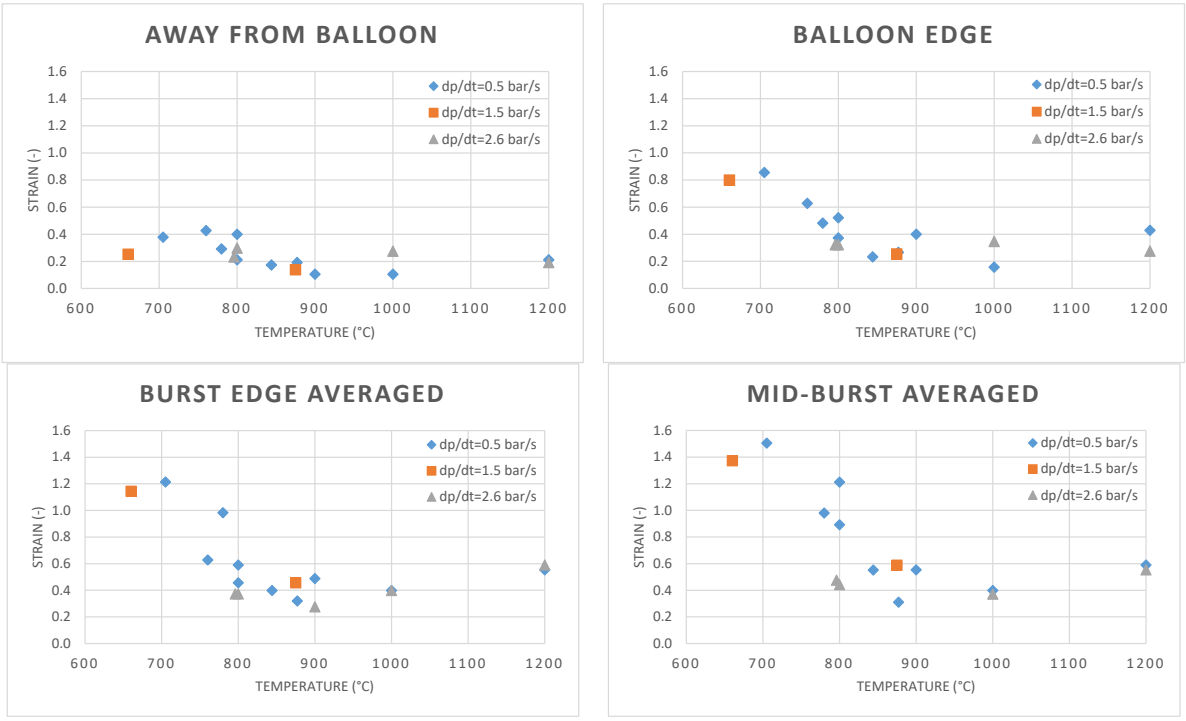

Figure 9. Average strains in different axial positions

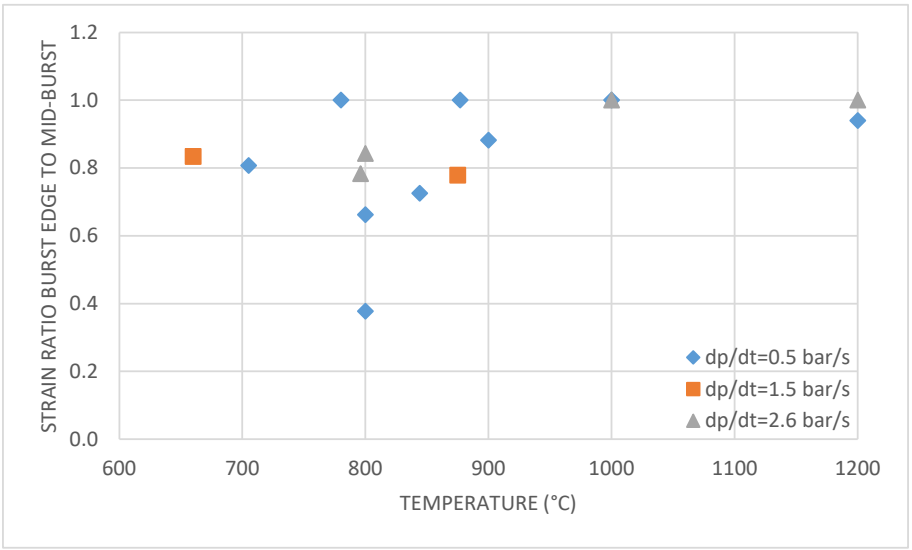

Figure 10. Ratio of the average strain at the edge of the burst to the average strain at the middle of the burst

Additional outcomes of the measurements

In addition to the correction of the strains, several features are of importance regarding Figure 6, which also appear in the other samples:

- The thickness is very much non-uniform, even far from the burst.
- The circumference cannot clearly be divided into a thinner balloon region and a thicker, 'uniform' region that would be the non-ballooned part of the cross-section.
- There are local minima in the thickness. This sample also shows what is even more pronounced in others: the burst could have occurred in several other locations as well, probably due to local weak spots in the cladding material.

New burst criteria

IRSN contribution

Different types of burst criterion were selected and tested during the R2CA project:

- Chapman-like burst criteria on **engineering** and **true stress** versus temperature taking into account the heating-rate,

$$T_{burst}(°C) = \mathrm{A} - \frac{B\ \sigma_{e\theta}}{1 + \frac{\frac{dT}{dt}}{C}} - \frac{\mathrm{D}\ \sigma_{e\theta}}{1 + \frac{\frac{dT}{dt}}{C}} + \mathrm{E}\ \sigma_{e\theta}$$

  Where T_{burst} is the burst temperature (°C), $\sigma_{e\theta}$ the engineering hoop stress (kpsi) and $\frac{dT}{dt}$ the heating rate (°C/s).
- Simple best-estimate exponential burst criteria on **engineering** and **true stress** versus temperature and various envelopes (lower, mean, mean ± std, upper) applicable in a limited heating range [1-20°C/s],

$$\sigma_{\theta burst}(T) = k * e^{-qT}$$

- Exponential burst criteria on **true stress** versus temperature taking into account the heating-rate,

$$T_{burst}(°C) = -\frac{\ln\left(\frac{\sigma_\theta}{A}\right)}{\mathrm{B}} + \mathrm{C}\frac{dT}{dt}\left(1 + \frac{D}{\sigma_\theta}\right)$$

  Where T_{burst} is the burst temperature (°C), σ_θ the true hoop stress (MPa) and $\frac{dT}{dt}$ the heating rate (°C/s)

For each type of criteria, various fits were performed on selected burst tests:

- All burst tests;
- Internal heating;
- Internal heating and as-received cladding.

During this analysis, several key observations were made:

- A significant impact of the heating mode was observed on burst temperatures, in particular at heating rates higher than 15°C/s. At a given engineering or true stress level, burst temperatures tend to be higher for internally heated rods.
- The higher the heating rate is the higher burst temperature is.
- Burst criteria based on engineering stress lead to more accurate burst temperatures than criteria on true stress and are less sensitive to cladding thermomechanical models.
- Burst criteria based on engineering stress lead to strongly underestimated burst strains.
- Cladding hydrogen content decreases burst temperature but available data is scattered as illustrated in Figure 11.

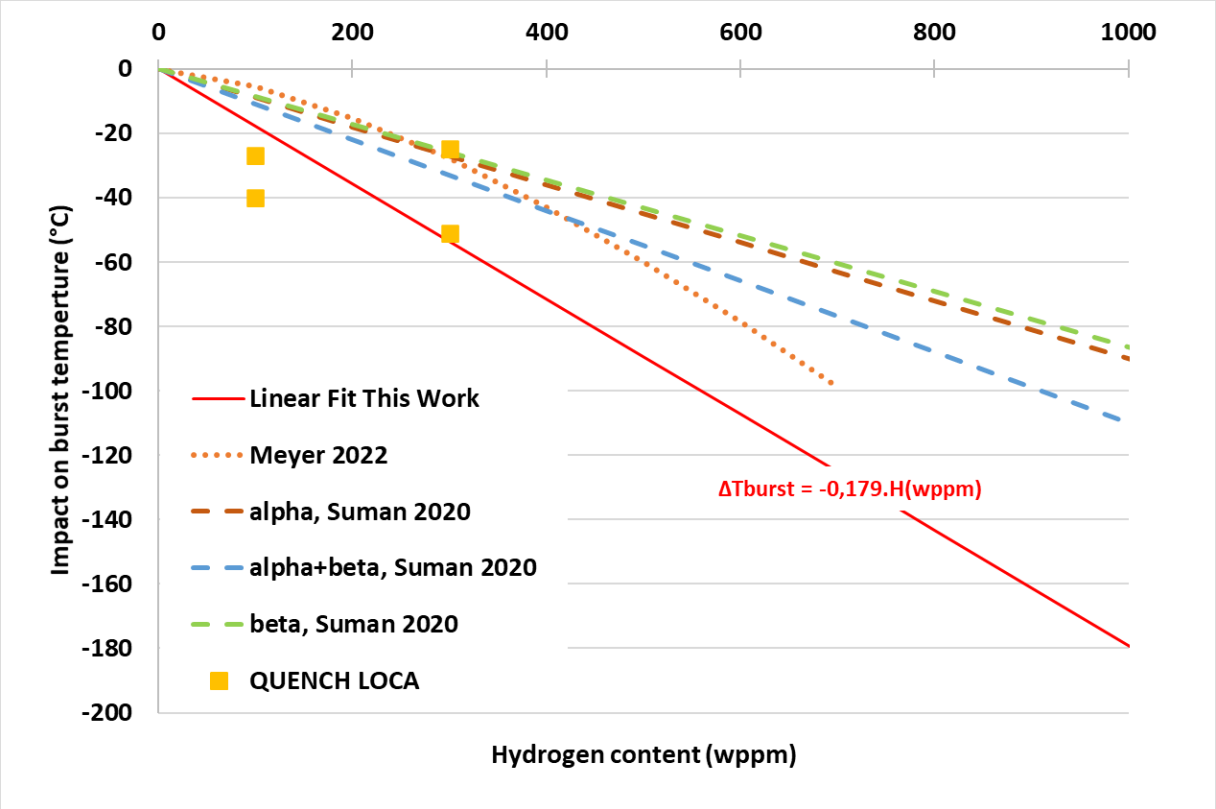

Figure 11: Impact of cladding hydrogen content on burst temperature from literature and fitted during this work.

From these observations, it was finally decided to only select Chapman-like models on tests performed with internal heating on as-received claddings on engineering stress. About 520 temperature ramp tests were selected, there were performed with heating rates in the range [0.8-38 °C/s] and pressure differences in the range [5-190 bar] (see Figure 1). With these test conditions burst occurred between 670 and 1170°C (mean value 771°C) with circumferential burst strain between 7 and 155% (mean value 47%). The strain distribution of all tests and internally heated cases with associated percentiles are given in Figure 12.

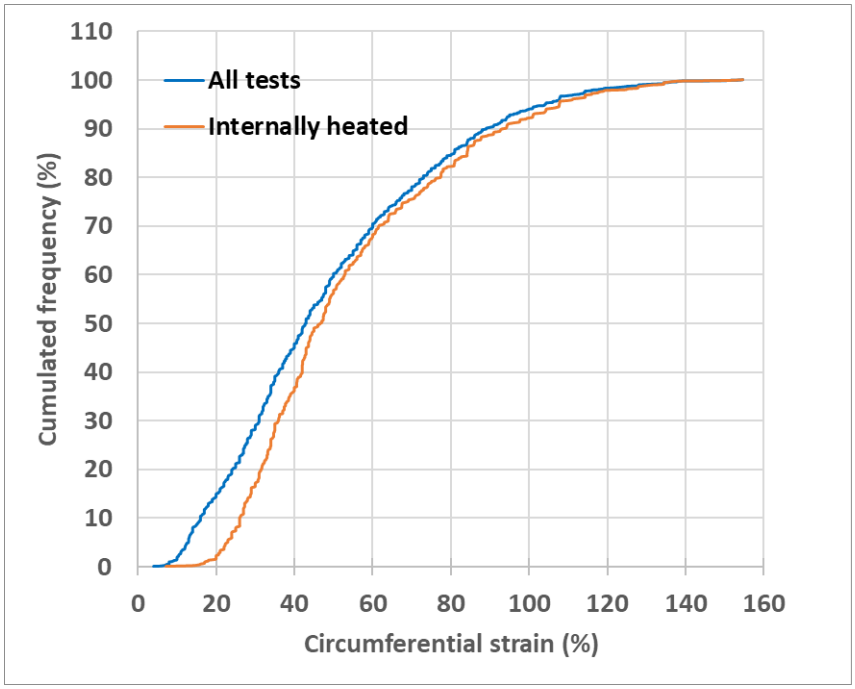

Percentiles	All tests Strain (%)	Internally heated Strain (%)
0	4,0	7,2
0,05	12,9	23,0
0,1	16,0	26,0
0,25	27,7	34,0
0,5	43,0	46,8
0,75	66,2	69,0
0,9	89,0	94,0
0,95	104,2	107,7
1	154,6	154,6

Figure 12: Circumferential burst strain cumulated frequency for all tests and for internally heated tests (left) associated percentiles (right).

Envelopes on true burst stress:

As a first approach, envelopes on true burst stress were fitted based on an exponential trend to allow sensitivity studies. To build these envelopes, data were filtered in the range 700-1000°C with a 25°C temperature step, outside this range there were not enough data. For each group, statistical data (minimum, mean, maximum values and standard deviation) were calculated and then each one was fitted as illustrated in Figure 13. The exponential envelopes $\sigma_{\theta burst}(T) = K * e^{-qT}$ K and q parameters are given in Table 8 and comparison to data is illustrated in Figure 14. The extrapolation of the models outside the 700-1000°C range seems acceptable even if a slight underestimation of true burst stress is observed. The best-estimate (BE) model was fitted on all the data and not restricted to the 700-1000°C range. The "mean envelope" is consistent with the BE model above 900°C, at lower temperatures it overestimates burst stress with an increasing difference for lower burst temperatures.

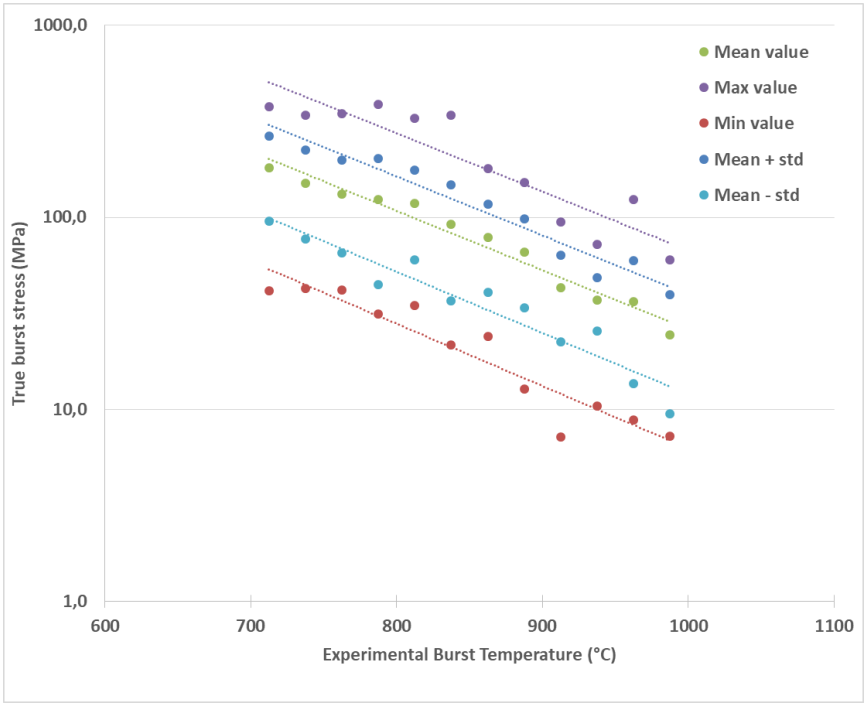

Figure 13: Maximum, minimum and mean values of true burst stress versus burst temperature

	σ_{min}	$\sigma_{mean-std}$	σ_{mean}	$\sigma_{mean+std}$	σ_{max}	σ_{BE}
K (MPa)	11015,44	18658,15	31817,96	46916,15	75541,69	9080,44
q ($°C^{-1}$)	0,007472	0,007351	0,007106	0,007075	0,007022	0,005817

Table 8: Parameters of the exponential correlations on true burst stress for various statistical parameters and the best-estimate model

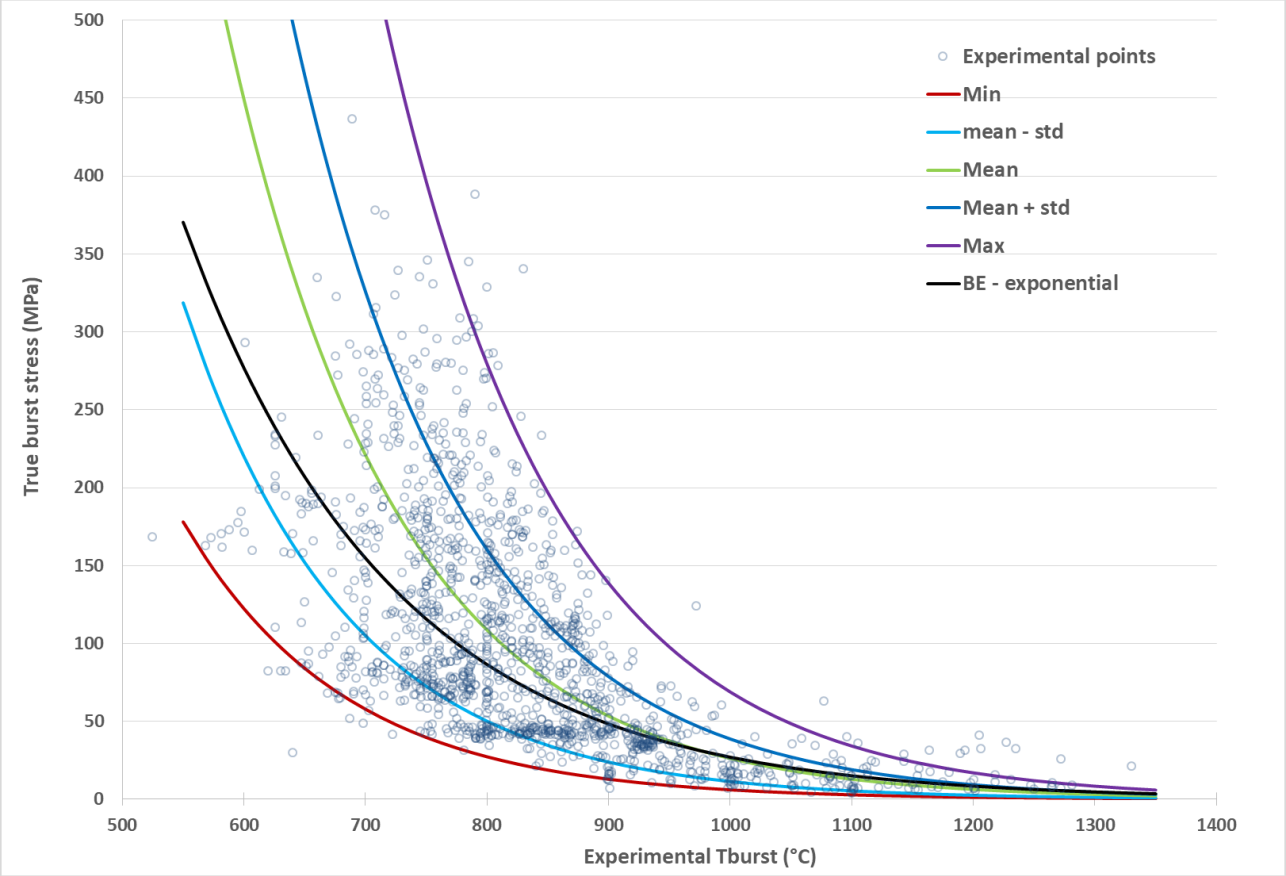

Figure 14: True burst stress versus experimental burst temperature, best estimate fit and exponential envelopes

Criterion on engineering burst stress:

The Excel solver with the nonlinear GRG (General Reduced Gradient) resolution method was used minimizing the sum of $(T_{calc}-T_{exp})^2$ with T_{calc} the calculated burst temperature and T_{exp} the experimental burst temperature. The fitting process beginning with the Chapman model led to a simpler model. The change in the function is mainly due to the addition of Quench LOCA tests.

$$T_{burst}(°C) = A - \frac{B\,\sigma_{e,\theta}}{1 + \frac{\min\left(\frac{dT}{dt}, 38\right)}{C} + D\,\sigma_{e,\theta}}$$

Where T_{burst} is the burst temperature (°C), $\sigma_{e\theta}$ the engineering hoop stress (kpsi) and $\frac{dT}{dt}$ the heating rate (°C/s). This model is only valid for heating ramps from 1 to 38°C/s.

A (°C)	B (ksi^{-1})	C(°C/s)	D (ksi^{-1})	Mean error $\lvert T_{calc} - T_{exp} \rvert$
1145,2	188,5	16,5	0,335	26.7 °C

Table 9 : Engineering burst stress fitting parameters for internally heated ramp tests on as-received cladding.

The comparison between calculated temperatures and experimental temperature is illustrated in Figure 15. The mean error is of 26,7°C and most of the tests are predicted within an error lower than 50°C. However, for a few cases the error is significantly higher (above 100°C).

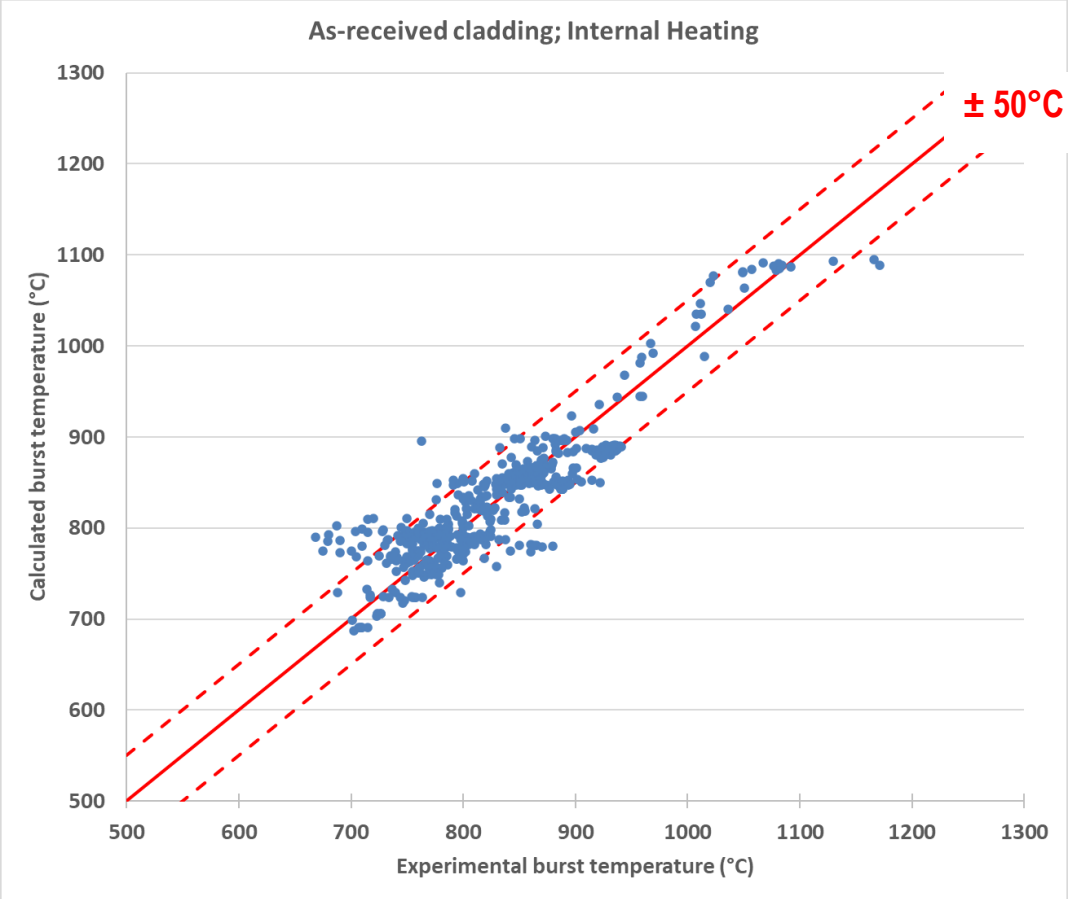

Figure 15: Calculated versus experimental burst temperature with the criterion on engineering stress. Doted lines correspond to ±50°C from the bisector line.

The analysis of burst criteria performances showed that:

- The absolute burst temperature error is lower than 50°C for 88.6% of the tests in the database.
- 85% of tests with absolute burst error higher than 50°C were performed in bundle configuration, for these tests burst conditions are not well known.
- The error versus the heating rate or the engineering burst stress does not follow any trend (cf. Figure 16).
- The higher the heating rate is (in the range 1-38°C/s), the higher the burst temperature is with an impact up to +150°C. (cf. Figure 17).

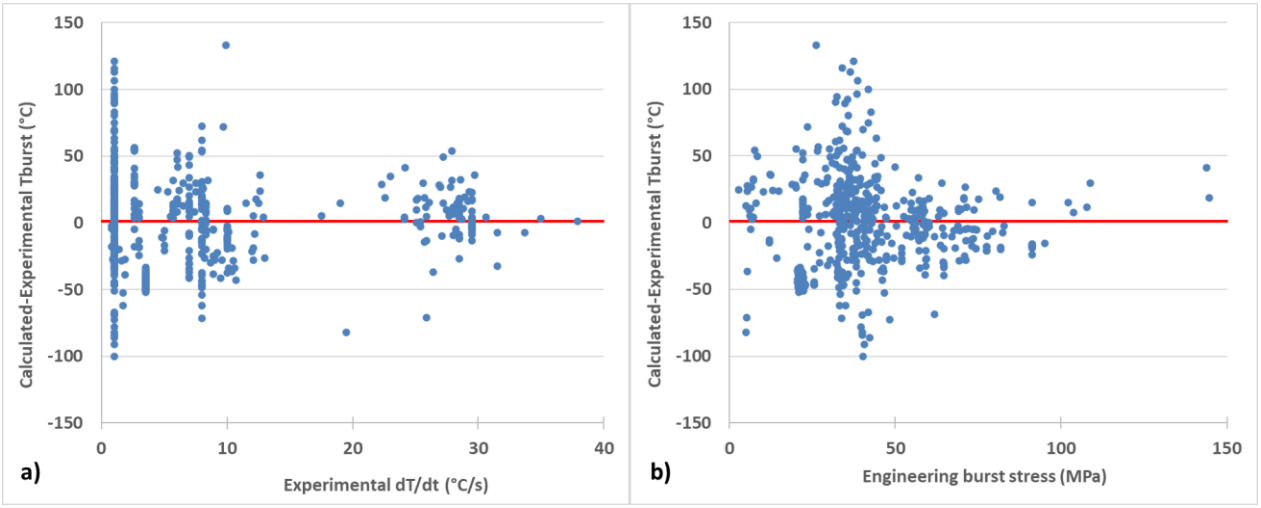

Figure 16: Burst temperature error (calculated-experimental) versus a) the heating rate (°C/s) and b) the engineering burst stress (MPa).

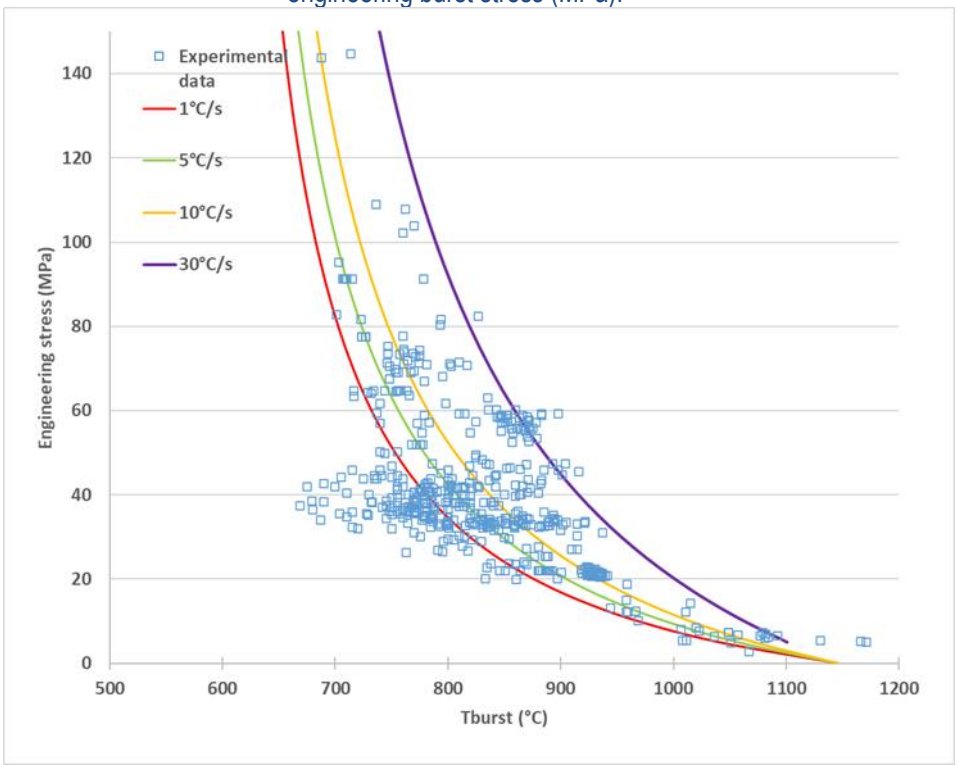

Figure 17: Engineering burst stress versus burst temperature for 1, 5, 10 and 30°C/s and data points.

The criteria fitted during the R2CA project was compared with the Chapman criteria and the Meyer for various heating rates (cf. Figure 18) and the following trends are observed:

- The stress limit versus temperature from this work and the Meyer criteria have a similar behaviour, with a sharp decrease of burst stress in the range 700-750°C. In particular for heating rates lower than 10°C/s.
- The differences between the three criteria decreases with increasing heating rates.
- At high engineering stresses (above ~80 MPa), burst temperature predicted with the R2CA criterion is between the ones predicted by Chapman and Meyer criteria.
- At 1°C/s, the R2CA criterion predicts lower burst temperatures than the two other criteria.
- For low stresses (< 20 MPa) the R2CA criteria predicts higher burst temperatures than the two other criteria in particular at 30°C/s.

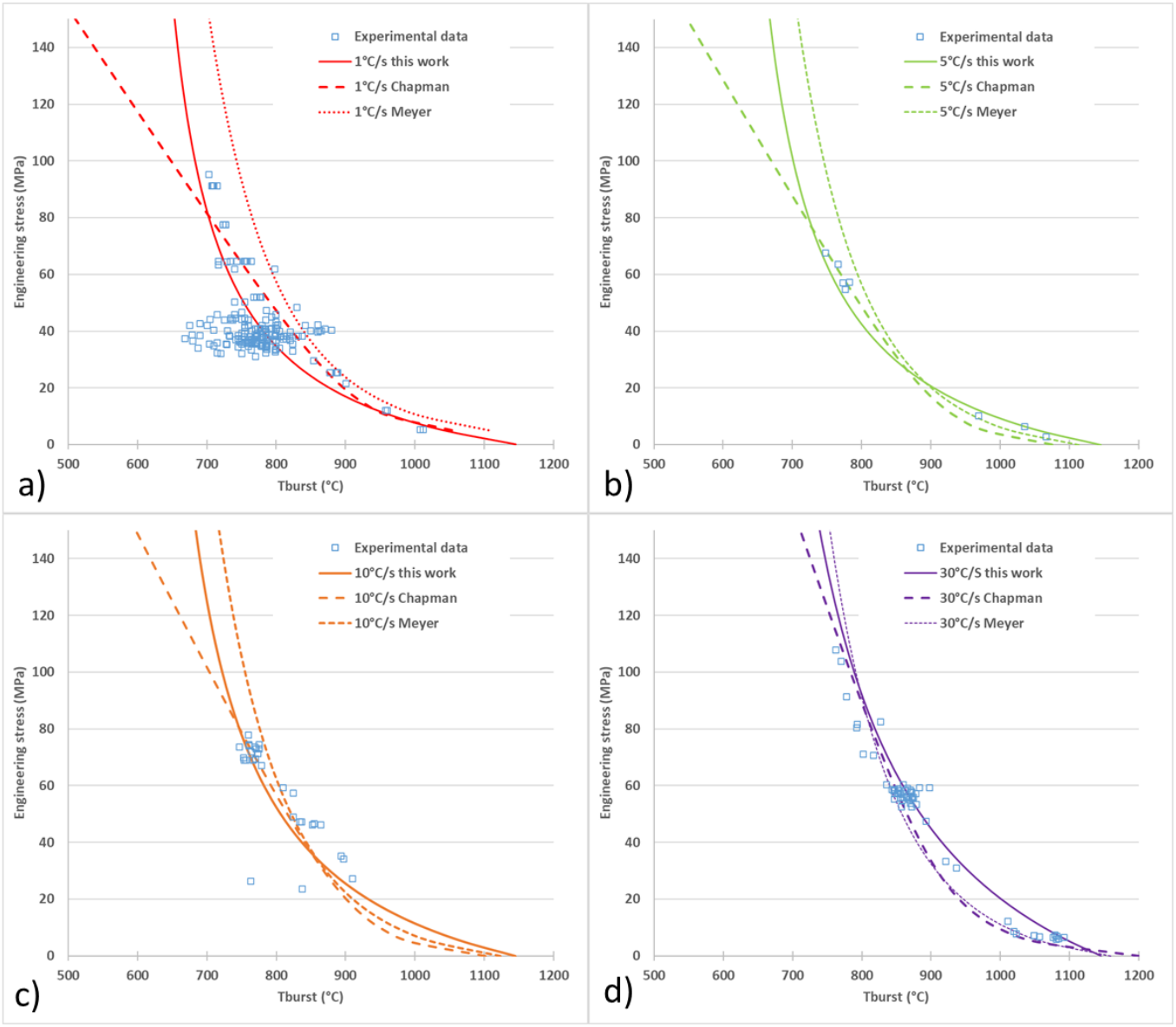

Figure 18: Burst criteria on engineering stress developed during R2CA, Chapman criteria and Meyer criteria for heating rates of 1, 5, 10 and 30°C/s.

EK contribution

Using all the available measurements ([5] [6] [7] [8] and further, unpublished data), including those corrected for the burst opening in the framework of the R2CA project, results in the following graph of strains at mid-burst:

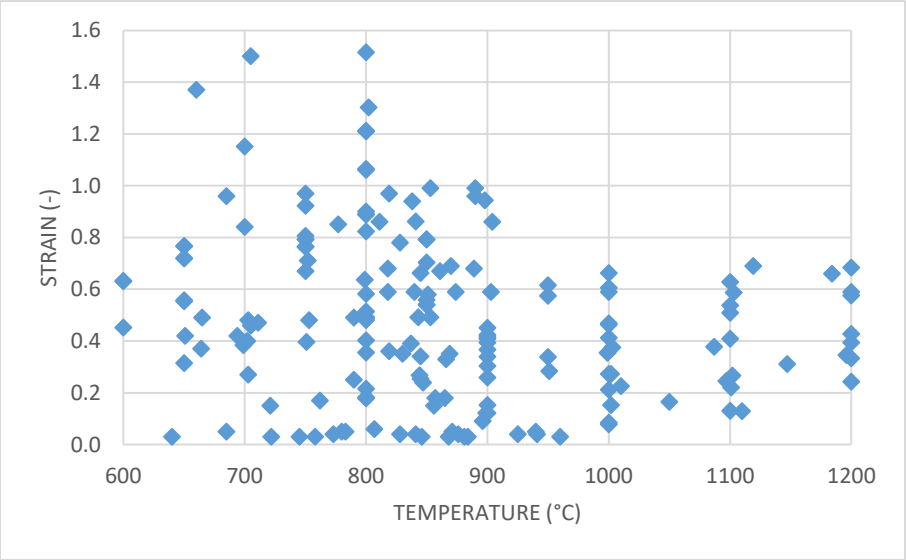

Figure 19. Available cladding burst strains

The data exhibit a significant scatter, without convincing trends. In addition, in the language of the FRAPTRAN models, the failures at low strain are probably due to high stresses, so using the lower envelope of the points would result in unrealistically low strains, which is counter-conservative from the oxidation point of view. Considering the fuel rod pitch of 12.3 mm of the VVER-440 assemblies and the outer cladding diameters of 9.1 mm for the previous and 8.9 mm for the latest fuel type, the maximum possible strain (assuming co-planar ballooning) is 0.35 and 0.38, respectively, so using the upper envelope of the points is also unrealistic. Some suitable middle limit has to be found.

Here an important point has to be made. The temperature-dependent parameters of plastic deformation implemented in the code FRAPTRAN are fitted *using the failure criteria* in such a way that the simulations agree to the best possible degree with the experimental results. Unless the failure criteria are really wrong, the set of failure criteria plus plastic deformation parameters will give good validation results even if the failure criteria are not perfect.

Based on the above, a constant best-estimate failure strain limit of 0.35 has been adopted for the FRAPTRAN parameter fitting, and a reduction by 60%, i.e. a strain limit of 0.21 has been used for the assessment of the failed fuel rod number.

Modified phase transformation and creep laws

EK contribution

The best-estimate failure limit of 0.35 mentioned above has been implemented in the code FRAPTRAN and the best-estimate parameters of the plastic deformation have been fitted. The fitting is an iterative process based on the Levenberg-Marquardt method, where in each iteration step the actual values of the model parameters are input to the code and the code output is compared to the measurements. The programs necessary to do this fitting were partly developed, partly finalised in the framework of the R2CA project.

The code FRAPTRAN [9] describes the cladding ballooning during LOCA as a plastic deformation governed by the equation

$$\sigma = K\left(\frac{\dot{\varepsilon}}{10^{-3}}\right)^{m}\varepsilon^{n}$$

where

σ is the true stress (Pa)
ε is the true total strain (–)
$\dot{\varepsilon}$ is the strain rate (–)
K is the strength coefficient (Pa), model parameter
m is the strain rate sensitivity constant (–), model parameter
n is the strain hardening exponent (–), model parameter

The data selected for the fitting are from three sources and only include samples from the Russian E110 alloy:

- Experiments performed by the Russian Kurchatov and RIAR Institutes for the US NRC [5] [6]. The reports contain data on ring tensile tests and ballooning and burst tests at constant temperature and increasing pressure on as-received and irradiated samples, and on a few axial tensile tests, carried out at different temperatures.
- Ballooning and burst tests performed by the German Forschungszentrum Karlsruhe at constant pressure and increasing temperature in steam atmosphere on as-received samples [7].
- Ballooning and burst tests carried out in EK on as-received samples at constant temperature and increasing pressure or on sealed tubes at increasing temperatures ([8] and so far unpublished data).

A total of approx. 290 data points was selected.

In order to achieve the best simulation results, we did not fit the three model parameters to obtain the best agreement for burst stress and strain data, but for burst times and pressures, following the methodology described in [10] The fitting is an iterative process based on the Levenberg-Marquardt method.This method is widely used for the fitting of non-linear models to experimental data. The problem to define the unknown parameters of any relation is attributed to the minimisation of an appropriate χ^2 function. Due to the non-linear dependence, the minimisation must proceed iteratively.
The N experimental data points, $(x_i, y_i)\quad i = 1, \dots, N$, are modelled by a non-linear function $y = y(x, \underline{a})$ (the FRAPTRAN code) with M adjustable parameters ($\underline{a} = [a_1, \dots, a_M]$). The χ^2 function appropriate for the minimisation is defined as follows:

$$\chi^2 = \sum_{i=1}^{N}\left(\frac{y_i - y(x_i, \underline{a})}{\sigma_i}\right)^2$$

where σ represents the individual measurement error of the ith data point. In each iteration step the actual values of the model parameters are input to the code and the code output is compared to the measurements for the entire set of experimental data used for the fitting.

The fitting procedure took tens of thousands of FRAPTRAN runs. The results of the fitting procedure are presented in Figure 20 to Figure 22, together with the first set of parameters implemented in the code FRAPTRAN by the Russian Kurchatov Institute [5] [6] and the previous set implemented by EK in 2018 (unpublished in international journals).
The large difference in the strength coefficient at low temperatures is caused by the very small number of experiments. At such low temperatures a liquid medium has to be used to achieve the high pressures necessary for burst, therefore only the original Russian experiments [6] were available. However, this coefficient gave the best agreement with the experiments with the new strain limit. The two exponents show significant differences between the different fitting efforts. This is due to the rather low sensitivity of the results to these parameters.
Compared to the 2018 fitting χ^2 has been reduced by 7%.

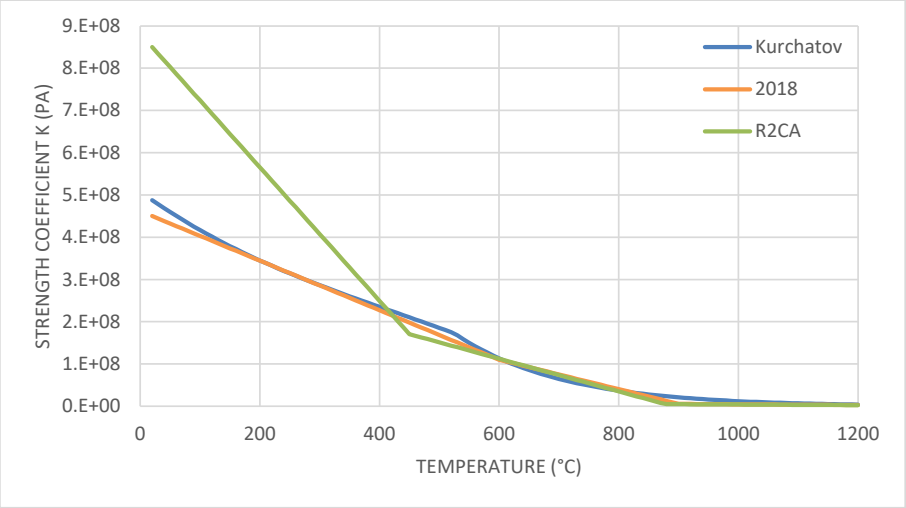

Figure 20. Temperature dependence of the strength coefficient K

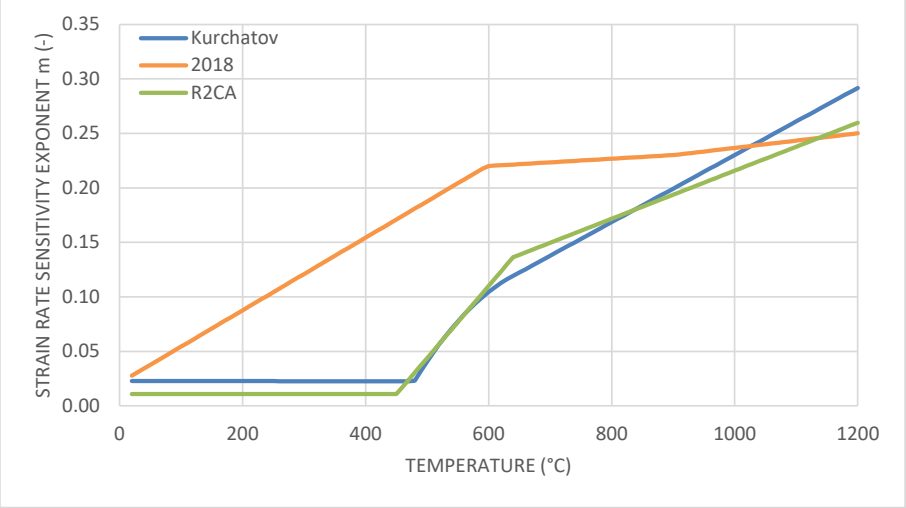

Figure 21. Temperature dependence of the strain rate sensitivity exponent m

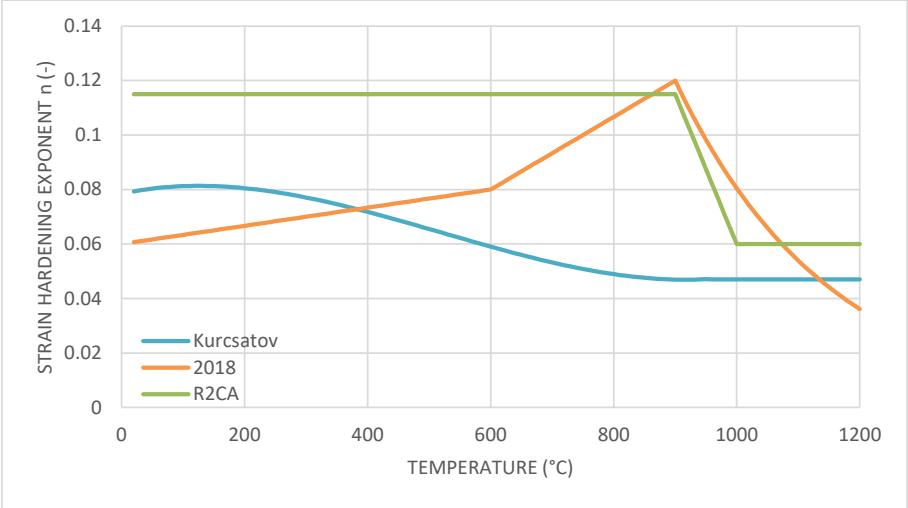

Figure 22. Temperature dependence of the strain hardening exponent n

VTT contribution

Current Loss of Coolant Accident (LOCA) failure criteria in FRAPTRAN have been established based on experimental data from decades ago. Since then, the development of new cladding material, the trend to go toward higher burnups, and plans to extend the operation of current nuclear power plants (NPPs) have highlighted the necessity of examining the viability of current failure criteria.

The report highlights the work carried out within Task 3.2 of the R2CA project. The purpose of the task is to improve the evaluation of the number of failing fuel rods in a whole core during the LOCA transient. The study examines different deformation models and burst criteria under LOCA transients in the FRAPTRAN code. Models from the code that need to be updated are identified and modified accordingly. The implemented models and failure criteria were tested for different LOCA validation cases and the obtained results are compared.

FRAPTRAN code

FRAPTRAN is US NRC fuel performance code for calculating the transient fuel behaviour at high burnup. At VTT, FRAPTRAN has been coupled with a subchannel thermal hydraulics code GENFLO (VTT's in-house code) for improved thermal hydraulics modelling. The coupled version is used for analysis of failing fuel rods within the calculation chain of the statistical methodology developed at VTT [11].

FRAPTRAN stress-strain behaviour:

Total cladding deformation in FRAPTRAN is calculated by considering the elastic strain (ε_θ), thermal expansion (ε_{th}) as well as the plastic strain ($\varepsilon_{plastic}$) according to the equation below

$$\varepsilon_{total} = \varepsilon_{th} + \varepsilon_\theta + \varepsilon_{plastic} \quad (2.1)$$

The basic equation to relate stress and plastic strain is the modified hollomon's equation (2.2) provided in MATPRO version 11:

$$\sigma = K\varepsilon^{n}\left(\frac{\dot{\varepsilon}}{10^{3}}\right)^{m} \quad (2.2)$$

σ is the true effective stress
ε is the true effective strain
$\dot{\varepsilon}$ is rate of change of true effective plastic strain (s^{-1})

K is the strength coefficient, m is the strain rate exponent and n is the strain hardening exponent. These parameters describe the metallurgical state of the cladding, and they are material dependent. Data used in fitting the parameters are listed in NUREG/CR-6150 [12] for generic zircaloy and for Zr-1%Nb in [13].

Plastic strain in FRAPTRAN is calculated by the mechanical model ***FRACAS-I*** for all nodes prior to ballooning (up to 5% strain). According to the manual***, FRACAS-I*** calculates the strain value from the stress-strain curve from MATPRO, where the stress worked out in the previous load step is used to obtain the new strain value in the following step. Under Pellet/cladding mechanical interaction (PCMI) condition, FRACAS-I calls *cstran* subroutine which calculates the time-independent strain from equation (2.2). Under no PCMI condition, *cstrni* subroutine is used instead. The later solves the time dependent strain as in equation (2.3).

$$\varepsilon_f = \left[\left(\frac{n}{m}+1\right)10^{-3}\left(\frac{\sigma}{\mathrm{K}}\right)^{1/m}\Delta t + \varepsilon_{\mathrm{i}}^{\left(\frac{\mathrm{n}}{\mathrm{m}}+1\right)}\right]^{\frac{\mathrm{m}}{\mathrm{n+m}}} \quad (2.3)$$

After the plastic strain exceeds 5%, the ballooning model (***BALON2)*** is called and the plastic strain is calculated for the ballooning node only. In ***BALON2*** model, plastic strain calculations are carried out in *"cstrni"* subroutine from the time integral of equation (2.3) as well.

Current LOCA Failure criteria in FRAPTRAN

The rod failure criterion in FRAPTRAN for ballooning in LOCA is based on empirical stress and strain limits. Under LOCA conditions, FRAPTRAN predicts cladding failure in the ballooning node if one of the following conditions is met:

- Cladding true hoop stress exceeds an empirical limit based on zircaloy data [14]. "*cmlimt"* subroutine calculates this true hoop stress limit which is then compared to the local true hoop stress in the baloning node to test for failure.

- The predicted cladding permanent hoop strain exceeds the FRAPTRAN strain limit defined in NUREG-0630 (Powers and Meyer, 1980). This limit is implemented in "*deform"* subroutine.

The primary cladding failure criterion under LOCA conditions is based on the true tangential stress component. There are essentially two different cladding type-specific stress limits. E110 cladding (cladding type 6 and 8 in FRAPTRAN) has an own model for the true tangential stress at burst, and all other cladding types (Zry-2, Zry-4, ZIRLO, Optimized ZIRLO, M5) use a common correlation which is a function of temperature, fast neutron fluence and cold work, heating rate and strain rate do not affect this criterion [12]. The E110 cladding correlation is only a function of temperature (various different correlations for different fast fluence and temperature ranges).

The generic burst stress limit is given in MATPRO [2]:

$$\sigma_{\theta B} = \begin{cases} 1.36\mathrm{K_A}, & \text{for} \quad \mathrm{T} \le 750\ \mathrm{K} \\ 46.861429\mathrm{K_A}\exp\left(\dfrac{-1.9901087\times10^{6}}{\mathrm{T}^{2}}\right), & \text{for}\ 750 < T \le 1050\ K \\ 7.7\mathrm{K_A}, & \text{for} \quad \mathrm{T} > 1050\ \mathrm{K} \end{cases} \quad (2.4)$$

$\sigma_{\theta B}$ the tangential component of true stress at burst (Pa)

K_A= strength coefficient for annealed cladding as determined with the MATPRO

Note: The material dependent variables (K, n, m) used in FRAPTRAN to predict the mechanical deformation for M5 cladding type are provided in the code by "*ckmn*" subroutine. However, these parameters are determined experimentally based on data for VVER type fuel claddings (E110) solely [13].

The burst stress limit on the other hand used to predict M5 cladding failure during LOCA is the same used for generic Zircalloy (M5 in FRAPTRAN is clad type 7). This experimental stress limit is based on zircaloy data and does not include M5 type cladding in the database. Therefore, the current LOCA models in FRAPTRAN need to be updated to model M5 cladding behaviour under LOCA conditions more adequately.

Code modifications within the R2CA framework

Different models for high temperature creep, phase transformation, in addition to new burst limits criteria have been implemented in the FRAPTRAN 1.4 code version. Those are described in detail in the following sections.

- High Temperature Creep

The mechanical deformation in the ballooning model was updated. The plastic strain calculated by FRAPTRAN in (2.3) was replaced by assuming deformation due to creep strain according to formula (2.6), making the total strain deformation as:

$$\varepsilon_{\text{total}} = \varepsilon_{\text{th}} + \varepsilon_{\theta} + \varepsilon_{\text{creep}} \qquad (2.5)$$

Two models for high temperature creep were implemented:

- Rosinger 1984 [15], developed based on Zircaloy-4 (Zy-4) data and is suitable for generic zircalloy claddings type.
- Kaddour et al. 2004 [16] creep law provides different parameters for both Zy-4 and Zr1%NbO (M5) types.

Both works report the creep strain rate in the form of a Norton creep formation:

$$\dot{\varepsilon}_{creep} = \frac{A}{T}\sigma^n \exp\left(-\frac{Q}{RT}\right) \qquad (2.6)$$

A is the strength coefficient, T is the temperature, Q is the activation energy and R is the gas constant and n is the stress exponent.

Important assumptions

-Although both Rosinger 1984 [15] and Kaddour et al. 2004 [16] creep models are developed for steady state conditions, deformation under LOCA circumstances during ballooning is assumed to follow the same law. As mentioned in [17], this assumption is more relevant at large strains approaching the burst strain, and it is consistent with the original work by [15] in developing the burst failure criteria. The same approach has been applied and proven for BISON code.

-When calculating the strain using the creep formula (2.6), one can assume the stress is constant during the time step integral, which is consistent with the assumption in FRAPTRAN original code calculations from equation number [14].

-Additionally, the creep strength coefficient A_z in the original works are reported from fitting to experimental data obtained under uniaxial testing. FRAPTRAN on the other hand calculates the effective isotropic strain and stress, therefore in order to implement the models consistently in FRAPTRAN, the strength coefficients A_f are recalibrated following the approach described in [18] according to equation (2.7) which is based on the Hill theory,

$$A_f = \frac{A_z}{(F+G)^{(n+1)/2}} \qquad (2.7)$$

F and G are the anisotropic factors defined by Hill. These parameters depend on the phase present in the cladding material. It has been shown previously that zirconium cladding under normal operation (*α* phase*)* is anisotropic, whilst under accident scenarios in the *α*+*β* phase and the *β* phase the cladding exhibits isotropic behaviour. Consistently, A_f calculations are performed with the assumption that the anisotropy factors F = 0.956, G = 0.304 in Zr-alpha and F = G = 0.5. Zr-beta [18].

Table 10 Kaddour et al., 2004 creep law parameters

Material phase \ Constants		$A_z\ [MPa^{-n}s^{-1}]$	n	$A_f[MPa^{-n}s^{-1}]$	$Q\ [KJ/mol]$	$Q/R\ [K]$
		Zy-4				
α-phase	$\sigma \leq 15\ MPa$	1.00E+06	1.3	7.67E+05	190	22852
	$\sigma > 15\ MPa$	1.63E+08	5	8.15E+07	316	38006
β-phase		1.00E+04	4.25	1.00E+04	150	18041
		Zr-1%NbO				
α-phase	$\sigma \leq 15\ MPa$	6.78E+03	1	5.38E+03	133	15996
	$\sigma > 15\ MPa$	2.28E+03	4	1.28E+03	194	23333
β-phase		1.23E+03	4.3	1.23E+03	142	17079

Table 11 Rosinger 1984 creep law parameters

Material phase \ Constants	Zy-4				
	$A_z\ [MPa^{-n}s^{-1}]$	n	$A_f[MPa^{-n}s^{-1}]$	$Q\ [KJ/mol]$	$Q/R\ [K]$
α-phase	1.94E+04	5.89	8750	3.20E+05	38487
β-phase	7.90E+00	3.78	7.9	1.42E+05	17079

In the mixed phase region (*α*+*β*) where both alpha and beta phases co-exist, linear interpolation with respect to the phase composition is applied to obtain the total creep rate ($\dot{\varepsilon}_{\alpha\beta}$)

$$\dot{\varepsilon}_{\alpha\beta} = \dot{\varepsilon}_{\alpha}(1-y) + \dot{\varepsilon}_{\beta} y \qquad (2.8)$$

$\dot{\varepsilon}_{\alpha}$ is the strain rate from *α* phase, $\dot{\varepsilon}_{\beta}$ is the strain rate from the *β* phase, y is the *β* phase volume fraction present in the cladding.

It is worth noting that FRAPTRAN plastic strain behaviour was initially changed by implementing the creep relation (2.6) in the mechanical model (FRACAS-I) and the ballooning model (BALON2). However, the preliminary results

had large error and inconsistencies especially with Rosinger model. This is likely due to the fact that the creep law (2.6) was previously developed and demonstrated for thin-walled cladding tubes in Rosinger work, FRACAS-I deformation on the other hand is based on the assumption that the cladding is a thick cylindrical shell and the strain rates are also not high enough during that stage for the assumption to remain valid. Therefore, calculations have been updated with modifications applied only to ballooning.

- Phase transition

Modelling the kinetics of crystallographic phase transformation is essential to obtain the volume fraction of β phase (y) in the cladding. The parameter is used in formula (2.8) with the creep law (2.6) to determine the right strain during ballooning. FRAPTRAN does not account for phase transition, hence a dynamic phase transition model for cladding phase transformation by [19] has been implemented in the code as described in [17].

The differential equation (2.9) provides the changing rate of the variable y which represents the volume fraction of the β phase, this is a function of time and temperature.

$$\frac{dy}{dt} = k(T)[y_s(T) - y] \quad (2.9)$$

Under non-isothermal conditions, the temperature is an arbitrary function of time, and hence Eq.(2.9) needs to be solved numerically.

y_s is the equilibrium β phase volume fraction at temperature T

$$y_s = \frac{1}{2}\left[1 - \tanh\left(\frac{T - T_{\text{cent}}}{T_{\text{span}}}\right)\right] \quad (2.10)$$

T_{cent} and T_{span} are material specific parameters which relate to the centre and the span of the mixed-phase temperature region.

$$T_{\text{cent}} = \frac{T_\alpha + T_\beta}{2}; T_{\text{span}} = \frac{T_\beta - T_{\text{cent}}}{2.3} \quad (2.11)$$

The temperatures T_α and T_β are those that, respectively, correspond to 99% α and β phase fractions in the cladding.

$k(T)$ is the rate parameter which is the inverse of the characteristic time of phase transformation $\tau_c(T)$.

$$k(T) = \tau_c(T)^{-1} = k_0 \exp\left[-\frac{E}{k_b T(t)}\right] + k_m \quad (2.12)$$

where:

$$k_0 = 60{,}457 + 18{,}129|\text{Q}|(\text{s}^{-1})$$

$$\frac{E}{k_b} = 16{,}650\ (K)$$

$$\begin{cases} k_m = 0 & \alpha \to \beta \\ k_m = 0.2 & \beta \to \alpha \end{cases}$$

Overall, the differential equation (2.9) is solved numerically using Runge Kutta 4th order scheme

For Zircaloy-4, the onset temperature for phase transition is a function of temperature rate Q [K/s] and hydrogen content w (weight parts per millions).

During heating:

$$T_{\alpha\to\alpha+\beta} = \begin{cases} 1083 - 0.152w & \text{for } 0 \leqslant Q < 0.1 \text{ K/s} \\ (1113 - 0.156w)Q^{0.0118} & \text{for } 0.1 \leqslant Q \leqslant 100 \text{ K/s} \end{cases} \quad (2.13)$$

During cooling:

$$T_{\beta\to\beta+\alpha} = \begin{cases} 1300 & \text{for } -0.1 < Q \leqslant 0\text{K/s} \\ 1302.8 - 8.333|Q|^{0.477} & \text{for } -100 \leqslant Q \leqslant -0.1\text{K/s} \end{cases} \quad (2.14)$$

$$0 \leqslant w \leqslant 1000 \text{ wppm}$$

For Zr1%Nb, the onset temperature is only a function of heating rate,
During heating:

$$T_{\alpha\to\alpha+\beta} = \begin{cases} 1060 & \text{for } 0 \leqslant Q < 0.1\text{K/s} \\ 1118Q^{0.023} & \text{for } 0.1 \leqslant Q \leqslant 100\text{K/s} \end{cases} \quad (2.15)$$

Table 12 Equilibrium phase transformation parameters

	T_{cent}	T_{span}
Zircaloy-4	$T_{\text{cent}} = 1159 - 0.096\text{w}$	$T_{\text{span}} = 44 + 0.026\text{w}$
Zr1%Nb	$T_{\text{cent}} = 1129$	$T_{\text{span}} = 49$

New LOCA burst limits implemented

IRSN true stress limits:

Following a comprehensive literature review performed by IRSN within the R2CA project, the experimental database for LOCA accidents has been updated and new failure criteria for stress limit (see page 31) were developed based on that database (see page 16). These correlations are developed for the true hoop stress as a function of temperature (T) [20], and they are consistently implemented in FRAPTRAN and compared with the true hoop stress (2.17) to check for failure.

$$\sigma_{\theta\,\text{burst}}(T) = k \times e^{-qT} \quad (2.16)$$

Table 13 Coefficients of IRSN true hoop stress limit correlations

Coefficients \ Stress limit	$\sigma_{\min}$	$\sigma_{\max}$	σ_{BE}
K(MPa)	11015.44	75541.69	9080.44
$q(^{\circ}\mathrm{C}^{-1})$	0.007472	0.007022	0.005817

FRAPTRAN calculates the true hoop stress in BALON2 model based on the perturbation theory [11]

$$\sigma_{\theta\theta} = \frac{P_i - P_o}{t_{\text{ave}}} r_{\text{ave}} - \frac{P_i + P_o}{2} - r_{\text{ave}} \frac{(P_i - P_o)}{t_{\text{ave}}^2} h_\delta + \frac{\sigma_{zz}}{(e^{\varepsilon_z})^2} r_{\text{ave}} \frac{\partial^2 \delta}{\partial z_o^2} \quad (2.17)$$

P_i is the inner pressure, $P_o$is outside pressure, σ_{zz} is the axial component of stress, r_{ave} is average radius.
$h_\delta = (t - t_{\text{ave}})$ is local perturbation of the cladding wall thickness (wall thickness - average wall thickness).
e^{ε_z} is the exponent of the average true axial strain component of the cylinder.
$\frac{\partial^2 \delta}{\partial z_o^2}$ is the term which describes the axial propagation of ballooned regions.

Full description of the derivation of equation(2.17) can be found in [22].

Burst temperature limit:

A new burst criterion based on temperature limit has been proposed by [23]

$$T_{burst} = 1385\sigma^{-0.129} - 0.0057H^{1.49} + 1.845R - 29 \quad (2.18)$$

T_{burst} is temperature [$^{\circ}C$], σ is stress [MPa], H is hydrogen content [wppm], and R is the heating rate [$^{\circ}C$/s]

The cladding stress σ is obtained from the burst pressure as follows:

$$\sigma = (d/2t)\Delta P \quad (2.19)$$

σ is the hoop stress, d is the undeformed cladding mid-wall diameter, t is the undeformed cladding thickness, and ΔP is the differential pressure across the cladding wall at the time of rupture.
The temperature limit has been implemented in the BALON2 model and the code was modified to predict failure if the local cladding temperature in the ballooning node exceeds this temperature limit. Note that the hydrogen pick-up is calculated by FRAPCON during the irradiation base. This value is then passed to FRAPTRAN from the restart file.

Rosinger optimised stress limit SSM 2021:

The latest optimised Rosinger stress limit (2.20) used in Quantum Technologies FRAPTRAN version was published in a report by the Swedish Radiation Safety Authority SSM [24]. The limit is only relevant for generic zircaloy (Zy-4 and Zy-2), it is not applicable to Zr-1%Nb cladding type. It takes into account the embrittlement effect and has been calibrated as a function of temperature (T) and excess oxygen in the cladding metal (x_{Met}). This correlation was successfully implemented and tested with few validation cases (Zy-4 and Zy-2) only with Rosinger 1984 plastic deformation model.

$$\sigma_{burst} = A_b e^{-B_b T} e^{-\left(\frac{x_{Met}}{C_b}\right)^2} \quad (2.20)$$

x_{Met} = average oxygen concentration excluding oxide layer – average oxygen concentration of as-received cladding (kg oxygen/kg zircaloy).

Table 14 Coefficients for Rosinger optimised stress limit corelation

Temperature region (K)	$A_b(Pa)$	$B_b\ (K^{-1})$	C_b (-)
873 to 1075	7.3757×10^{10}	5.9298×10^{-3}	5.888×10^{-4}
1075 to 1250	5.1513×10^{12}	9.8798×10^{-3}	5.888×10^{-4}
1250 to 1873	2.3301×10^{7}	3.4814×10^{-5}	5.888×10^{-4}

FRAPTRAN 1.4 contains both the Cathcart-Pawel 1979 (C-P) and Baker-Just 1962 (B-J) oxidation models [14]. Cathcart-Pawel correlations implemented in FRAPTRAN provide the oxygen concentration in the metal. Calculations carried out by *metweb* subroutine for Baker-Just are based on the assumption that there is no oxygen diffusion into the metal. Therefore, C-P should be the standard oxidation model when selecting Rosinger optimised stress limit.

The oxygen weight fraction in the alpha phase is assumed constant at 0.047 and no calculation is necessary for this parameter, It is simply listed in the code. For the beta layer, diffusion of oxygen into the region does not begin until the temperature is greater than 1239 K. Detailed description of the correlations used to calculate the oxygen concentration in the cladding metal by *cobild* subroutine is provided in section 4.15.1.2 of the MATPRO [12].

It should be noted that the Cathcart model predicts the oxygen uptake a lot faster than the oxidation model (Leistikow and Schanz, 1987) used in developing the criteria, this will overpredict the embrittlement effect in the oxygen.

Forgeron et al. 2000 stress limit:

Forgeron et al 2000 correlation (2.21) has been obtained from fitting to burst stress data for M5 cladding type [25].

$$\sigma_{burst} = A_b e^{-B_b T} e^{-\left(\frac{x_{\text{Tot}}}{0.00095}\right)^2} \qquad (2.21)$$

x_{Tot} is the weight fraction of the total oxygen uptake in high temperature metal-water reactions

Table 15 Coefficients for Forgeron et al. 2004 stress limit corelation

Temperature region (K)	A_b (Pa)	$B_b\ (K^{-1})$
< 1084	7.464×10^{10}	6.260×10^{-3}
1084 to 1191	4.940×10^{13}	1.225×10^{-2}
>1191	2.213×10^{8}	1.909×10^{-3}

ENEA-JRC contribution

TRANSURANUS, thanks to its clearly defined mechanical and mathematical structure, has been developed and extended aiming at proposing a versatile tool capable of tackling all the conditions considered in licensing procedures [26] [27]. In this view, significant efforts have been devoted to make the code applicable to LOCA transients. In this domain noticeable advances have been achieved in the models for cladding ballooning [28] [29] and cladding-steam reaction [30] [36]. In parallel, the number of cladding materials that can be used in

TRANSURANUS calculations has been extended with E110 [30] and Zr-1%NbO (M5™) alloys [37]. The crystallographic phase transition and high temperature creep play a relevant role for LOCA simulations. Code correlations of Zircaloy-4 have been updated to consider hydrogen concentrations up to 1000 ppm[2] and heating\cooling rates with absolute values up to 100 K/s [38] [39][40].

In the frame of R2CA, ENEA, in strict coordination with JRC, has performed a review on M5™ [40][41]. Results of this review have suggested to consider in more detail the model published by Massih and Jernkvist (model B) for the crystallographic phase transition [41] and a combination of Kaddour's and Massih's models for the high temperature creep [42] [43]. These models have been implemented in the TRANSURANUS subroutines for verification by means of a standalone program. Additional considerations on Zircaloy-4 crystallographic phase transition have permitted to propose a preliminary modelling. Results of this activity have been presented at the NENE2022 conference [44]. These models will be tested against current TRANSURANUS modelling of LOCA transients.

Crystallographic phase transition of M5™

M5™ is a Zr-Nb alloy devoid of Sn with a controlled O, Fe and S content; see Table 16 . M5™ is characterized by a homogeneous dispersion of β-Nb precipitates in fully recrystallized microstructure which enhances creep resistance [22]. The absence of Sn, the controlled alloy chemistry, and optimized heat treatment lead to a very high corrosion resistance and better mechanical properties in high burnup and high dose irradiations [45]. In the temperature domain of LOCA transients (600–1200 °C) crystals of zirconium-based alloys undergo a transition from a hexagonal close-packed (hcp) to a body centered-cubic (bcc) structure of the lattice. Phase transition is affected by hydrogen concentration and heating\cooling rate of thermal transients [38][46].

Table 16: Nominal composition of M5™ alloy (wt.%) [46]

	Sn	Nb	O	Fe	Cr	Ni	Zr
M5™	-	1.0	0.125	-	-	-	balance

The model selected for the crystallographic transition of M5™ has been published by Massih and Jernkvist [40][41]. The β phase fractional volume y is calculated by means of Eq. 1.

$$\frac{\mathrm{dy}}{\mathrm{dt}} = \frac{1}{\tau(\mathrm{T})}\left[\left(\mathrm{y}_{eq}(\mathrm{T}) - \mathrm{y}\right) \pm \frac{\mathrm{b}}{\mathrm{y}_{eq}(\mathrm{T})}\left(\mathrm{y}_{eq}(\mathrm{T}) - \mathrm{y}\right)^2\right] \quad (1)$$

Rate of β phase fractional volume is proportional to the deviation from equilibrium (y_{eq}) according to $\frac{1}{\tau(\mathrm{T})}$ where $\tau(\mathrm{T})$ in the characteristic time that is presented in Eq. 2.

$$\tau(T) = B \exp\left(\frac{E}{T}\right) \quad (2)$$

In Eq. 1 the plus sign is used for the description of heating transients while the minus sign is used for cooling transients. Authors introduced in this model an additional parameter b and a condition on the characteristic time $\tau(T)$: during cooling its value should not be higher than 6 s. This limit has been imposed to prevent that at the end of cooling calculations predict the presence of a significant fraction of β phase instead of a fully α phase [41]. The equilibrium phase transition of M5™ is shown in Eq. 3.

$$\mathrm{y}_{eq} = \frac{1}{2}\left[1 + \tanh\left(\frac{\mathrm{T} - \mathrm{T}_{cen}}{\mathrm{T}_{span}}\right)\right] \quad (3)$$

[2] The unit of measure *ppm* stands for *wt.ppm* throughout this part of the report.

The fractional volume of β phase y_{eq} depends on T_{cen} and T_{span}. The first one is the middle temperature of the two-phase domain while the second one gives an indication on the width of this temperature domain; see Eq. 4.

$$T_{cen} = \frac{T_\alpha + T_\beta}{2}; \quad T_{span} = \frac{T_\beta - T_{cen}}{2.3} \tag{4}$$

Values proposed by authors for M5™ are: E = 54000 K, b = 0.3, $B = 1.55\ 10^{-19}$ s [11]. T_α and T_β are 1016 K and 1240 K, respectively. The model of M5™ doesn't account for the effect of hydrogen concentration. Based on the experimental findings, we assume that the effect of hydrogen on M5™ phase transition is consistent with the effect measured on Zircaloy-4 [38]. In our modelling the transition temperatures T_α and T_β are diminished by hydrogen concentration according to the coefficients of Zircaloy-4 [41]. Expressing the concentration of hydrogen in ppm, T_α is diminished by $1.52\ 10^{-1}$ K per ppm and T_β by $2.20\ 10^{-2}$ K per ppm. Under transient conditions the concentration of hydrogen affects the phase transition of Zircaloy-4 by means of a factor that modifies the characteristic time [41]. This approach has been replicated for M5™ by using a value of 5300 K for the coefficient in the exponential function; see Eq. 5. This parameter is set to 5000 K in the case of Zircaloy-4 [41]. In the same way, coefficient B of Eq. 2 has been tuned to achieve phase transition curves that are consistent with the curves obtained for Zircaloy-4 at the same conditions of heating rate and hydrogen concentration [46].

$$\tau(T) = \frac{B \exp\left(\frac{E}{T}\right)}{1 - 0.0003\bar{x}_H\left(1 - \exp\left(\frac{5300}{T}\right)\right)} \tag{5}$$

Authors do not clearly state if this factor is to be applied during cooling transients . Concerning Zircaloy-4, they do not present calculations on the effect of hydrogen during cooling where experimental measurements are lacking.

High temperature creep of M5™

The model proposed for M5™ is based on the correlation developed by Kaddour et al. that is presented in Eq. 6 [42].

$$\dot{\varepsilon} = \frac{A}{T}\sigma^n exp\left(-\frac{E}{RT}\right) \tag{6}$$

This correlation is applied in our proposal in the α and β single-phase domains as well as in the (α+β) two-phase domain for values of effective stress higher than 5 MPa. The experimental findings indicate that in the α phase, besides dislocation, a diffusion mechanism contributes to creep rate. The diffusion mechanism is dominant if values of stress are lower than 15 MPa, whereas above this threshold the creep strain rate is ruled by the dislocation mechanism. In the β phase the creep rate is described by a dislocation mechanism. Values of the pre-exponential constants, activation energies and stress exponents can be found in the original paper [42]. Concerning the (α+β) domain, a linear combination of single-phase creep rates is applied if values of stress are higher than 5 MPa; see Eq. 7.

$$\dot{\varepsilon}^{\alpha+\beta} = (1-y)\dot{\varepsilon}^{\alpha} + y\dot{\varepsilon}^{\beta} \tag{7}$$

Below this value of stress the creep rate is determined according to the model published by Massih [43]. This model is based on the theoretical approach to the superplasticity of zirconium alloys published by Ashby and Verrall [47]. Two mechanisms are used to describe the behaviour of M5™ creep rate in the two-phase domain: diffusion and dislocation. At high values of stress the diffusion mechanism is substituted by the dislocation one. In an intermediate region these two processes are superimposed and act independently (superplasticity). Correlations are given in Eq. 8 (diffusion term) and in Eq. 9 (dislocation term).

$$\dot{\varepsilon}_{diff}^{\alpha+\beta} = C_a\tilde{\sigma}\frac{\Omega\bar{D}_V}{k_B T d^2}\left(1 + \frac{\theta\delta\bar{D}_S}{d\bar{D}_V}\right) \tag{8}$$

In Eq. 8 C_a and θ are geometrical constants, Ω the atomic volume, d the grain size, $\overline{D}_V$ the average bulk diffusion coefficient, $\overline{D}_S$ the average grain boundary surface diffusion coefficient, δ the thickness of the grain boundary, and $\tilde{\sigma}$ is the effective stress.

$$\dot{\varepsilon}_{disl}^{\alpha+\beta} = \frac{1}{k_B T}\left(\frac{b}{d}\right)^{p} exp\left(-\frac{Q_d}{RT}\right)\left[A_\alpha \mu_\alpha \left(\frac{\sigma}{\mu_\alpha}\right)^{n_\alpha}(1-y) + A_\beta \mu_\beta \left(\frac{\sigma}{\mu_\beta}\right)^{n_\beta} y\right] \quad (9)$$

In Eq. 9 $A_{\alpha/\beta}$ is a material-dependent (dimensionless) constant in the *α/β* phase, $\mu_{\alpha/\beta}$ the shear modulus in the *α/β* phase, b the magnitude of the Burgers' vector, p an empirical inverse grain size exponent, and Q_d the activation energy for dislocation creep. Parameters of this model are p and $n_{\alpha/\beta}$. In their calculations the grain size remains constant with values lying in the interval 5-11 μm [43]. In compliance with this indication, the value of grain size used here is 6 μm. The original models show discontinuities at the boundaries between single-phase and two-phase domains. Concerning the concluding part of the *(α+β)* to *β* transition, Trego showed that in this region a significant increase of grain size occurs leading to a markedly decrease of creep in a narrow temperature interval [48]. Based on this indication, we have identified a small interval of the *β* fractional volume between the two- and single-phase region. In this domain the continuity of creep rate curves has been assured by construction with a linear combination of the values at the boundaries. An identical approach has been used for the transition region from *α* to *(α+β)*.

Crystallographic phase transition of Zircaloy-4

Authors have reported that in the case of Zircaloy-4, model B shows deviations from the experimental measurements performed at high heating rates [41]. Aiming at discussing this inaccuracy of model B, we have developed phase transition correlations based on the first-order model proposed by Massih [49]. While most of the original model has been maintained unchanged, we have introduced an additional parameter. This factor is applied under the condition that the beta phase fractional volume is lower than 10%. The use of this factor, having values between 0.0 and 1.0, diminishes the phase transition rate. Above 10% of *β* phase fractional volume this factor is set to 1.0 in order to attain a full phase transition rate. This smooth increase of the transition rate is seen especially at high heating rates (+100 K/s) [50].

Verification of models

Phase transition and high temperature creep correlations presented in previous sections have been introduced in the corresponding subroutines of TRANSURANUS. A standalone program that couples both models has allowed us to perform calculations in the domains of interest concerning heating\cooling rate, hydrogen concentration, effective stress. With regard to the effect of hydrogen, an upper limit of 1000 ppm has been adopted. This value is consistent with the modelling of Zircaloy-4 conditions but much higher than observed at end of M5™ irradiations. Therefore, these calculations are intended mainly for verification purposes of TRANSURANUS subroutines. Some results of our calculations are presented with the objective of considering issues of interest for future development or relevant for the following step of verification. In this second step we plan to perform LOCA calculations with TRANSURANUS. This will be a good opportunity to make a comparison between the predictions of models presented here with the results of existing modelling in TRANSURANUS.

Crystallographic phase transition of Zircaloy-4 and M5™

Phase transition correlations (model B) of Zircaloy-4 and M5™ have been compared at increasing values of heating\cooling rate neglecting the effect of hydrogen. Results are presented in Figure 23. They confirm that the lower diffusion of niobium induces a delay of M5™ phase transition. Results at +10 K/s are quite consistent. A small delay of M5™ is noticed at +100 K/s [46].

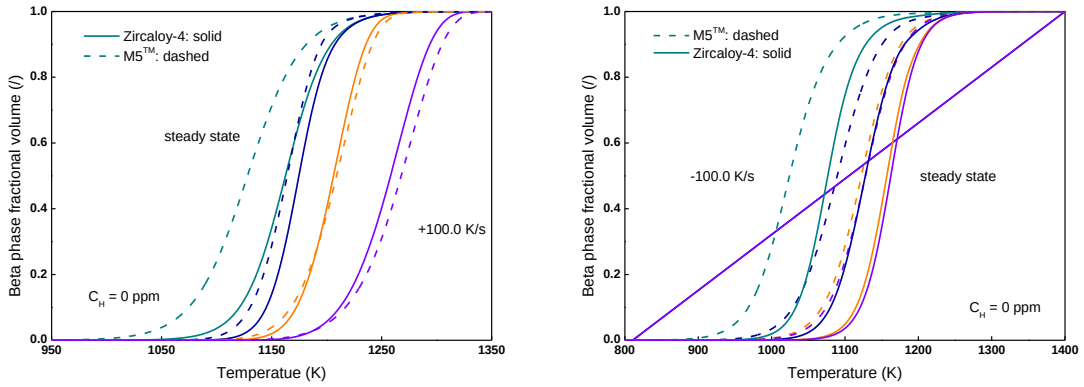

Figure 23: Zircaloy-4 and M5™ phase transition at 0, +1, +10, +100 K/s (left) and 0, -1, -10, -100 K/s (right)

Hydrogen pick-up is much more intense in Zircaloy4 than M5™. Figure 24 presents the phase transition curves of Zircaloy-4 if a concentration of 1000 ppm is assumed. According to the authors, the effect of hydrogen has been determined by using an expression that modifies the characteristic time as shown in Eq. 5 [41]. Results of Zircaloy-4 during cooling transients have been obtained taking into account only the effect of hydrogen on the transition temperatures that has been determined under quasi-equilibrium conditions. Due to the fast desorption of hydrogen at temperatures above the β transition temperature, it was not possible to perform the study of the inverse phase transformation kinetics upon cooling [38]. The use for Zircaloy-4 of the characteristic time as in Eq. 5 has shown that results obtained during cooling were loosely correlated with a possible effect of hydrogen (not shown). Based on these considerations, it has been decided to neglect this factor during cooling transients where, as above mentioned, the effect of hydrogen is not well established.

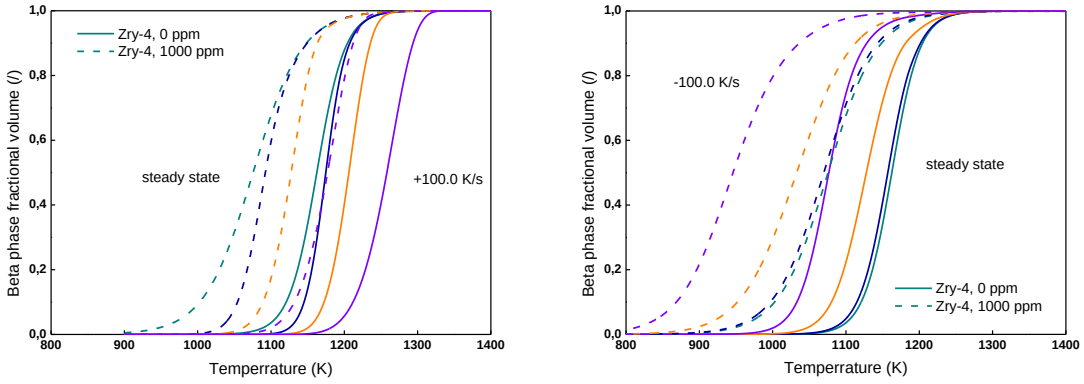

Figure 24 : Zircaloy-4 phase transition at 0, +1, +10, +100 K/s (left) and 0, -1, -10, -100 K/s (right); effect of hydrogen concentration (1000 ppm)

Effect of hydrogen concentration on M5™ phase transition

As shown in Figure 24, the effect of hydrogen is of great importance for Zircaloy-4 phase transition. The use of M5™ is quite beneficial from this point of view as much lower concentrations of hydrogen are expected [45]. Nevertheless, the effect of hydrogen on M5™ is of interest to make the code capable of estimating its effect and of treating an ample domain of conditions. The duty in charge of ENEA and JRC within Task 3.2 is to provide an updated model\subroutine for M5™ that could cope with domains of applicability comparable with the existing TRANSURANUS model for Zircaloy-4 [9]. A comparison of the model of M5™ [41] with the modified one assuming

increasing concentrations of hydrogen is presented in Figure 25. The interval of concentrations considered in the comparison ranges from 0 ppm up to 500 ppm.

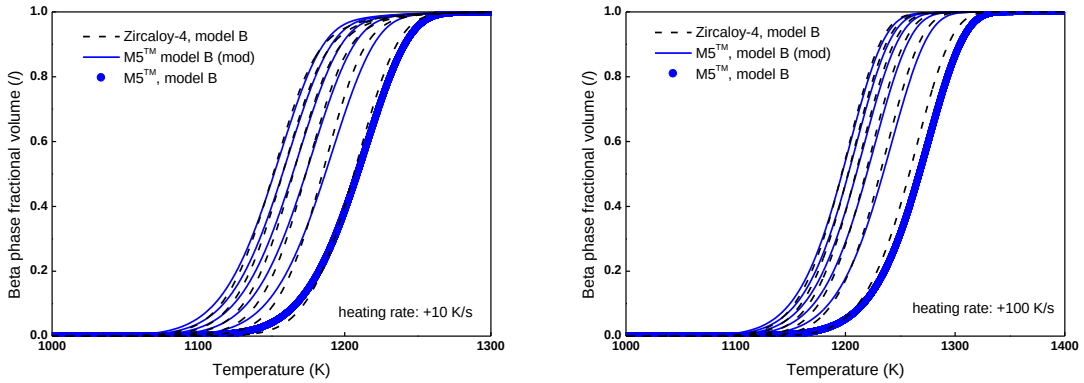

Figure 25 : Phase transition with concentrations of hydrogen in the interval 0-500 ppm (every 100 ppm): comparison of models at +10 K/s (left) and +100 K/s (right) [41]

Values of hydrogen concentration representative of the operating conditions and burn-ups typical of M5™ irradiations lie in the interval 60-100 ppm. In agreement with the findings presented in [38], our results confirm that predictions of the model proposed for M5™ are quite consistent with Zircaloy-4.

Creep rate of M5™ in the (α+β) region

Literature has underlined that modelling of M5™ creep rate is not well established in the (*α+β*) region [42]. Results of the model proposed here are presented in Figure 26. In this figure the creep rate of M5™ has been calculated as a function of temperature under two heating rate conditions: +10 and +100 K/s. Values of stress employed in calculations are 3 MPa, 10 MPa, 20 MPa, and 30 MPa. The first value lies in the stress domain where it has been assumed that Massih's model is applied [43]. Results have been obtained by assuming a constant grain size (6 µm). Transition regions from Kaddour's to Massih's model and back from Massih's to Kaddour's model across the (*α+β*) region have been tentatively imposed. Under these conditions our results show a peak of creep rate at 3 MPa that tends to shift toward higher temperatures and to increase with increasing heating rate. Calculations are consistent with predictions presented in the literature [42][43].

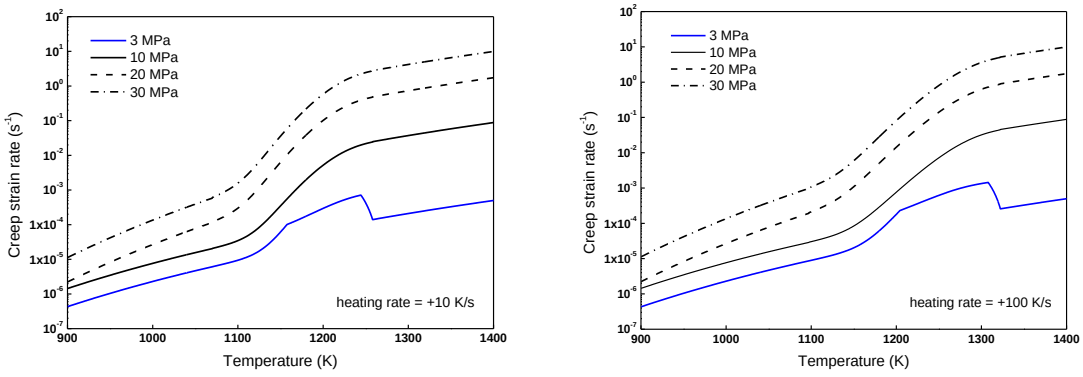

Figure 26 : Creep rate of M5™ as a function of temperature and heating rate: +10 K/s (left) and +100 K/s (right)

Preliminary model for phase transition of Zircaloy-4

In this section we discuss a comparison of predictions obtained with two different models of Zircaloy-4 phase transition: model B [41] and model A [49]. Correlations of model A have been partly modified on purpose. As stated by authors, model B shows deviations from the experimental results at high heating rates [41][50]. Results of models at +5, +10, +50, and +100 K/s are presented in Figure 27. Model A shows reasonable agreement with model B at low values of heating rate and a more satisfactory agreement with the experimental results at +100 K/s [50]. While great part of model's correlations [49] has not been modified, a tuning factor of absolute value lower than 1.0 has been applied to the rate of phase transition when the β fractional volume is lower than 10%. This proposal relies on the hypothesis that the full rate of phase transition is attained in the region above 10% of beta fractional volume. This hypothesis has been confirmed especially at high heating rates in [50], moreover, uncertainties affecting beta volume measurements are higher below 10% [38] [46]. In principle, this tuning factor could improve accuracy of phase transition predictions especially at high heating rates where model B tends to underestimate the experimental measurements [38][50].

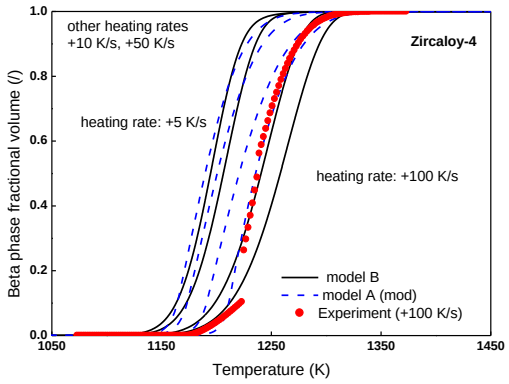

Figure 27 : Phase transition of Zircaloy-4: comparison of model B and model A (mod.) with experimental measurements [50]

Conclusions

This section of the report presents some results of the activity performed by ENEA in strict coordination with JRC within Task 3.2 of R2CA. Our contribution has been focused on the identification of correlations for the crystallographic phase transition and high-temperature creep of M5™ that could update and eventually improve the existing models of TRANSURANUS. The initial review has identified some models fitting for our purpose. They have been presented here and results of corresponding TRANSURANUS subroutines discussed. If on the one hand, it has been confirmed that predictions are consistent with the literature, on the other hand, relevant aspects are still not well established such as the effect of hydrogen during cooling transients and creep rate across the phase transition of M5™. In this view, our proposal tends to be conservative with regard to the effect of hydrogen (no modelling during cooling transients) while it has been attempted to model the creep rate in the two-phase domain. Besides this, preliminary indications on a novel phase transition model for Zircaloy-4 have been proposed in the concluding part of this section. In principle, this model could improve accuracy of predictions at high heating rates where model B showed to be less precise. In conclusion, this stage of verification has given positive indications addressing several aspects of modelling relevant for TRANSURANUS. In the following step these models will be compared to the existing modelling by performing code calculations on LOCA experimental tests. It is expected that this future activity could provide recommendations useful to the community of TRANSURANUS users.

Code validation tests with new thermomechanical models

IRSN contribution: test of the criterion on DRACCAR validation tests

In order to test the developed criterion on engineering stress, the DRACCAR code developed at IRSN has been used on tests not used in the validation data base. This study was performed on 125 LOCA relevant transients. First the new criterion was tested on EDGAR temperature ramp tests (0.1-100°C/s), performed on Zy-4 cladding directly heated by Joule effect. Results are illustrated in Figure 28. The two burst criteria lead to predictions within ±10% of experimental burst temperature. However, the R2CA burst criteria leads to best estimate predictions whereas the true stress burst criteria generally overestimates burst temperature. The mean absolute errors are similar, 29°C for R2CA criteria and 32°C for the DRACCAR true stress criteria.

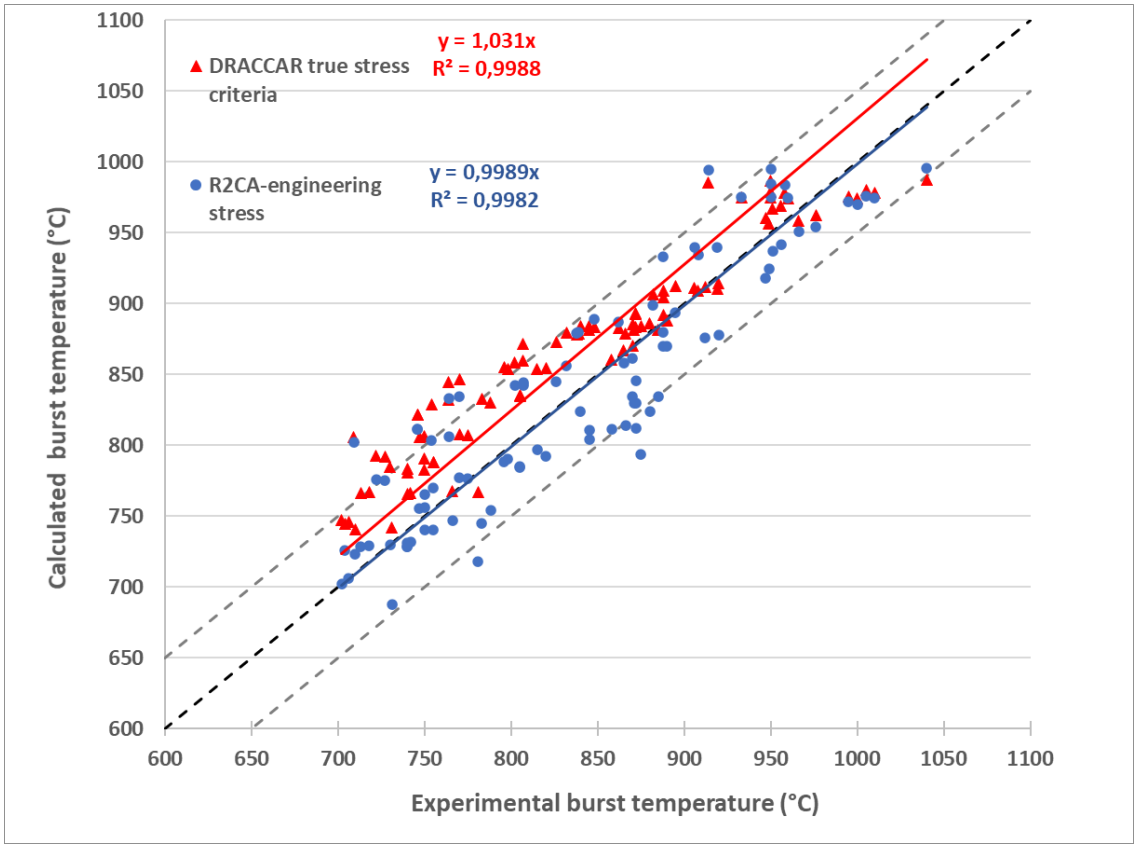

Figure 28: Calculated burst temperature versus experimental temperature on EDGAR test on Zry-4 with DRACCAR true stress criteria and R2CA Engineering burst criteria and linear fitting (y=ax). Dotted lines correspond to ±10%.

Then Halden LOCA tests were calculated with the new criterion and DRACCAR reference criteria (which depends on the cladding alloy), results are gathered in Figure 29. Both criteria lead to a wrong prediction of burst occurrence for one test. The R2CA criteria leads to better predictions but with some underprediction of burst temperature up to 100°C. DRACCAR reference criteria tend to overestimate burst temperatures.

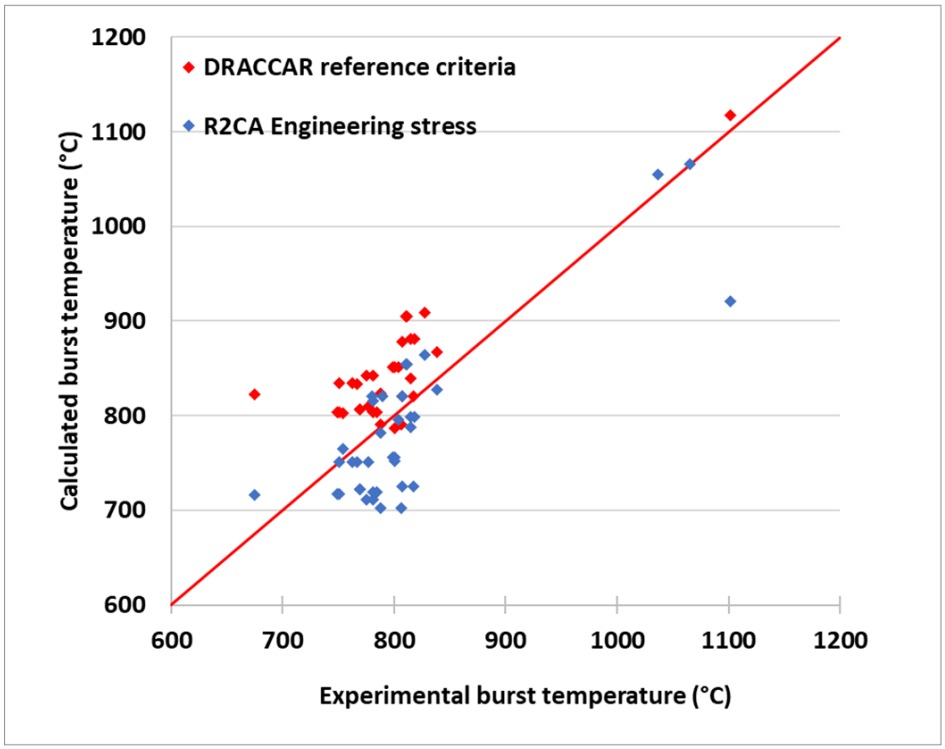

Test	Burst	DRACCAR	R2CA
IFA650-2	Yes	Yes	Yes
IFA650-3	Yes	Yes	Yes
IFA650-4	Yes	Yes	Yes
IFA650-5	Yes	Yes	Yes
IFA650-6	Yes	Yes	Yes
IFA650-7	Yes	Yes	Yes
IFA650-9	Yes	Yes	Yes
IFA650-10	Yes	Yes	Yes
IFA650-11	Yes	Yes	Yes
IFA650-12	Yes	No	Yes
IFA650-13	Yes	Yes	Yes
IFA650-14	No	No	Yes
IFA650-15	Yes	Yes	Yes
IFA650-16	Yes	Yes	Yes

Figure 29: Calculated versus experimental burst temperatures for Halden LOCA tests with DRACCAR reference criteria and R2CA Engineering burst criteria.

Finally, the SCIP III LOCA tests were recalculated, calculated temperatures are given in Figure 30. Both criteria tend to overpredict burst temperature and the R2CA burst criterion leads to far better burst temperature prediction. However, R2CA burst criterion led to burst occurrence for two tests whereas no burst was observed experimentally (low peak cladding temperature or low internal pressure) and DRACCAR reference criteria missed one burst occurrence (low internal pressure).

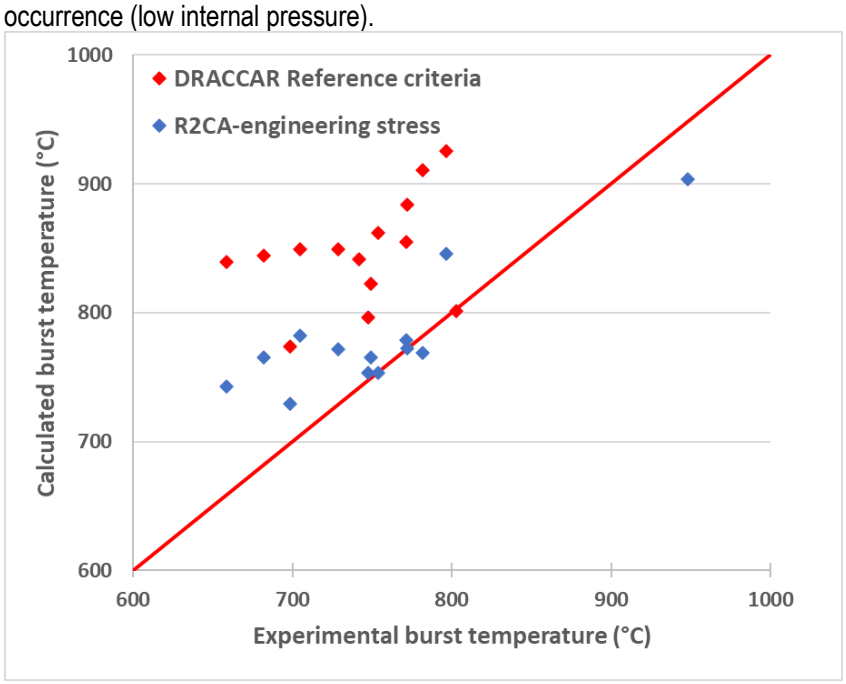

Figure 30: Calculated versus experimental burst temperatures for SCIP III LOCA tests with DRACCAR reference criteria and R2CA Engineering burst criteria

To conclude on DRACCAR simulations versus experimental results, R2CA criterion based on engineering stress allows a better evaluation of burst temperatures than reference criteria used in the DRACCAR validation tests. For studied cases, the use of the R2CA criterion led to 3 burst occurrences not experimentally observed (over 125 tests), whereas the use of DRACCAR reference criteria led to miss two burst predictions. Therefore, the use of the R2CA burst stress limit based on engineering stress leads to the best burst temperature evaluations for the cases considered in this study. However, burst criteria based on engineering stress are not well-suited to predict burst cladding strain as illustrated in Figure 31. Indeed, for most of the cases calculated strain is significantly underpredicted with the R2CA criteria.

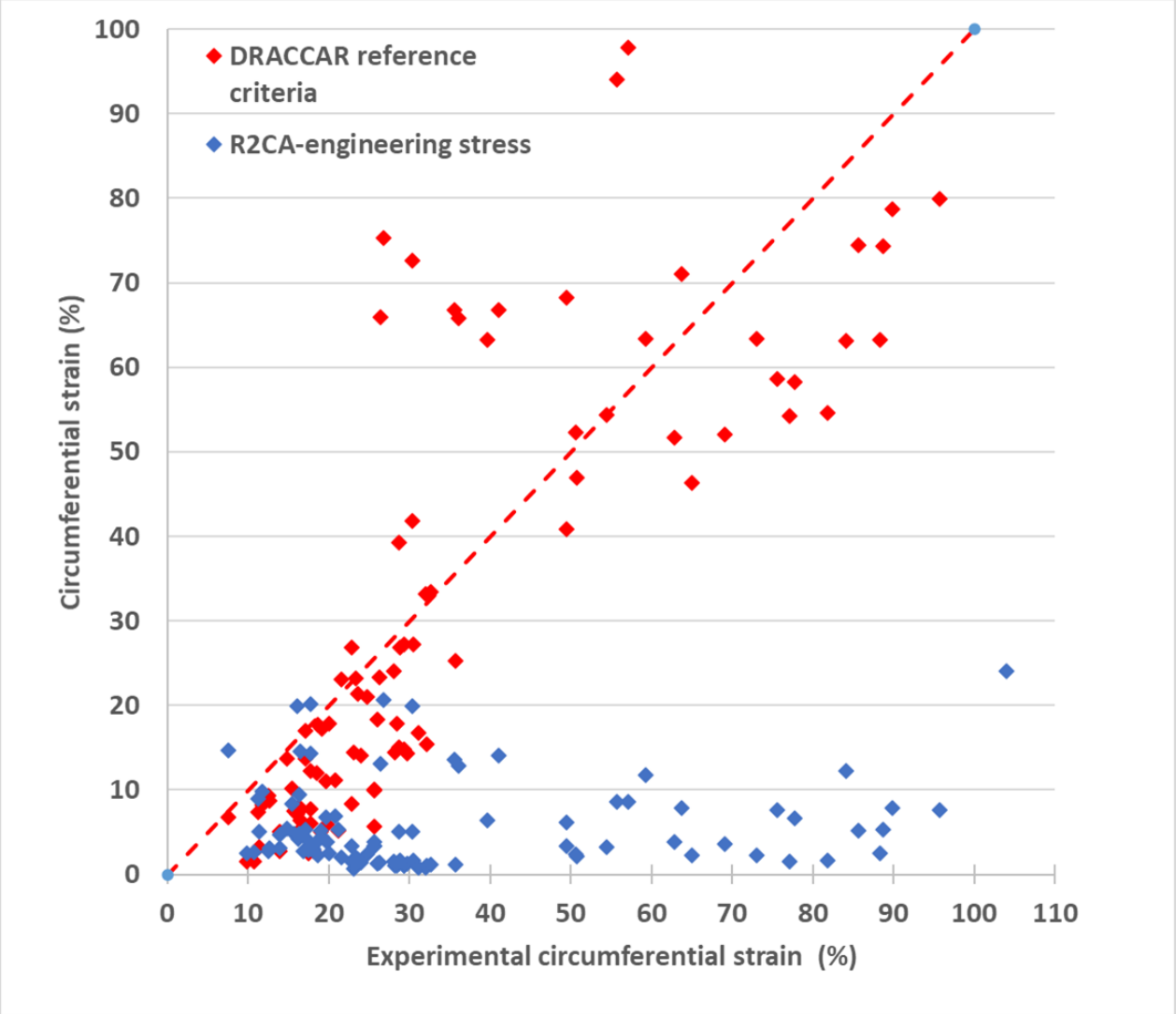

Figure 31: Calculated circumferential strain versus experimental circumferential strain for temperature ramp tests.

Conclusions on burst criteria

During the R2CA project a large burst database was built and used to fit new burst criteria dedicated to the prediction of burst occurrence. During this study, no simple criteria based on burst temperature, strain, engineering or true stress was found to fulfil the two following goals:

- Best-estimate prediction of burst occurrence (time and temperature).
- Best-estimate prediction of burst strain.

This may be due to uncertainties on burst data but is mainly related to the very high variation of strain close to burst and therefore there is a strong dependence of strain estimation to temperature and to the thermo-mechanical laws used to model cladding ballooning.
From the analysis performed, it has been decided to select a temperature limit versus engineering stress and the heating rate as the so-called Chapman criteria. The selected test cases are internally heated and performed with as-received cladding. The proposed criterion does not take into account hydrogen content and is only valid for heating rates between 1 and 38°C/s. Various correlations on hydrogen impact are presented in the document and can be used combined with the proposed limit.
The burst database used in this work is mainly composed of burst occurrences during a temperature ramp. For low heating rates, like a temperature plateau or even slow temperature decrease at reflooding beginning in LOCA transients, the criteria may miss some burst occurrences or even not be applicable. These phenomena have particularly been observed when using true stress criteria. Indeed, in these cases the temperature decreases and the stress limit may increase if the pressure difference is constant or decreasing. Therefore, when using burst criteria based on stress it is recommended to use a strain limit as a safeguard. The strain limit must be chosen consistently with the goal of the study. The NUREG 630 limit can be considered as an upper envelope for flow blockage evaluations (cf. Figure 2). When studying rod fuel failures for radiological consequences evaluations, a fixed strain limit around 20-25% is recommended based on observed circumferential strains (cf. Figure 12).
When dealing with small and intermediate break LOCA scenarios, maximum temperature plateau is often in the burst occurrence temperature range (~700-900°C), whereas for large break LOCA scenarios the maximum plateau was generally significantly higher than the burst occurrence range. Therefore, burst studies based on temperature ramp tests with representatives heating rates and pressure differences are well suited to study burst in large break LOCA conditions but may not be sufficient for small and intermediate breaks. More experimental tests with representative thermomechanical transients are needed to validate creep and burst current models.

VTT contribution : M5 validation case : IFA-650.15

IFA-650.15 is the first LOCA test with M5 cladding material tested in the Halden BWR. The test segment was cut from a PWR UO2-M5 fuel rod (36U-N05) that has been irradiated in the Ringhals 4 PWR NPP for five cycles. The active length of the test segment was 442.5 mm, and the fuel has been irradiated to a burnup of up to 57 MWd/kgOx. The refabricated test segment was pressurized to 4 MPa with a mixture of 95 % argon and 5 % helium. Full description of the experiment is detailed in the Halden report [31].

Base irradiation :

Power history data (Figure 32Figure 33) and fuel rod characteristics are obtained from [32], [33], [31]. The base irradiation was simulated with FRAPCON in two stages:

-In the first step, the whole mother rod (36U-N05) was simulated with FRAPCON VTT 3.5 version which provides the coolant boundary conditions for the elevation corresponding to the tested segment, as well as the pressure conditions at the end of the base irradiation.

-In the second step, only the tested segment is simulated, the boundary conditions from the first step are utilised and the volume plenum in this case is changed until the same pressure at the end of the first step is obtained. The calculation is then continued with the refabrication feature enabled to change the gas composition. The conditioning phase at Halden was also simulated after refabrication. At the end of this step, a restart file is produced which is then used to initialise FRAPTRAN transient calculations.

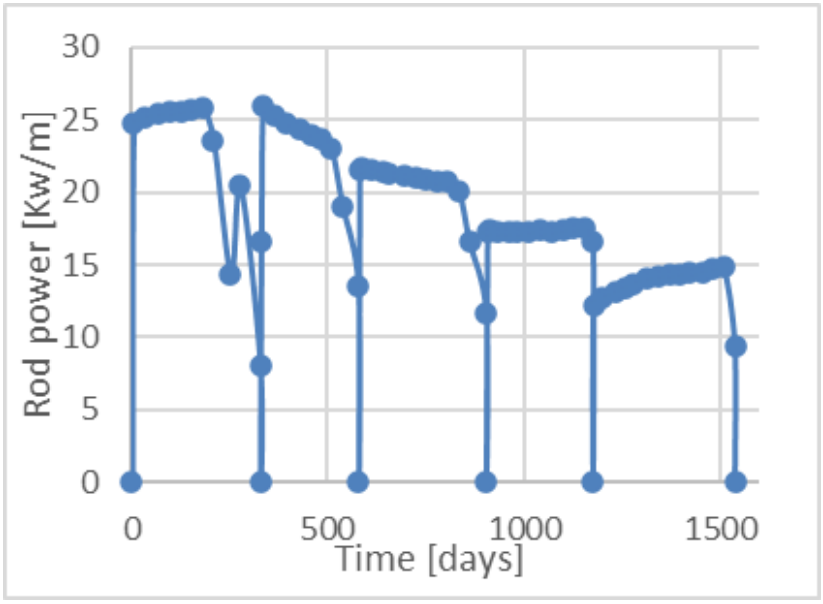

Figure 32 : irradiation power history

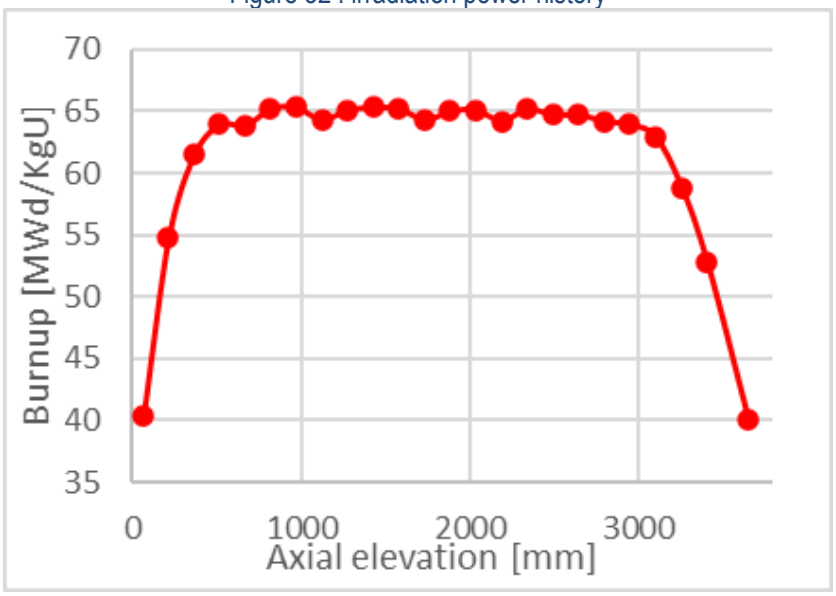

Figure 33 : Axial burnup profile

LOCA transient calculation

IFA-650.15 LOCA transient case was calculated with FRAPTRAN 1.4 version with the restart file from FRAPCON 3.5. The rod mechanical deformation was modelled with FRACAS-I and the updated ballooning model as well as the original BALON2 for comparison.

The same methodology used in modelling previous FRAPTRAN's validation cases from Halden was adopted to generate the input file for IFA 650-15. Simulations were carried out by dividing the cladding into 9 axial nodes and 5 radial nodes, the cladding surface temperature and coolant pressure were provided as boundary conditions. Subchannel thermal-hydraulics code GENFLO was not used in this case; the temperature is imposed on the outside walls of the cladding without clad-to-fluid heat transfer evaluation. Cladding surface temperature was recorded from three thermocouples during the experiment: TCC1 at 100 mm and both TCC2 and TCC3 at 366 mm elevation of the fuel rod from the bottom. The average value from TCC2 and TCC3 was imposed on the

corresponding upper part of the cladding, and values from TCC1 on the lower part of the rod. There are thus two axial zones for cladding temperature in FRAPTRAN input; similar division is used also in original FRAPTRAN validation cases IFA-650.5, -650.6 and -650.7. FRAPTRAN then interpolates to set the cladding outer surface temperature for each axial node.

Two sets of calculations were performed:
In the first run, internal pressure is calculated by FRAPTRAN. In the second run, the experimental rod internal pressure is supplied as an input. In FRAPTRAN it is possible to give the rod internal pressure history as a boundary condition. This can be done in the $model data block by setting “prescri=1” and entering values for the keyword “gasphs”.

- Resulsts & discussion

Overall results:

Overall, selected validation cases from FRAPTRAN integral assessment were recalculated with original and updated deformation models and burst criteria. 8 validation tests were calculated with FRAPTRAN original model and Kaddour et al 2004, each test against 5 different failure criteria: FRAPTRAN original criterion, IRSN BE, IRSN min, IRSN max, T limit (8 x 5 calculations each). Rosinger model on the other hand is not suitable for Zr1%Nb cladding type and therefore only 6 validation cases were tested against 6 different failure criteria (6 x 6 in total), Rosinger optimised limit was added. Detailed results for the calculations are presented in appendix page 203.

The number of total calculations for each creep model along with the number of inaccurately predicted cases are illustrated in Figure 34. False predictions refer to cases where the model falsely predicts burst or when it fails to trigger cladding burst.

FRAPTRAN original is the most conservative deformation model; rod failure was falsely predicted for one test (LOC-11C rod 2) with all 5 burst criteria. Kaddour model had one false occurrence of burst for the same test when selecting IRSN min criterion. Rosinger model, on the other hand, exhibits a more relaxed behaviour, with two false occurrences of burst and two cases where the model fails to predict rod rupture. The two missed burst occurrences went undetected by Rosinger-SSM limit and the original FRAPTRAN criterion. In the case of Rosinger-SSM, this could be attributed to the embrittlement effect by the excess oxygen, as x_{Met} is not calculated in the same way to calibrate the criterion. In addition, whilst C-P model was used in these calculations, a different oxidation model (Leistikow and Schanz 1987) was employed in the original work [24]. Therefore, this criterion is not recommended at this point without further modifications.

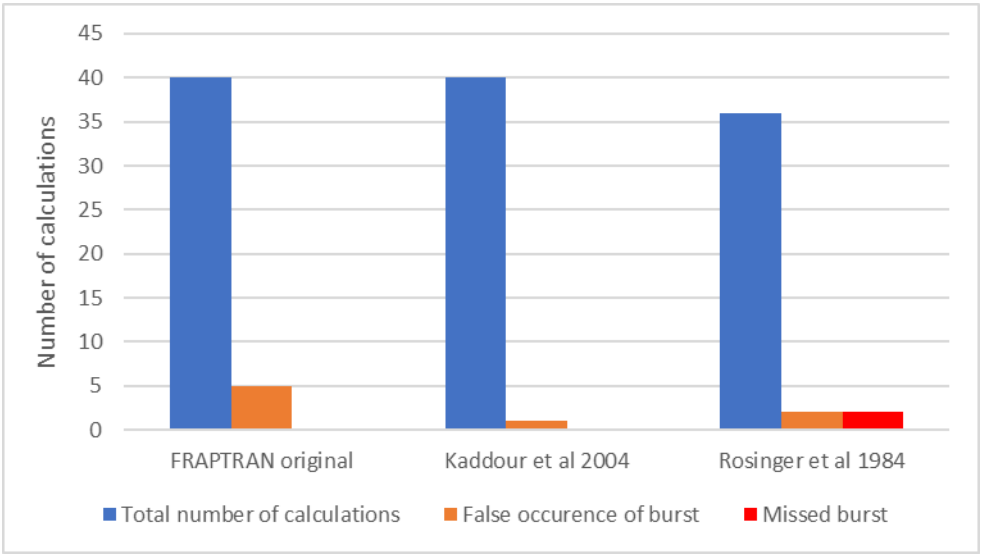

Figure 34 : Overall results of validation cases calculations.

Calculations results for all deformation models and burst criteria are plotted and compared to experimental burst temperature and maximum residual hoop strain in Figure 35 and Figure.36, respectively. FRAPTRAN original plastic model and Kaddour et al. show more conservative predictions in terms of burst temperature. In terms of employed burst criterion, IRSN min is the most conservative stress limit.

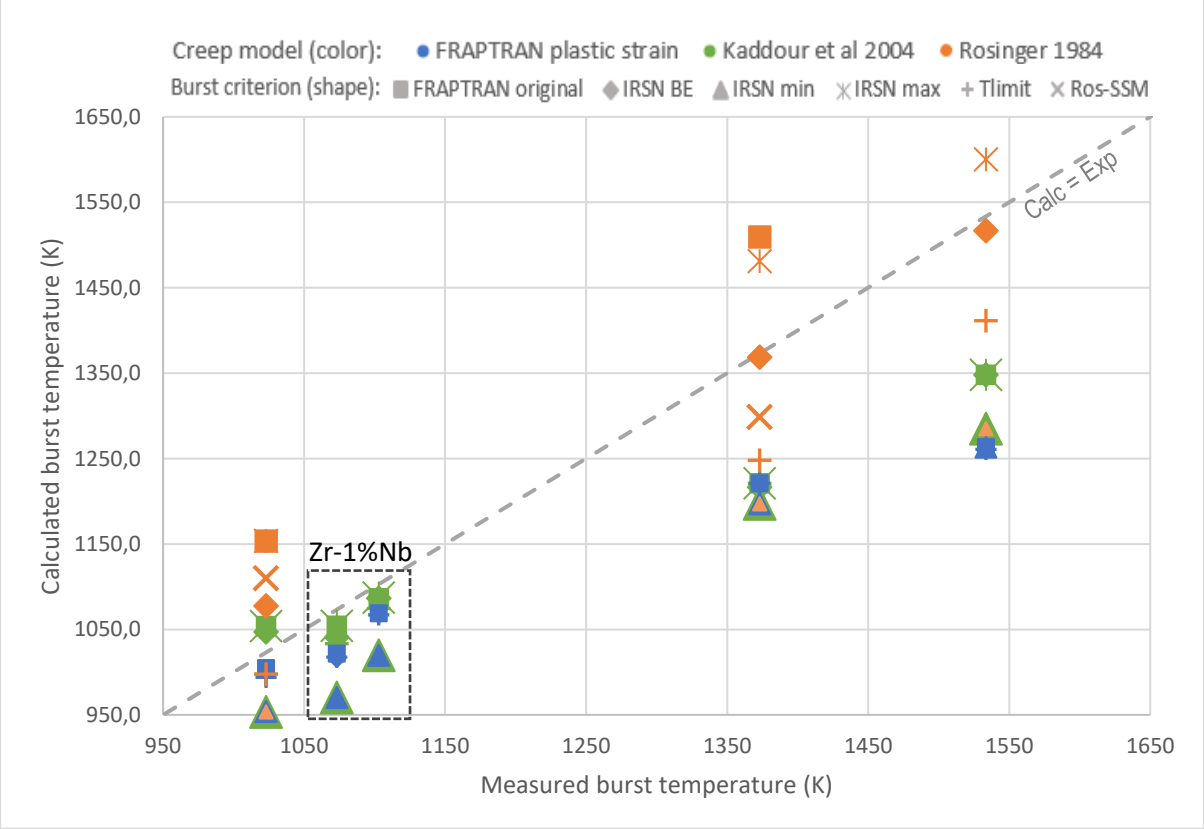

Figure 35 Calculated versus experimental burst temperature for simulated validation cases

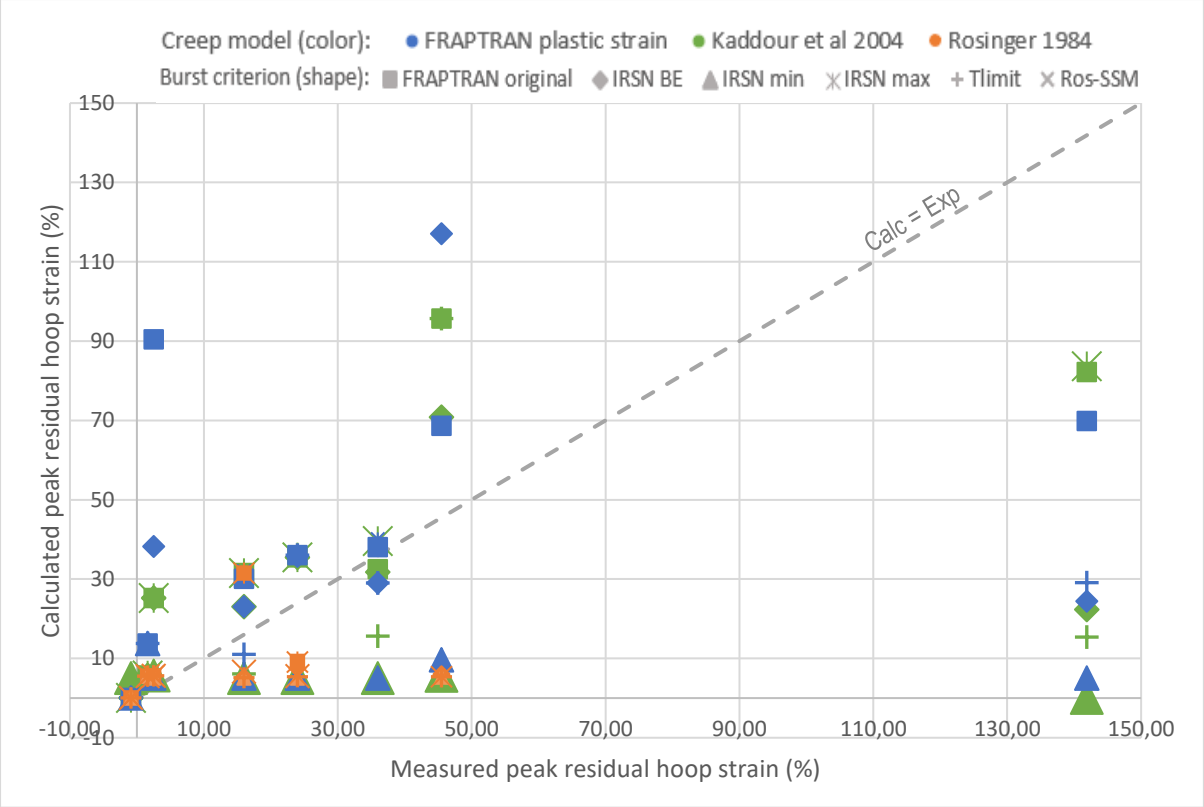

Figure.36 Calculated versus experimental max residual hoop strain for simulated validation cases

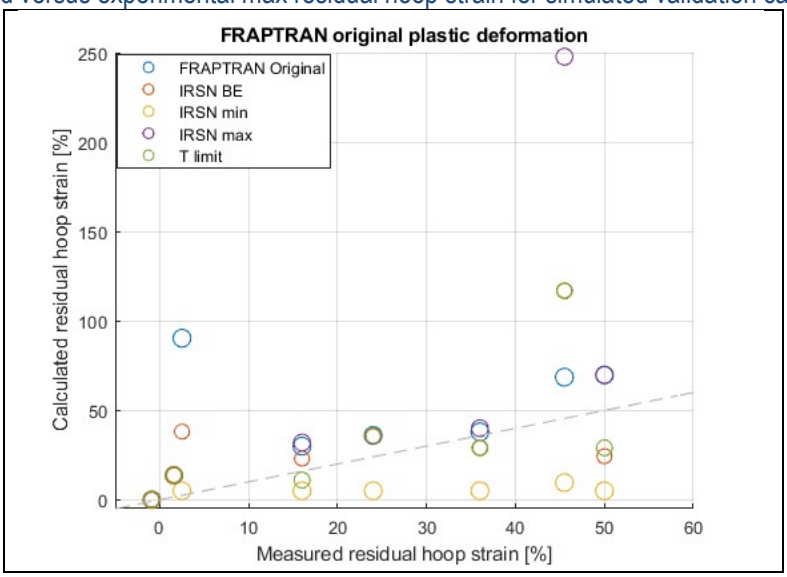

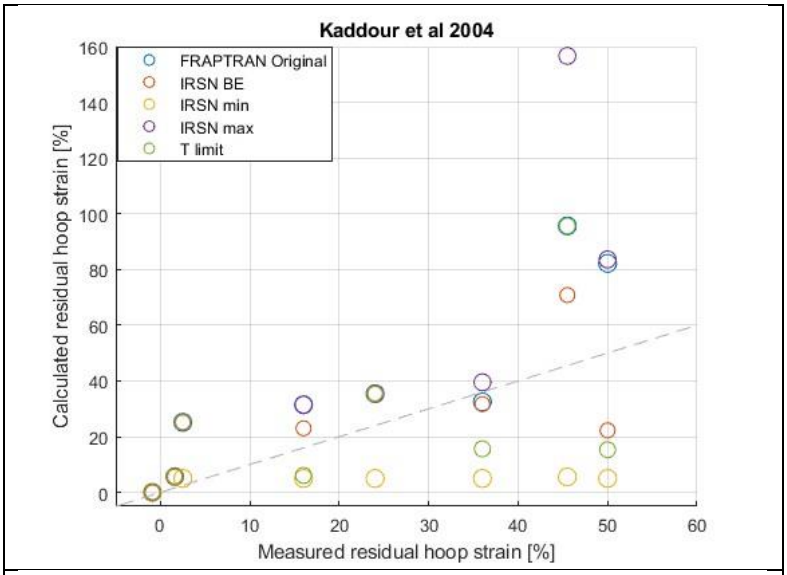

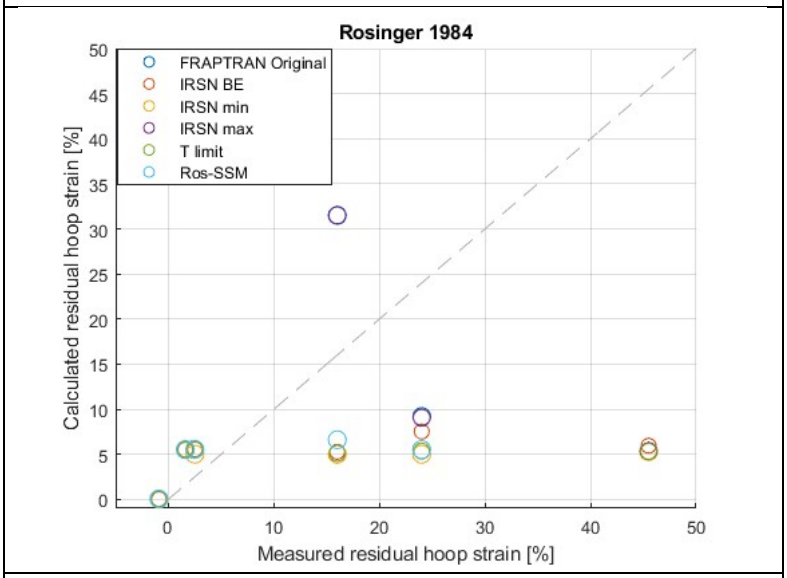

Figure 37 Calculated vs measured residual hoop strain results

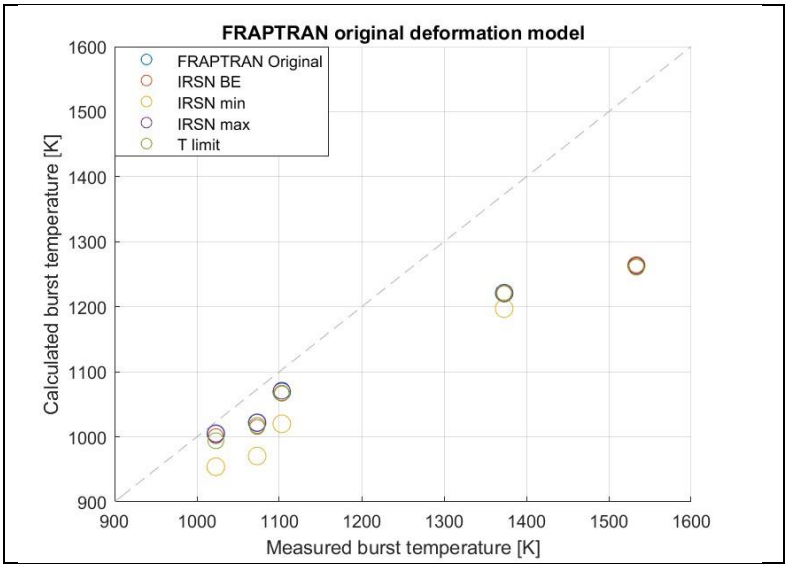

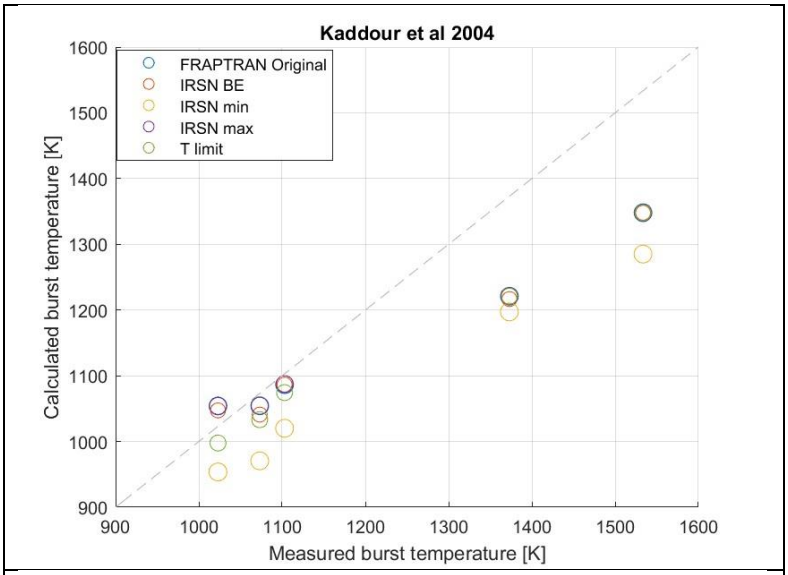

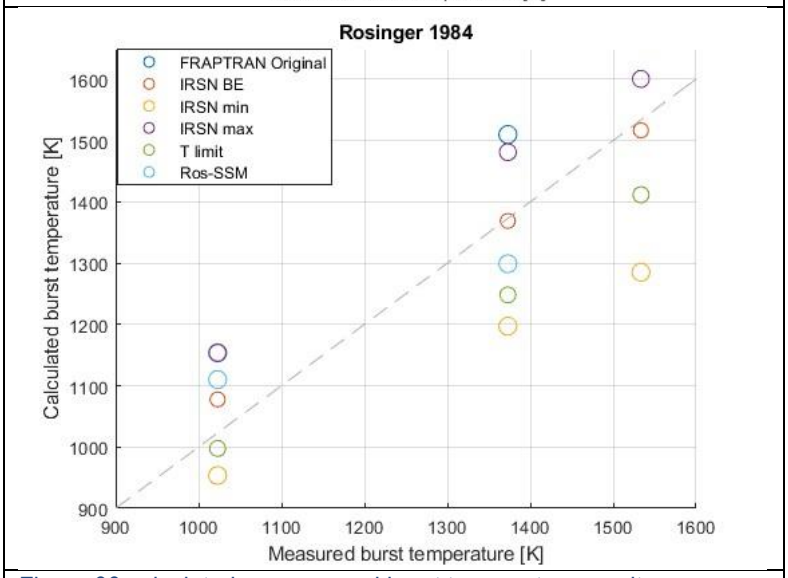

Figure 38 calculated vs measured burst temperature results

Error calculations:

The mean absolute error (MAE) of correctly predicted calculations for each creep model are presented in Figure 39. For time and temperature parameters, error is calculated from correctly predicted burst occurrences. For strain calculations, data include correctly predicted cases of burst and non-burst (LOC-11C rod 3 and LOC-11C rod 1 and 4 did not rupture**)**. The error compares predicted variable to the recorded experimental value. The newly implemented creep models show relatively lower error in terms of predicted burst time, temperature and strain. Although Rosinger creep has the lowest error, the model has less validation cases and therefore more calculations would be required in the future. The methodology used to calculate the overall mean absolute error for each creep deformation model and burst criterion is described in the appendix page 207. It should be noted that in addition to the FRAPTRAN assessment cases, the error estimates also include the IFA-650.15 predictions.

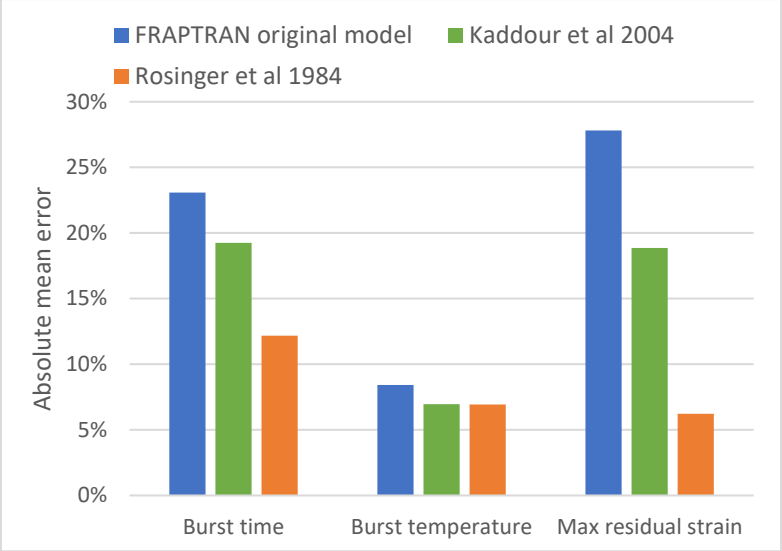

Figure 39 Comparison of absolute mean error for utilised deformation models

Figure 40. illustrates the MAE for each burst criterion from overall correctly predicted burst occurrences across all deformation models. The implemented limits (IRSN BE, IRSN max, and T limit) show comparable results to the original criterion employed in FRAPTRAN in terms of burst time and temperature. IRSN min is the most conservative limit. In terms of strain results, FRAPTRAN original criterion had the least error since it incorporates an additional strain limit to check for failure in parallel with the stress limit (stress+strain). Hence, it is recommended to enable the strain limit in combination with the new implemented criteria as well for better predictions.

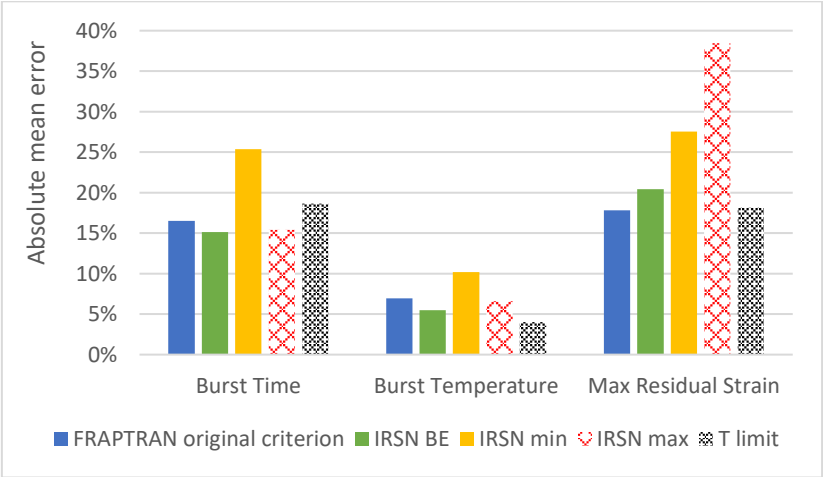

Figure 40 Comparison of absolute mean error for burst criteria

IFA-650 results:

IFA-650.15 transient calculations in Figure D.1 (cf. appendix) are shown for the case where FRAPTRAN calculates the rod internal pressure. FRAPTRAN clearly overpredicts the rod pressure during LOCA as compared to the measured value. The selected default static pressure model assumes that all volumes inside the fuel rod equilibrate in pressure instantaneously [14]. In the Halden test rodlet, however, the free volume of the plenum is significantly larger ($17 cm^3$) than in full length rod and is located outside the heated region. As a result, the pressure increases only slightly during the experiment, which may explain the discrepancy between the calculated and measured results. It should also be noted that the plenum temperature was not provided separately, and thus the default option in FRAPTRAN for plenum gas temperature is applied: it is set equal to local bulk coolant temperature plus 10 °F. Consequently, rod failure is predicted considerably earlier than in the experiment The same pattern can be observed for other Halden validation cases (IFA-650 series) in the integral assessment report [34].

Table 17 summarises initial calculations results with two different deformation models and FRAPTRAN original failure criterion (stress+ limit). Summary of experimental results for IFA-650.15 LOCA test are reported in [32] and [35]. Two different values for the cladding maximum residual hoop strain have been published: 141.89% [32] and 50% [20] [35]. The latter was deemed more consistent with the IFA-650.15 metallography report and is therefore used for the purpose of comparison in this report.

Table 17 IFA-650.15 initial calculations results

Ballooning deformation / Parameter	FRAPTRAN original model	Kaddour et al 2004	Measured
Time to burst (s)	161	182	245
Burst Temperature (K)	952.82	1003.3	1073.15
Max hoop strain (%)	50.76	74.05	50
Pressure (MPa)	10.18	9.94	5.98

In the second run, the measured internal rod pressure was provided as input. FRAPTRAN 1.4 however allows only 10 data pairs of (pressure, time) to be given to describe the internal pressure history, this is plotted in Figure D.2. In this case, the pressure at each time step is found by linear interpolation.

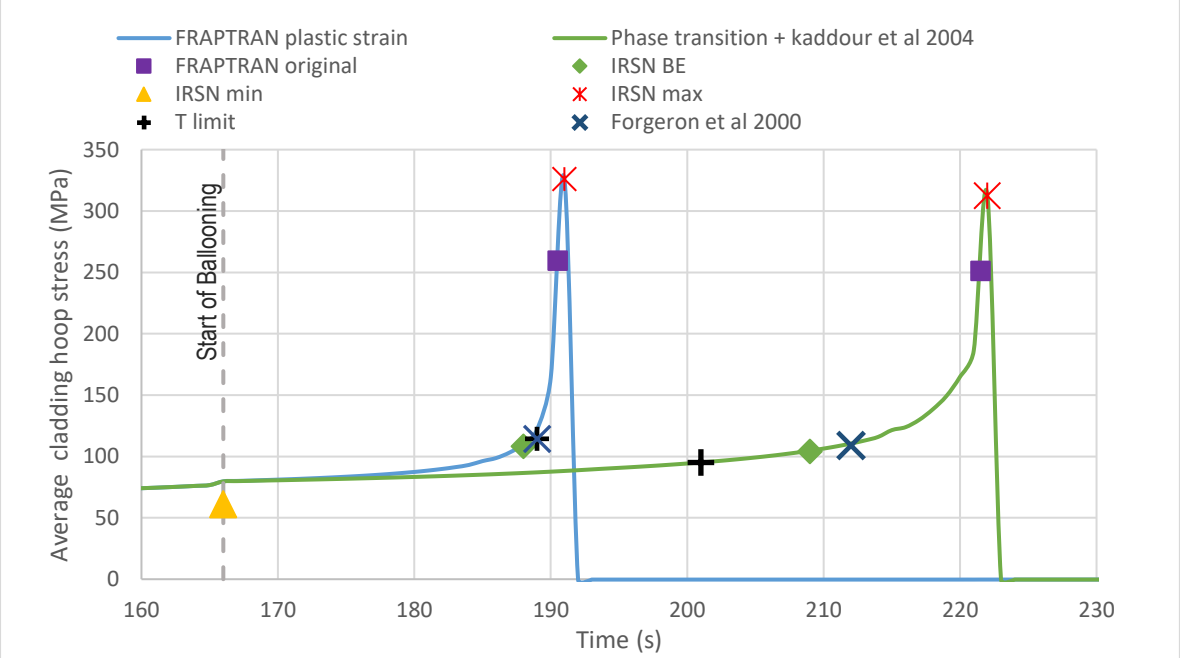

Figure 41 FRAPTRAN stress calculations with different deformation models and burst criteria for IFA-650.15

The stress evolution in the ballooning node for the second run is plotted in Figure 41. As can be seen, ballooning starts at 166s, the code is structured to check for failure only after BALON2 is called and at that point, the stress is already over IRSN min criterion and hence the cladding is assumed to fail at that time in that case. Other criteria trigger failure at different times as detailed in Table 18 and Table 19. Kaddour et al. 2004 creep deformation produces relatively better predictions.

Table 18 IFA-650.15 LOCA results with Kaddour et al creep deformation and different burst criteria

	Kaddour et al. 2004						
Burst criterion / Parameter	**FRAPTRAN original (stress + strain)**	**IRSN BE**	**IRSN min**	**IRSN max**	**T limit 2022**	**Forgeron et al. 2000**	**Experiment**
Time to burst (s)	222	209	166	222	201	212	245
Burst Temperature (K)	1054.3	1040.9	970.57	1054.3	1033.2	1044.3	1073.15
Peak residual strain (%)	82.19	22.26	5.00	83.60	15.31	25.92	50

Table 19 IFA-650.15 LOCA results with FRAPTRAN original deformation and different burst criteria

	FRAPTRAN original plastic deformation						
Burst criterion / Parameter	**FRAPTRAN original (stress + strain)**	**IRSN BE**	**IRSN min**	**IRSN max**	**T limit 2022**	**Forgeron et al. 2000**	**Experiment**
Time to burst (s)	191	188	166	191	189	189	245
Burst Temperature (K)	1021.7	1015.5	970.57	1021.7	1017.6	1017.6	1073.15
Peak residual strain (%)	69.83	24.35	5.00	69.83	29.05	27.61	50

Summary and conclusions:

The work carried out in this study outlines the modifications applied to the FRAPTRAN code for improved prediction of cladding behaviour during a LOCA event. Cladding deformation in BALON2 was modified by employing two high-temperature creep laws in combination with a dynamic crystallographic phase transformation model. The models are relevant for generic zircalloy and Zr1%NbO (M5) cladding types. In addition, different burst criteria were also implemented and tested. The implemented developments have been validated by detailed thermal mechanical modelling of FRAPTRAN integral assessment LOCA-tests. Furthermore, a new validation case for M5 cladding type was simulated.

The produced results show that the original ballooning deformation dictates failure to a certain extent in most cases regardless of the burst criterion applied. Nonetheless, the newly implemented creep models are more sensitive to burst criteria as more variation is observed. Kaddour et al. 2004 produces better predictions for M5 cladding type and more cases should be modelled with Rosinger 1984 creep law for accurate assessment.

In terms of burst criteria, IRSN BE and IRSN max produce comparable results to the original criterion in the code. On the other hand, IRSN min and the temperature limit exhibit a more conservative boundary. Rosinger-SSM limit requires further modifications to the oxidation model before it can be used reliably. For better strain predictions, it is recommended to enable the strain limit alongside the new implemented failure criteria of temperature and stress.

Further developments are suggested for improved predictions in future work:

The implemented high-temperature creep laws could be updated in terms of excess oxygen to account for embrittlement effect. Calibrated models have been published in the open literature [24].

With respect to phase transition, creep calculations in the mixed phase region could be updated in line with latest studies in the literature and hydrogen effect should be considered for Zr1%NbO cladding types.

Additionally, Leistikow and Schanz 1987 oxidation model is suggested in FRAPTRAN for consistent use of Rosinger optimised limit and Forgeron et al. 2000 limit. Since these criteria have been calibrated based on that model.

3. Full core modelling

In this project, partners selected a methodology to evaluate the number of failed fuel rods during a LOCA transient. Two main approaches were used:

- Chaining of a fuel performance code with a system thermohydraulic code. In this case, the core and the reactor core system (RCS) is simulated given a chosen scenario and assumptions and results in terms of thermohydraulics are used as boundaries conditions by the fuel performance code.
- Integral approaches with codes dealing with RCS, thermohydraulics and fuel thermo-mecanical modelling in the same simulation.

The different approaches used in task 3.2 are detailed in Table 20.

Partner	System model (core+RCS)			Fuel perfomance modelling	
	Thermo-hydraulic modelling	Thermo-hydraulic Code	Core nodalization	Thermo-mechanical modelling	Code
Fuel performance code chained to T/H code					
SSTC	2D Axi-symetric	RELAP5	Groups	2D Axi-symetric	TRANSURANUS
UJV	2D Axi-symetric	RELAP5	Groups	2D Axi-symetric	TRANSURANUS
Integral system approach					
LEI	2D Axi-symetric	ASTEC	4 Groups (rings)	2D Axi-symetric	ASTEC
HZDR	3 D	ATHLET-CD	Rings + azimuthal sub-division	2D Axi-symetric	ATHLET-CD
IRSN	3 D	DRACCAR	at least 1 / FA	2,5 D	DRACCAR

Table 20 : Summary of approaches used to evaluated the number of failed fuel rods during a LOCA

Fuel performance code chained to a system thermohydraulic code

JRC Summary of methods used with TRANSURANUS

In an effort to contribute to the harmonisation of methods for evaluation of the radiological consequences of accidents, the JRC provided an overview of the experience gained by means of the TRANSURANUS code, in particular for LOCA analysis.

Historical development of LOCA analysis with TRANSURANUS

The TRANSURANUS fuel performance code developed and distributed by the JRC is involved in various countries for the licensing of nuclear fuel. Based on the different experiences gained, and in an effort to support harmonisation at EU level, a summary is made here for the methodology applied to compute the number of failed rods in the event of a LOCA by means of the TRANSURANUS code. The methodology is intended for the LOCA licensing analyses of fuel in the European Union and is in line with internationally accepted procedures and guidelines [51][52][53].

The enveloping hypothetical accident considered (LB LOCA) is a guillotine type break of one primary loop at the reactor vessel inlet, initiated at full power. Often an additional single failure of the passive core flooding system of the emergency core cooling system is assumed. Owing to the pressure drop in the primary system, the void increases rapidly in the core resulting in fast reactor power reduction because of the negative reactivity feedback. Due to flow reversal during blowdown, the heat transfer radically decreases, DNB occurs and the cladding temperature increases. The decreasing primary pressure actuates the different ECCS's that eventually refills and finally re-floods the core after several hundred seconds.

The scope of the methodology considered here is limited for the LOCA hot rod and failure rate analyses and focuses on the insertion of a new fuel type in an existing NPP. Therefore, it focuses on the thermo-mechanical simulation of the fuel rod during a LOCA and it is assumed that there is a valid safety evaluation of the plant from which boundary conditions can be utilized (i.e. an analysis of record).

The fuel licensing procedures established in East-European countries prior to their entrance in the EU entailed the intensive utilization of the TRANSURANUS code for Russian type VVER reactors. The code had been selected to be the standard fuel rod performance code used for regulatory purposes in several countries operating VVER reactors, as e.g. Hungary, Slovak Republic and Bulgaria [54]. However, the involved VVER-specific material functions were limited to normal operating conditions, and consequently, the code was not applicable in VVER accident analyses.

The EXTRA project of the EURATOM 5th Framework Programme was therefore initiated in 2001 with the aim to address this incompleteness through the systematisation of the knowledge on experimental data of the Russian Zr1%Nb cladding alloy and the extension of the applicability of the TRANSURANUS code[55] [56]. A consortium of three research organisations carried out this project: the JRC- Karlsruhe (formerly Institute for Transuranium Elements), the VUJE Nuclear Power Plant Research Institute (Slovak Republic) and the MTA EK (formerly KFKI Atomic Energy Research Institute). Thanks to parallel activities for the extension and application of the TRANSURANUS in PWR safety analyses, the German technical safety organisation in Hannover (TÜV) was also involved in the project as an observer, providing a forum for work harmonization and broad discussions.

The EXTRA project aimed to provide an analytical tool for the consistent simulation of the VVER fuels' performance under both normal and off-normal conditions [55]. Prior to the EXTRA project, no European fuel performance code with the above capabilities was available. Thanks to the implemented equations and general code structure, as well as the wide scope of the covered phenomena and the involved comprehensive materials databank, the

TRANSURANUS code could be straightforwardly extended to improve the safety analyses capabilities [56][57]. More precisely, in the second work package of the EXTRA project, the TRANSURANUS code was extended with new models for the high temperature steam oxidation, plastic deformation and failure of the fuel cladding. The model development was focusing on the exact description of the zirconium-steam reaction, the plastic deformation and the rupture of the nuclear fuels' cladding tube under varying conditions. New VVER-specific empirical correlations for the mass gain rate, the zirconium oxide layer growth rate and the deformation rate were evolved and adopted to the models. The multidimensional Levenberg-Marquardt minimisation procedure was applied to fit the material constants of the correlations on the compiled experimental data. The resulting mechanical model took into account not only the temperature and the crystallographic phase of the cladding, but also the oxygen concentration as a parameter of the deformation rate. In this manner, the effect of the oxidation on the strength and deformation of the cladding can be simulated in an accurate way.

In the fourth work package of the EXTRA project, the code was applied to evaluate the number of failed fuel rods in a hypothetical double-ended cold leg LBLOCA in the Units V2 of the Bohunice NPP in Slovakia. The application of the TRANSURANUS code to assess the extent of core damage improved the methodology of the safety analyses and allowed for a more detailed evaluation of the radiological consequences of the DBA. This was possible thanks to the development of an automatic transfer of data from the RELAP code as boundary conditions for the fuel rod performance calculations, as illustrated in the following figure:

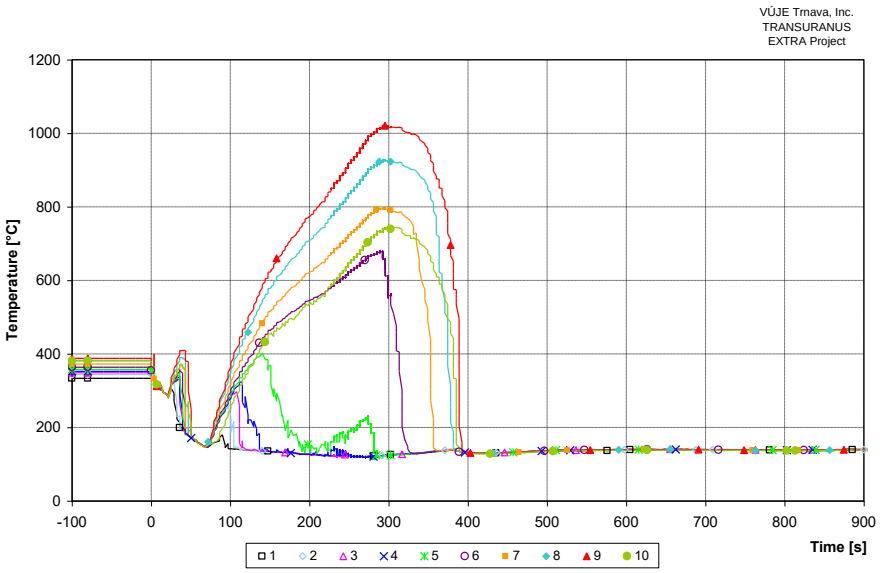

Figure 42: Cladding temperature history in 10 axial nodes during 2F-LBLOCA by means of a RELAP analysis [56].

Following the EXTRA project, a bilateral project has been funded by the European Commission and carried out by MTA EK [58]. The main objectives were to simulate the hydrogen uptake by the Zr-1Nb alloy and its effect on the cladding performance under accident conditions, which was triggered by the Paks fuel cleaning tank incident in 2003. On the basis of experimental data, an empirical stand-alone model was developed in 2006 to calculate the hydrogen absorption in Zr-1Nb cladding during steam oxidation and in a gaseous atmosphere [59]. The model is based on a quasi steady-state approach of the actual hydrogen concentration defined on the basis of the solubility limit and an appropriate kinetics constant fitted separately to experimental data. This model for Zry4 cladding is being implemented in the TRANSURANUS code in the frame of the R2CA project. Independent verification is planned by NucleoCon in the Slovak republic and PreussenElektra in Germany. Extension to M5 cladding properties is planned by ENEA in the frame of the R2CA project as well.

The earliest application for LOCA analysis with TRANSURANUS in the frame of licensing was made by TÜV in Germany [60]. The aim of the PWR hot channel analysis in the German regulatory framework was to demonstrate that the fuel temperature stays below the melting temperature and the transient tangential cladding strain remains below its licensing limit.

More recently, the industry demonstrated a methodology for how the core can be more realistically modelled in the sense that only individual rod parameters are treated conservatively without the need for further conservative assumptions regarding the clustering of rods into thermohydraulic channels. For the introduction of fuel from Westinghouse Sweden Electric by E.ON in a German PWR, such clustering was based on the maximum stored energy and the mean stored energy per rod, the mean stored energy of the hot assembly and the mean stored energy of the surrounding assemblies are shown in Figure 43 as a function of burnup. The mean stored energy of the surrounding assemblies and of the residue assemblies (not shown) is practically constant regardless of burnup.

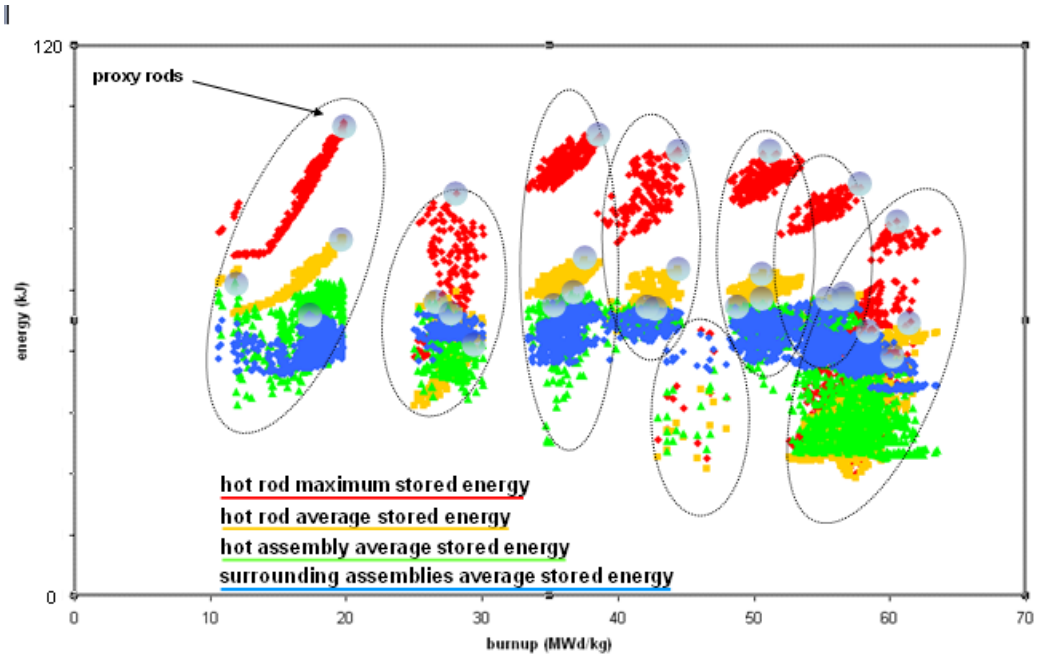

Figure 43: Fuel rod clusters as a function of burnup applied in the LB LOCA analysis by E.ON [61].

Such clustering was also considered in the methodology for quantification of fuel cladding failure as a result of a LOCA in the Slovak republic and was developed in the frame of the EXTRA project of Euratom 5th framework programme[55] [56]. That clustering considers division of all fuel rods into four groups based on fuel rod power. Since there is five-year-load scheme applied, each of the power group of rods is split into five groups (if relevant) to reflect time of irradiation. The safety analysis relies on external coupling of the RELAP5 code and TRANSURANUS code, and was applied for typical maximum design basis accident of the VVER-440 reactor in order to assess the failure rate for this type of accident [62]. Stefanova et al [63] applied a similar approach for the VVER-1000 LB LOCA analysis in Kozloduy.

In parallel to the applications to PWRs and VVERs, colleagues from the university of Pisa developed and applied a procedure involving the TRANSURANUS code to address the fuel rod failures during LB-LOCA transients in Atucha NPP operated in Argentina [64]. The methodology implies the application of best estimate TH and neutron physics codes in combination with the TRANSURANUS fuel performance code, with the objective to verify the compliance with the specific acceptance criteria. The fuel pin performance code is applied with the main objective to evaluate the extent of cladding failures during the transient. The procedure consists of a deterministic calculation by the fuel performance code of each individual fuel rod during its lifetime and in the subsequent LB-LOCA transient

calculations. The boundary and initial conditions are also provided by core physics and three-dimensional neutron kinetic coupled thermal-hydraulic system codes calculations.

In 2017 the TRANSURANUS code of the JRC was also selected for the licensing of the fuel from Westinghouse Sweden Electric for the VVER-440 reactors in the EU and Ukraine in the frame of the ESSANUF project [65] [66]. Finally, most recently Hyvönen [67] prepared the TRANSURANUS code for LOCA analysis by FORTUM in Finland.

Today, not only numerous universities, research centres and several key industrial partners in the EU, but the majority of ETSON members have a TRANSURANUS user licence agreement: Bel V, EK, ENEA, IRSN, VTT, LEI, TÜV, INRNE, VUJE, UJV Rez, RATEN ICN, PSI, and SSTC. The active participation of the users in the development and independent verification and validation enables to keep pace with all current developments in terms of new materials as well as adapted operating conditions being considered, although it also is challenging in view of the different regulations in place in each country. Nevertheless, on the basis of all this experience, the present methodology is briefly outlined in this document.

General methodology

The general methodology for performing the safety evaluation of reload cores assumes that a valid conservative safety analysis exists, the so-called plant analysis of record or reference analysis, along with a set of key safety parameters for each accident or transient under consideration. The values of the input safety parameters, or frame parameters, in the reference safety analysis are selected to conservatively bind the values expected in subsequent cycles. If all reload safety parameters for a core are conservatively bound, the reference safety analysis is assumed to be valid, and no further analysis is considered necessary. When a reload safety parameter is not bound, further analysis is considered necessary to ensure that the required margin of safety is maintained for the accident in question, in this case a LOCA. When the key safety parameters are not bounding specific analyses are required to ensure that the margin to the safety criteria is maintained throughout the accident.

When a new fuel design is introduced, it has to be demonstrated that the safety analysis of the plant is still valid. In addition, any criteria affected by the insertion of a new fuel design have to be evaluated. The methodology presented here consists of three different parts. The first is about how the existing safety analysis can be validated for also being applicable to the new fuel. The second is about how the acceptance criteria can be evaluated for new fuel rods using the so called hot rod approach. The third part is a failure rate methodology which aim is to define the expected radioactive release during an LOCA. These three parts are outlined in the following sections.

Verification of the thermal hydraulic data

The fuel stored energy is ranked as one of the most important parameters with respect to heat-up analysis, especially during blowdown, since the resulting pellet temperature distribution undergoes a readjustment that determines the temperature of the cladding after DNB. The fuel stored energy is also directly dependent on the specific fuel design. Thus, in order to verify the applicability of the TH data from the reference LOCA analysis, it has to be demonstrated that the fuel stored energy of the new fuel design is bounded (or similar) to those in the reference LOCA analysis. The fuel stored energy is evaluated by means of the TRANSURANUS code with the same conservative level as in the reference analysis. The calculations are conducted using conservative models and fuel rod design parameters that can also take into consideration uncertainties [61].

Hot rod analysis

The evaluation of the PCT and the equivalent cladding reacted (ECR) during the postulated LOCA is based on the thermo-mechanical analysis of the behavior of the hot fuel rod in the core applied by Westinghouse Electric Sweden and PreussenElektra (formerly E.ON Kernkraft) [68]. The analysis covers the consistent simulation of the fuel performance under normal operation and accident conditions with is possible thanks to the capabilities of the TRANSURANUS code. An overview of the proposed methodology is presented below.

Initial Conditions:

The fuel rod condition at the initiation of the LOCA depends on the heat rate and the burnup of the fuel rod. The burnup dependent fuel rod parameters (pellet and cladding geometry, free volume, pressure, fission gas fraction, corrosion, etc.) and material properties (e.g. fuel thermal conductivity) are calculated via the simulation of the normal (steady-state) operation. The simulations are conducted using conservative models and conservative (bounding) power histories. Lower or upper bound models are considered such that the most conservative conditions for the PCT / ECR evaluation are achieved. The coolant conditions and the heat transfer between the cladding and the coolant under normal operation is calculated by the thermal model of TRANSURANUS.

Prior to the LOCA event, conservative linear heat rate profiles have to be assumed at the initiation of the accident, in accordance with the thermo-hydraulic analyses. Consequently, the relative axial power profile at the evaluation is distorted to a conservative profile in a hypothetical pre-LOCA transient in the hot rod analysis. The most conservative relative heat rate profile is assumed to be provided on input for TRANSURANUS and should be defined in a system-level parametric study and applied throughout the postulated LOCA event. The duration of this hypothetical pre-LOCA transient is typically 1 h and followed by a steady-state period (about 48 h) prior to the LOCA initiation.

LOCA Transient

The thermo-mechanical performance of the fuel rod under LOCA conditions is calculated using the best-estimate models of TRANSURANUS considering the appropriate clad material properties that were implemented in the wake of the EXTRA project. These models cover all the phenomena relevant for LOCA simulations such as plastic deformation, ballooning, high-temperature oxidation and cladding failure due to overstress or overstrain. The effects of the crystallographic phase transformation in zircaloy and the hydrogen absorption on the cladding deformation and burst are also considered thanks to the new developments in the frame of the R2CA project. Cladding failure is simulated according to combined criteria, i.e. burst occurs due to overstress, overstrain or rod-to-rod contact as outlined above. Cladding oxidation must be calculated with Baker-Just kinetics separately for the outer and the inner surfaces. Inner-side steam oxidation is taken into account only after rod burst. Reaction heat in the cladding wall is considered as an additional heat source.

The maximum local linear heat rate and a conservative axial heat rate profile are assumed at the initiation of the LOCA and shall be consistent with the reference analysis. At the beginning of the LOCA the core power suddenly drops due to the void feedback effect. Afterwards it follows the decay curve. In the hot rod analysis the maximum linear heat generation rate curve follows the decrease of the core power relative to the initial core power. The axial power profile at the burnup for evaluation is distorted to a fixed conservative profile prior to the LOCA initiation. The conservative axial heat rate profile is defined through a parametric study in the system-level thermo-hydraulic (e.g. ATHLET or RELAP) analyses. The same relative power profile is applied throughout the postulated LOCA event.

The simulation of the fuel rod performance under LOCA conditions is carried out at the thermo-hydraulic boundary conditions provided by the customer on the basis of system-level analyses by means of ATHLET or RELAP for example. The system model of the core generally consists of parallel hydrodynamic channels with different cooling conditions (e.g. [61][62]). The effects of bypass and flow distribution between the parallel channels on the heat transfer conditions are simulated by the TH code. Therefore the TRANSURANUS code does not calculate the coolant conditions and the HTC under accident conditions. The TU code uses the data of the hot channel that simulates the cooling conditions of the fuel rods at the highest power. The time evolution of the system pressure, the linear heat rate, the HTC between the coolant and the cladding, the mass flow rate and the coolant temperature have been prescribed as boundary conditions in the TU input. Such data transfer can either be made via interfaces created for transferring data between ATHLET and RELAP in the frame of the EXTRA and ESSANUF projects (e.g. [3-5]), or can be achieved automatically by means of code coupling in the frame of the McSAFE project for example [69], which is based on the SALOME open source platform. On the basis of these boundary conditions the code calculates the actual cladding temperature for each axial node, the cladding mechanical response and the Zr-steam reaction. Consequently the axial profiles of the cladding temperature and oxidation can be evaluated throughout the LOCA transient and the peak cladding temperature and equivalent cladding reacted can be extracted from the code output.

Failure rate analysis

It is crucial to evaluate the total number of perforated fuel rods in the core in order to define the expected radioactive release. The proposed methodology is based on deterministic TRANSURANUS simulations of the fuel rod performance under the base irradiation and the subsequent postulated accident using realistic power histories in a consistent manner. The applied calculation methodology is consistent with that applied by Westinghouse Sweden for German PWRs [61]. An overview of the proposed methodology is presented below.

Initial Conditions

The simulation of the base irradiation provides the burnup-dependent conditions e.g. rod internal pressure, gap conductance, etc. for all fuel rods in the core at the defined time point of the postulated LOCA. The power history data (linear heat generation rates and axial profiles) of the fuel rods are derived from the core design computations provided by the utility for instance, together with an uncertainty of the heat rate computations. The fuel performance analyses are carried out with these realistic power histories (increased with the uncertainty) but using conservative fuel rod and model parameters.

Prior to the LOCA event, the axial power profile of the core has to be set in a limiting condition consistent with the reference analysis. This is translated to each rod by applying a modulation function that re-distributes the axial power profile while retaining the rod average power. In a similar way as for the hot rod analysis above, the duration of this hypothetical pre-LOCA transient is typically 1 h and followed by a steady-state period (about 48 h) prior to the LOCA initiation.

LOCA Transient

The postulated LOCA is initiated at the end of the steady-state phase. During the transient, the TH boundary conditions are used to specify the time evolution of the fuel rod linear heat generation rates, coolant temperature and mass flow rate, heat transfer coefficients and the coolant pressure in the fuel rod calculations. The core-wise thermo-mechanical simulations require a complete set of thermo-hydraulic data defined for different assembly power, rod power and burnup intervals. TÜV organises this by means of the TITANIA software [60], while VUJE has established a semi-automatised data processing procedure for a reduced number of rods based on power and burnup [62]. Such data transfer can be done automatically at any time for any rod when using a coupled set of codes like PARCS-SUBCHANFLOW-TU [70], or fully automatized in the SALOME platform [71]. The boundary conditions applied for a specific rod are selected from this set of data on the basis of the actual heat rate and burnup values at the LOCA initiation.

At the defined time point of the LOCA initiation, the DBA-specific best-estimate models of TRANSURANUS for the assessment of cladding effective strain rate, oxidation rate, burst stress and burst strain are automatically activated and the built-in cladding failure criteria (over-stress and over-strain) are verified for each time-step. If a criterion has been violated, cladding burst is indicated in the code output. At the end of the core-wise simulation cycle the number of failed rods is summarized and the failure rate (number of failed rods / total number of rods in the core) is defined.

Statistical post-processing with TRANSURANUS

In parallel to the summary of the methodologies for LOCA analysis, progress has been made for the statistical analysis based on the build-in capabilities of the TRANSURANUS code. More precisely, the statistical post-processing program TUPython of the TRANSURANUS package was further improved in order to support the Best Estimate Plus Uncertainty (BEPU) analyses [71]. Thanks to the Monte Carlo input sampling approach, uncertainties of up to 40 safety-relevant modelling variables can be statistically estimated. In a paper submitted to TOPFUEL2021 conference to be held in Santander, Spain from 24-27 October 2021 [72], the main functionalities of this tool were outlined and illustrated using a test case and a numerical experiment based on Wilks' formula. In particular, it was illustrated how the standard statistics can be calculated with the new graphical user interface and a numerical experiment with 1st to 6th order Wilks' methods was demonstrated. Based on the numerical experiment we showed that the 1st order Wilks' method for calculating the 0.95/95% uncertainty estimator contains

also uncertainty in itself and can deliver very conservative values for a safety-relevant variable. More details are provided in Task 5.3.

Inclusion of the effect of Hydrogen in Zry4 on LOCA properties

The properties concerned are the high-temperature creep, the crystallographic phase transition, and the burst stress in the TRANSURANUS code. By the end of January 2021, the JRC implemented new models in the current version of the TRANSURANUS code to describe the influence of the hydrogen content on the creep behavior of Zircaloy-4 cladding tubes. This was largely based on the previous work of U. Dackermann [73] at the Technical University of Münich with support from E.ON, but also on more recent models for phase transition in the open literature such as that of Massih et al [74] and Pastore et al. [75]. The former developments of Dackermann were made in Fortran77 and have been converted to modern Fortran. The correlations were based on calorimetry and dilatometry data that were used to modify the static and dynamic phase transfer models of TRANSURANUS. The new phase transfer models should be able to be applied for temperature gradients between -100 and +100 $C.s^{-1}$ and for hydrogen contents up to 1000ppm. The Zircaloy-4 creep model has been calibrated on isothermal burst experiments performed for hydrided and non-hydrided specimens by Forgeron et al. [76] For that purpose, Norton creep parameters (structure parameter, stress exponent) have been adopted in each crystallographic phase domain. The new models allow to assess the increase of damage extent due to the influence of the hydrogen in Zircaloy-4 [77]. Nevertheless, on this basis new correlations for other cladding tube materials can be implemented easily in order to take into account the influence of hydrogen. As an example ENEA has prepared corresponding properties for M5 cladding, which were presented at the NENE2021 conference in Slovenia [78].

UJV methodology

Plant description

The analysed plant is light water pressurized reactor VVER-100/V320 located in the southern part of the Czech Republic. The powerplant facilitates two reactor units with power increased to 104% of the nominal power. The primary system consists of four main loops with horizontally placed steam generators. The reactor and the primary circuit are surrounded by a single full pressure containment system.

Parameter	Value
Thermal power [MWth]	3120
Core inlet temperature [°C]	290
Core outlet temperature [°C]	321
Primary system pressure (UP) [bar]	15.7
Primary circuit flow rate [m^3/s]	88000
Number of coolant loops [-]	4

Table 21 : Main plant parameters

Parameter	Value
Number and type of fuel assemblies [-]	163
Fuel lattice [-]	Triangular
Fuel pitch [mm]	12.75
Pellet diameter [mm]	7.8
Pellet composition [-]	UO_2, UO_2 + $Gd2O_3$
Active fuel height [mm]	3680
Cladding inner and outer diameter [mm]	7.93/9.1
Cladding material [-]	E110
Control rod number [-]	61
Control rod material [-]	DyTi, B_4C

Table 22: Main core parameters

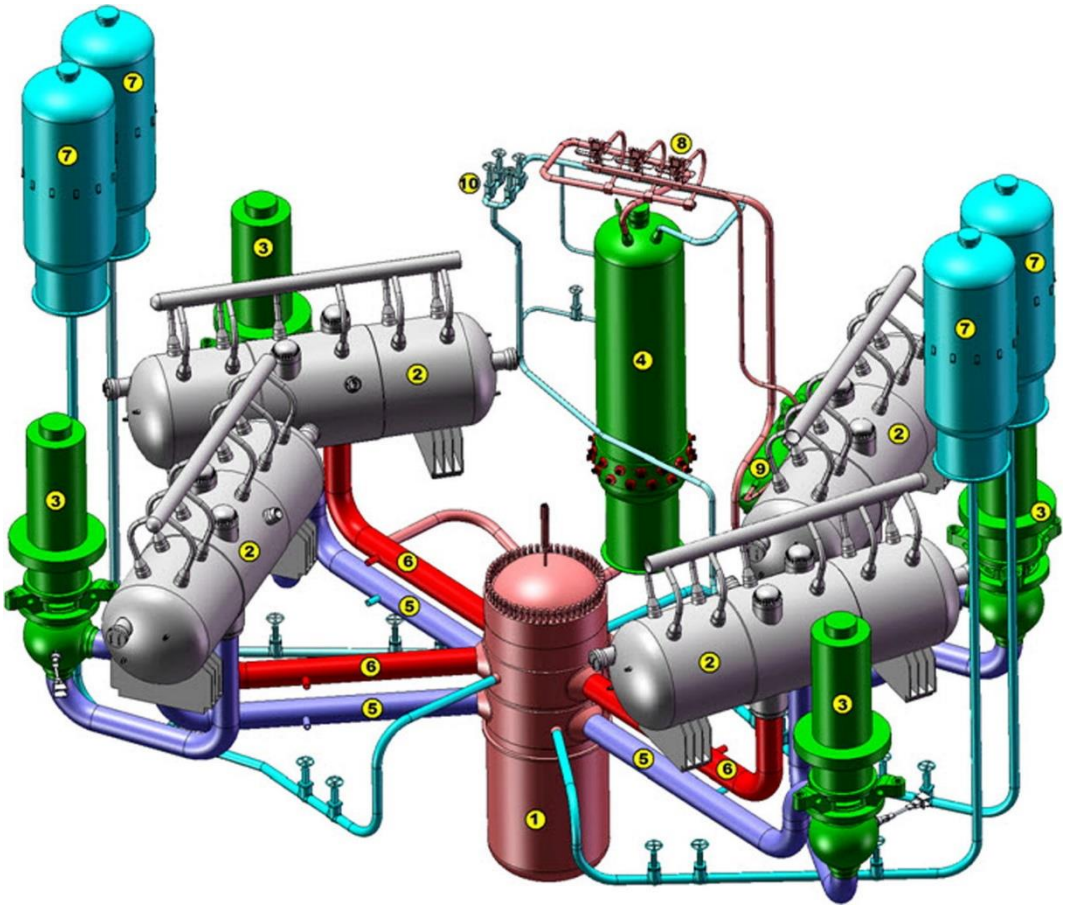

Figure 44 : VVER1000 primary system configuration (V320) [79]

Reactor type.

The VVER 1000 /V 320 is Russian design of pressurized water reactor. This design is quite common and has several specific features. e.g. a hexagonal fuel grid, four horizontal aligned steam generators and a full pressure containment. Design basis accident is a double end large break LOCA with equivalent leak diameter equal to 2 x 850 mm.

Core information.

The core consists of 163 hexagonal shroudless fuel assemblies. Each fuel assembly contains 312 fuel rods, 18 guide tubes and 1 central tube. Cladding dimensions are almost equivalent to the 17x17 OFA (cladding outer diameter 9.1 or 9.1444 mm). Fuel pellets (UO2) with or without central hole are used depending on the fuel type. Assembly length is 4570 mm, with quantity and layout of the grids depending on the fuel type. A homogeneous core consisting of 12 SG fuel assemblies with solid pellets was used as a reference one for the analysis.

Reactor cooling systems.

The reactor has a four-loop configuration. Each of the four loop has its main cooling pump on the cold leg. Unlike the western PWRs, the VVER-1000/V320 has horizontally oriented steam generators.

Safety injection systems.

High-high pressure injection system (TQx4):

Number 3
Start 10 s
Level 3,1 m
Temperature 30 °C
Concentration of H_3BO_3 42 g/kg

High pressure injection system (HPIS, TQx3):

Number 3
Start 10 s
Level 1,25 m
Temperature 30 °C
Concentration of H_3BO_3 42 g/kg

Low pressure injection system (LPIS, TQx2):

Number 3 (Suction from Containment Sump)
Start 5 s
Level 3,5 m
Temperature 55 °C
Concentration of H3BO3 14,2 g/kg

Accumulators:

Number 4
Pressure 5,9 MPa
Level 7,35 m
Temperature 50 °C
Concentration of H_3BO_3 14,2 g/kg

Scenario description

LB LOCA modelled within the D2.5 of R2CA project ([79]) was used as an input for TRANSURANUS ([80]) calculation. The version / settings of the TRANSURANUS code used corresponded to those used for the safety assessment of the Czech NPPs performed at UJV ([81]).

The effective coolant temperatures and heat transfer coefficients, core pressure and core power calculated by the system code through the course of the transient were used as the boundary condition for the LOCA part of the TRANSUNRUS power history. The steady-state operation of the fuel modelled by the TRANSURANUS code before the LOCA event was input based on the bounding power histories for the current core design.

The goal of the TRANSURANUS analysis was to statically assess the number of the failed fuel rods. Based on the conservative analysis (see D2.5), the group of the rods with relative power between the 1.3 – 1.65 was considered as this was the only one to fail in the conservative analysis. The corresponding burnup range of such rods in the plant reference core design was 15 – 20 MWd/kgU.

The merits of interest of ta analysis is the distribution of the clad failure times and the probability of rod failure.

Two groups of the uncertainties were considered in the statistical analysis – fuel rod parameter uncertainties and code model uncertainties. 100 input files were generated, executed and evaluated by the set of automated tools. The code model uncertainties were treated as random, but the fuel parameters underwent several checks and the combinations out of the allowed range of the correlated parameters were discarded.

- Total length of fuel stack and plenum was kept constant
- Total mass of fuel was checked – known tolerances of fuel mass are narrower than full range of fuel density and dimensions effect
- Although the fuel and cladding parameters were generated randomly at each of 50 axial segments considered in the simulation, their variation along the length of the rod was restricted (e.g. one run could be generated with cladding outer diameter between 9.09 and 9.11 mm, another between 9.10 and 9.12, but 9.09 to 9.12 variation was rejected)
- Minimum cladding thickness was checked

Unfortunately, the specific values of the fuel uncertainties cannot be given due to intellectual property rights of the fuel vendor.

Parameter
Fill gas He content
Fuel pellet inner radius
Fuel pellet outer radius
Cladding inner radius
Cladding outer radius
Fuel pellet surface roughness
Cladding tube inner surface roughness
Fuel stack length
Plenum length
Fuel grain size
Fuel pellet open porosity fraction
Fuel pellet as fabricated density
Fuel densification
Fuel stoichiometry
Fill pressure
Fill temperature
Plenum free fraction (spring volume)
Fuel-cladding friction coefficients

Table 23 : Fuel rod parameters varied in the statistical analysis

The code model uncertainties were represented by multipliers used for the key correlations describing the pellet and cladding behaviour. The list of the considered models is given below:

MODEL	DISTRIBUTION	MEAN / MIN VALUE	SIGMA / MAX VALUE
Fuel-cladding heat transfer	Normal	1.0	0.027
Fuel			
Relocation	Uniform	0.5	1.0
Young's modulus	Normal	1.0	0.02
Swelling	Normal	1.0	0.05
Thermal expansion	Normal	1.0	0.05
Thermal conductivity	Normal	1.0	0.025
Creep rate	Normal	1.0	0.05
Specific heat	Normal	1.0	0.03
Cladding			
Young's modulus	Normal	1.0	0.01
Irradiation growth	Normal	1.0	0.13
Thermal expansion	Normal	1.0	0.013
Thermal conductivity	Normal	1.0	0.033
Creep rate	Normal	1.0	0.08 / 0.25[3]
Yield stress	Normal	1.0	0.03
Specific heat	Normal	1.0	0.03

[3] Low temperature / LOCA

Results & discussion

The main results of the calculations are shown in the figures below. There are two distinct groups of PCT curves in Figure 46. As shown on Figure 50, the high PCT group in the 2nd temperature peak corresponds to the rods which were predicted to fail within the 1st peak.

Of timing of the cladding failures, which is of the most interest to the radiological consequence evaluation is shown in the Figure 48**Erreur ! Source du renvoi introuvable.**. The highest power rods (relative power > 1.55) are predicted to fail within the 1st PCT peak in 7 – 12 seconds after the initiating event. It must be stressed that although such high power rods are allowed at Czech VVER-1000, the core designers avoid such cycles. The failures within the 2nd peak are predicted to happen between 130 – 250 s after the initiating event. The rods with a relative power between 1.50 and 1.55 fail either during the 1st or during the 2nd peak, the rods with a relative power 1.40 and 1.50 either remain hermetic or fail only during the 2nd peak. No rod failures are predicted below 1.40. In the current core loading patterns od Czech VVER-1000 there are therefore no high burnup rods which would reach high enough power to fail in the LB LOCA.

For this reason, the gas flow model developed as a standalone module within the T3.3. project was not coupled with the TRANSUNUS code for the LOCA analysis – for the low burnups rod the impact of this model is negligible due to large fuel cladding gap as may be seen from Figure 51 and Figure 52.

The summary of the clad failure probabilities is provided in Table 24.

ROD POWER [/]	NON-BURST [%]	BURST [%]	Burst time [s]
1.30 - 1.35	100	0	-
1.35 - 1.40	100	0	-
1.40 - 1.45	82	18	130 - 250
1.45 - 1.50	44	56	130 - 250
1.50 - 1.55	0	100	7-12 or 130-250
1.55 - 1.60	0	100	7-12
1.60 - 1.65	0	100	7-12

Table 24 : Burst probability as a function of rod relative power (15 – 20 MWd/kgU)

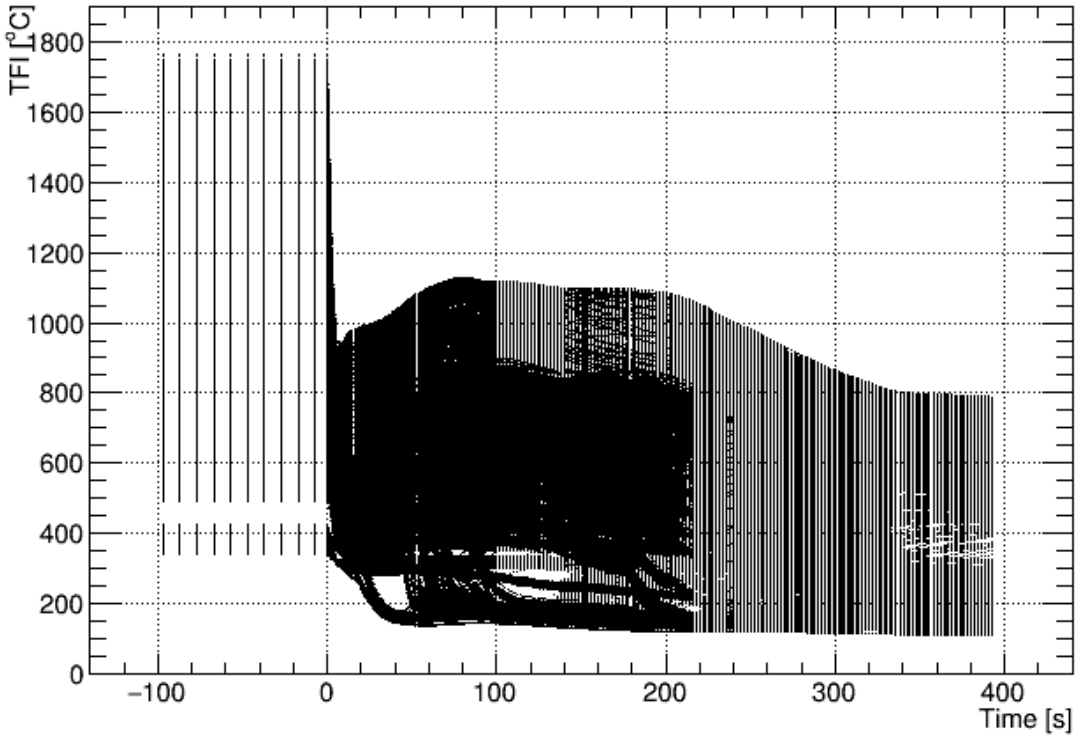

Figure 45: Fuel centerline temperatures

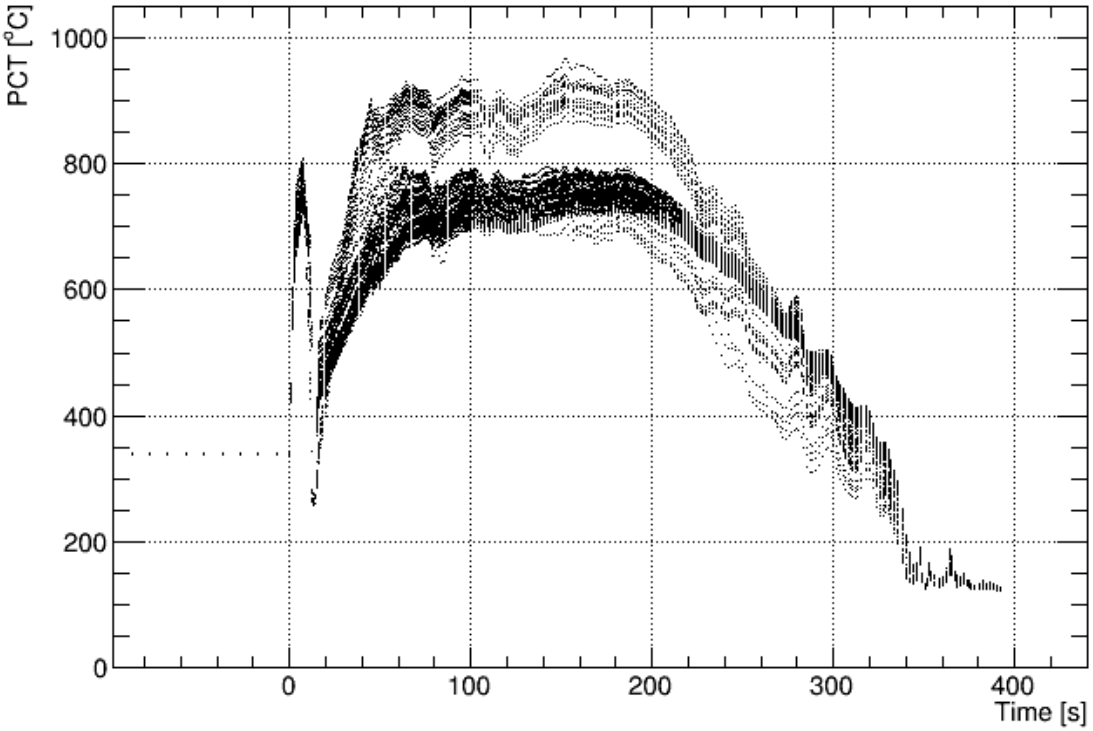

Figure 46: Peak Cladding Temperatures

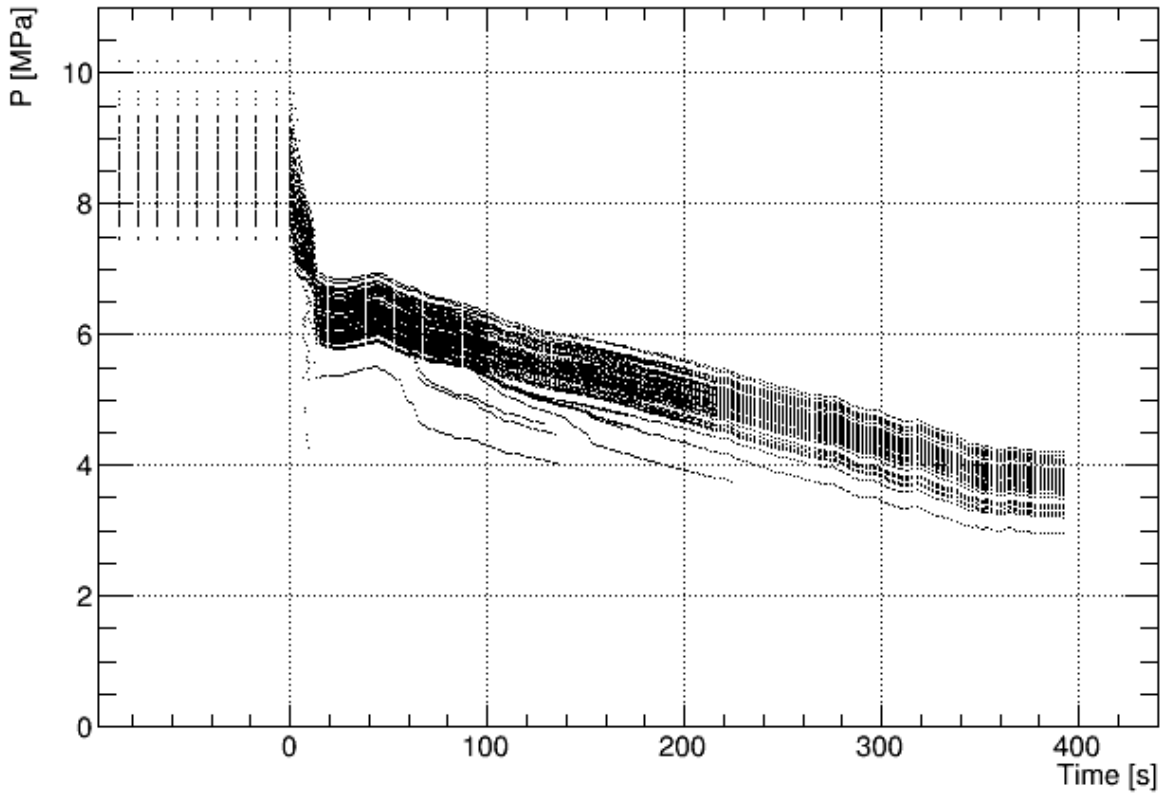

Figure 47: Rod Internal Pressure

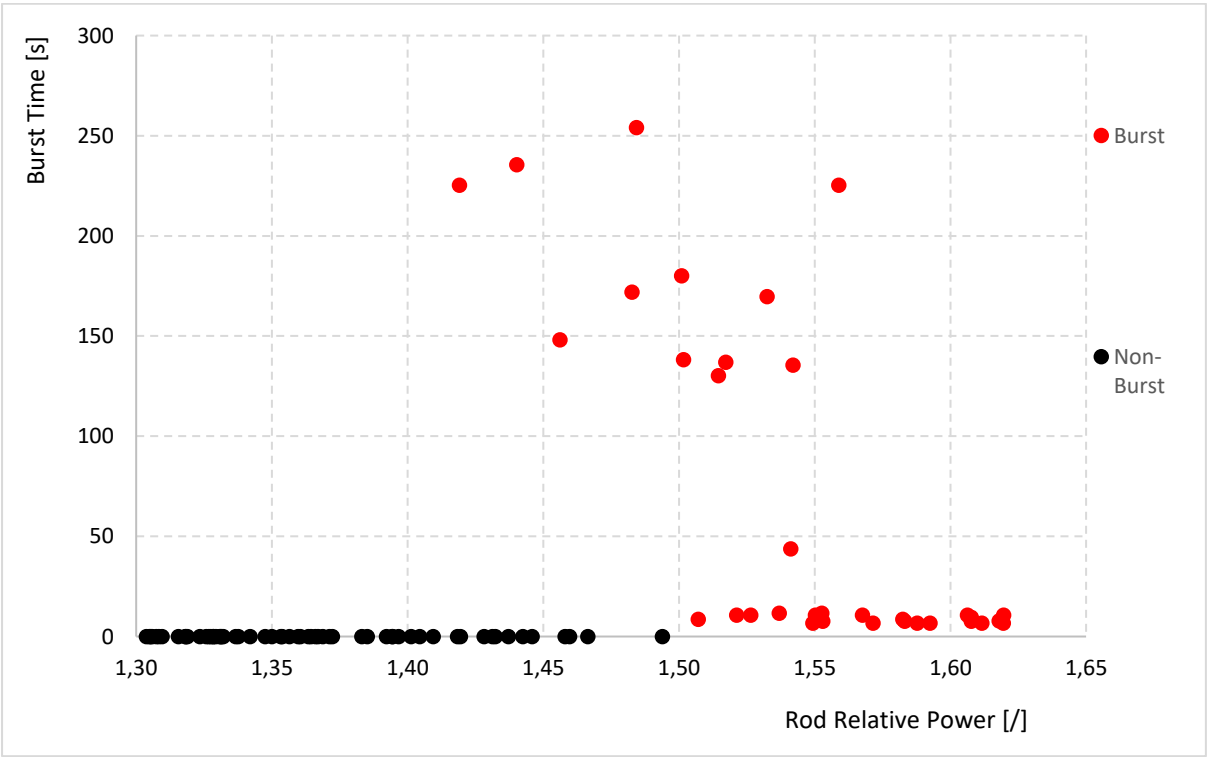

Figure 48: Rod Burst Times

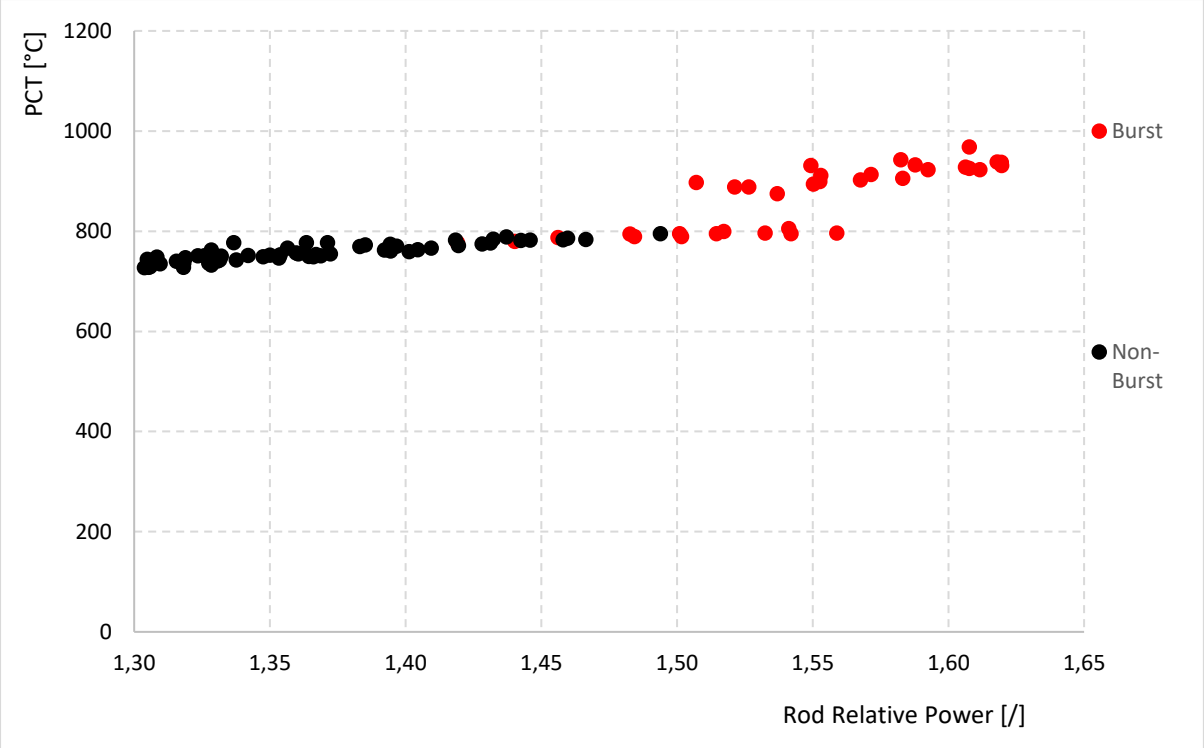

Figure 49 : PCT as a function of rod relative power

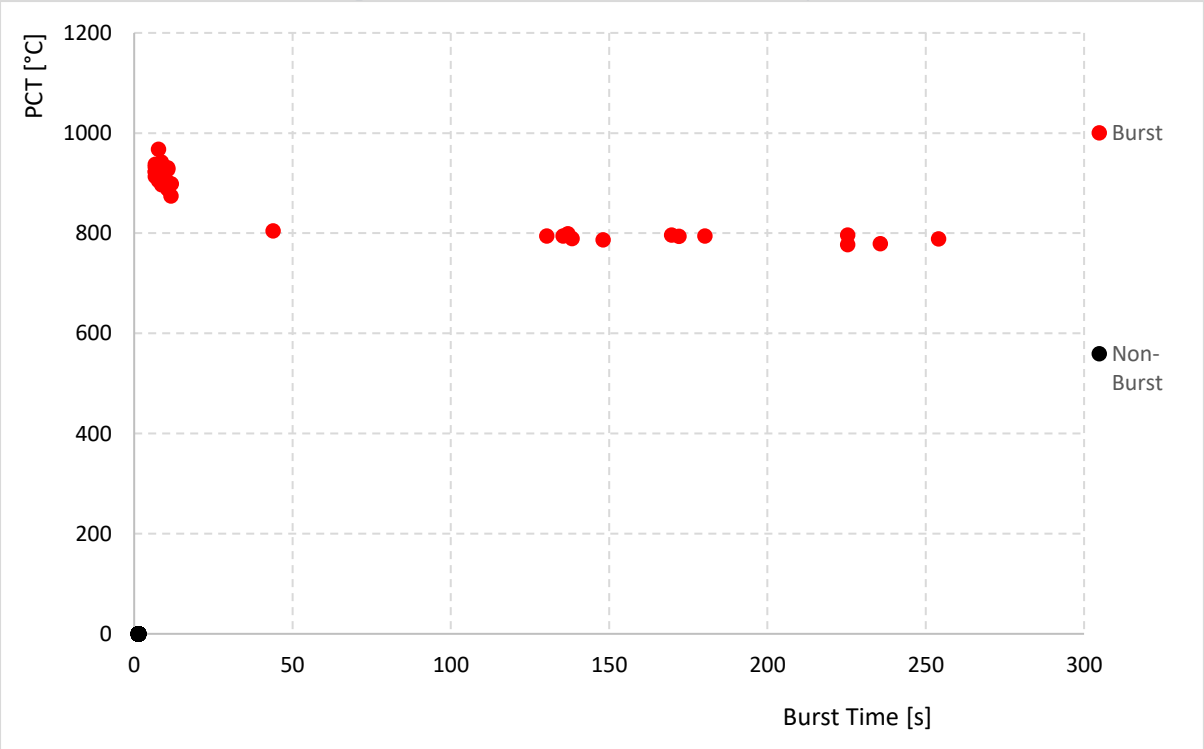

Figure 50 : Correlation between the PCT and the burst time

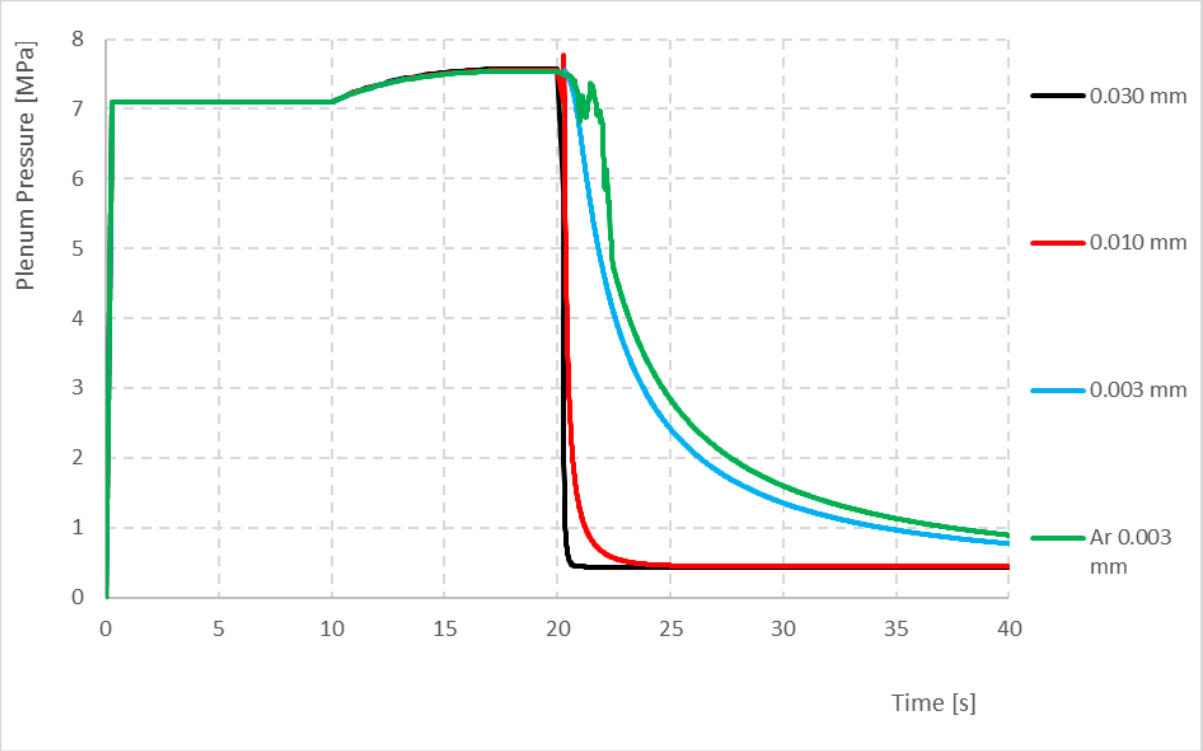

Figure 51 : Standalone Gas Flow model results for LOCA conditions

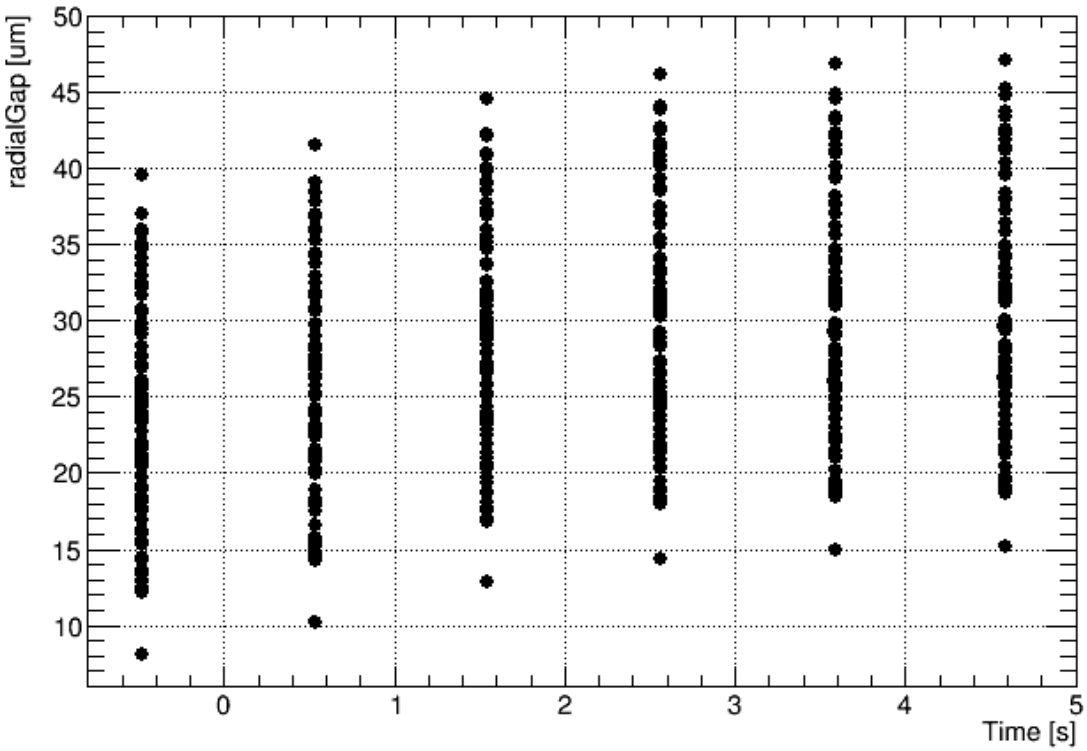

Figure 52 : Radial fuel – cladding gap predicted by the TRANSURANUS code for LB LOCA VVER-1000 case in the statistical analysis

Conclusions

TRANSURANUS simulation of rod response to VVER-1000 LB LOCA was performed using the statistical treatment of the fuel rod and code model uncertainties combined with the sensitivity study with respect to the rod power.
The critical group od the rods with a burnup of 15 – 20 MWd/kgU was studied as only these rods have high enough power to fail during the postulated LB LOCA. The correlation between the burst time and rod power was studied as the burst time is critical to the realistic radiological consequence calculations. The highest power rods were predicted soon in the transient when there is still a large mass release from the primary circuit to the containment. However, the cores with such high power rods are not normally operated. For the realistic assessment of the radiological consequences, the delay between the break of the primary circuit pipe and the onset of the majority of the fuel failures may be credited.

SSTC methodology

Codes listed below are used in SSTC methodology, a general description of each code is given in the appendix page 203 :

- HELIOS – libraries of neutronic constants XS preparation
- DYN3D – power history in core fuel rod
- RELAP – T/H boundary conditions of fuel rod under LOCA
- TRANSURANUS (v1m3j21) – behaviour of fuel rod under normal conditions and during LOCA
- SCALE – calculation of libraries of accumulation of gaseous fission products during burnup (depletion sequences T6-DEPL)

To prepare the initial data on the power history and burnup of fuel rods before the start of the LOCA, the calculation of the VVER-1000 (V-320) reactor core was carried out. For calculations, a four-year fuel cycle based on fuel assemblies of the TVSA type was chosen. Four cycles are calculated. Cycle refueling schemes are selected by the implemented fuel cycles at Ukrainian NPPs. Initial data on fuel and core design are presented below.

Initial data

The general view of the TVSA FA is shown in Figure 53 [82] . The design of the fuel assemblies of the TVSA type uses stiffening plates in the FA corners to improve geometric and mechanical stability.
The relevant design characteristics and material data of the TVSA needed for modelling are provided in Table 25. Data on the materials and compositions used in the design of the stiffening angels also are provided in Table 25.

The several core loadings use fuel assemblies of TVSA design with different enrichment, different numbers of fuel pins with different enrichment (radial profiling) as well as different pin numbers (pins) with burnable absorber and weight percentage of the burnable absorber material Gd_2O_3 mixed with different enriched UO_2 fuel. The various TVSA FA configuration designs used in the reactor core loading patterns are listed in Table 26. Table 25, Table 26 and Figure 53 also provides the design data for the fuel pins with burnable absorber and the control rods (CRD). The pin lattice layouts of the different FA types are shown in Figure 54, Figure 55.

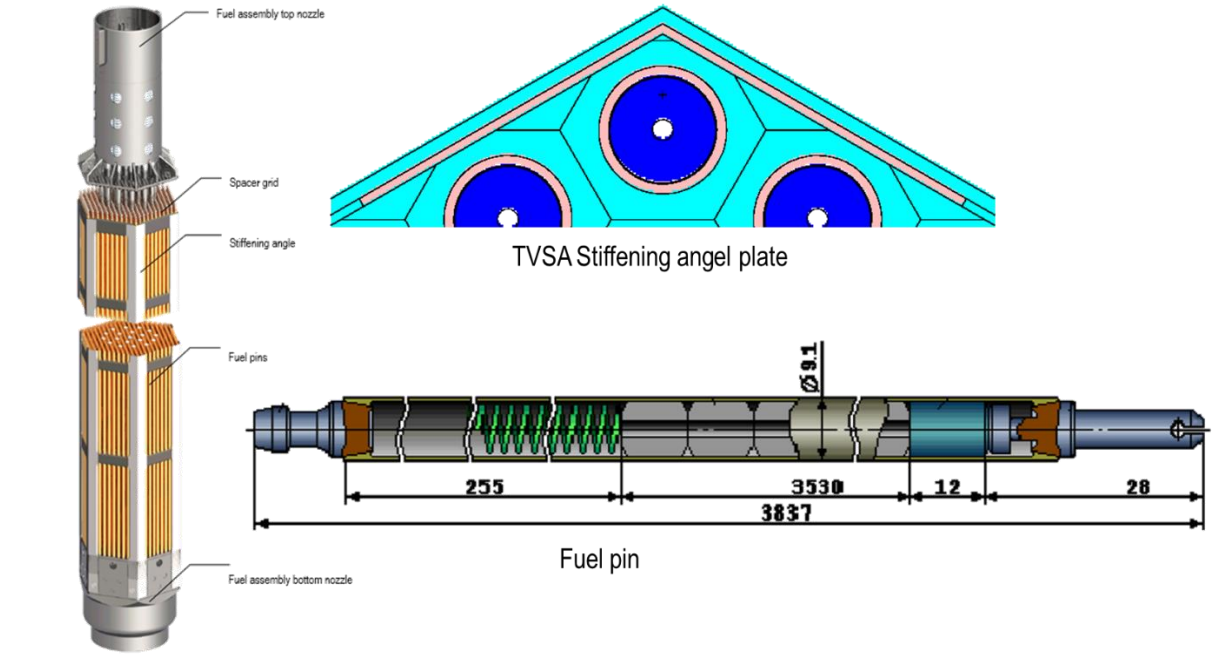

Figure 53: TVSA fuel assembly, stiffening angel plate and fuel pin

Description of the FA design data	Value
General Design Data	
Length of TVSA, mm	4570
Mass of TVSA, kg	ca. 730
Assembly pitch, mm	234,8
Assembly lattice pitch in the core, mm	236.0
Lattice type	hexagonal
Number of pins in the TVSA	312
Mass of UO_2 or (UO_2+Gd_2O_3) in TVSA, kg	494,4±4,5
Fuel pin rod	
Number of fuel pins	312
Lattice layout	uniform triangular
Lattice pitch, mm	12,75
Outer diameter of the pins, mm	9,10
Inner diameter of the pin clad, mm	7,73
Material of the fuel pin cladding	alloy Э110
Composition, %	98.97 Zr+1 Nb+ 0.03 Hf

Description of the FA design data	Value
Density, g/cm^3	6.4516
Material of the fuel pellet	sintered UO_2
Mass of the fuel UO2 in the fuel pin, kg	ca. 1,585
Length of the fuel column in the pin (cold), mm	3530
Outer diameter of the fuel pellet, mm	7,57
Diameter of the pellet central hole, mm	1,40
Fillgas pressure, MPa (at 20 °C)	2.0
High free volume, mm	352.0
Burnable absorber pin	
Number of Gd absorber rods in the TVSA	6
Absorber material	Gd_2O_3 [4]
Mass fraction of Gd_2O_3 in the fuel of the absorber rods, % w/o	5
Fillgas pressure, MPa (at 20 °C)	2.0
Guide Tubes	
Number of guide tubes	18
Material	alloy Э635
Composition, %	98.47Zr+1Nb+0.5Fe+0.03Hf
Density, g/cm^3	6.55
Outer diameter, mm	12,6
Inner diameter, mm	10,9
Central Guide Tube	
Material	alloy Э635
Composition, %	98.47Zr+1Nb+0.5Fe+0.03Hf
Density, g/cm^3	6.55
Outer diameter, mm	13,0
Inner diameter, mm	11,0
Spacer grids	
Number along the FA height	15

[4] the gadolinium with natural abundance of isotopic composition is used:
^{152}Gd - 0.20%, ^{154}Gd - 2.18%, ^{155}Gd - 14.80%, ^{156}Gd - 20.47%, ^{157}Gd - 15.65%, ^{158}Gd - 24.84%, ^{160}Gd - 21.86%.

Description of the FA design data	Value
Number in the active part of the core	13
Material	alloy Э110
Composition, %	98.97 Zr+1 Nb+0.03 Hf
Density, g/cm^3	6.45157
Mass of one spacer grid, kg	0,55
Stiffening angel plates	
Number	6
Material	alloy Э635
Composition	98.47Zr+1Nb+0.5Fe+0.03Hf
Density, g/cm^3	6.55
Width, mm	25
Thickness, mm	0,65
Control rod cluster	
Number of control rods	18
Absorber material of the control rods - upper part - lower part	 B_4C $Dy_2O_3 \bullet TiO_3$
Length of the absorber column, mm - general - upper part - lower part	 3500 3200 300
Density of the absorber material, g/cm^3 - upper part (B_4C) - lower part ($Dy_2O_3 \bullet TiO_3$)	 1,8 5,1
Composition of B_4C, %	^{10}B14.3346, ^{11}B63.918, C 21.736
Composition of ($Dy_2O_3 \bullet TiO_3$), %	^{10}O29.647, ^{11}Ti37.020, ^{158}Dy0.0338, ^{160}Dy0.7808, ^{161}Dy6.3369, ^{162}Dy8.5047, ^{163}Dy8.3050, ^{164}Dy9.3717
Outer diameter of the control rod clad, mm	8,2
Thickness of the control rod clad, mm	0,6
Material of the control rod clad	steel 08X18H10T
Density of the control rod clad, g/cm^3	7.75
Composition, %	0.08C, 18.5Cr, 10.5Ni, 1Ti ,69.92FE

Table 25 : Basic design data of the fuel assemblies TVSA and their components

FA Design	FA Type	Enrichment/ Pu_{fiss}-content (w/o %)	No. of UO_2 pins / enrichment	Number of Gd-pins (w/o Gd_2O_3/^{235}U)	Diameter of the central hole, (mm)
TVSA	398GO	3.99	306 / 4.00	6 (5.0/3.3)	1.4
TVSA	439GT	4.39	306 / 4.40	6 (5.0/3.6)	1.4

Table 26 : TVSA FA types used in the reactor core loading patterns

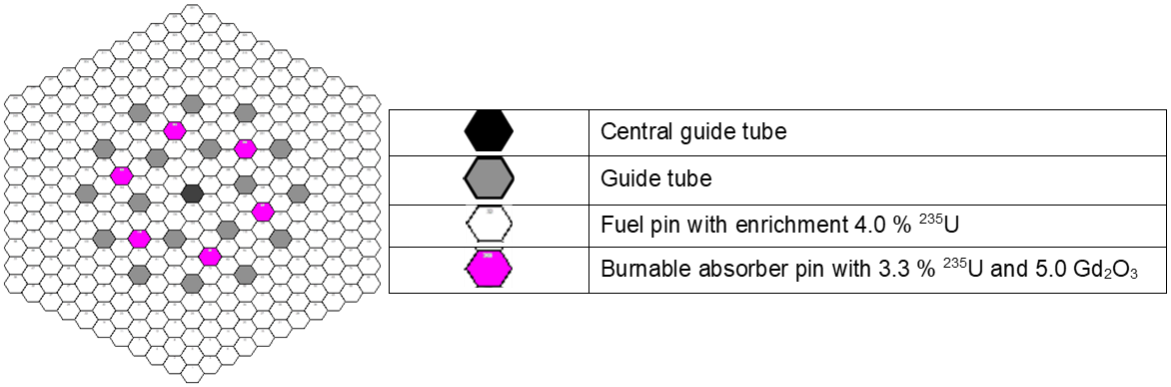

Figure 54: Pin layout of fuel assembly type 398GO

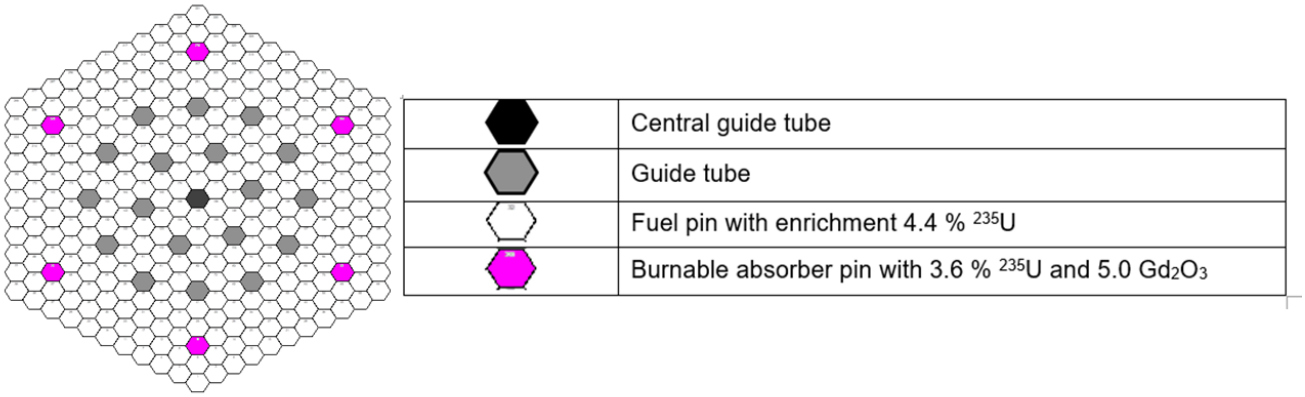

Figure 55 : Pin layout of fuel assembly type 439GT

Core description

The general characteristics of the VVER-1000 core are presented in Table 27. The duration of all 4 cycles are presented in Table 28. The schemes reloading of fuel assemblies are the same for all cycles are presented in Figure 56. The types of fuel and the year of their operation in the core are shown in Figure 57 and Figure 58. The numbering of the cassettes in the core and the numbering of the fuel rods in the cassette are shown in Figure 59 and Figure 60.

Items	Value
Number of fuel assemblies	163
Power, MW	3000.0
Coolant temperature at the core inlet T_{in}, °C	287.0
Position of CR, cm from the bottom	318.6
Core mass flow rate, kg/s	22000.0
Coolant pressure at the upper boundary of the core, MPA	16.0

Table 27 : General data for core operational

Cycle	Length, fpd
A	287.8
B	305.1
C	304.1
D	303.0

Table 28: Length of cycles

FA 439GT

2	22	154	122
3	30	135	163
4	32	110	121
5	145	152	158
9	11	20	
13	123	21	8
16	100	137	157
17	85	39	76
24	47	46	
25	73	129	107
26	40	84	111
36	45	131	149
37	65	86	102
48	72	108	93
49	28	114	98
61	130	104	89
63	38	51	
74	120	59	14
90	44	105	150
101	126	113	
103	34	60	75
115	136	50	66
116	92	56	71
127	99	78	62
128	119	33	15
138	124	80	53
139	91	35	57
140	117	118	
147	79	125	88
148	64	27	7
151	41	143	156
155	153	144	82
159	19	12	6
160	132	54	43
161	134	29	1
162	142	10	42

FA 398GO

55	133	96	146
67	112	83	87
70	106	95	141
94	58	69	23
97	52	81	77
109	31	68	18

Figure 56 : Reload pattern for all cycles

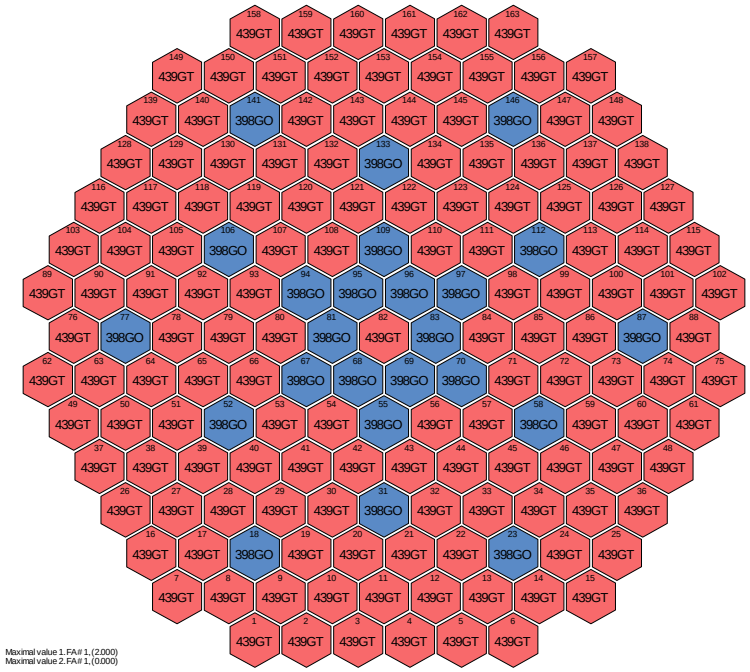

Figure 57 : Core loading pattern of the all cycles

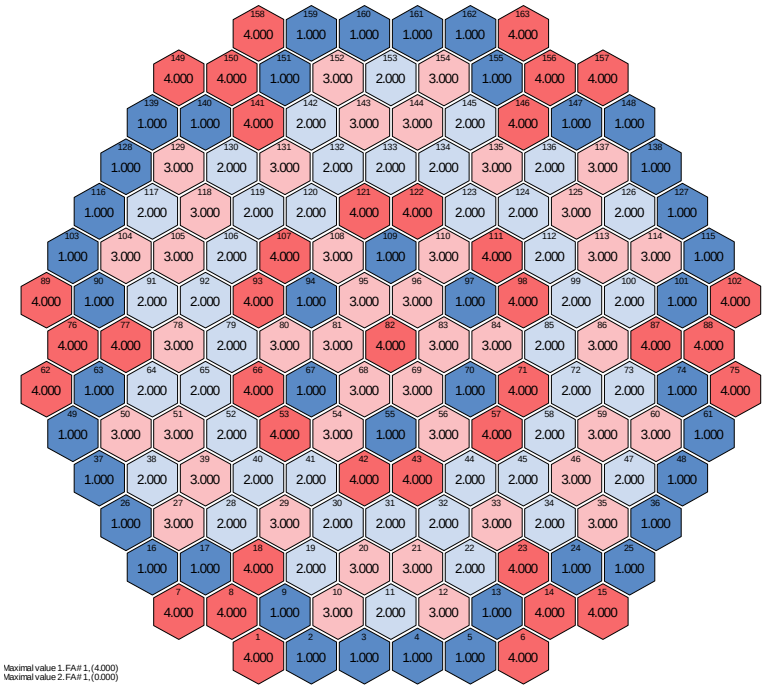

Figure 58 : FAs years of operation for all cycles

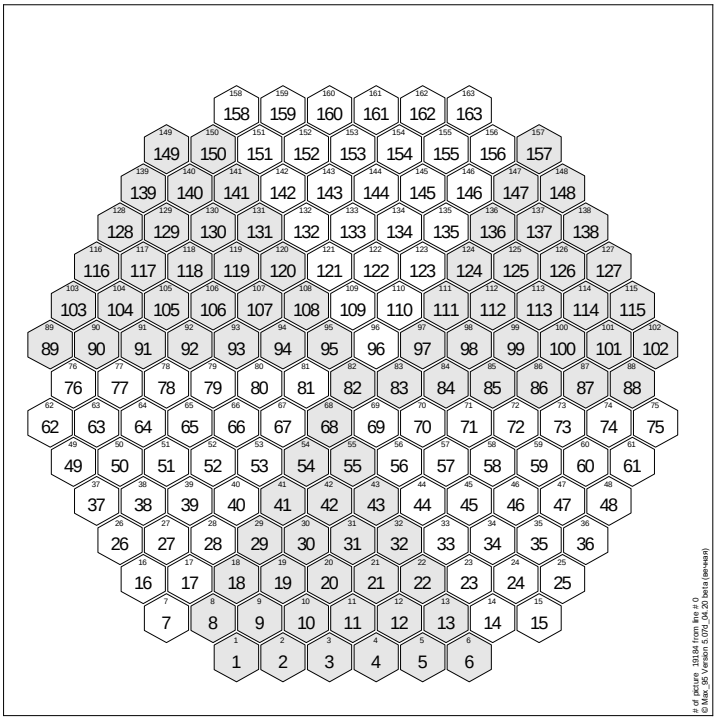

Figure 59 : Core numbering

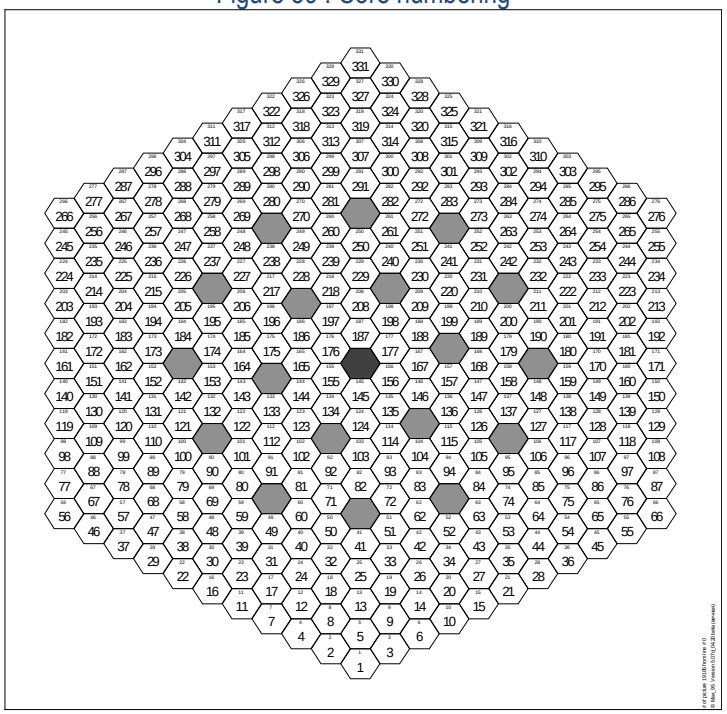

Figure 60 : FA numbering

Core calculation results

As a result of core calculations, the characteristics of power history and burnup of all fuel rods of all fuel assemblies for the entire core were determined. Obviously, for the subsequent calculation of the behavior of fuel rods during LOCA, considerable interest is the rods with the maximum power. They have the highest probability of failure and release of gaseous fission products. Below in this section, the results of the analysis of the distribution of fuel rod power are namely presented number of fuel rods with different power for different moments of the cycle is estimated. The relative power of fuel rod Kr was chosen for evaluation. All estimates are given for calculations at a rated power of 3000 MW without taking into account correction factors and engineering margins. Figure 61 shows the change in the maximum value of Kr during the cycle. It can be seen from the presented data that the maximum is reached for the cycle time of about 10 fpd. Figure 62 shows the distribution of fuel rods with different power Kr for a cycle time 10 fpd. Similar data for the cycle moments 105 fpd and 303 fpd are shown in Figure 63 and Figure 64.
Another important characteristic for the analysis of LOCA is the burnup of fuel rods with high values of power. The activity that enters the primary circuit from failed fuel rods depends on their burnup and the accumulation of fission gases. Burnup of fuel rods with power Kr>1.40 for the beginning of the cycle is shown in Figure 65. For fuel rods Kr>1.40 burnup doesn't exceed 20 MW*days/kgU, Kr>1.45 10 MW*days/kgU.

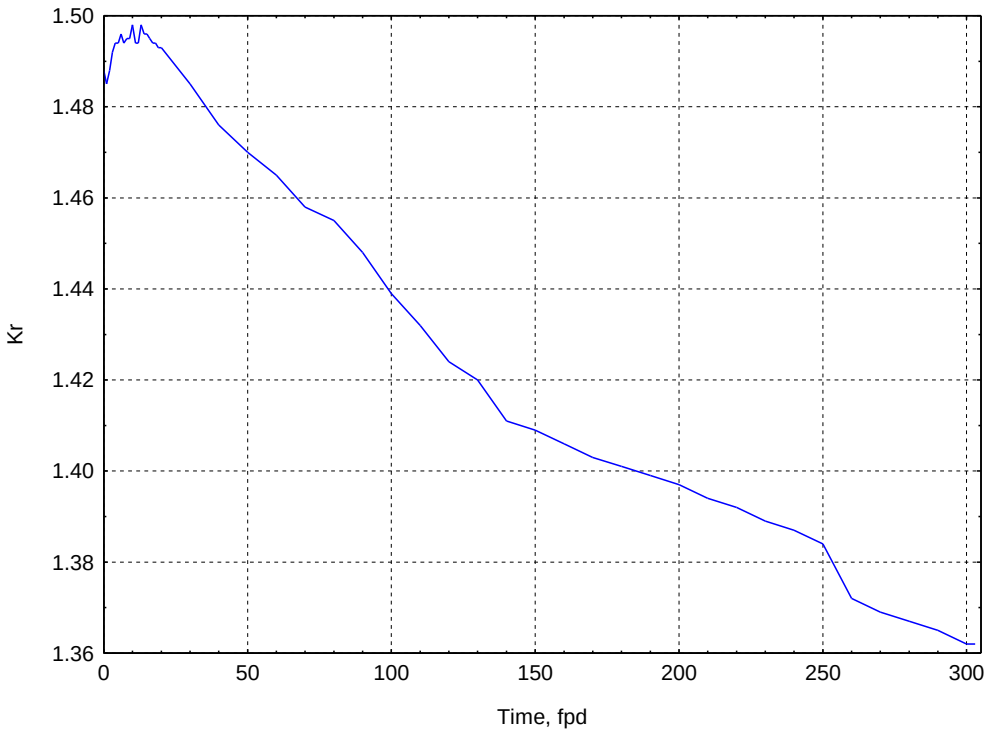

Figure 61 : Maximal Kr during cycle

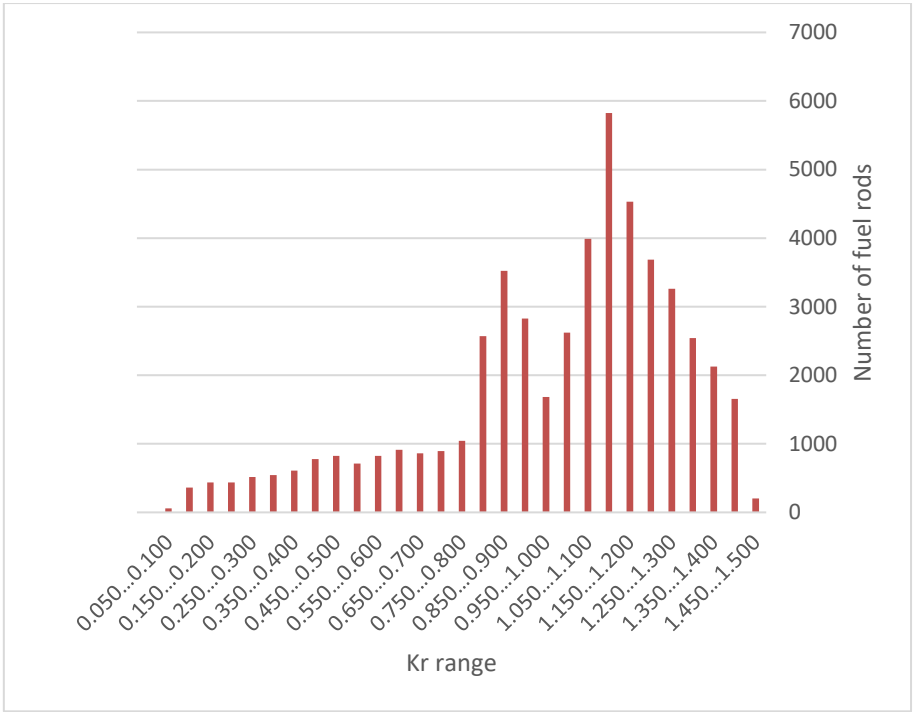

Figure 62 : Distribution of fuel rods with different relative power Kr for a cycle time T=10 fpd

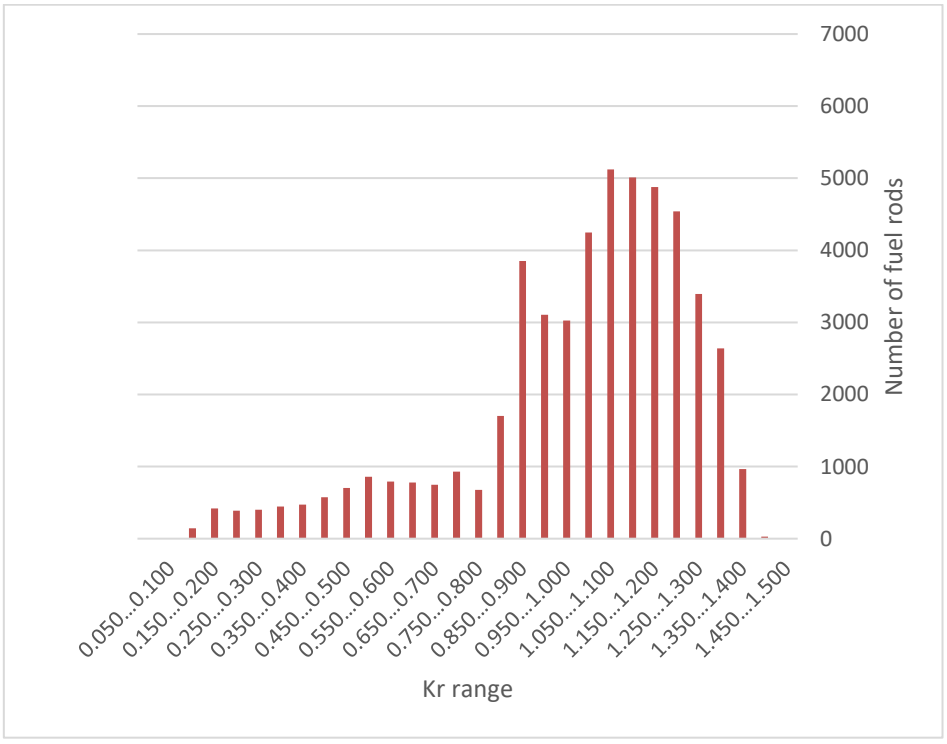

Figure 63 : Distribution of fuel rods with different relative power Kr for a cycle time T=105 fpd

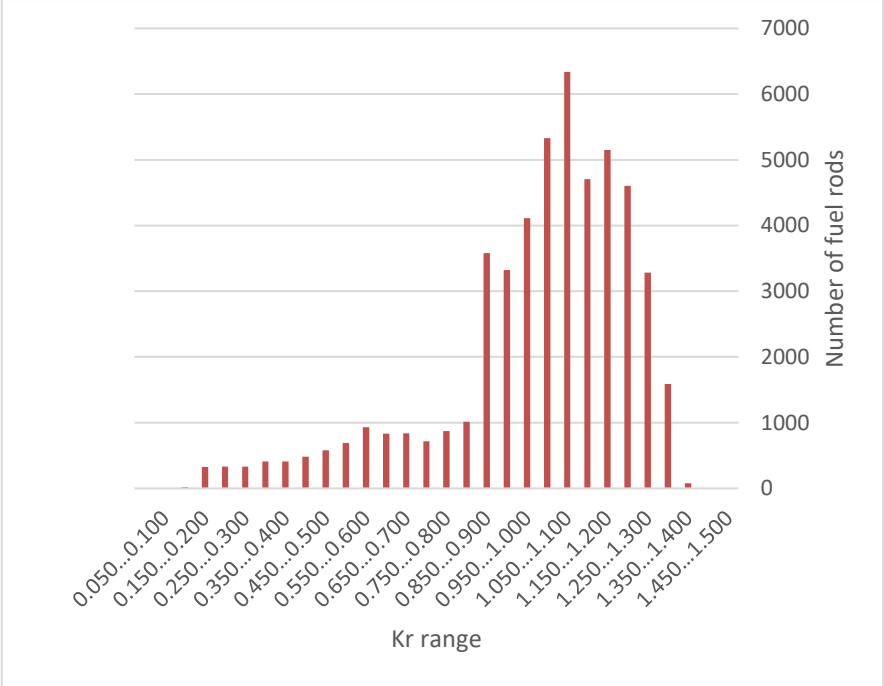

Figure 64 : Distribution of fuel rods with different relative power Kr for a cycle time T=303 fpd

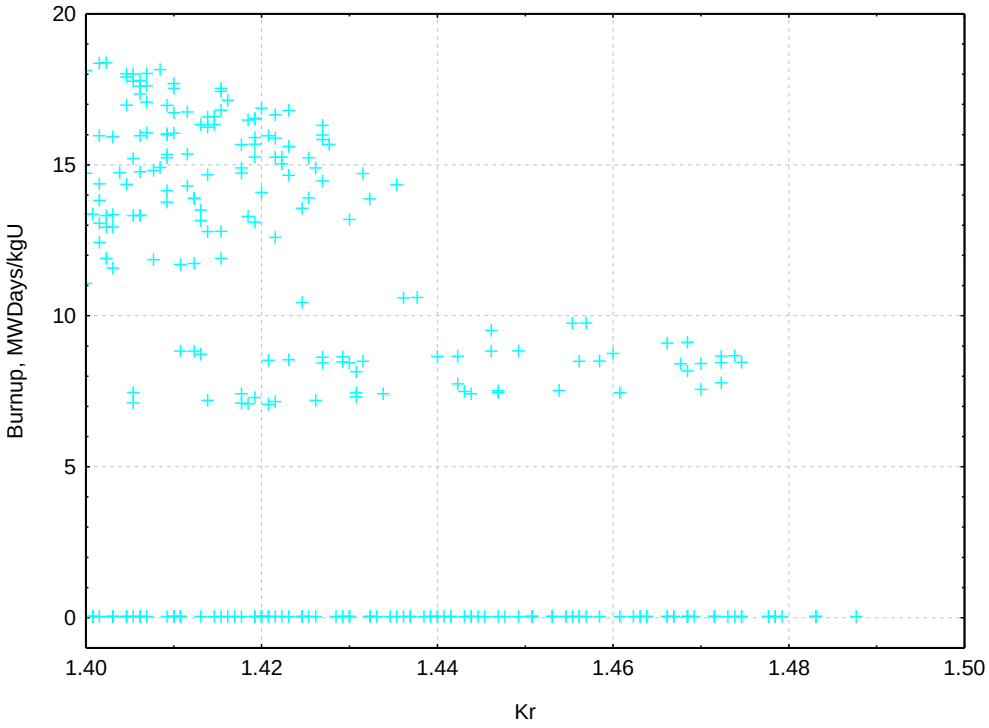

Figure 65 : Burnup of fuel rods with relative power Kr=1.4…1.5 for the beginning of the cycle

LOCA

General methodology:

The general procedure for the calculations performed is as follows. In the first stage, the power of fuel rods was calculated for four cycles using the DYN3D code. The calculation results are stored in separate libraries for all four cycles. In parallel with this, boundary conditions were calculated for modeling the behavior of fuel rods during LOCA. Boundary conditions (external fuel cladding temperature Tout and external coolant pressure Pout during LOCA) were calculated using the RELAP5 code in the form of libraries for various fuel-rods power Kr. Further, using the calculated power of fuel rods and libraries of boundary conditions for Tout and Pout, the behavior of fuel rods was simulated using the TRANSURANUS code (v1m3j21). DYN3D and TRANSURANUS calculations were performed for 20 axial layers along the core height. The split is uniform. Libraries of boundary conditions are prepared for 10 layers along the core height. The split is also uniform. When developing the fuel rod model for the TRANSURANUS code, the results of the FUMAC project were used to the maximum, including modeling the behavior of the VVER fuel rod in the LOCA (experiment IFA-650.11,[85] , [86]).

Also, within the framework of the project, libraries of accumulation of gaseous fission products during irradiation for various types of fuel rods were calculated. The calculations were performed using the SCALE, depletion sequences T6-DEPL software package (cf. p 214). Based on these libraries and the characteristics of the release of gaseous fission products from the fuel pellet under the cladding, the release of activity into the primary circuit from failed fuel rods was estimated.

The general calculation scheme is shown in Figure 66.

It is necessary to stop separately on the service module, which was developed as part of this project. The main function of this module is preparing input files for TRANSURANUS code, running of the code, selecting the necessary reference calculation results, and saving files to libraries.

Main features of the service module:

- formation of an input file for various types of fuel rods;
- formation of fuel rods load history before the LOCA. All cycles of operation of the fuel assemblies are taken into account, its movement in the core during refueling, power reduction schedules during shutdowns, and power increase at the startup of the cycle;
- formation of fuel rod power history and boundary conditions during LOCA based on the libraries of T/H boundary conditions and fuel rods power at the beginning of LOCA;
- adjustment (if necessary) of the fuel rod power Kr in the form of Kr×Keng separately for each fuel cycle;
- execution of the calculation for the full core, symmetry sector and individual assemblies;
- reading from the output files of the necessary reference calculation results;
- determination of the number of failed fuel rods during the LOCA;
- assessment of the activity release to the primary circuit from failed fuel rods;
- saving all input and output files for the possibility of performing additional calculations of individual fuel rods.

Below are examples of resulting tables that are generated by the service module based on the results of the calculations performed. Table 29 shows an example of data for the moment before LOCA, in Table 30 for LOCA. Table 31 shows an example of information on failed fuel rods during LOCA. Table 32 shows an example of information on the assessment of the activity release into the primary circuit from failed fuel rods.

An example, of the formation of the power history of a fuel rod before the LOCA is shown in Figure 67. An example of setting the boundary conditions - the temperature of the fuel cladding - during the LOCA is shown in Figure 68 (for K_{eng}=1.00).

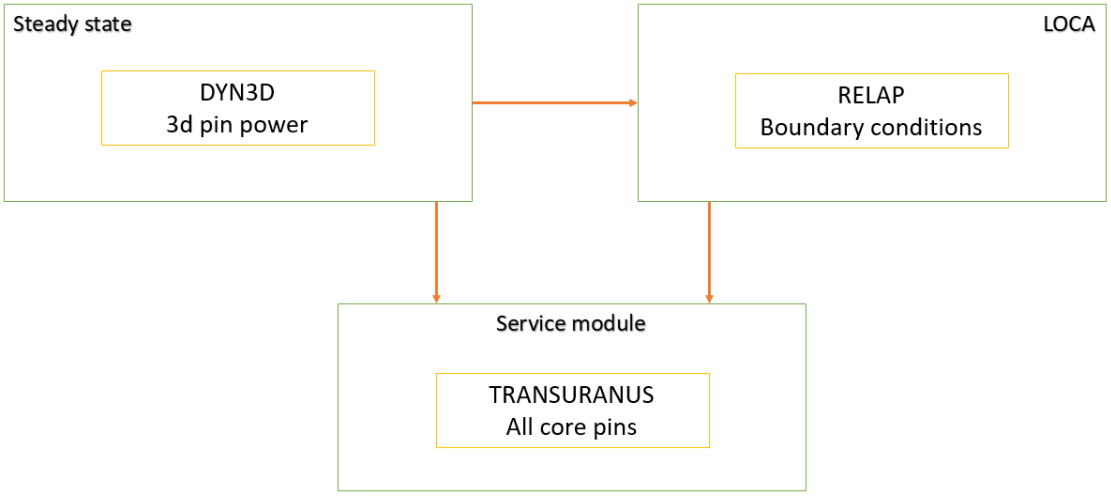

Figure 66 – The general calculation scheme

	time hrs	time sec	time msec	value	#FA	#FP	#AxL
Inner fuel radius, minimal (mm)	25251.0	3375.0	843.8	0.697	1	10	5
Inner fuel radius, maximal (mm)	16984.0	74.0	25.3	0.717	20	32	6
Outer fuel radius, minimal (mm)	8267.0	2469.0	44.4	3.802	43	193	20
Outer fuel radius, maximal (mm)	25252.0	368.0	843.7	3.891	18	272	6
Inner cladding radius, minimal (mm)	24770.0	1838.0	933.8	3.863	6	12	8
Inner cladding radius, maximal (mm)	8738.0	936.0	312.5	4.742	30	20	8
Outer cladding radius, minimal (mm)	24770.0	1838.0	933.8	4.538	1	9	15
Outer cladding radius, maximal (mm)	8738.0	935.0	312.5	5.335	30	20	8
Inner fuel temperature (°C)	8281.0	295.0	312.5	1296.648	11	307	10
Outer fuel temperature (°C)	481.0	695.0	960.4	1030.353	4	39	9
Maximal fuel temperature (°C)	8281.0	295.0	312.5	1296.648	11	307	10
Inner cladding temperature (°C)	481.0	685.0	960.4	926.823	9	278	10
Outer cladding temperature (°C)	481.0	685.0	960.4	924.163	9	278	10
Inner gas pressure (MPa)	25252.0	230.0	843.8	8.563	18	272	20
Fractional fission gas release (/)	25251.0	3213.0	528.1	0.019	1	282	0
ZrO2 layer thickness [mm].	25252.0	458.0	843.8	0.014	1	10	18
Average tangential stress in cladding, maximal (MPa)	24050.0	1840.0	32.5	122.994	1	9	4
Average tangential stress in cladding, minimal (MPa)	0.0	0.0	0.0	-92.720	31	194	1
Axial deformation, fuel (mm)	25252.0	368.0	843.7	70.922	18	272	20
Axial deformation, cladding (mm)	25252.0	351.0	843.7	31.695	18	272	20
Average enthalpy of the fuel (J/g)	481.0	695.0	960.4	332.366	4	39	9
Heat flux density (W/mm2)	22.0	1224.0	0.6	1.226	21	59	9
Averaged Burn-up in section or slice (MWd/kgHM)	25252.0	458.0	843.8	61.705	1	282	5
Averaged Burn-up of FP (MWd/kgU)	25252.0	78.0	843.7	56.157	1	10	0

Table 29 – Some data for the moment before LOCA

	time hrs	time sec	time msec	value	#FA	#FP	#AxL
Maximal fuel temperature (°C)	8281.0	295.0	312.5	1296.648	11	307	10
Inner cladding temperature (°C)	481.0	685.0	960.4	926.823	9	278	10
Outer cladding temperature (°C)	481.0	685.0	960.4	924.163	9	278	10
Inner cladding radius, maximal (mm)	8738.0	936.0	312.5	4.742	30	20	8
Outer cladding radius, maximal (mm)	8738.0	935.0	312.5	5.335	30	20	8
Gap width between fuel and cladding (um)	8738.0	944.0	312.5	883.648	11	64	8
Axial deformation, fuel (mm)	25252.0	368.0	843.7	70.922	18	272	20
Axial deformation, cladding (mm)	25252.0	351.0	843.7	31.695	18	272	20
Inner gas pressure (MPa)	25252.0	230.0	843.8	8.563	18	272	20
Fractional fission gas release (/)	25251.0	3213.0	528.1	0.019	1	282	0
ZrO2 layer thickness [mm]	25252.0	458.0	843.8	0.014	1	10	18
Equivalent Cladding Reacted ECR (%)	25252.0	458.0	843.8	1.712	1	10	18

Table 30 - Some data for LOCA

```
 Number of calculated rods - 8736
 Number of failured rods   -  908
 Time of fail, h (from LOCA start)
                minimal   -     0.1288786564D+00
                maximal   -     0.1700000000D+00
 Failured layers
      # of layer     1     2     3     4     5     6     7     8     9    10    11    12    13    14    15    16    17    18    19    20
      # of fails     0     0     0     0     0     0     0   712   220    18     0     0     0     0     0     0     0     0     0     0
```

Table 31 – Information on failed fuel rods during LOCA

	Activity, bq
cs134	0.111E+14
cs135	0.705E+08
cs137	0.156E+14
cs138	0.644E+15
cs139	0.604E+15
xe133	0.640E+15
xe135	0.213E+15
xe137	0.610E+15
xe138	0.595E+15
i129	0.330E+07
i131	0.317E+15
i132	0.466E+15
i133	0.676E+15
i134	0.769E+15
i135	0.639E+15
kr85	0.174E+13
kr85m	0.102E+15
kr87	0.204E+15
kr88	0.276E+15
Total	0.679E+16

Table 32 - Gap Gas release from failure FP, LOCA calculations

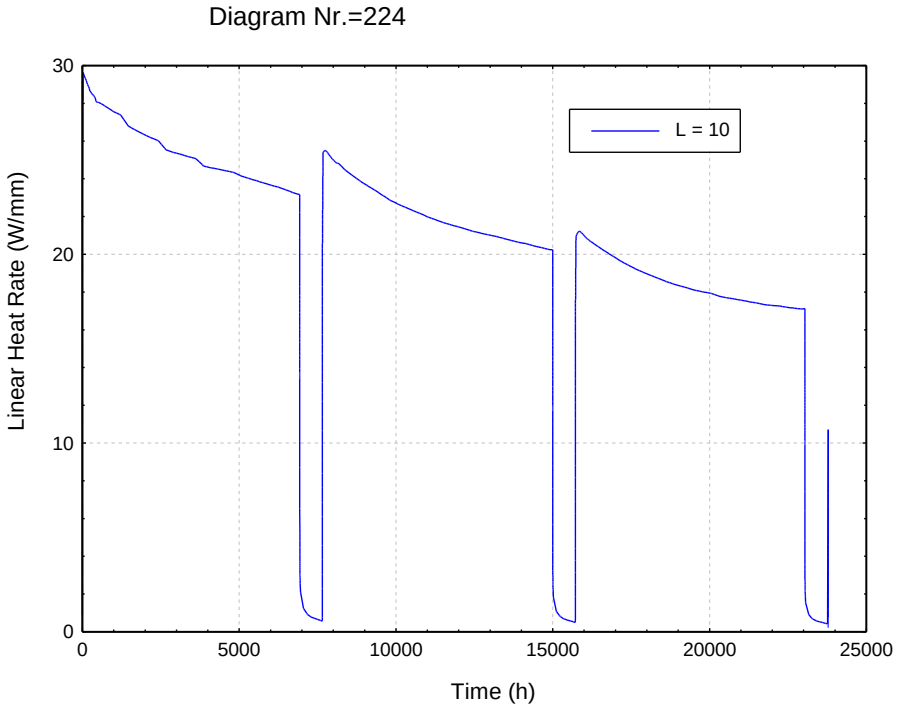

Figure 67 – Power history of a fuel rod before the LOCA

This project has received funding from the Euratom research and training programme 2014-2018 under the grant agreement n° 847656

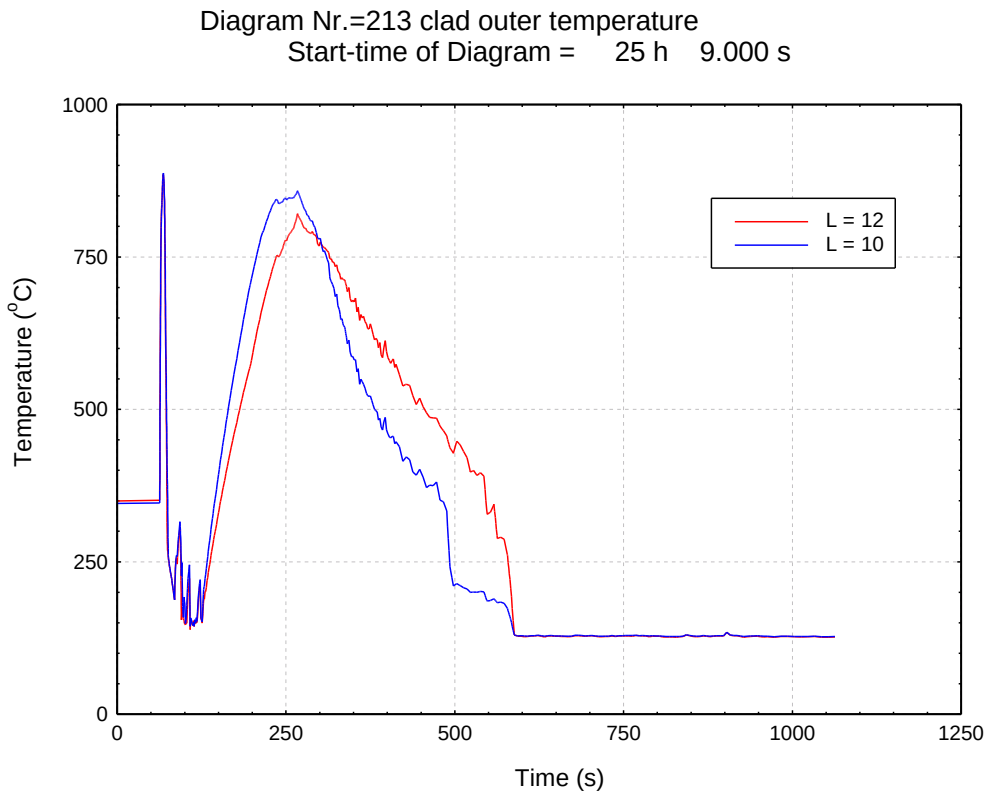

Figure 68: Boundary conditions - the temperature of the fuel cladding during LOCA of layer 10 and 12

Number of failed fuel rods

As mentioned above, the calculation of the behavior of the fuel rod during a LOCA was performed using the TRANSURANUS code. The standard code version v1m3j21 was used. Details on initialization parameters and models of importance regarding cladding burst prediction during the LOCA transient are summarized in Table 33.

Initialization	Imposed/calculated by	Grouping	Sensitivity analysis/studies
Rod Internal Pressure	Calculated by TRANSURANUS	rod	
Power	Neutronic code - DYN3D	3d core by rods	**Study on the impact of relative power ratio (Kr)**
Decay heat	Approximation	rod	
Initial temperature field	Outer cladding temperature imposed by RELAP and 2D from TRANSURANUS	rod	
BU	Calculated by TRANSURANUS	rod	
Cladding hydrogen content	Calculated by TRANSURANUS	rod	

Transient	Model type	Sensitivity analysis/studies
Transient fission gas release	Modelled : yes, stand alone model	
Axial gas transport in the gap	yes (TRANSURANUS)	
Zr alloy phase transition	yes (TRANSURANUS)	
Creep modeling	TRANSURANUS creep laws for E110 and Zr1Nb	
Radial/Axial fuel relocation before burst	no	
Burst criteria	Failure is assumed if the tangential stress or the tangential strain limit is achieved.	

Table 33 : Initialization parameters and key models regarding cladding burst used in SSTC methodology

Failure is assumed if the tangential stress or the tangential strain limit is achieved. The iclfail=1 and iclfail=4 options were used in calculations. Both options gave the same result in estimating the number of failed fuel rods. The calculations were carried out for a symmetry sector of 60°. Considering that the considered core is completely symmetrical, the use of the 60° symmetry sector is completely correct. The TRANSURANUS model used 20 axial layers along the core height. The split is uniform.
The calculation of the nominal parameters of the core (reactor power 3000 MW) at LOCA at the initial stage of the operation of the cycle (at the moment of maximum Kr) showed the absence of failed fuel rods. Using the ability of the service module to correct the value of rod power Kr×Keng at a value of Kr=1.513 (Keng≈1.02), 6 failed fuel rods appear (out of 50856, for the full core). Calculations were also made for Keng=1.20 and Keng=1.30 (cf. Table 34). For all calculations, the failure occurred in the 11th layer along the height of the core (numbering - from the bottom).

Table 34 - # of failure fuel rod for different K_{eng}

K_{eng}	# of failure fuel rod (from 50856, full core)
1.00	0
≈1.02	6
1.20	9390
1.30	16980
1.00 EOC	0
≈1.02 EOC	0

To assess the nature of the dependence of the number of failed fuel rods for different moments of the cycle, the LOCA calculation was carried out for different moments of the cycle. The calculation was made for increased relative power of the fuel rods (K_{eng}=1.20). The results are shown in Figure 69. It can be seen that although there is a decrease in Kr over the cycle, the increase in burnup (as a result of the residual decay heating and internal pressure) leads to an increase in the number of failed fuel rods with a maximum value at the end of the cycle. Taking into account the obtained increase in the number of failed fuel rods by the end of the cycle for K_{eng}=1.20, additional calculations were made at K_{eng}=1.00 and K_{eng}≈1.02 for the end of the cycle (EOC). In both cases, there are no failed fuel rods.

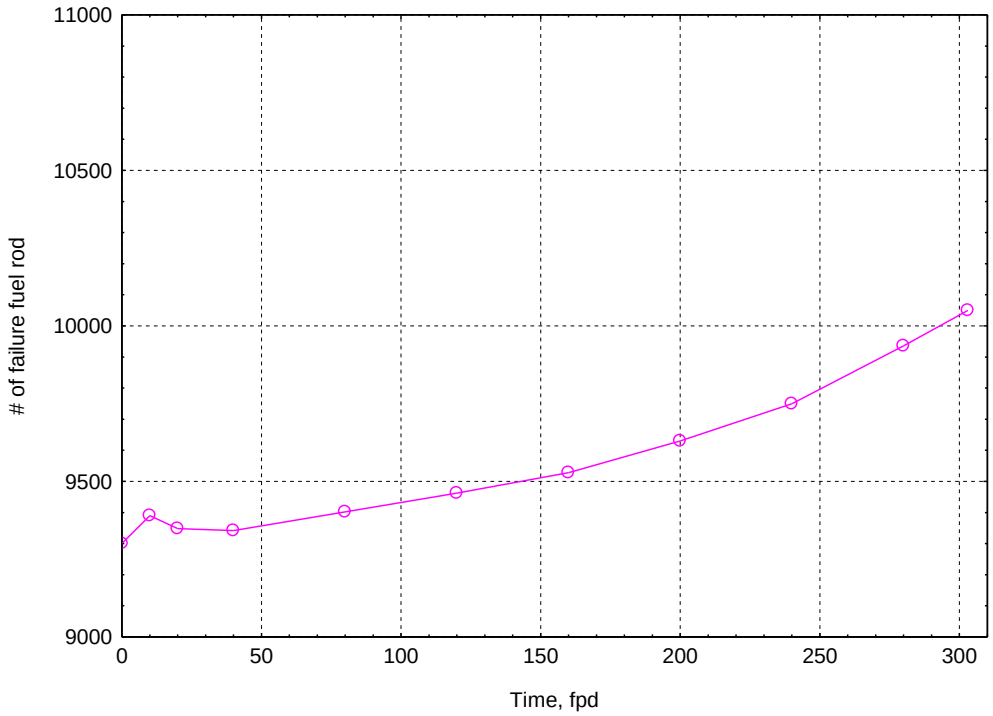

Figure 69 – # of failure fuel rod during cycle (Keng=1.20)

Results: Activity release to primary circuit

Estimation of activity release to the primary circuit from failed fuel rods is implemented in the service module based on the libraries of gaseous fission products accumulation during burnup for various types of fuel rods (A=f(bur), Bq) and characteristics of the release of gaseous fission products from the fuel pellet under the cladding (FGR). It was assumed that 100% of the gas from the cladding of failed fuel rods enters the primary circuit. The libraries for the accumulation of gaseous fission products take into account the following isotopes:

- Cs - 134, 135, 137, 138, 139
- Xe - 133, 135, 137, 138
- I - 129, 131, 132, 133, 134, 135
- Kr - 85, 87, 88

Taking into account that according to the results of calculations at the nominal parameters of the core (K_{eng}=1.00) there are no failed fuel rods, the activity calculation was carried out for increased power of fuel rods - K_{eng}=1.20 and K_{eng}=1.30 (cf. Table 35). For K_{eng}=1.20, the activity output was calculated for different moments of the cycle (Figure 70).

Table 35 - Gap Gas release activity from failure FP

K_{eng}	Activity, bq
1.20	0.679E+16
1.30	0.276E+17

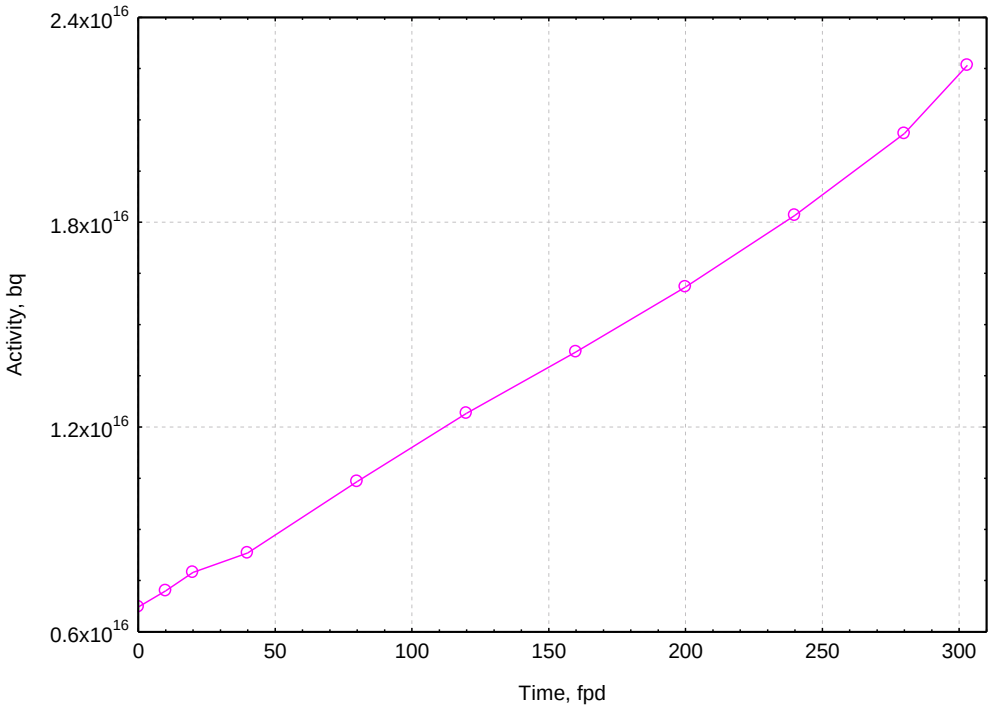

Figure 70 – Gap Gas release activity from failure FP during cycle (K_{eng}=1.20)

Conclusion

In the course of work on the R2CA, WP3.2 project (LOCA. Evaluation of the failed rod number), the following was done:

- calculation of power history of fuel rods for four cycles using the DYN3D code. Libraries of neutronic constants (XS) were calculated by the HELIOS code;
- based on calculations using the RELAP5 code, the boundary conditions (external temperature of the fuel cladding Tout and external coolant pressure Pout during LOCA) were determined in the form of libraries for various relative power of the fuel rod Kr;
- fuel rod models were developed for the TRANSURANUS code, including the possibility of modeling the behavior of a VVER fuel rod in LOCA;
- a service module has been developed that provides calculations of the behavior of fuel rods during normal operation of the reactor and a LOCA for all fuel rods in the core;
- libraries of accumulation of gaseous fission products during burnup were calculated for various types of fuel rods;
- calculations of the number of failed fuel rods in the LOCA were performed and the output of activity to the primary circuit was estimated.

The developed method for calculating the LOCA is ready for use at the SSTC NRS in the framework of studies of the consequences of the LOCA as state-of-the-art. If necessary, it can be adapted to other types of fuels and fuel cycles.

Integral approach

LEI : ASTEC and TRANSURANUS calculations

Principal aspects of LEI activities in this task are to provide calculations using the ASTEC code, complete calculation results with the TRANSURANUS code and evaluation of the failed rod number using ASTEC and TRANSURANUS codes.
Overall, LEI activities in task 3.2 could be divided in 4 main tasks and provided work:

1. Sensitivity analysis for the ASTEC oxidation parameters. The result of this task allows to estimate the influence of the different oxidation, creep, and cracking parameters on the calculation results. Also, this task will help for the selection of the modelling parameters for the reference calculations in task 2.3. Sensitivity results main focusing on to the cladding burst time, total hydrogen generation, and to see how these parameters influence the fission product release to environment.
2. Verification of the ASTEC calculation results with calculation results made by the TRANSURANUS code.
3. Different ASTEC nodalizations for the core region of BWR-4. The result of this study gives a more precise evaluation of the possible fuel assemblies ruptures during selected LOCA scenario in the DEC-A conditions. This task is led by the verification of the ASTEC calculation results with calculation results made by the TRANSURANUS code.
4. Detail analysis using the TRANSURANUS code and uncertainty quantification for the calculation results.

Details on initialization parameters and models of importance regarding cladding burst prediction during the LOCA transient are summarized in Table 36.

Initialization	Imposed/calculated by	Grouping	Sensitivity analysis/studies
Rod Internal Pressure	3MPa, the highest value, according [[87]]	Same for all rod groups	
Power	BE	Same for all rod groups	
Decay heat	Calculated by neutronic code - SCALE	Same for all rod groups	
Initial temperature field	Generic model of BWR was modeled. Initial temp. field was imposed according to the relevant temp. for BWR type reactors	Same for all rod groups	
BU	Burn up and initial fission inventory was calculated by neutronic code - SCALE	Same for all rod groups	
Cladding hydrogen content	Not considered		
Transient	**Model type**		**Sensitivity analysis/studies**
Transient fission gas release	Yes, modelled by ASTEC		zirconium oxidation physical laws (Cathcart, Urbanic, Prater), the minimum temperature to start the reaction of oxidation, maximal hoop creep allowed before burst and axial extension of the cracking after the clad burst. ASTEC Parameters varied: CATHCART; URBANIC; PRATER; TBEG; EPMX; CRAC
Axial gas transport in the gap	No, for the transport of FP the SOPHAEROS module was used		
Zr alloy phase transition	No		
Creep modelling	Norton, …, H impact? O impact? Phase dependence		
Radial/Axial fuel relocation before burst	No		
Burst criteria	EDGAR model on hoop stress + maximum hoop strain 40% (EPMX)		

Table 36 : Initialization parameters and key models regarding cladding burst used in ASTEC LEI calculations

Sensitivity analysis for the ASTEC modelling parameters

The sensitivity calculations were performed in order to evaluate several ASTEC modelling parameters impact on fuel rod failure time, hydrogen generation, and then on the source term prediction. It is obvious that the biggest influence on the fuel rod failure is linked to the choice of the burst criterion model available in the ASTEC code. In ASTEC [87], [89] 3 different burst criteria models can be used to determine the cladding rupture event: NUREG, CHAPMAN and EDGAR:

- The NUREG-630 model [[90]], based on a correlation between the cladding strain and the burst temperature. Two different strain limits are available depending on heat-up rate (≤10K/s or ≥ 25K/S).
- The CHAPMAN model, setting a temperature limit versus engineering hoop stress depending on thea heat-up rate (up to 28 K/s [[91]].
- The EDGAR model setting a true hoop stress limit depending on the alpha phase fraction. this burst criterion is derived from French EDGAR experimental on Zry-4 alloy.

It must be outlined that, in ASTEC, only EDGAR and CHAPMAN are alternative concurrent models. The NUREG-630 and the simple user criterion on a contact strain limit can be used only in combination with EDGAR or CHAPMAN models. The NUREG-630 model can be activated or deactivated by users.

In the frame of the R2CA project, ENEA provided sensitivity analysis on above mentioned burst criteria with ASTEC. This analysis confirmed a high sensitivity of calculation results to the burst criteria. Taking this information into account for LEI calculations it was decided to fix the burst criteria model and to vary other parameters. EDGAR model is used for the reference case calculations, and it was fixed for the further analysis. In total 6 calculations (Table 37) were provided. In each calculation case only one parameter was changed. Sensitivity was provided for: zirconium oxidation physical laws (Cathcart, Urbanic, Prater), the minimum temperature to start the reaction of oxidation, maximal hoop creep allowed before burst and axial extension of the cracking after the clad burst.
Calculation results using different parameters are presented in Figure 71 - Figure 75.

Table 37. Different parameters for the sensitivity analysis

Case 0	Basic	Zirconium oxidation physical law - BEST-FIT TBEG (minimum temperature to start the reaction of oxidation) – 700 K Burst parameters: EPMX 0.25; CRAC 0.50.
Case 1	CATHCART	Zirconium oxidation physical law - CATHART
Case 2	URBANIC	Zirconium oxidation physical law - URBANIC
Case 3	PRATER	Zirconium oxidation physical law - PRATER
Case 4	TBEG	TBEG (minimum temperature to start the reaction of oxidation) – 600 K
Case 5	EPMX	EPMX (maximal hoop creep allowed before burst, involving then the clad to burst immediately when fulfilled) - 0.4 (standard value according to manual)
Case 6	CRAC	CRAC (axial extension of the cracking after the clad burst) - 0.0 (standard value according to manual)

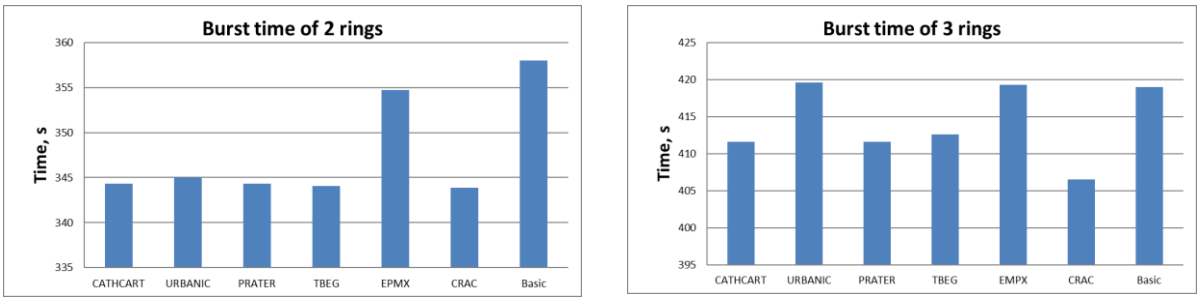

(a) (b)

Figure 71. Cladding burst time: a) the second ring, b) the third ring

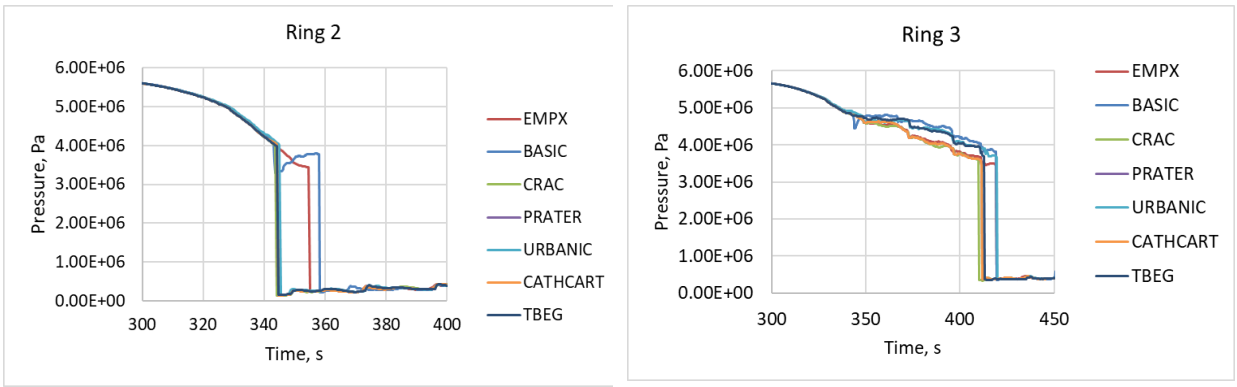

(a) (b)

Figure 72. Fuel internal pressure: a) the second ring, b) the third ring

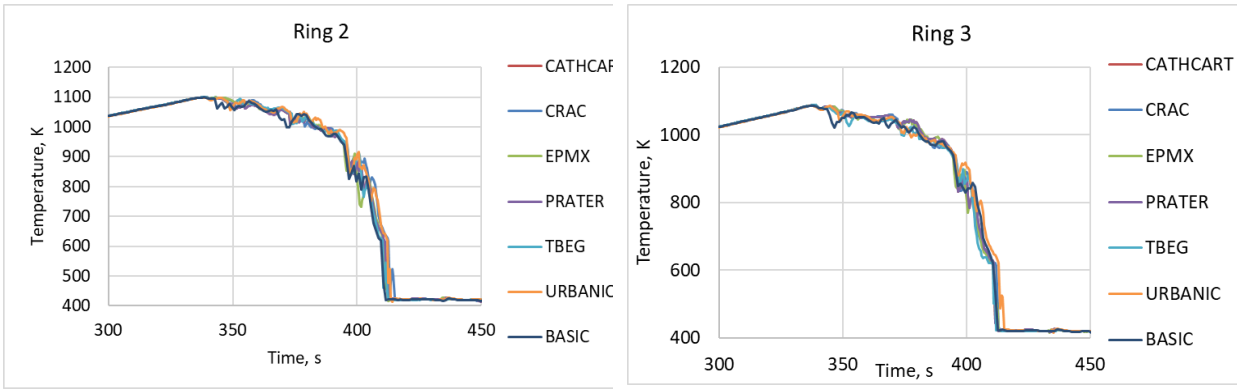

(a) (b)

Figure 73. Peak cladding temperatures: a) the second ring, b) the third ring

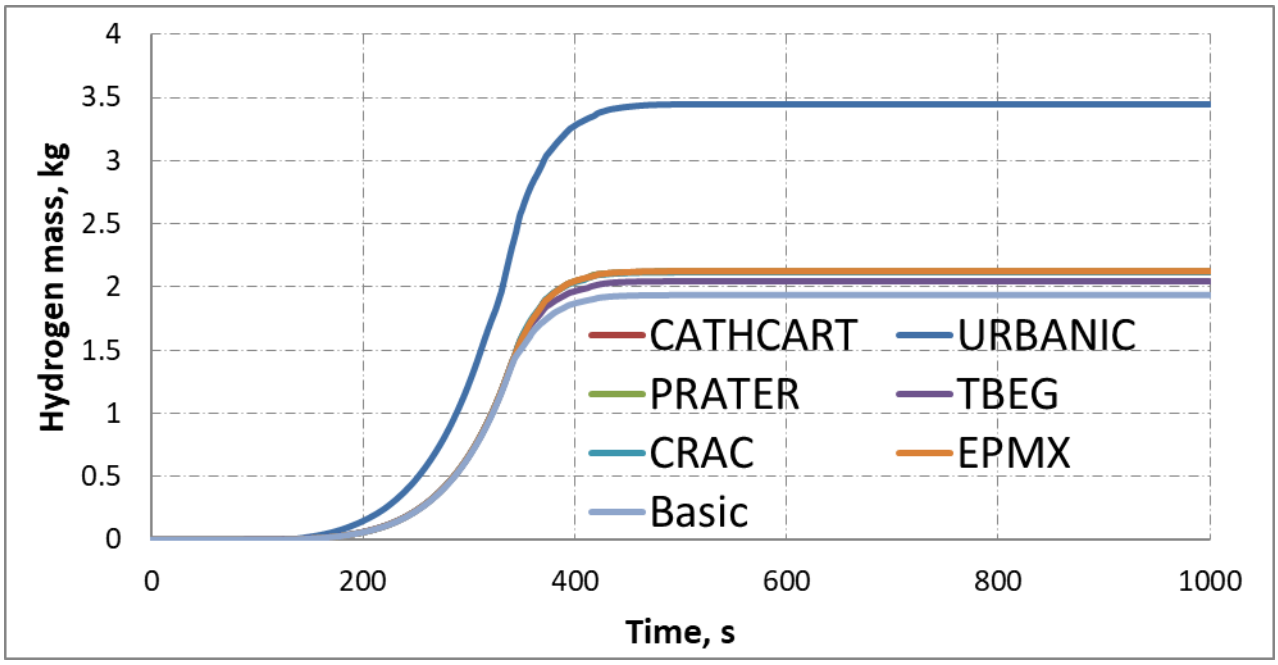

Figure 74. Total hydrogen generation

(a)

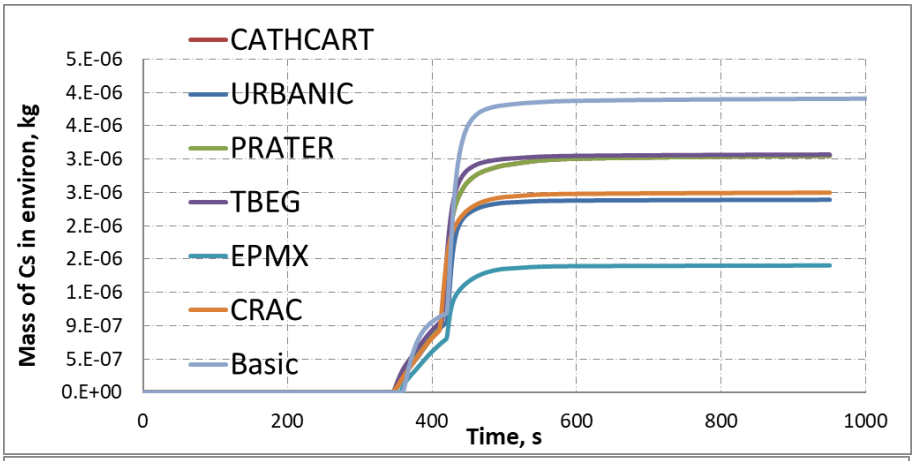

(b)

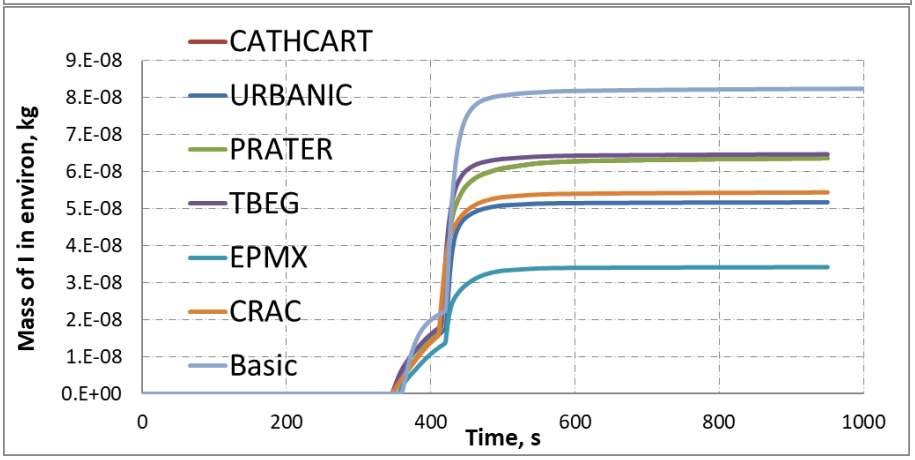

(c)

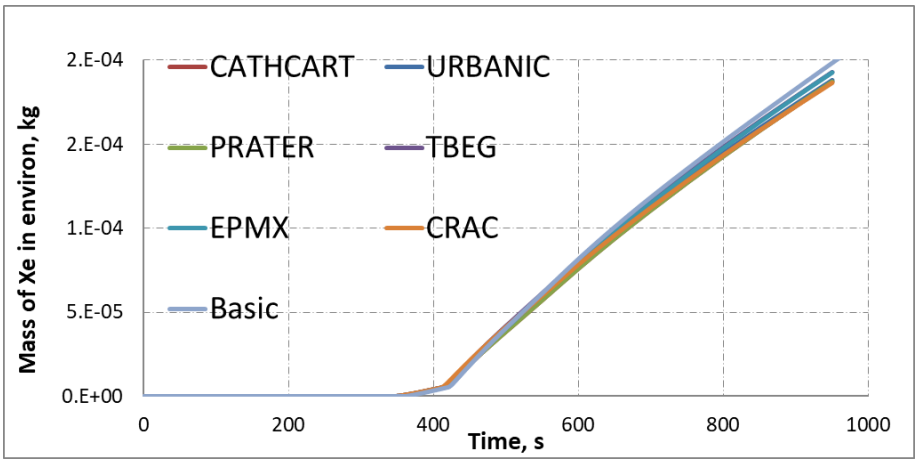

Figure 75. Fission product release to the environment: a) Cs mass, b) I mass, c) Xe mass

Conclusions

The result of provided sensitivity analysis showed that parameters have a small effect on the cladding burst time. The latest burst time was achieved using a standard value according to the manual for the EPMX parameter and is very close result as the basic calculation result (see Figure 71).
Influence of the analysed parameters to the fuel internal pressure and maximal temperatures have also minimal impact to the calculation results (see Figure 72 and Figure 73)
Analysing hydrogen generation and the fission product release, it was observed a significant influence. Using URBANIC zirconium oxidation physical law the highest amount of total hydrogen was calculated. The result was ~60% higher compared to other calculation results. Using PRATER zirconium oxidation physical law and changing TBEG the higher fission product release in the environment was achieved.
Parameter indicating the minimum temperature to start the reaction of oxidation (TBEG) have a significant influence on fission product release calculations, especially for Zs and I (see Figure 75). However, for the gaseous fission products (for example Xe) the difference is minimal.

Verification of the ASTEC calculation results with TRANSURANUS code.

For the analysis in the R2CA project the LEI considered a generic Boiling Water Reactor (BWR) of class 4 with Mark I containment. The thermal power of the reactor is 2381 MW. The calculation results of the basic ASTEC BWR model considered analysed LOCA accident showed rupture of two concentric rings. With this basic model nodalization concept corresponds to the 55% of all active zone claddings rupture. To verify the ASTEC calculation results the calculations were provided using TRANSURANUS code.

TRANSURANUS modelling parameters and assumptions

For thermomechanical analysis two cases were considered:

I) Axial cladding temperature profile is homogenic. Temperatures in all axial segments are equal.
II) Axial cladding temperature profile is heterogenic. Each axial segments have specific temperatures taken according to ASTEC calculation results.

Outer cladding temperatures are imposed for LOCA case. This is achieved by setting the infinitely large heat transfer coefficient and assigning previously calculated outer cladding temperatures to the coolant.
BWR fuel rod model with a total length of 4081.4 mm is considered. Pellet diameter, inner cladding, outer cladding diameters are 8.67, 8.84, 10.5 mm respectively. Cooling channel of rod is presented in Figure 76 and has 27.500

mm hydraulic diameter. Lower plenum is 388.60 mm in length. Pressure in plenum is 3 MPa. Fill gas is helium. Fuel pellets are made of Uranium Oxide with 3.987 % U-235 enrichment. This value corresponds to the average enrichment between all rod fuels in BWR ATRIUM-10 design. For cladding material Zirconium is considered.

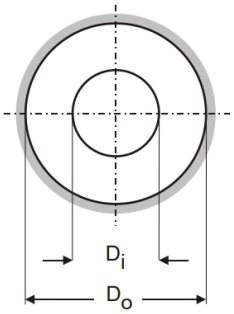

Figure 76. Fuel Rod hydraulic cross-section [[87]]

TRANSURANUS native modelling parameters. URGAS-model is used for fission gas release. Empirical model of densification is used. Visco-elastic treatment of creep in the fuel and explicit treatment of creep in the cladding are assumed. Oxygen redistribution is not considered. An interaction layer between fuel and cladding is considered in the gap conductance model. Relocation volume is treated as a free volume. Surface boiling is assumed. Grain growth model of Ainscough and Olsen is considered. The Hydrogen content is not considered. No stress dependent fission gas release and swelling model is considered. 0.001 mm of oxide layer is considered at the start of irradiation. Details on initialization parameters and models of importance regarding cladding burst prediction during the LOCA transient are summarized in Table 38.

Initialization	Imposed/calculated by	Grouping	Sensitivity analysis/studies
Rod Internal Pressure	3MPa, the highest value, according [[87]]	Single rod calculations	
Power	BE, according to ASTEC calculations		
Decay heat	Power taken according to ASTEC calculations		
Initial temperature field	Initial temp. taken as for ASTEC calc.		
BU	Burn up is calculated by TRANSURANUS code according to the giving power history.		
Cladding hydrogen content	No		
Transient	**Model type**		**Sensitivity analysis/studies**
Transient fission gas release	No		oxide layer thickness (initial and before the transient). Full Uncertainty and sensitivity analysis have been provided. Selected uncertain parameters: Pellet radius; Inner cladding radius; Outer cladding radius; Gap pressure; Outer pressure. Burst parameters: Overstress; stress/strain; epslim[1]; strlim[2].
Axial gas transport in the gap	No		
Zr alloy phase transition	Dynamic model		
Creep modeling	Norton, alpha-phase, (beta phase starts from ~900 C, which we did not reach in current calculations)		
Radial/Axial fuel relocation before burst	Relocation in gaps between pellets, Modified KWU relocation model		
Burst criteria	True tangential stress (material specific temperature and oxidation level dependence), plastic instability criterion (effective true strain and the strain rate), radially averaged true tangential permanent strain.		

[1] epslim - effective strain limit for plastic instability

[2] strlim - effective strain rate limit for plastic instability (1/h)

Table 38 : Initialization parameters and key models regarding cladding burst used in TRANSURANUS LEI calculations

As for the irradiation scenario (prehistory) region 3 scenario (Figure 77 and Figure 78) was considered. It lasts for roughly 1000 days and has three break periods. During this phase an average linear power equal to 14.3 kW/m is

assumed. Neutron flux was calculated from the derived relationship between neutron yield and linear heat rate from the previous calculations and it stands as $6 \cdot 10^{12}$ neutrons per kW/m. Prehistory provides some cumulative strain such as creep strain that furthers influence the rupture possibility in cladding. So far, the selection of prehistory brings some degree of uncertainty to the work presented.

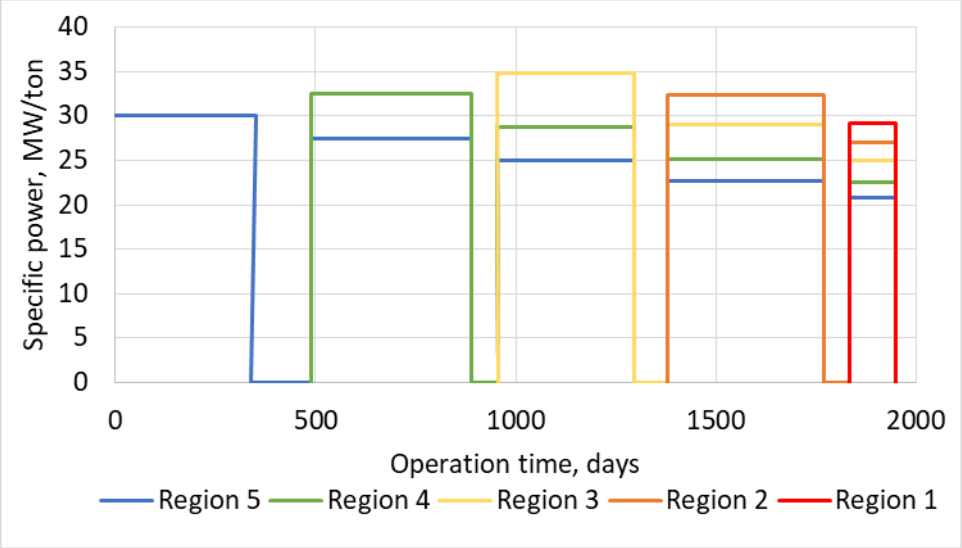

Figure 77. Fuel Rod hydraulic cross-section [[93]]

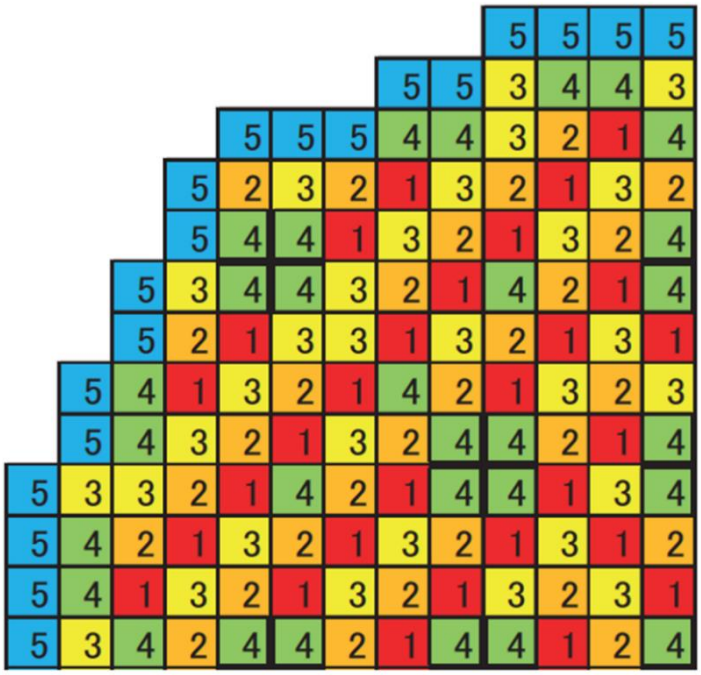

Figure 78. Fuel assembly region locations in reactor core [[93]]

Fuel rod is divided into 29 axial segments with a specific power fraction seen in Figure 79 as axial power profile. Peak linear power resides in 10th and 11th axial segments (112.5% power) in TRANSURANUS model. However, in the examined cases the peak temperature is consistently witnessed in 14th segment therefore is fair to assume

that such segment is most likely to rupture. For the further analysis 14th segment will be used as a point of reference.

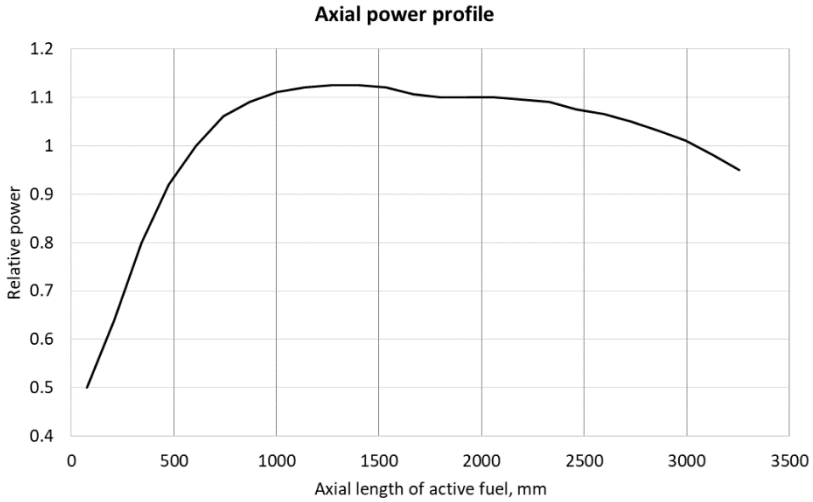

Figure 79. *Axial power profile assumed for irradiation*

During LOCA event linear power (Figure 80) is gradually reduced to 11.5 kW/m and then suddenly drops (SCRAM event) to ~0.7 kW/m and gradually declines. Before linear power drop there is 900 s lasting transition period from the operational regime to the LOCA initial conditions.

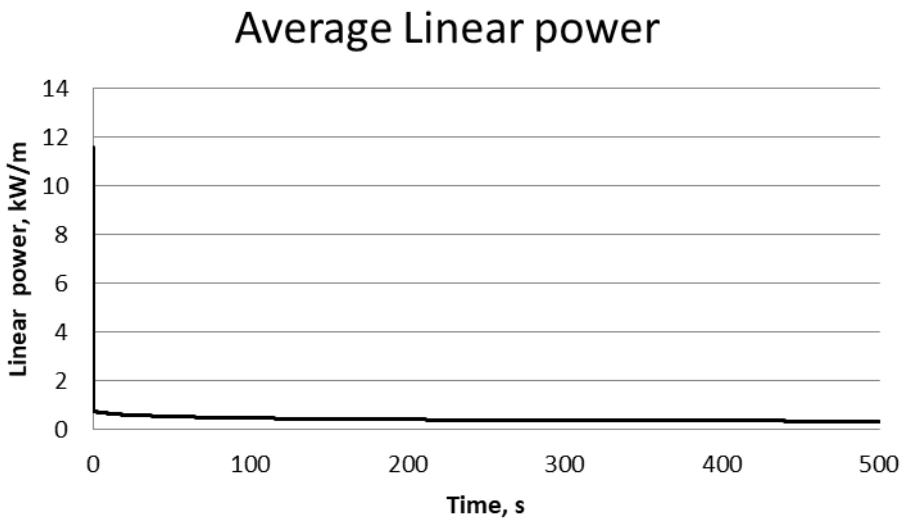

Figure 80. *Linear power during the LOCA event.*

Outer cladding temperature (Figure 81) is imposed in accordance with the results of previous ASTEC calculations are presented here. For further analysis, 4 rings in reactor core will be considered. Ring 2 has the highest peak temperature. Peak temperatures will be analysed in the homogenic temperature profile cases.

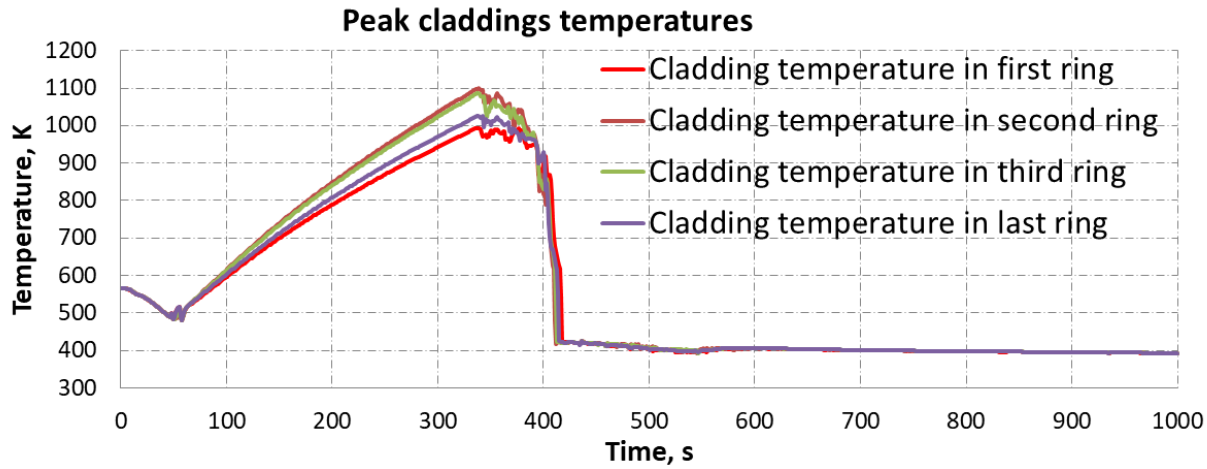

Figure 81. *Outer cladding temperatures at different reactor core ring locations (14th segment).*

In heterogenic temperature profile case 2nd, 3rd and 4th rings were analysed. Outer cladding temperatures for ring 2 different axial segments are presented in Figure 82. Temperatures were obtained for axial segments 10-11 from top to bottom. Missing temperature values were set from the interpolation operation.

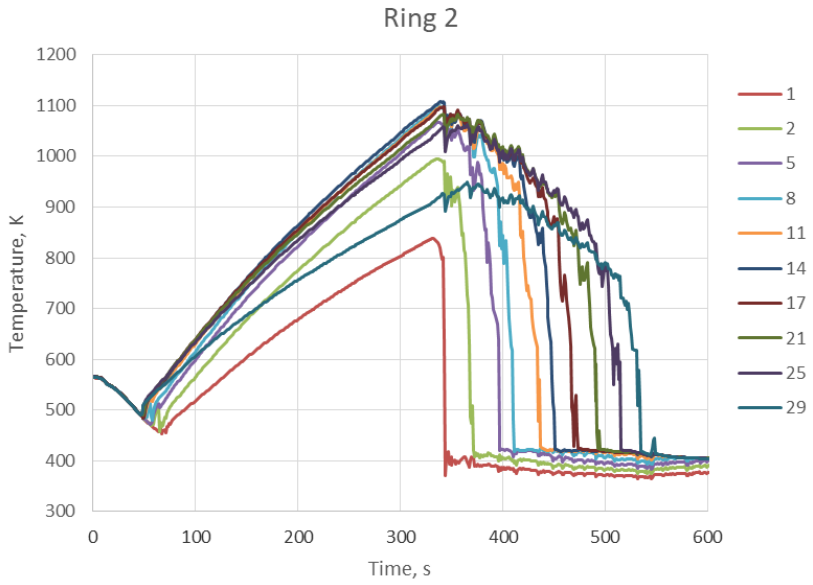

Figure 82. *Temperature profiles in different axial segments.*

In Figure 83 axial temperature profiles for all examined cases are presented.

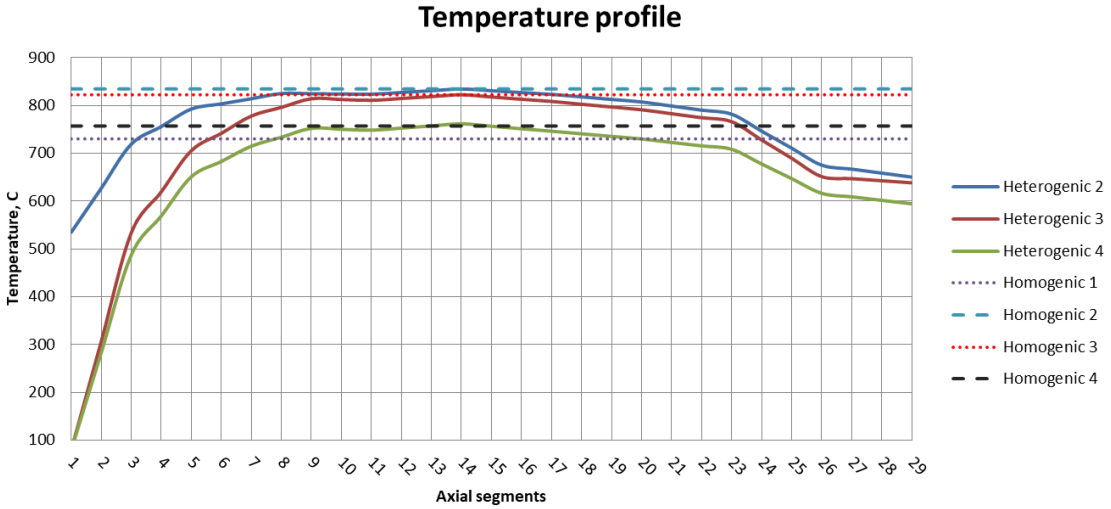

Figure 83. *Axial temperature profiles for examined cases.*

TRANSURANUS modelling results

There are 4 different cladding rupture criteria available in TRANSURANUS and they can be used either separately or in combination. Presented graphs depict results obtained with combined method, however each parameter was investigated separately (tab. 1, 2). For reference, failure parameters were selected with regards to HALDEN BWR LOCA test input files.

Preliminary results correspond are consistent with ASTEC results. Rupture is witnessed in two out of four fuel rods (Ring 2, Ring 3). After the rupture pressure inside gap is set to the outer pressure of the coolant (Figure 84). However, in ASTEC calculations rupture occurs at 358 s for ring 2 and at 419 s for ring 3. In TRANSURANUS case the rupture occurs before at ~320 s and ~330 s for respective rods. In Figure 85 it is seen that the gap pressure is higher in homogenic temperature profiles cases. This is caused by larger gap gas heating, however it doesn't result in rupture or faster rupture times.

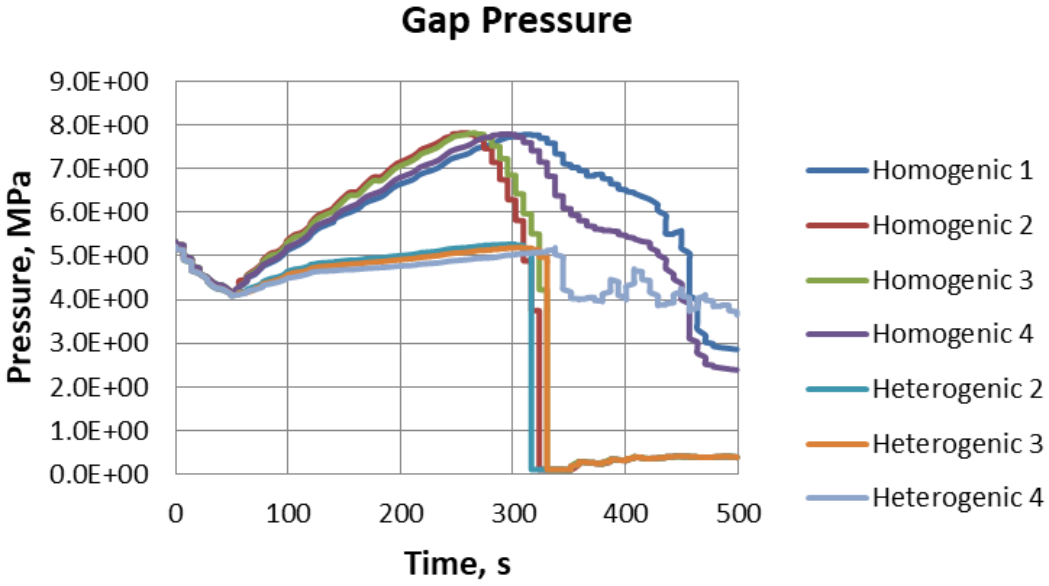

Figure 84. *Pressures inside gap (14th segment).*

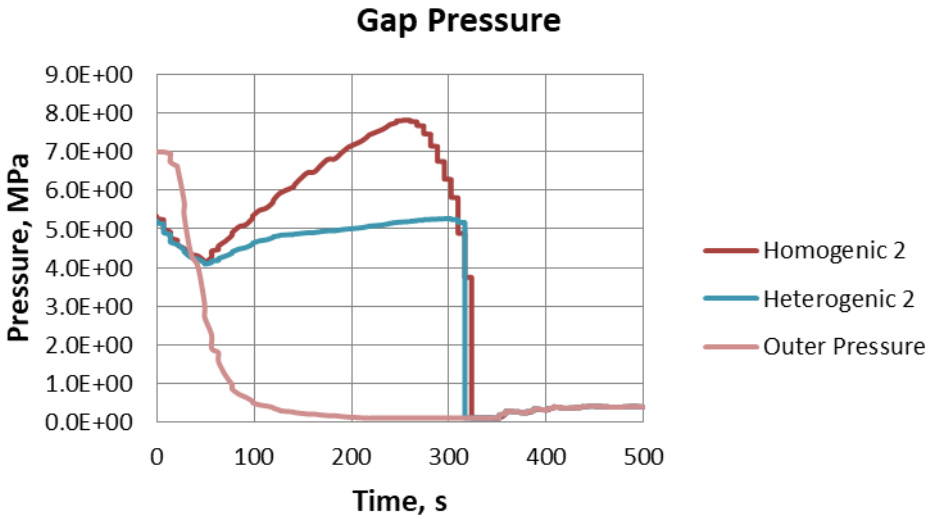

Figure 85. *Outer and inner pressures (14th segment).*

Figure 86 and Figure 87 depict average equivalent stresses and burst stresses in rings. It is seen that average equivalent stress decreases after rupture. Equivalent stress corresponds to the pressure, temperature and temperature gradient product. Burst stress indicates when the cladding rupture is caused by overstress or overstrain.

In this TRANSURANUS case full dynamics of thermohydraulic description is not being considered: Only one direction of mass flow is being considered, coolant characteristics are described same in each axial segment, meaning there is no gradual drying process within the rod.

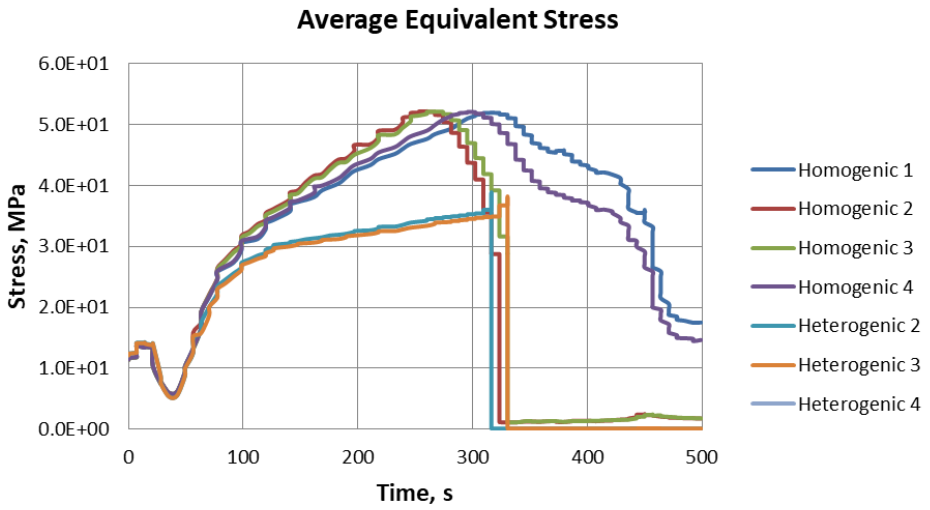

Figure 86. *Average equivalent stresses (14th segment).*

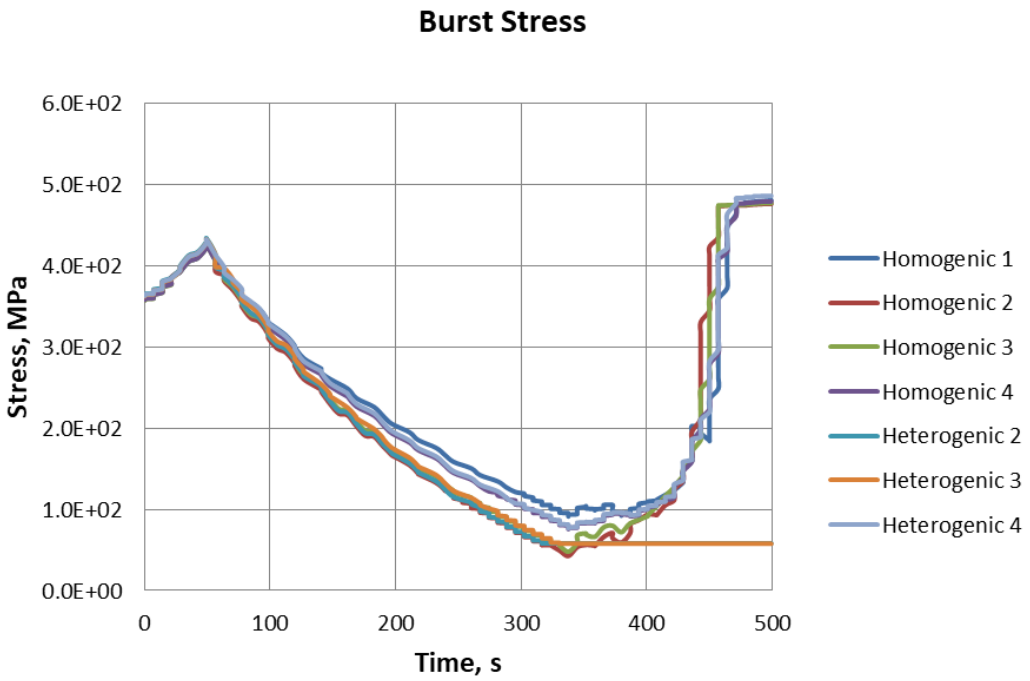

Figure 87. *Burst stresses (14th segment).*

As for the cladding failure, In TRANSURANUS cases, it occurs with a response to the temperature threshold, meaning that the main factor is a rising temperature and pressure difference as opposed to some cumulative property that keeps cladding intact for a prolonged time.

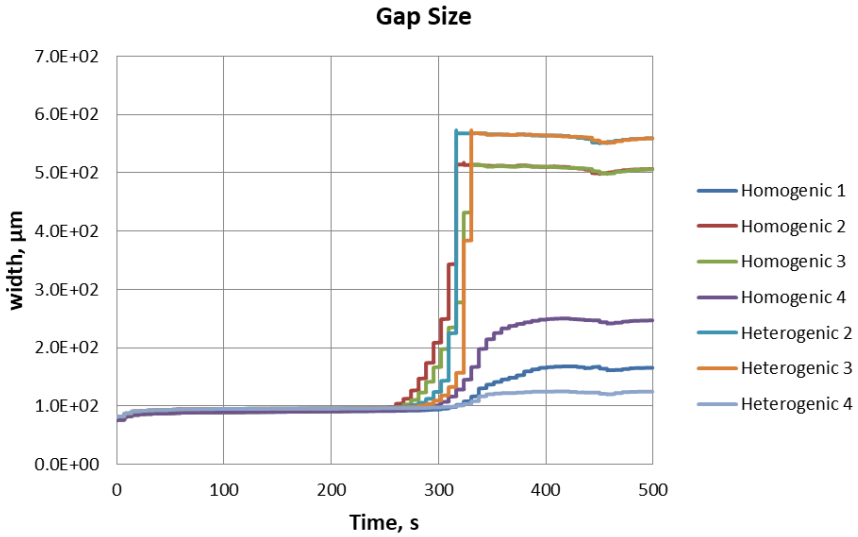

Figure 88. *Gap width size (14th segment).*

Gap size width (Figure 88) is very similar during cladding heat up phase among examined cases. Main differences start after the expected LOCA time. In cases where cladding rupture is expected, gap width significantly increases due to gap depressurization. Other gap widening causes are related to the cooling temperature.
In Table 39, Table 40 and Table 41 the rupture analysis is presented with regards to different burst parameters. Despite relatively larger temperatures for homogenic temperature profiles and consequently higher gap pressure the rupture occurs only a few seconds before than for the the heterogenic cases. The rupture only occurs due to strain limit/limit of plastic instability. In heterogenic cases these limits are achieved faster due to possible temperature gradient across the rod axis. In heterogenic case rupture occurs due to tangential stress being larger than failure stress. Since rupture occurs due to couple criteria as opposed to one, heterogenic case can be considered more reliable and less arbitrary option when analysing LOCA cases.
In Table 41 oxidation layer influence on rupture time was analysed. 4 initial conditions with 0,1,2,4 µm layers were analysed. According to the calculations, the thinner the oxide layer is the faster rupture occurs. Zirconium oxidation is exothermic reaction meaning that energy is being produced in the process and it should result in higher outer cladding temperatures. However, oxidation reaction rates don't indicate significant difference and it is probable that all excess heat is negated by TRANSURANUS LOCA mechanism. Difference in rupture time between 0 µm and 4 µm is roughly 5 seconds in all criteria examined.

Table 39. *Cladding failure event (homogenic temperatures).*

Parameter	**Rupture Time, s**			
	Ring 1	Ring 2	Ring 3	Ring 4
Overstress[1]	n/a	n/a	n/a	n/a
stress/strain[2]	n/a	n/a	n/a	n/a
epslim[3] **0.1**	n/a	320.1 s	330.4 s	n/a
strlim[4] **5**	n/a	320.1 s	330.4 s	n/a
Combined	n/a	320.1 s	330.4 s	n/a

Table 40. *Cladding failure event (heterogenic temperatures).*

Parameter	Rupture Time, s			
	Ring 1	Ring 2	Ring 3	Ring 4
Overstress[1]	n/a	321.8	332.5	n/a
stress/strain[2]	n/a	321.8	332.5	n/a
epslim[3] **0.1**	n/a	318.1	328.9	n/a
strlim[4] **5**	n/a	318.1	328.9	n/a
Combined	n/a	318.1	328.9	n/a

Table 41. *Cladding failure event (ring 2, oxide layer (OL)).*

Parameter	Rupture Time, s			
Initial OL	0 μm	1 μm	2 μm	4 μm
Pre LOCA OL	0.2 μm	1.1 μm	2.9 μm	4.9 μm
OL during rupture	0.8 μm	1.7 μm	3.6 μm	5.6 μm
Rupture time[1,2]	319.7	321.8	323.0	325.1
Rupture time[3,4]	316.2	318.1	319.2	321.3

1- Overstress is assumed if the average true tangential stress was larger than the failure stress calculated by the material property function SigmaB
2- Failure is assumed if the tangential stress or the tangential strain limit is achieved
3- Effective strain limit for plastic instability
4- Effective strain rate limit for plastic instability (1/h)

- epslim and strlim are co-dependent parameters. For the analysed cases the standard values are assumed to be at 0.1 (correspond to 10%) and 5 correspond to (5/h) respectively (HALDEN LOCA).

Conclusions

- ASTEC calculations were completed with TRANSURANUS code leading to similar cladding failure conditions.
- There is some time discrepancy in rupture times when compared TRANSURANUS results with ASTEC.
- Homogenized axial temperatures don't result in overstress related cladding failures compared to Heterogenic temperature cases.
- Rupture in TRANSURANUS is propagated first by strain and strain rate limits for plastic instability. However, in examined heterogenic temperature cases rupture can occur few seconds later from the overstress as well.
- Minor changes in linear heat rate or neutron flux doesn't affect cladding failure much due to gap conductance.

There are number of differences between TRANSURANUS and ASTEC rupture estimation. TRANSURANUS require some irradiation prehistory as well has higher number of parameters that might influence the outcome of calculations. Failure criteria in TRANSURANUS mainly described as mechanical process (stress/strain), ASTEC using EDGAR burst model which is best estimate model based on burst criterion determinate after the EDGAR experiments data. In ASTEC calculations, rupture stress depends on temperature and hoop stress.

New nodalization of the core region for better evaluation of the fuel clad failures

ASTEC Calculation results

For the selected LOCA accident analysis assumed fuel assemblies load pattern and power history is presented in Figure 77 and Figure 78. According to that information relative horizontal distribution have been calculated [[93]] and presented in Figure 89. According to the taken assumptions and developed core active zone model the analysed core could be divided in 5 groups according to the relative power presented in the Table 42.

Table 42. *Groups according to the selected relative power*

Group	***Relative power of FA***	***Quantity of FA in a reactor***
1	0.81	72
2	0.89	124
3	0.98	120
4	1.07	116
5	1.19	116

In the basic model developed for ASTEC code BWR-4 core were modelled using 4 concentric rings. These rings include 4, 80, 224, and 240 fuel assemblies respectively. Different rings of fuel assemblies are presented with a different colour in Figure 89. Each concentric ring has average relative power (Table 43).
Initially, for the task3.2 it was planned to make a new ASTEC nodalization for the core region of BWR-4 and update the input deck. It was planned to increase the number of concentric rings, change axial and radial nodalization. However, it was decided to move in a different direction and to change only the relative power of the existing concentric rings. This allows to indicate with which relative power burst of the claddings occurs at the selected accident scenario with a given burst criteria.
With respect to the relative powers of the loading groups (Table 42), the ASTEC model was modified giving different relative power values. Selected relative powers for the basic and modified ASTEC model is presented in Table 43.

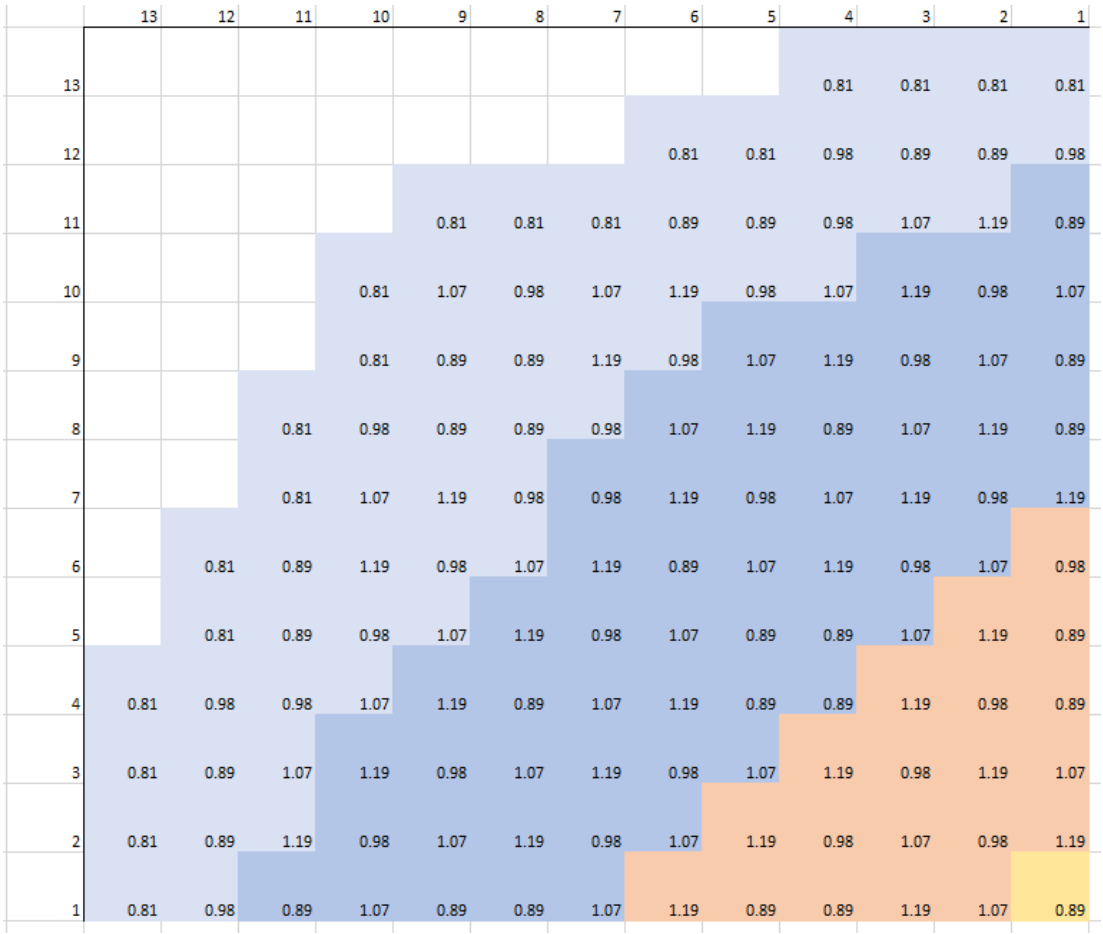

Figure 89. Relative horizontal distribution (a quarter of reactor core)

Table 43. *Radial power distribution through the rings, for nodalization with 4 rings*

Fuel ring	Number of fuel assemblies	Number of control rods	Relative power (basic calculation)	Relative power (modified)
1	4	1	0.89	0.89
2	80	20	1.066	1.066
3	224	56	1.043	1.005
4	240	60	0.943	0.98

The previous analysis (basic calculation) provided in the frame of task 2.3 showed that during our analysed LOCA accident second and third concentric rings were ruptured – relative power 1.066 and 1.043 respectively. So, it is obvious that according to our specified core load fuel assemblies (FA) groups 4 and 5 will be damaged. However, it is not clear if FA in group 3 with the relative power of 0.98 will be damaged during our analysed scenario. Thus, it was decided to change the relative power of the existing ASTEC nodalization to check if the concentric ring with 0.98 relative power will burst. The relative power of all rings was recalculated Table 43.

Before the starting of the transient analysis (LOCA), it is needed to provide a steady state calculation to check if the flow rate through the modelled concentric rings with modified relative power is adequate to the previous calculation case. The flow rate through the model rings is related to the relative power – increasing relative power should also increase flow rate and vice versa. These dependencies should be linear. Flow rate could be regulated changing the form loss coefficient in the modelled ring. Figure 90 represents coolant flow rates versus relative

powers of rings for the basic and modified relative power calculations. As it could be seen from the figure, flow rate versus relative power is congruent in one line. This result shows that further (LOCA) analysis could be performed.

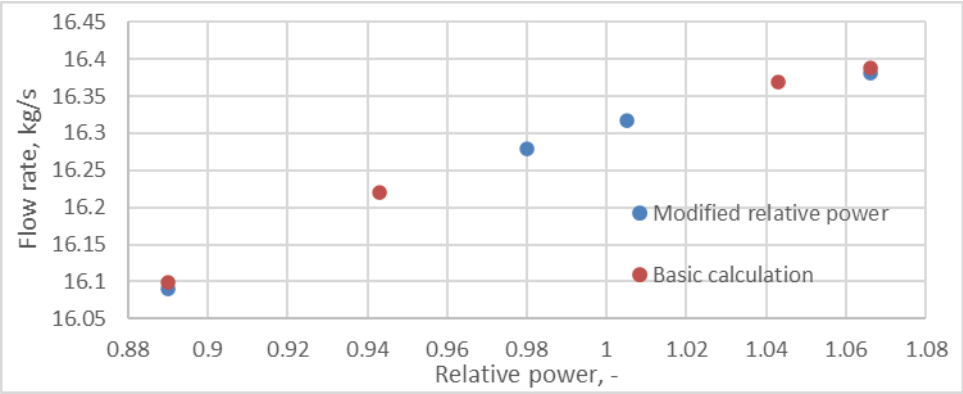

Figure 90. Coolant flow rate versus relative power of rings

Transient (LOCA in DEC-A conditions) calculation results of modified relative power showed only burst in ring 2 (burst time 344.8 s) which has a relative power of 1.066. This result means that FA having relative power of 0.98 will not rupture during the analysed accident. Regarding this result, it could be concluded that only groups 4 and 5 will burst from the selected core load during analysed LOCA accident. Group 4 and 5 correspond to 232 FA, thus ~42% from all core region will be damaged. Previous results showed ~55% of core region damage (cladding burst).

Verification of the ASTEC calculation results with the TRANSURANUS code.

The 4th ring with the relative power of 0.98 was selected for the analysis using the TRANSURANUS code. Assumptions for the TRANSURANUS modelling is presented in section 0 and it is applicable for the modelling presented in this section. Heterogenic temperature profile was taken from the ASTEC calculation results. In Figure 91 axial temperature profile is presented at the period (~350 s) when temperature reaches the peak cladding temperature of 782 °C.

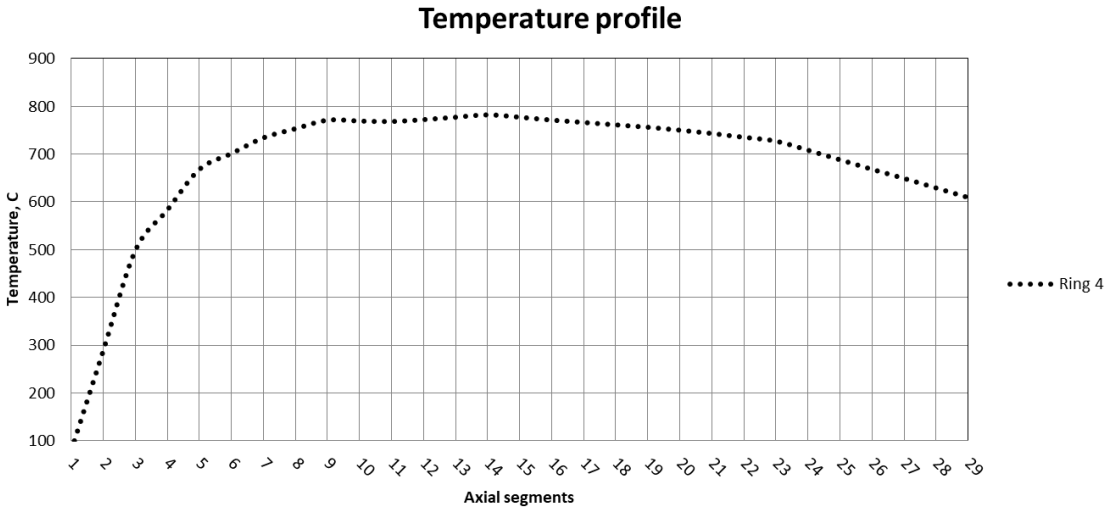

Figure 91. *Axial temperature profile during peak temperature.*

TRANSURANUS calculation results did not lead to cladding rupture in accordance with the cladding failure parameters presented in Table 44.

Table 44. *Cladding failure event (heterogenic temperature profile).*

Parameter	Rupture Time, s
	Ring 4
Overstress[1]	n/a
stress/strain[2]	n/a
epslim[3] **0.1**	n/a
strlim[4] **5**	n/a
Combined	n/a

Figure 92 - Figure 95 present outer cladding oxide layer thickness, gap width during LOCA, average equivalent stress and burst stress, inner and outer pressures for the 14th axial segment.

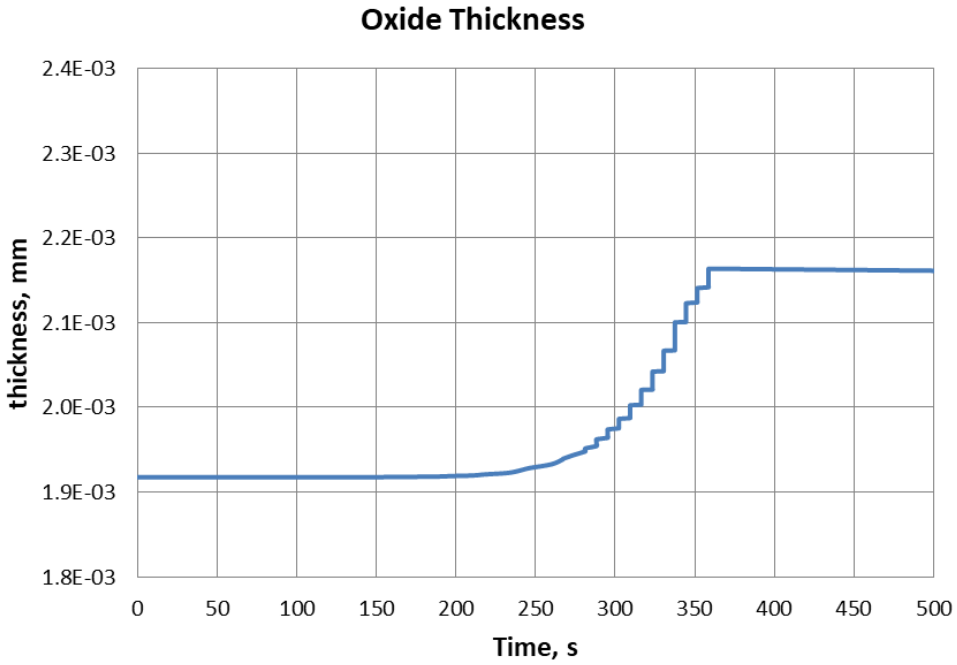

Figure 92. *Cladding oxide layer thickness (14th segment).*

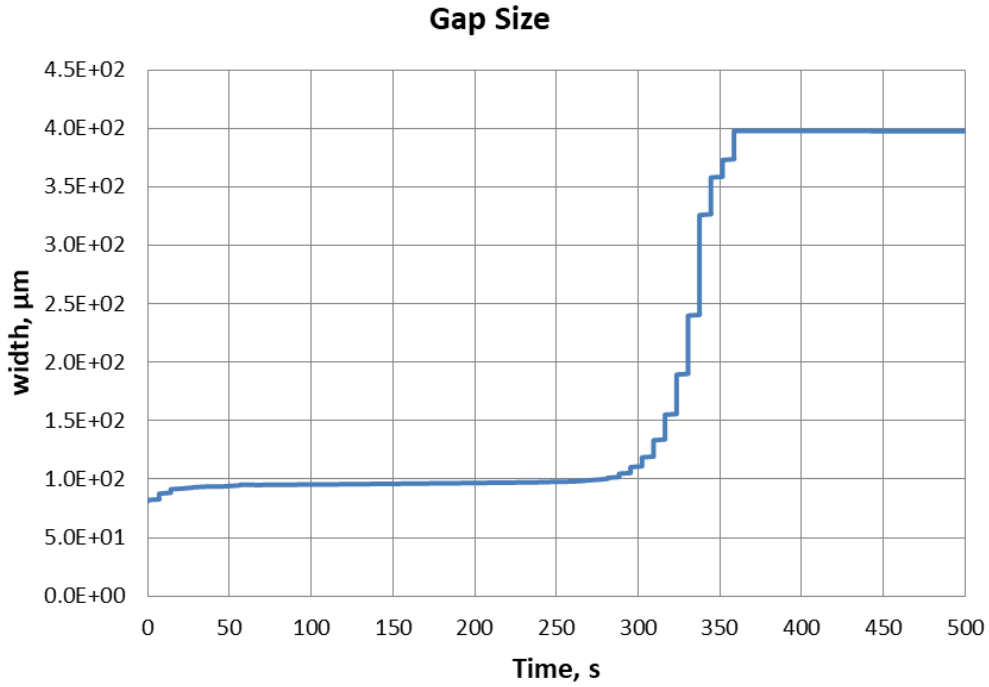

Figure 93. *Gap width size (14th segment).*

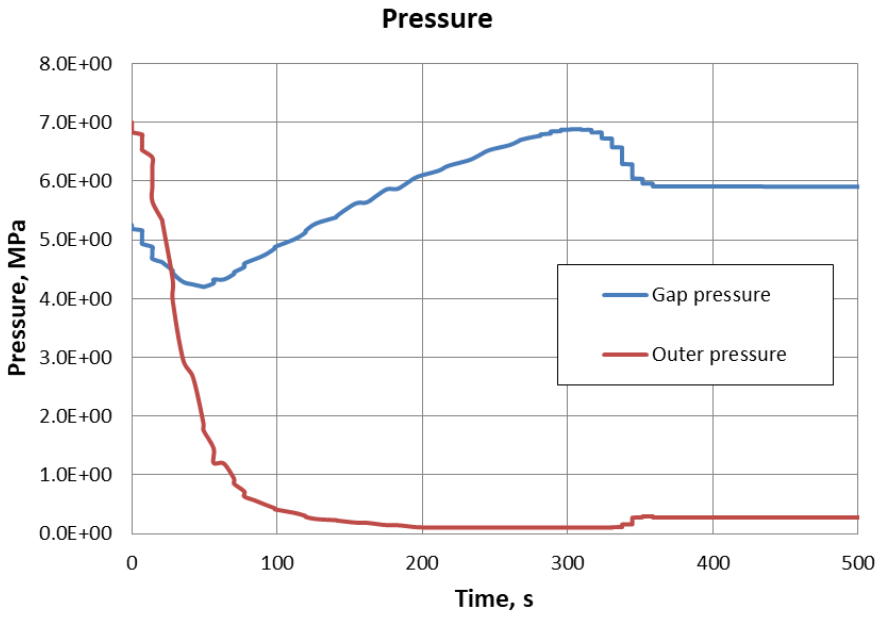

Figure 94. *Outer and inner pressures (14th segment).*

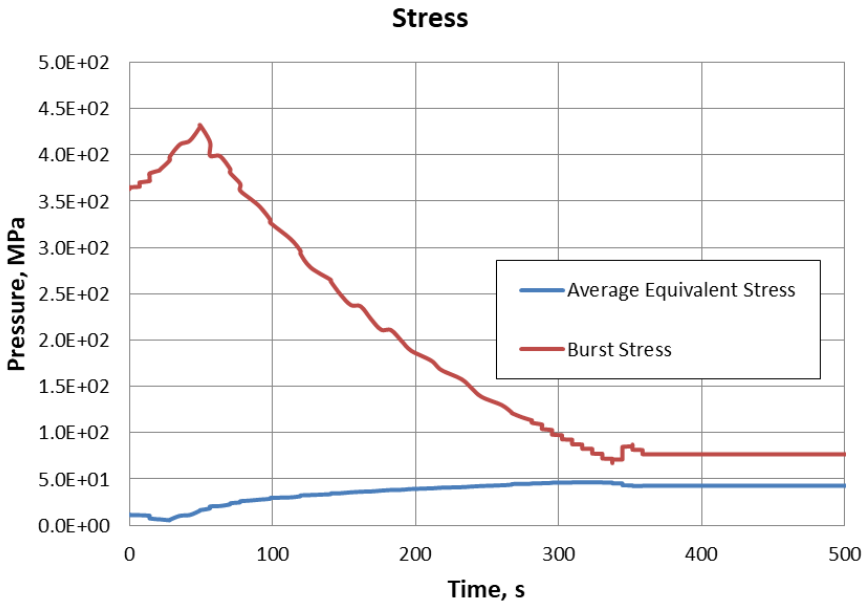

Figure 95. *Average equivalent stress and burst stress (14th segment).*

Conclusions

- ASTEC Transient (LOCA in DEC-A conditions) calculation results of modified relative power showed only burst in ring 2 (burst time 344.8 s) which has a relative power of 1.066. This result means that FA having relative power of 0.98 will not rupture during the analysed accident. Regarding this result, it could be concluded that only groups 4 and 5 will burst from the selected core load during analysed LOCA accident. Group 4 and 5 correspond to 232 FA, thus ~42% from all core region will be damaged. Previous results showed ~55% of core region damage (cladding burst).
- TRANSURANUS code was used for more detailed analysis of the processes in fuel behaviour during LOCA in the DEC-A conditions taking into account ASTEC calculation results with modified relative power. 4th ring with the relative power of 0.98 was selected to the analysis. Calculation results did not show cladding rupture. This confirms calculation results obtained by ASTEC.

Uncertainty quantification for the TRANSURANUS calculation results

In the Figure 95 the average equivalent stress is presented together with the calculated burst stress. At the time ~340 s after the beginning of the LOCA accident the distance between burst and equivalent stress is very narrow. Therefore it was decided to perform uncertainty and sensitivity analysis for the TRANSURANUS calculation results in order to make sure that even with uncertainties bound claddings of the fuel with 0.98 relative power will be intact.

Conservative rupture parameters are being considered as presented in other cases (see section 0). Five parameters were considered for uncertainty quantification. Uncertain parameters and selected uncertainty ranges for the uncertainty quantification presented in the Table 45. Uncertainty ranges and PDF was selected according to the previous provided work [[94]-[96]] and engineering judgment, after the separate sensitivity analysis.

Table 45. *Uncertain parameters and selected uncertainty ranges for the uncertainty quantification*

Uncertain parameter	Default value	Uncertainty range	PDF	Max case	Min case
Pellet radius, mm	4.335	±1%	Normal Distribution	4.292	4.378
Inner cladding radius, mm	4.420	±1%		4.464	4.376
Outer cladding radius, mm	5.025	±1%		4.975	5.075
Gap pressure, MPa	3.000	±2%		3.060	2.940
Outer pressure, MPa	According to ASTEC calculations	±1%		-1%	1%

Max case calculation

Case with parameters that correspond to the maximal values was analysed (Table 45). This case is assumed to have highest likelihood to rupture, however such event is not being observed in calculation results (Figure 96, Figure 97). Pellet radius variation has a peculiarity where both increase in radius and decrease in radius can affect the rupture probability negatively. In case of pellet radius reduction, gap pressure increases during start up and exerts larger force on the cladding, while pellet radius increase would result in lower gap size and better thermal conductivity between fuel and cladding. This could increase the temperature of the cladding, however in examined case this effect is less relevant than gap pressure increase therefore maximal critical value was assumed to be the reduction of pellet radius.

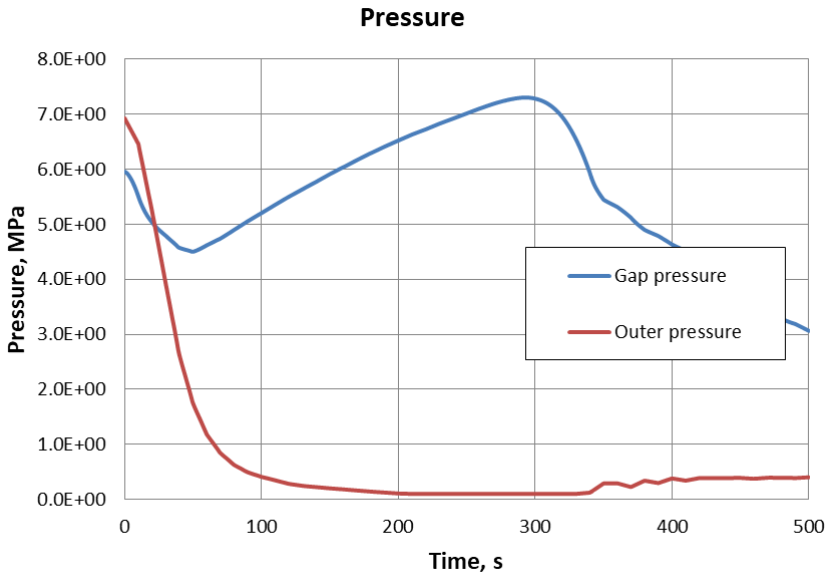

Figure 96. *Outer and inner pressures (14th segment).*

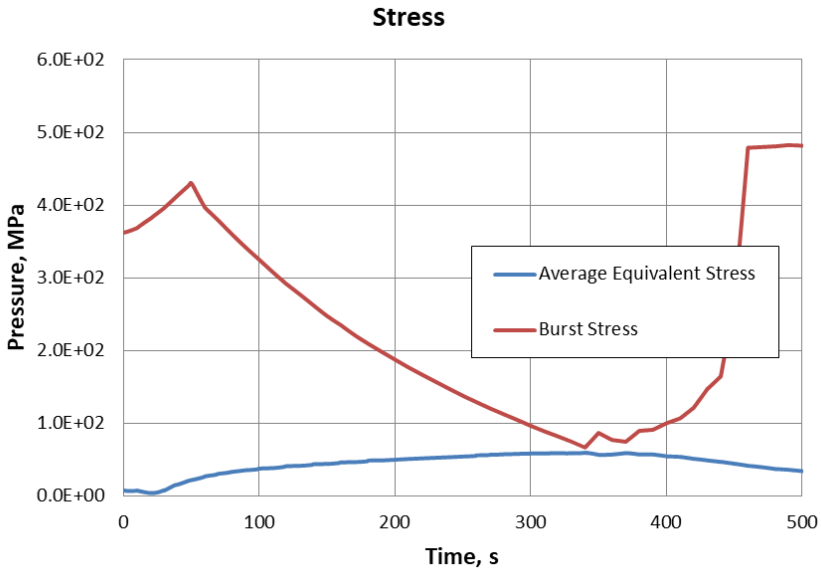

Figure 97. *Average equivalent stress and burst stress (14th segment).*

Uncertainty analysis

TRANSURANUS code has his in-build Uncertainty and Sensitivity tool [[97]]. For the uncertainty analysis 100 calculation were performed. Results of the uncertainty analysis are presented in Figure 98 - Figure 102. All presented figures show the results obtained at the 14th axial segment of TRANSURANUS fuel model. This node has the highest axial relative power.

As it is presented (Figure 98) the average equivalent stress varies in the range ~30 to ~60 MPa. However, the calculated burst stress did not show any uncertainty (Figure 99). This burst stress is calculated by the code using other parameters which does not have effect for the assumed uncertain parameters.

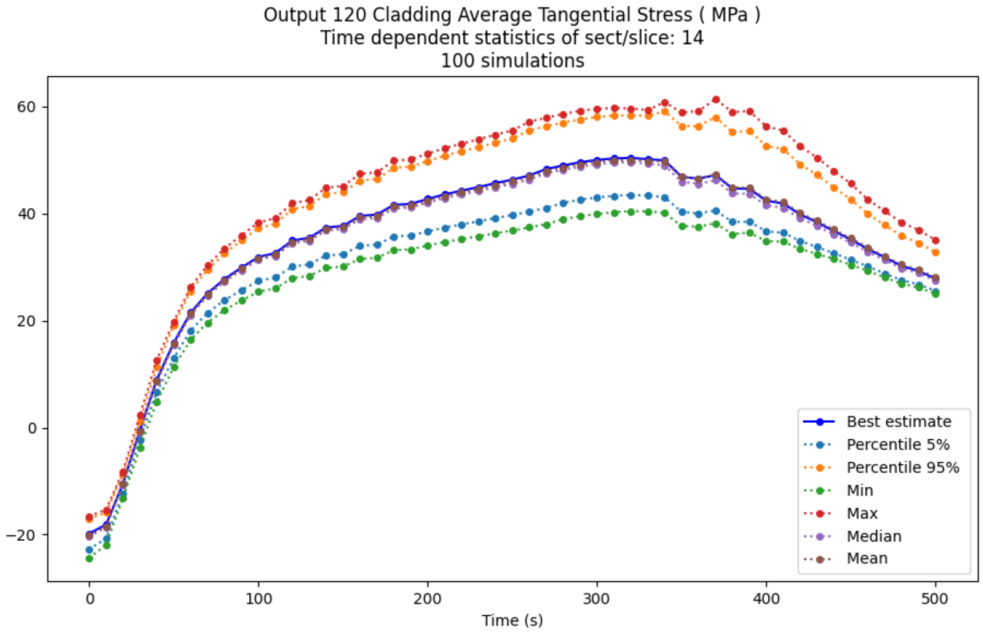

Figure 98. *Average equivalent stress (14th segment).*

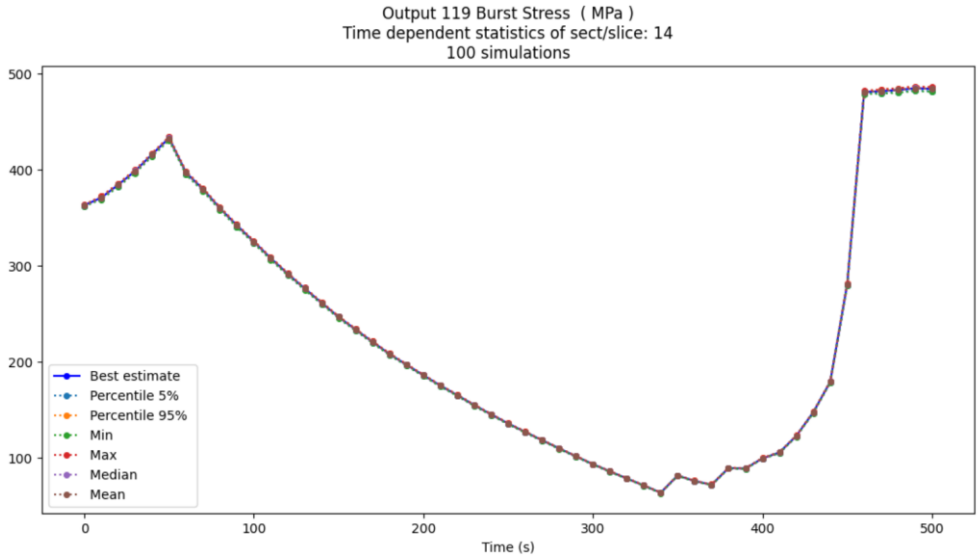

Figure 99. *Burst stress (14th segment).*

Figure 100 and Figure 101 present the pressure evolution in the gap between fuel pellet and cladding and gap width changes at the 14th segment. Especially high variations are observed in the gap width at 300 s after the transient initiation. Minimum gap with was ~200 μm, while maximum values ~1600 μm. However, these extreme values was not often, because the percentile values are more narrow.
Outer oxide layer at the 14th segment is presented in Figure 102. Discrepancies of the calculation results are uniform during all presented calculation period.

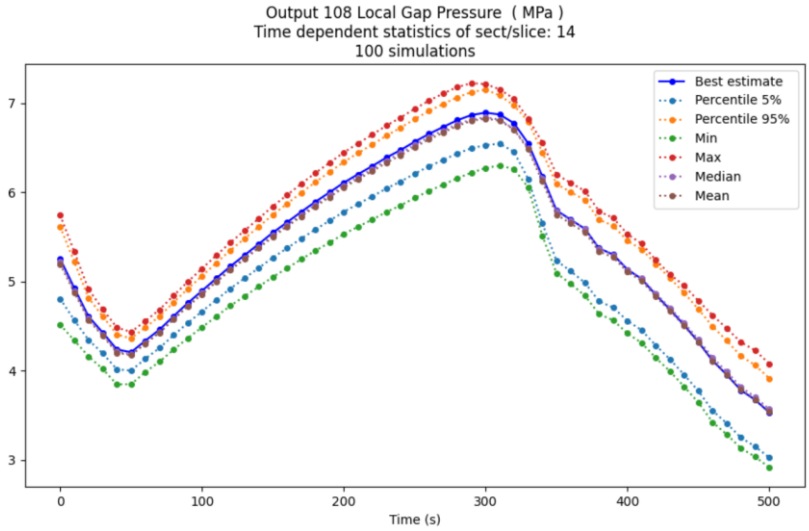

Figure 100. *Gap Pressure (14th segment).*

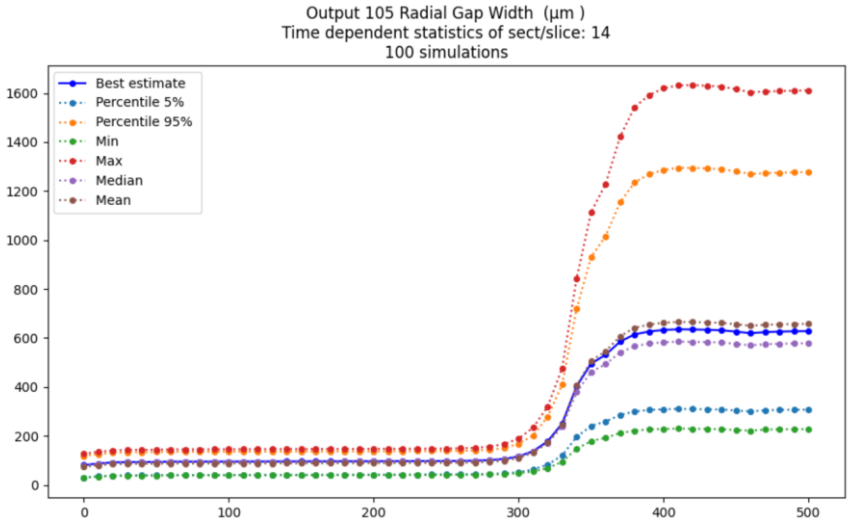

Figure 101. *Gap Width (14th segment).*

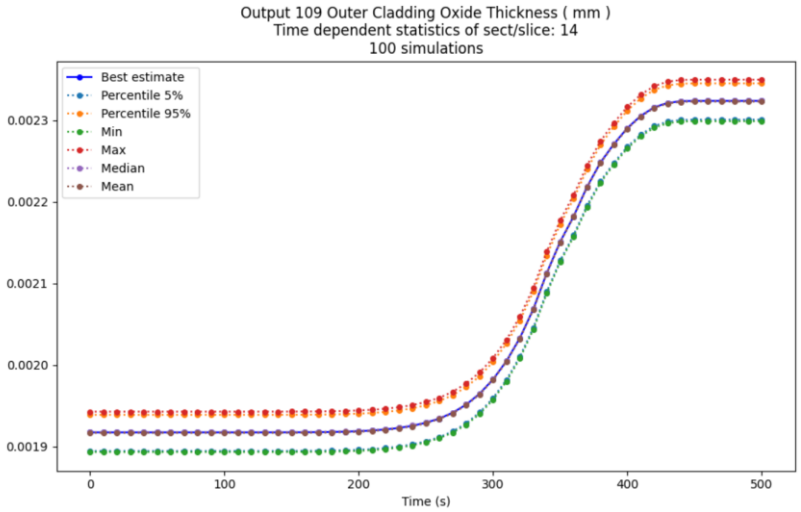

Figure 102. *Outer oxide layer (14th segment).*

Sensitivity analysis

For the Sensitivity analysis the Spearman corelation was used. Figure 103 - Figure 105 presents the sensitivity analysis results (Spearman's ranks and scattering plots for time moment at the beginning of the LOCA transient and 340 s after the LOCA transient) to the gap pressure calculation results. The results of the sensitivity analysis to the gap pressure calculation shows that in the first ~300 s of the start of the accident the cladding inner radius and fuel outer radius have highest effect. Later the influence is changing – the most important parameter become cladding outer and inner radius. Scatter plots provided in the moment at the beginning of the LOCA transient and 340 s after the LOCA transient confirms this this. However, it is needed to note that the results scattering amplitude is high.

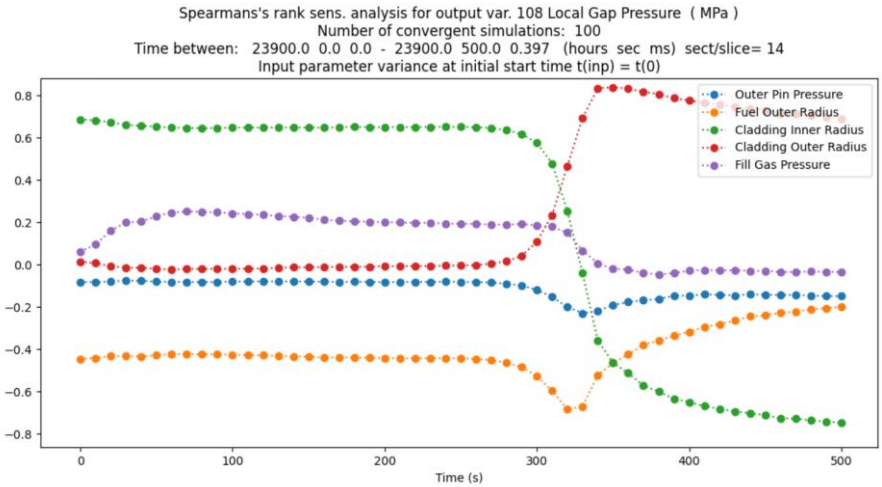

Figure 103. *Spearman's ranks for gap pressure (14th segment).*

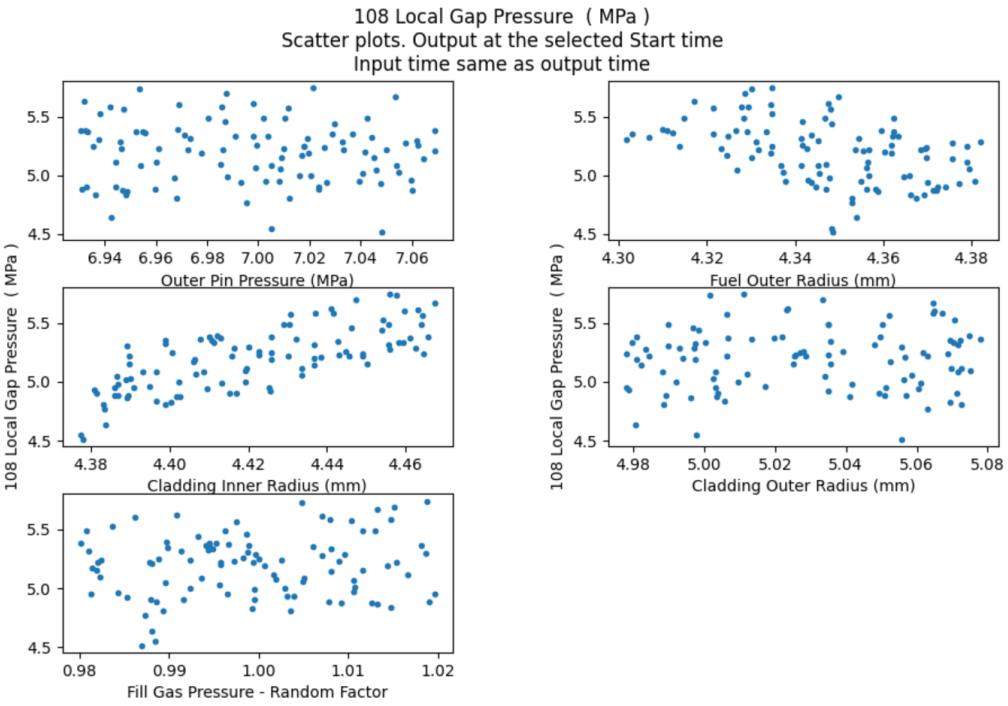

Figure 104. *Scatter data plots for gap pressure (14th segment), at the beginning of the LOCA transient*

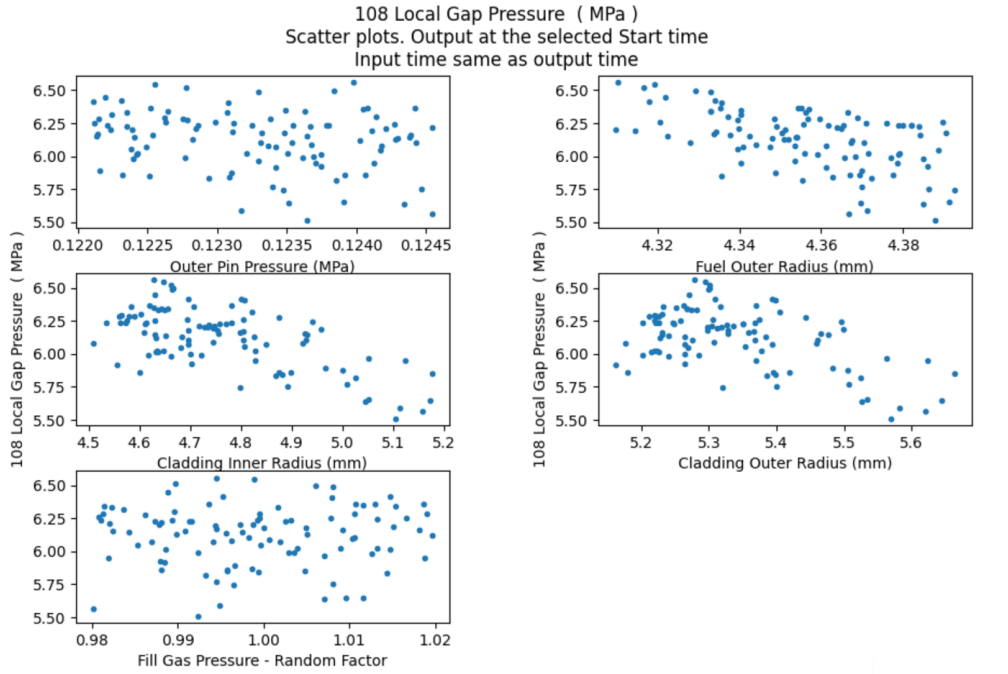

Figure 105. *Scatter data plots for gap pressure (14th segment), 340 s after the LOCA transient*

Figure 106 - Figure 108 presents the sensitivity analysis results (Spearman's ranks and scattering plots for time moment at the beginning of the LOCA transient and 340 s after the LOCA transient) to the average equivalent stress calculation results. The results of the sensitivity analysis to the equivalent stress shows that the cladding

inner and outer radius have highest effect during all calculated transient period. This in principle indicates the thickness of the cladding. Scatter plots provided in the moment at the beginning of the LOCA transient and 340 s after the LOCA transient confirms this.

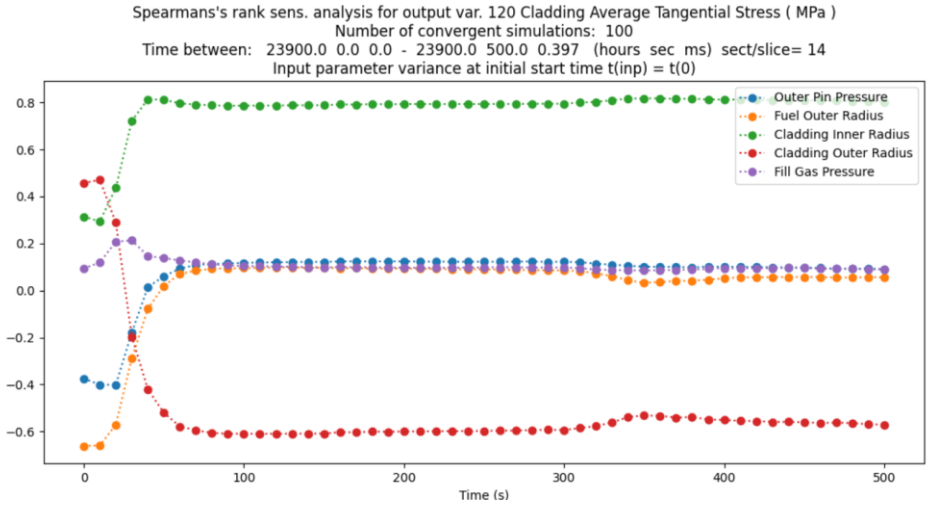

Figure 106. *Spearman's ranks for average equivalent stress (14th segment).*

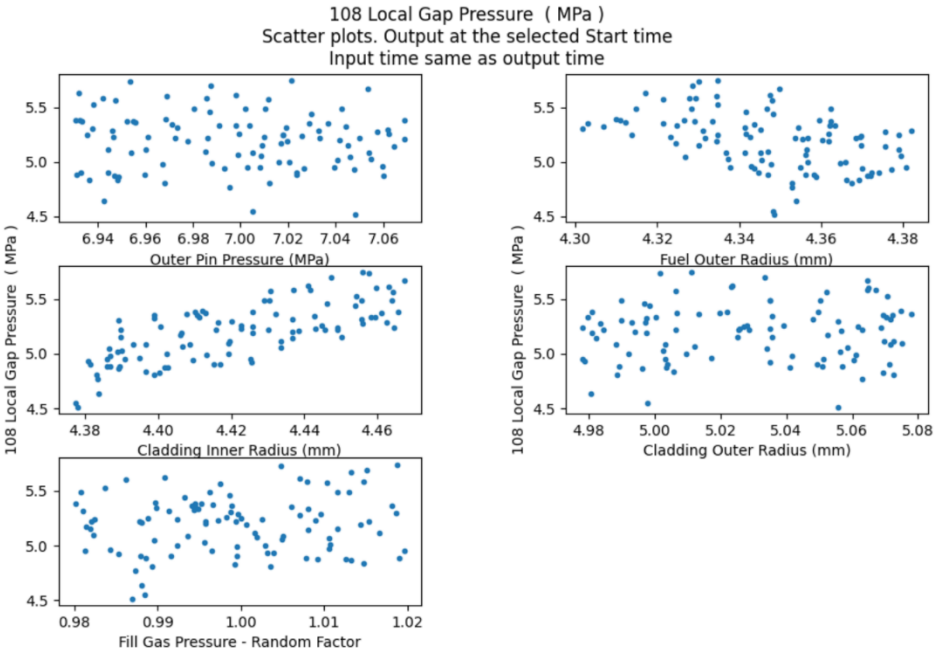

Figure 107. *Scatter data plots for average equivalent stress (14th segment), at the beginning of the LOCA transient*

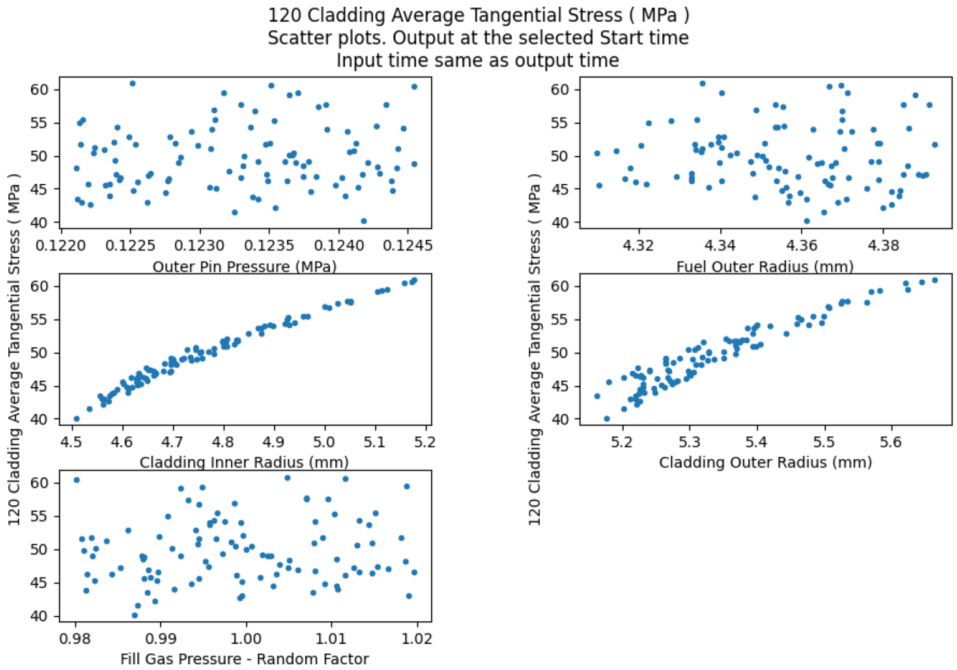

Figure 108. *Scatter data plots for average equivalent stress (14th segment), 340s after the LOCA transient*

Conclusions

Provided uncertainty analysis confirmed that even with uncertainties bound claddings of the fuel with 0.98 relative power will be intact. It was observed large variations of the calculated average equivalent stress and for the maximal case the distance between burst stress and average stress is very narrow.
Sensitivity analysis indicated that the most influencing parameter is cladding inner and outer diameter.

IRSN : DRACCAR New LOCA methodology

A new whole core modelling approach has been developed using available codes applicable to LOCA at IRSN. In particular, IRSN develops the DRACCAR multi-rod and multi-physics code at the assembly scale dedicated to LOCA. The code is based on a coupling between 2.5D multi-rods thermal-mechanical modelling and a 3D thermalhydraulics description at sub-channel scale. Compared to system thermalhydraulic codes classically used in LOCA for DBA assessment, DRACCAR is able to model fuel assembly behavior under LOCA conditions by coupling rod deformation to flow blockage. Thus DRACCAR proposes interesting insights regarding impact of LOCA on fuel rod behavior and coolability.

Introduction

In the frame of the FUEL+ platform, IRSN is developing a set of computer codes dedicated to the simulation of fuel behaviour all along the fuel cycle under normal and accidental conditions. This platform regroups a fuel performance code FIRST for normal operation and transient conditions – transport and storage accidents, SCANAIR devoted to reactivity insertion accidents, DRACCAR dedicated to loss-of-coolant accidents and SHOWBIZ which focuses on the embrittling effect of H and O species on claddings. DRACCAR software [98] is developed by IRSN with the financial support of EDF since 2006. It's latest version 2022 proposes 3D advanced modelling of multi-rod configurations accounting for the coupling of thermal-mechanics and thermal-hydraulics – influence of the deformation and contact between rods on the heat exchanges and flow distribution. In addition,

recent models focusing on fuel behaviour allow to perform parametric studies of fuel relocation, gas axial transport in free volumes or fission gas release. Typical application of DRACCAR focuses on fuel assembly and provides assessment of the coolability by the evaluation of PCT (peak cladding temperature), rod deformation, clad burst and flow blockage.

The classical methodology used for design basis accident safety (DBA) demonstration for LOCA are based on idealistic modelling - using thermal-hydraulic system code such as CATHARE-3 [CEA] combined with relatively simple modelling of fuel behaviour during LOCA and penalizing the rod response by a set of assumptions and additional margins. The response of the hottest rod is one of the main concerns by evaluating (PCT), equivalent cladding reacted (ECR) and concluding on the core coolability including efficiency of reflooding. Such idealized model cannot be used to determine the behaviour of all the fuel rod of the core as it captures mainly the behaviour of the hottest rod, the hottest fuel assembly and the average core responses to LOCA. Moreover, the set of assumptions and modelling are not realistic as this method aims at evaluating the envelope response to a given transient. Contrarily to DBA, the evaluation of the number of failed rods during LOCA requires to evaluate the behaviour of each fuel assembly and the burst potential of fuel rod belonging to it. Therefore, the classical methodology developed for DBA cannot be used for the evaluation of the number of failed rods and it motivated the development of a new core methodology in the frame of R2CA. This section exposes the work that conducted to this new methodology with DRACCAR focused on burst risk assessment.

The workplan proposed by IRSN in the frame of WP3.2 of R2CA project aimed at extending DRACCAR applicability to the evaluation of the number of failed rods under LOCA conditions. This task is completed by activities in the WP2.5 corresponding to the development of DRACCAR/ASTEC PWR900 demonstrative application coupling DRACCAR new core modelling to the ASTEC source term evaluation code [99][99].
To propose a new core model and associated methodology to predict the number of failed rods, several studies on idealized cases were built and provided insight on modelling needs. In parallel, some developments were brought to DRACCAR software to better represent core characteristics and to use burst criteria well adapted to burst risk assessment (which were developed by IRSN within the same task 3.2, see section page 29. Several core models were developed based on PWR900 demonstrative case and oriented on the proposed methodology. Outlooks are provided as a conclusion of this work to better highlight the status and the possible prospects for new DRACCAR core model.

On the need to consider 3D PWR core model to evaluate the number of failed rods during LOCA

Core loading in PWR is composed of a set of fuel assemblies whose characteristics distribution are heterogeneous and linked to the fuel type (UO_2 or Mixed (U, Pu) O_2) and irradiation history. Core loading is changed at the end of each irradiation cycle. New loading is voluntarily built for different purposes (flattening neutron flux, reducing vessel damage, …) by reorganizing irradiated fuel assemblies and introducing new fresh fuel assemblies. As a result, a core region cannot be associated to an equivalent rod with average values for burn-up (BU), rod internal pressure (RIP), neutron power and decay heat factors (cf. Figure 109). This is clearly one issue when using the classical core ring method with only one equivalent rod per ring. Indeed, focusing on the burst risk in LOCA conditions requires to evaluate creep and then stresses in cladding. The stresses are directly linked to the RIP which at initial state before accident varies a lot from one fuel assembly to another one as it depends on fuel type (MOX or UO_2) and initial gas filling as well as on the burn-up. The RIP strongly evolves due to fission gas production during the irradiation (more than 2.5 MPa between BOL and EOL, cf. Figure 111).
Regarding such heterogeneous distribution of the fuel assembly characteristics in the core, an evolution of the core ring method using several equivalent rods per ring was investigated in the frame of R2CA (refer to the contribution by ENEA) it appears that 3D model accounting for the specificities of each fuel assembly is necessary to assess burst risk in a best estimate manner. Advanced simulation should focus on taking into accout the specific

fuel rod state and fuel assembly location in the core. This led to questioning the feasibility of providing input data and initializing with enough detail each fuel rod representative of the fuel assemblies in the core application.

Available tools and data required for fuel rod initialization in the core application

Fuel performance codes such as FRAPCON 4.0 [100] (developed by PNNL for US NRC) or TRANSURANUS [101][101] (developed by JRC) can predict the behaviour of a representative fuel rod during its irradiation during normal operation. Such codes provide with more or less details the initial state of the fuel pellets and of the clad which are necessary to obtain a proper initialization of DRACCAR simulation before LOCA (geometry, fuel porosity/density, RIP, temperature field [r, z], …). However, such codes do not provide burn-up, decay heat and neutron power accounting for the location of the fuel rod in the core. Moreover, when assessing radiological consequences, the fission products inventory of the core and if possible, of each fuel assembly should be known. To obtain these data, it's necessary to rely on neutron physics simulation. Of course, these simulations must account for the core configuration, initial fuel loading and irradiation program.
IRSN develops VESTA [102] depletion code which can provide detailed data on each fuel assembly using a 4th core model. Such modelling of neutronic evolution is a basis for proposing the initialization of the decay heat, the neutron power and the fission products isotopes inventory.

Therefore, the proposed new DRACCAR core model can use data produced by VESTA (power factor, decay heat factor, isotopes inventory) and by the fuel performance code FRAPCON (temperature field [r, z], fuel porosity, rod internal pressure, …) to best initialize each of the fuel rod considered in the simulation. To ease this process, a procedure was developed in the frame of this task to chain results produced by FRAPCON to DRACCAR software. Thus, a library of FRAPCON simulations can be read automatically to connect DRACCAR input data to the relevant initializations depending on the selected PWR core loading.

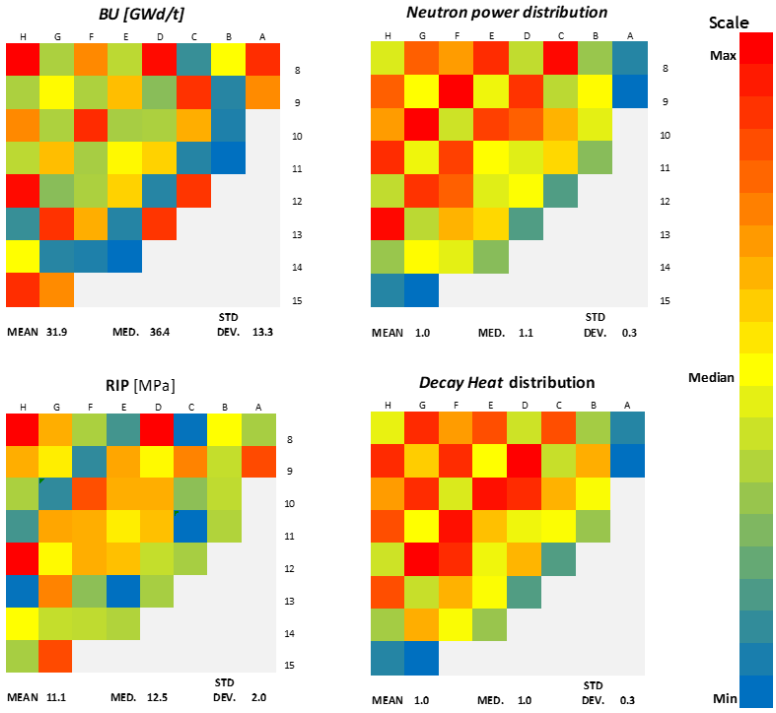

Figure 109: Example of heterogeneities of a PWR core loading map with respects to fuel assemblies' average characteristics (power factors, burn-up and rod internal pressure)

Of course, refining description of the fuel rod – for instance by improving their individual initialization – can be only fruitful if these efforts are consistent with respect to the other phenomena. Distinguishing the initial fuel rod state for each fuel assembly suggests that simulation try to discriminate their response to LOCA conditions. This is strictly consistent if the selected thermal-hydraulic model for the core is able to differentiate the thermal-hydraulic conditions for each simulated fuel rod accounting for 3D core configuration and LOCA phenomena such as local ballooning. This means that advanced method for LOCA should use 3D thermal-hydraulic model coupled to detailed fuel rod model describing at least each fuel assembly of the reactor core.

Preliminary analysis of DRACCAR meshing capabilities for PWR core modelling

One of the major constraints when performing a 3D simulation concerns the CPU cost of the simulation. The current numerical method used in the DRACCAR software is an implicit scheme coupling thermal-hydraulics and thermal-mechanics. Moreover, model management operates with Open MP parallelism. However, the coupling of thermal-hydraulics and thermal-mechanics embedded in the 3D meshing remains costly for a large domain involving several hundred of hydraulic sub-channels. Consequently, preliminary cases were launched to identify if the cost of full core simulation was sustainable for PWR LOCA simulation.
The detailed representation at sub-channel scale using 3D meshed rods of a 17x17 PWR fuel assembly requires a number of hydraulic sub-channels which overgoes widely the order of magnitude manageable by DRACCAR software in a reasonable CPU time. Indeed, the 3D detailed description of a single 17x17 PWR fuel assembly requires more than 322 thermal-hydraulics channels - which means approximately 12880 hydraulic cells. For the same reason, the 3D detailed fuel assembly is not useable for PWR simulation in a reasonable computational time with respects to the fact that more than 150 fuel assemblies should be simulated. Therefore, a whole core model using 3D detailed fuel assembly meshed at sub-channel scale cannot be at this stage managed by DRACCAR software.

So, with current version DRACCAR 2022, the core should be represented using average channels to regroup sub-channels. This work proposes to use one channel per fuel assembly thus averaging thermal-hydraulic flow within a fuel assembly. Of course, other subdivisions and grouping are possible (such as subdivisions in 4^{th} of fuel assembly proposed by HZDR with ATHLET-CD in the frame of this task). The use of one channel per fuel assembly regrouping sub-channels leads to replace 3D (r-θ-z) detailed rod model by 2D (r-z) equivalent rod model. According to the development carried out in the frame of R2CA, the 2D (r-z) rod model from DRACCAR was upgraded to evaluate creep on 2D (θ, z) clad contour accounting for rod pitch. Thus, DRACCAR equivalent rod model differs from the one of ASTEC as it can reproduce non-circular shapes representing rod-to-rod contact due to ballooning and the associated reduction of friction perimeter and wall-to-fluid exchange surface.

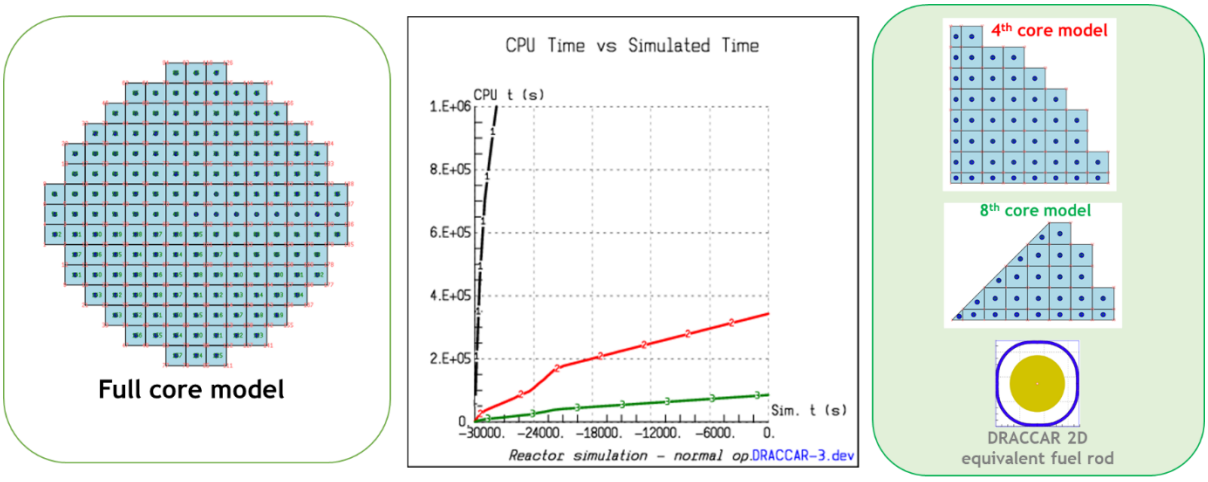

Figure 110: Cut view of DRACCAR core meshing with 2D equivalent fuel rods and associated CPU cost.

Even using one channel with one equivalent fuel rod per fuel assembly, a PWR 900MW full core model corresponds to 157 thermal-hydraulics channels and it leads to CPU times which are not sustainable to perform plant transient studies (or even worst to run parametric studies or to associate uncertainty methodology due to the required number of simulations). Therefore, the proposed core model with DRACCAR was simplified. Even if the LOCA is a non-axisymmetric accident which affects one of the primary loops and induces non uniform flow distribution in the core, the compromise between the detail of modelling and CPU cost imposed to restrict the DRACCAR core model to a part of it by considering only part of the core. Fortunately, such simplification is consistent with the core loading map and characteristics symmetries which allow to consider only the 4th or the 8th of the core (both are suitable for DRACCAR PWR simulation however to obtain better CPU performance 8th core model is recommended). The 8th core model uses 26 thermal-hydraulics channels, each of them considering at least one equivalent representative fuel rod – this means at least one per fuel assembly. The minimum recommended height of the thermal-hydraulic meshes, and fuel rod slices is 10 cm. It implies that core is represented by 1040 thermal-hydraulic cells in 3D meshing and nearly 1500 2D meshed structures (fuel rods, control rods, spacer grids).
Because of the simplification to the fraction of the core, the complete core vessel cannot be modelled in a 3D Reactor Pressure Vessel (RPV) model. Therefore, the reactor pressure plena and downcomer should use a 1D description because the simplified core domain provides an overall response of the complete core. The 3D distribution of flow in the RPV resulting from the behaviour at the loop connections and the non-symmetric behaviour of primary loops during LOCA cannot be captured by such a model.

Need to model fuel assembly behaviour under LOCA conditions at the sub-channel scale

The use of the equivalent rod model is accompanied by neglecting the local characteristics and phenomena which impact distinctively the fuel rod within the fuel assembly. Indeed, due to its location in the core, the boundaries of the fuel assembly are not subject to the same neutronic, thermal and flow conditions. These conditions are possibly influenced by neighbouring fuel assemblies' characteristics and behaviour during the accident. The possibility of propagation of the heat-up zone from one assembly to another is uncertain. This point is furtherly discussed with the help of specific case studies.
Moreover, by design, the fuel rod characteristics and environment are not homogeneous among the fuel assembly as illustrated for a MOX PWR fuel assembly on Figure 111. The neighbouring of the guide tubes is associated to thermal cold spots. Moreover, some of the fuel rods in the assembly can be filled with different types of fuel oxide pellets, the initial enrichment of which can differ. Within the same fuel assembly, the fuel rod initial state and in particular the local power or the rod internal pressure (RIP) can vary significatively as illustrated by the evolution

of RIP evaluated for MOX PWR-like fuel assembly with fuel performance code FRAPCON 4 PNNL / US-NRC (Figure 111).

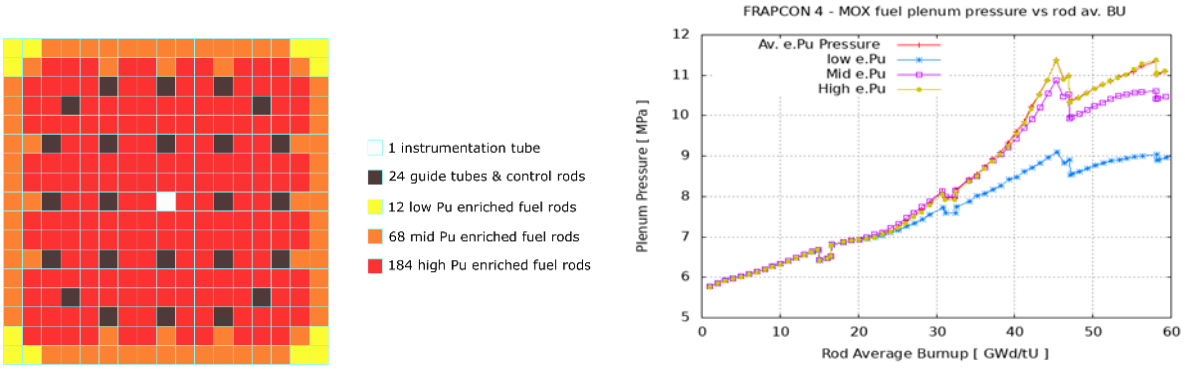

Figure 111: PWR 17x17 MOX type fuel assembly configuration with 3 distinctive Pu enriched fuel rods and associated rod internal pressure evolution with burn-up computed by FRAPCON 4.0 PNNL - USNRC

Based on a fuel assembly case representative of an intermediate break in PWR, the magnitude of deviance in the rod response among a MOX type PWR fuel assembly at end of life was studied. Two levels of modelling were compared:

- One corresponding to the fuel assembly description in the 8th core model – a single average thermal-hydraulics channel with a single equivalent rod representative of the considered fuel assembly;
- Another corresponding to the 3D detailed model of a fuel assembly restricted to 8th of fuel assembly description and proposing details such as 3D meshed fuel rods, guide tubes and accounting for fuel rod specificities (non-uniform power distribution in fuel assembly, several Pu enrichments, …).

The whole thermal-hydraulic circuits are not modelled in this simplified case and results from system thermal-hydraulic simulation are imposed at bottom and top of the DRACCAR fuel assembly domain to reproduce the two-phase flow conditions in the core channels occurring during the LOCA (using IRSN CESAR thermal-hydraulic module). In both cases, boundary conditions are used to close the two-phase thermal-hydraulics problem by imposing flow and pressure conditions at inlet and outlet of the fuel assembly channels. The flow distribution at bottom is insured by defining a homogeneous volume.

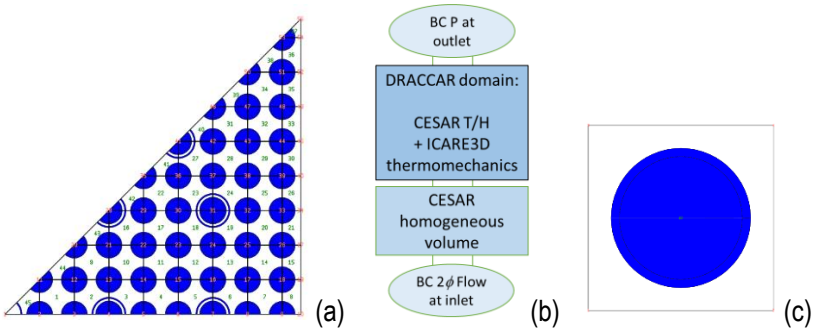

Figure 112: DRACCAR 3D modelling of one eighth of a PWR 17x17 fuel assembly (a), 2D single equivalent rod model in square cell of side the fuel rod pitch (c)
and schematic view of the DRACCAR model network and boundary conditions (b).

Table 46 regroups the main characteristics of the 3D modelling and of the 2D single equivalent rod model of PWR 17x17 MOX fuel assembly.

DRACCAR modelling	3D (r,θ,z) detailed modelling	2D (r,z) single equivalent rod
Fuel assembly type	MOX 17x17 fuel assembly	
Modelling	3D meshing reduced to 1/8th of FA	1 equivalent rod for the FA: 1 square cell of side rod pitch
Number of modelled fuel rods	39 rods 3D meshed	1 rod 2D meshed
Other modelled FA elements	5 control rods & guide tubes 1 instrumentation tube 8 spacer grids	-
Thermal-hydraulic channels	45 sub channels	1 sub channel
Axial discretization	40 axial levels over the active fuel length	
Cladding azimuthal discretization	3 to 4 thermal nodes 20 to 40 mechanical nodes	1 thermal node 20 to 40 mechanical nodes

Table 46 : Main characteristics of DRACCAR fuel assembly cases

Two different 3D detailed models were developed. The first one aims at comparing the 3D detailed model and the 2D single equivalent rod model on an idealized configuration focusing on “cold rod” effect driven by guide tubes position. To make the comparison easier between the fuel assembly 3D detailed model and the equivalent rod model, the same initial rod state and uniform distribution of power within all rods of the fuel assembly are assumed in this “idealized” case. It corresponds neither to a realistic distribution of the power over the rods of the fuel assembly nor to a realistic initial state of the rods. But even with identical rod states and uniform power distribution, this fuel assembly case does not correspond to a uniform configuration when using 3D meshing as the 24 guide tubes and the instrumentation tubes are represented. As a consequence, the 3D detailed model on this “idealized” case highlights the influence of the non-heated rods on the fuel rod responses to LOCA.

The second case using 3D detailed model relies on realistic assumptions by distinguishing the fuel rod characteristics such as rod power factors and the initial Pu enrichments. This corresponds to a “realistic” simulation using 3D detailed model with non-uniform distribution of power in rods of the fuel assembly (varying in 90-105% range of nominal power) and accounting for different initial rod states (evaluated by FRAPCON and using the 3 different types of initial Pu enrichment).

The thermal-hydraulic conditions correspond to a 15 inches LOCA break associated to a delayed cooling which leads to significant rod ballooning. The fuel assembly studied is a PWR 17x17 MOX fuel assembly with an average burn-up of 55 GWd/tHM. Several assumptions were selected to maximize the rod response in terms of strain (and cannot be considered fully representative for the safety analysis).

Main DRACCAR results	Unit	3D detailed model		2D Single equivalent rod idealized
		idealized	realistic	
Maximum circumferential strain	%	21 to 42	9 to 47	35
Mean of max. circ. strain ± std deviation (over all modelled rods)	%	37 ± 5.5	34 ± 10.5	
PCT	°C	673 to 707	664 to 713	692
Mean PCT± std deviation (over all modelled rods)	°C	689 ± 9	690 ± 13	

Table 47 : Comparison of 3D detailed meshing to an equivalent rod approach on an idealized single fuel assembly modelling.

The comparison of main results in Table 47 shows that the mean value of circumferential strain and PCT are well reproduced by the equivalent rod approach. However, one can notice on 3D meshing results that the obtained strain distribution is dispersed around the mean value (cf. Figure 113). Considering this scattering, differences on the evaluated strain between 3D model and 2D equivalent rod model are significant. Indeed, the presence of guide tubes whose locations generate a non-uniform temperature distribution and the local characteristics of rod (power and initial state associated to Pu enrichment) play a non-negligible role in rod response to LOCA. It's important to underline those discrepancies cannot be only attached to rod local characteristics and therefore that results are transposable to UO_2 17x17PWR fuel assembly. Indeed, even with iso-characteristics of fuel rods (same initial rod state and power), the presence of guide tubes impacts enough the temperature distribution to significatively influence strain and rod response to LOCA (cf. Figure 114).

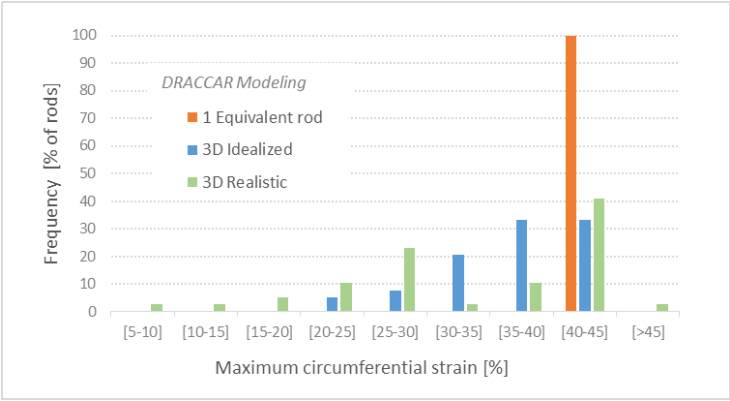

Figure 113: Distribution of rod maximum strains for MOX PWR 17x17 fuel assembly cases using equivalent rod approach and 3D meshing with idealized or realistic assumptions.

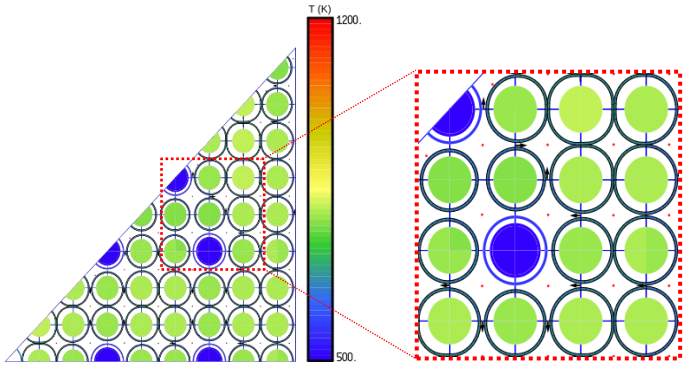

Figure 114: Thermal field and rod deformations simulated with DRACCAR 3D detailed PWR 17x17 fuel assembly model highlighting cold region close to guide tubes and non-symmetrical balloon contour.

The difference on maximum strains for rods belonging to the same fuel assembly on this case evaluated by DRACCAR are sufficient to create discrepancies on burst occurrence. Therefore, the 3D detailed modelling of fuel assembly is recommended to predict with confidence the number of failed fuel rods. The single equivalent rod model is nevertheless able to capture mean behaviour but cannot be considered as "best estimate". Therefore, one should take care that even if the burst threshold is not reached using an equivalent rod model, equivalent model cannot represent scattering among rods described by this model. This scattering could be such that the burst threshold would be reached by some of these rods. It means that using several equivalent rods to represent

fuel assembly (as proposed with ASTEC model and tested by ENEA) is not enough to have a good estimation of the number of failed rods.
Therefore, 3D model at sub-channel scale with azimuthal thermal meshing for rods is needed to predict with higher confidence fuel assemblies' behaviour during LOCA. Due to a compromise regarding the CPU cost, equivalent rod model for the whole core description was chosen for DRACCAR simulation but this work demonstrates that these simulations should be coupled with an analysis using a 3D detailed model (in particular for the fuel assembly whose average response is close to burst threshold). Therefore, based on this work, the proposed methodology to evaluate the number of failed rods under LOCA conditions with DRACCAR was chosen to mix both scales: full core approach using equivalent rod models and additional detailed fuel assembly studies using 3D fuel assembly model at sub-channel scale.

Analysis of the interaction between fuel assemblies during LOCA

Considering the heterogeneous distribution of power factor and burn-up in the core, one issue concerns the influence of a "hot" fuel assembly on its "colder" neighbours. In particular, the fuel rods located at the border of the fuel assembly could be influenced by the fuel rod belonging to the neighbouring fuel assembly.
For neighbouring fuel assemblies, the discrepancies of response between fuel rods are expected to be in relation with stored energy, decay heat and burn-up (influencing fuel rod characteristics, free volumes and rod internal pressure). A specific case study was built to investigate this issue. It consists in a slice of length of the fuel assembly pitch, composed of 17 sub-channels and filled by two rows of half fuel rods. This configuration is supposed to represent two neighbouring fuel assemblies separated by fuel assembly gap. To do so, two groups of fuel rods are considered (cf. Table 48); these are selected to represent the maximum difference in stored energy related to neutron power during normal operation.

Characteristics of the group	Unit	Fuel group 1 "cold"	Fuel group 2 "hot"
Average Power factor (representative of stored energy)	-	0.98	1.21
Average burn-up of fuel assembly	GWd/tHM	~50	~25

Table 48 : Comparison of 3D detailed meshing to an equivalent rod approach on an idealized single fuel assembly modelling.

For each of these groups, the condition of the representative rod has been assessed by fuel performance simulation using FRAPCON 4 software. In addition, a specific decay heat factor was set from VESTA results that are representative of the respective burn-up of the group.

Three configurations are compared, the first one representing two fuel assemblies each composed of rods from one group. The two other configurations represent two fuel assemblies, both composed by fuel rods from the same group.

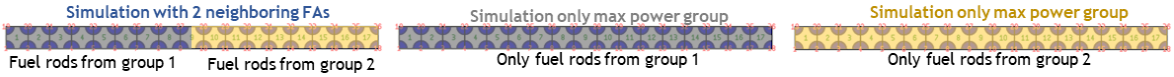

Figure 115: Three cases based on 1D slice of subchannels representative of 2 neighbouring fuel assemblies.

The thermal-hydraulic conditions correspond to a 15 inches LOCA break associated to a delayed cooling which leads to significant rod ballooning and are imposed at boundaries of the DRACCAR domain (similarly to 8th fuel assembly case study presented previously).

The PCT and strain evolutions were analysed with attention to the influence of higher power of group 2 on the rod of group 1 in the first configuration. As shown in Figure 116 (b), when considering two groups of fuel assemblies, the overall response of rods is close to the limit cases considering only one group of rods. At a given time as illustrated in Figure 116 (a), the PCT for the rods located at the boundary do not show a heat-up of the "coldest" assembly by the "hottest" one. Indeed, the coupling between thermal-hydraulics and thermal-mechanics lead to a slight increase of convective heat transfer on "cold" rods due to flow redistribution as "hottest" rods deformation is higher. This effect tends to lower the "cold" rod temperatures at the fuel assembly boundary.
Therefore, the case which was studied with DRACCAR shows that the influence of the neighbouring fuel assembly is mainly carried by the thermal-hydraulic redistribution of the flows. The heat-up effect of higher stored energy fuel assembly on its neighbour is not demonstrated by DRACCAR simulation. Consequently, it suggests that there's no need to explicitly model specific interactions from one fuel assembly to another except by representing thermal-hydraulics in 3D. This work suggests that the proposed core model must represent each fuel assembly in separated thermal-hydraulics channels and that the refinement of the modelling scale at fuel assemblies' boundary is not required.

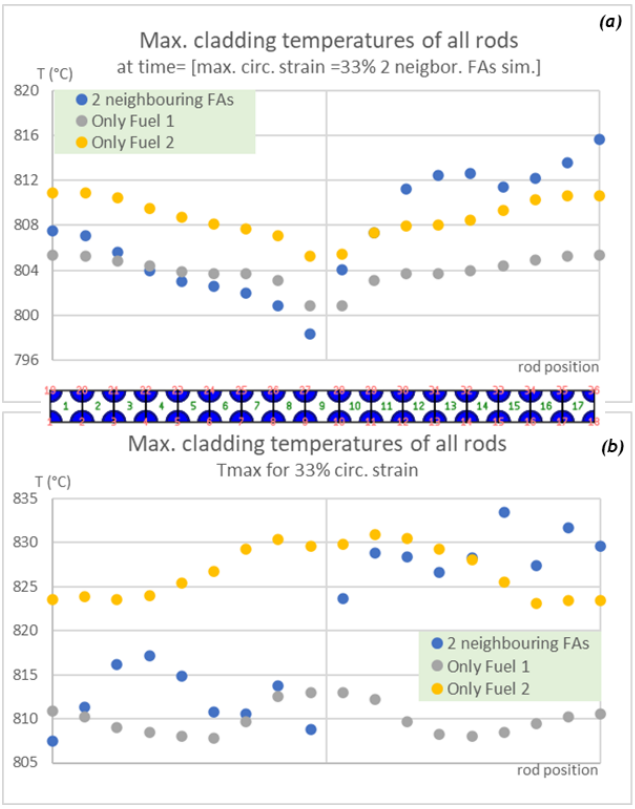

Figure 116: PCT for each rod obtained when max circumferential strain 33% is reached for first time by one rod *(a)*
PCT for each rod when rod circumferential strain is 33% *(b)*

Fuel rod modelling choices for whole core application

Fuel rod modelling

Specific physical modelling dedicated to LOCA phenomena is recommended to assess burst risk in the frame of R2CA. From 2006, DRACCAR software was specifically developed for LOCA simulation and gathered the knowledge acquired on the LOCA phenomenology. DRACCAR proposes classical heat transfer description of the

fuel rod, rod-to-rod interaction (including heat radiation between rods, contact) and specific wall-to-fluid heat transfer (including reflooding model) coupled to 2-phase flow 3D modelling. The creep of the cladding is described by a 2.5D model assuming thin shell formulation and in which the creep rate is represented by a Norton-law associated to a phase transformation model. Thermal-hydraulics and thermal-mechanics are strongly coupled within an implicit scheme which accounts for the impact of the clad deformation and of the contact on the flow characteristics (friction, section) and wall-to-fluid heat exchanges.

In addition, recent parametric models developed in DRACCAR are now available to investigate impact on rod behaviour of some phenomena such as:

- the fission gas release associated to fuel temperature evolution during LOCA heat-up ramp;
- the gas transport within rod directly related to rod internal pressure distribution and ballooning;
- the fuel relocation in rod balloon which influences the local power in the deformed zone.

The proposed methodology for evaluating the number of failed rods benefits directly from the development effort of the DRACCAR software which proposes advanced modelling of fuel rod specific to LOCA. These efforts were pursued in the frame of R2CA and are depicted in this section.

Improvement of contact modelling in DRACCAR when using 2D meshed equivalent rod

The proposed DRACCAR model for the core considers equivalent rods. This solution simplifies the core modelling in order to reduce CPU cost of the LOCA simulation. In DRACCAR application, outside from R2CA project frame, the equivalent rod model was almost never used to model creep as the 3D modelling was mainly the target of DRACCAR. The equivalent rod model was very simple and its use in the frame of R2CA studies required some model updates.

In DRACCAR, this equivalent fuel rod model consists in a single rod located in a thermal-hydraulic channel and associated to a numerical weight which corresponds to the number of “real” rods represented by this equivalent rod. The physical modelling associated to equivalent rods is simple and close to the one of ASTEC fuel rod model. In this equivalent rod model, cladding creep was evaluated assuming that the clad contour remained circular and could extend freely without any limitation. This model presented a major drawback because it did not take into account the fact that fuel rods are organized in a lattice and that the clad only extends freely until it comes into contact with its neighbours. Therefore, its use for balloon prediction led to erroneous heat exchange surface evaluations.
In view of using an equivalent rod model for modelling the whole core, it seemed necessary to propose a more realistic modelling of creep with an equivalent rod model. New feature was developed for equivalent rod model cladding creep in order to restrict ballooning to the rod pitch. The DRACCAR equivalent rod model uses 2D (θ, z) meshed clad contour discretized using nodes. Creep rate is evaluated at each node of the meshed contour. When the node radius exceeds half of the rod pitch, the contact at this node is assumed by the new equivalent rod model. Thus, the same assumptions about contact are made as for the DRACCAR 3D detailed rod model. This new feature allows to account for progressive contact, noncircular shape clad contour as well as fluid-clad exchange surface reduction. Therefore, the equivalent rod behaves as if it was included in a square pitch lattice composed of identical rods as shown in Figure 117.

This development is suitable in DRACCAR modelling which is based on 2D (θ,z) meshed clad contour. However, such meshing is not available in some system codes. Therefore, IRSN proposes an algorithm to better account for rod deformation at contact for codes using equivalent fuel rods with 1D(z) meshed clad such as in ASTEC system code for source term evaluation.

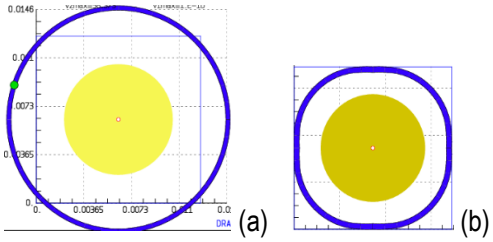

Figure 117: Example of DRACCAR fuel rod simulation using the 2D equivalent rod model with previous mode assuming free development of balloon with circular clad contour (a) and the new model which limits the clad contour extension to the rod pitch (b).

Proposal of contact surface evaluation for codes using equivalent rod with 1D(z) meshed clad contour

Some system codes such as ASTEC use an equivalent rod model with 1D (z) meshed clad contour. At each elevation, a single creep rate is evaluated according to a Norton-based creep law. Therefore, assuming circular shape for the clad lead to compute an average clad radius which is updated at each time step according to the creep deformation. Without specific management of the contact, this radius can exceed the rod pitch. So, the first improvement could consist in restricting (if not already done) the equivalent clad radius to $\frac{p}{\sqrt{\pi}}$ with p the rod pitch.

However, even with this limitation, when the radius is greater than $\frac{p}{2}$, it seems relevant to consider that the equivalent rod is in contact over a part of its clad contour with its neighbours. But the circular shape contour is not adapted to predict this contact ratio. So, for such simple modelling, a second interesting improvement is to use a mathematical expression to deduce non-circular clad contour shape when the radius exceeds half of the rod pitch. This method shows its benefits when evaluating the contact surface ratio to correct wall-to-fluid heat exchange surface.

The basic principle of the method is exposed in Figure 118. From initial configuration, the radius of the clad progressively increases due to the cladding creep. As soon as the diameter of the clad exceeds the fuel rod pitch, a shape function could be used to evaluate the non-circular shape corresponding to the surface area occupied by the equivalent circular clad contour.

Concerning the shape prediction, the following function is suggested: $|x|^k + |y|^k = \left|\frac{p}{2}\right|^k$, with *x, y* the Cartesian coordinates of midline clad contour, *p* the rod pitch and *k* a real number in $[2, +\infty[$.
This function presents the interest to correspond to a circle for k=2 and its shape tends progressively to the square when $k \to +\infty$ as shown in Figure 118. Therefore, the proposed algorithm on this figure aims at evaluating the clad heat exchange areas accounting for contact based on the equivalent rod deformation obtained using circular assumption. The contact ratio is deduced from the computed iso-surface area non-circular shape. This solution could be easily implemented in system codes such as ASTEC in order to refine and to reduce the fluid-to-clad exchange surface as well as the radiative exchange surface.

Of course, such a method does not provide an exact solution of the clad shape and especially when clad undergoes non-axisymmetric thermal loading. Nevertheless, it's a simple method that can significantly improve codes which assume circular clad contour during the whole development of the balloon.

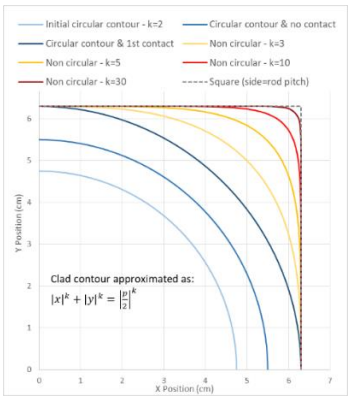

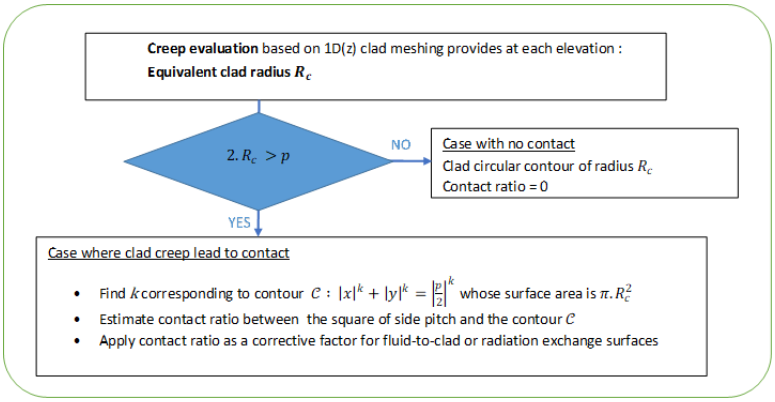

Figure 118: Shape function approximating the clad contour all along its deformation (at left), corresponding algorithm to evaluate contact surface ratio when using a 1D(z) equivalent rod model as in ASTEC code (at right).

Impact of the radial discretization of the fuel column in DRACCAR simulations

In DRACCAR software, fuel pellets and fragments are represented by a fuel column which can be meshed in 3D (r,θ,z). During a LOCA, the SCRAM occurs in the first seconds after initiator and leads to a rapid decrease in neutron power. Therefore, fuel power is driven mainly by decay heat and radial temperature gradients within the fuel are less than during normal operation. The fuel modelling in DRACCAR mainly focus on heat transfer (power generation, heat conduction in fuel column and gap exchange to the clad) and model associated to fuel relocation. Considering magnitude of the radial thermal gradients and the simplified modelling, the use of a high number of radial fuel meshes is not necessary. However, a specific study aims to identify the recommended number of radial meshes for the fuel that must be considered for the DRACCAR core model.
To do so, the 8th fuel assembly model was used and associated to a parametric study on the number of radial fuel meshes. The results shows that the consistency of results on the PCT is obtained using 9 radial meshes. It's also important to underline that PCT is not highly sensitive to the fuel meshing.
The use of 9 radial meshes for the fuel column increases the number of thermal elements which describe the core in DRACCAR simulation. For example, for the DRACCAR PWR900 MWe 8th core model, using 9 fuel radial meshes instead of 1 increases of more than 800 the number of thermal elements. However, the number of thermal-hydraulic channels remaining unchanged, the final CPU cost of the radial meshing on LOCA simulation is still suitable for a reactor core application.

Fuel rod characteristics initialization
To better define the fuel rod characteristics in DRACCAR, an automatic procedure was developed to generate input data for DRACCAR from FRAPCON 4.0 results. This procedure is used to initialize distinctively the 26 equivalent fuel rods modelled in DRACCAR 8th of core application.

Burst risk assessment using the new burst criterion proposed by IRSN in the frame of R2CA
In the frame of task WP3.2, IRSN revisited the experimental burst database and new burst criteria were proposed specifically to assess the burst risk. These new burst criteria were implemented in the Material Data Base (MDB) of the DRACCAR software. These new criteria are presented page 29, recommendations for the choice of criteria suitable for LOCA simulation targeting the evaluation of the number of failed rods are proposed.

New methodology for the prediction of the number of failed rods under LOCA conditions

Several features and characteristics needed to assess the number of failed rods were identified through preliminary analysis and complementary DRACCAR case studies. Those ones were considered to propose the new methodology in particular:

- LOCA simulation requires specific management of the coupling between thermal-hydraulics and thermal-mechanics. Moreover, some phenomena related to fuel behaviour can modify significatively the clad response to the LOCA conditions such as the fuel fragmentation and the fission gas release;
- Due to wide range of fuel assembly characteristics (power, burn-up, location, …), assessment of the burst risk should rely on the simulation of the behaviour of each fuel assembly from the core accounting for its own characteristics (location, power, fuel type and rod state);
- 3D core thermal-hydraulic is needed to compute the flow distribution among the different fuel channels and the possible crossflows due to ballooned zone;
- Burst assessment needs specific burst criteria dedicated to rod failure assessment which are slightly different from coolability assessment;
- Modelling fuel assembly at a refined scale is needed to account for local phenomena at subchannel scale such as the presence of guided tubes or to distinguish the fuel rods among the fuel assembly. Indeed, DRACCAR case studies showed that scattering of rod responses among a fuel assembly can be significant and should be captured by 3D detailed fuel assembly modelling (and not only by equivalent rod approach);
- No heat-up propagation from higher stored energy fuel assembly to other fuel assemblies was found from DRACCAR case studies, however thermal-hydraulic redistribution of the flow between the ballooned zone and the less blocked channels was identified.

Based on these requirements, the new methodology proposed by IRSN with DRACCAR software is presented on Figure 119.

One key element of this methodology concerns the input data. Indeed, this approach is based on several data which mix information on plant and fuel design, assumptions on transient and safety system availability and also a set of input which can be produced by simulation using neutron physics software (IRSN VESTA evolution code) or fuel performance code (such as the US NRC software FRAPCON 4.0 developed by PNNL). As the new DRACCAR core approach aims to discriminate fuel assembly behaviours during LOCA and should also propose detailed analysis of the response of each fuel rod within fuel assembly, it is necessary to collect relevant data to describe the condition and characteristics on each fuel assembly or fuel rods. These data are used to set the initial state (geometries, stored energy, decay heat, rod internal pressure, fission gas composition, …) in each fuel rod modelled by DRACCAR to account as best as possible for the parameters which impact the rod response during the LOCA.

Those data are used for DRACCAR simulations. The new approach is built by mixing two kinds of DRACCAR simulations at different scales. The first scale corresponds to the whole core modelling coupled to reactor coolant system modelling. The core simulation evaluates the response of the different fuel assemblies composing the core using a set of representative equivalent rods (at least one per fuel assembly). The second scale corresponds to a detailed modelling of the fuel assembly in order to simulate the response of each fuel rod belonging to the fuel assembly accounting for specificity of rods (local power, fuel type, ...) and location (neighbourhood of guided tubes, …). The approach is based on the simulation of the average response of each fuel assembly to LOCA conditions. This provides thermal-hydraulics conditions averaged for each fuel assembly. Those results can be used as boundary conditions coupled to 3D detailed fuel assembly models. Therefore, each fuel assembly analysis can be

refined at sub-channel scale. The main characteristics of the DRACCAR models making up the new approach are depicted in Table 49.

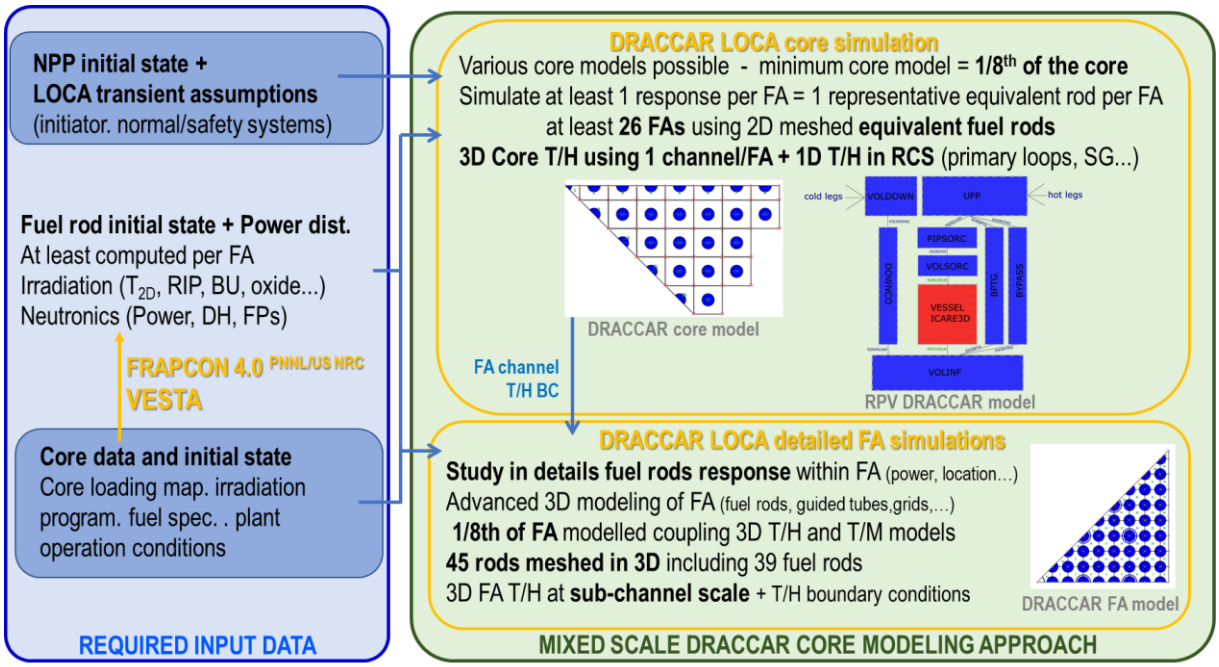

Figure 119: DRACCAR new core modelling approach to evaluate the number of failed rods during LOCA for LWR developed in the frame of R2CA project.

The new approach can provide response of each fuel assembly to LOCA transient both simulating thermal-hydraulics in the core (3D) and in the reactor circuits (1D). The different systems and events of the transient are modelled using the models available in the thermal-hydraulic code (CESAR IRSN or CATHARE-3 CEA) and allow to predict the whole LOCA transient and especially the influence of emergency safety systems by injection of water and the induced reflooding of the core. The main difference of this approach with classical DBA model is that each fuel assembly is represented using a “realistic approach”. The thermo-mechanical behaviour of the fuel rods of each fuel assembly is evaluated and coupled to thermal-hydraulic conditions using a channel for each fuel assembly and embedded in a whole 3D core domain. Due to CPU cost constraint, the whole core cannot be modelled at sub-channel scale, but the proposed approach allows to connect core model providing average fuel rod response for each fuel assembly to detailed 3D simulation at sub-channel scales. These 3D detailed simulations can be run in stand-alone for each of the fuel assembly of the core. As local phenomena occurring at sub-channel scale can significantly influence the rod response to LOCA, it seems necessary to focus on the fuel assembly in detail. This can be done using the 3D detailed 8th fuel assembly model whose boundary conditions can be fed by whole core simulation based on equivalent rod approach. So, this approach is a good compromise between details of modelling and CPU cost. It allows to perform core and detailed fuel assembly simulations providing the evaluation of the number of failed rods under LOCA conditions in a reasonable computational time which allows to perform sensitivity studies or to combine these best-estimate simulations to uncertainty methods (BEPU).

DRACCAR modelling	DRACCAR core & RCS model	DRACCAR detailed fuel assembly model
Description scale	Core (assuming symmetries) + RCS minimum: 1/8th of core = 26 FA	Fuel rod sub-channels 1 fuel assembly described in detail
Fuel assembly description	Average 2D model At least 1 equivalent fuel rod 1 equivalent control rod+guide tube 1 equivalent instrumentation tube 8 spacer grids + support grid	8th FA Detailed 3D model 39 fuel rods 5 control rods & guide tubes 1 instrumentation tube 8 spacer grids
Fuel rod description	Equivalent rod model 2D (r,z) thermal meshing Creep: 2.5D (θ,z) clad contour	3D detailed rod model 3D (r,θ,z) thermal meshing Creep: 2.5D (θ,z) clad contour
Fuel rod axial discretization	At least 40 axial slices	
Cladding azimuthal discretization	1 thermal node At least 40 mechanical nodes	At least 3 to 4 thermal nodes At least 40 mechanical nodes
Fuel thermal meshing	Azimuthal: same as clad 9 radial meshes	
Fuel rod heat transfer modelling	3D (r,θ,z) conductive heat transfer including at contact between rods Wall-to-fluid convective heat transfer including 2-phase flow regimes, reflooding model and accounting for ballooning and contact	
	Simplified FA to FA radiation heat transfer based on effective conductivity and equivalent radiative resistance of FA	Rod-to-rod radiative heat transfer accounting for deformation and shading (based on Hottel methods)
Fuel heat generation	Normal power evolution (rod power factor, axial profile, time evolution) Decay Heat from time evolution law (rod power factor, axial profile, time evolution) or from FP isotopes decay (evaluated by ISODOP module) Relocation of fuel associated to mass and energy transfer within fuel rod	
Thermomechanical modelling	2.5D (r,θ,z) secondary creep model with contact detection (Norton-law for creep rate + phase transformation) New burst criteria specific to burst risk assessment (developed in frame of R2CA) Advanced phenomenology: gas transport within fuel rod, fuel relocation	
	Rotational symmetry of clad contour over the rod axis Contact management: non-circular clad contour if radius exceeds rod pitch	Non-axis-symmetrical deformation rod-to-rod contact management Impact of azimuthal thermal gradients
Core thermal-hydraulic description	3D 2-phase flow model with implicit coupling to thermal-mechanics (CESAR[IRSN] or CATHARE-3[CEA]) Same axial discretization as the one used for fuel rods	
Core thermal-hydraulic channels	26 FA channels	45 sub-channels
	Same axial discretization as the one used for fuel rods (40 axial levels)	
RCS thermal-hydraulic description	Full RCS model using thermal-hydraulics 1D system description for circuits (CESAR[IRSN] or CATHARE-3[CEA])	Boundary conditions from DRACCAR LOCA core+RCS or system code RCS simulations
RPV modelling	3D core domain 1D downcomer 0D lower and upper vessel plenums Junction to RCS model (connection to 1D meshed primary loops)	3D core domain only
FPs release	evaluated for each FA - Evolution of Initial FP isotopes total inventory of the core from ISODOP module and release evaluation from ELSA module (ELSA and ISODOP modules from ASTEC V2.2.0 are embed in DRACCAR software)	
Automatic chain to source term evaluation tool	Chained to ASTEC simulation with FP transport and release modelling based on same RCS description	No (Since no RCS is modelled)

Table 49 : Description of the new DRACCAR PWR modelling approach proposed in the frame of the R2CA project and used to predict the number of failed rods.

Prospects and possible improvements for the new approach

In the frame of R2CA, IRSN proposes a new methodology with the DRACCAR software to predict the number of failed rods during LOCA which is a key parameter influencing the source term and the radiological consequences of LOCA. DRACCAR development is pursued to improve physical modelling or to extend the software capabilities. This work is directly associated to the R&D activities at IRSN and the production of knowledge relative to the thermal-hydraulics under LOCA conditions (reflooding, impact of ballooned zone on core coolability), to the mechanical behaviour of the cladding materials (influence of azimuthal temperature gradients on ballooning, influence of contact on burst, description of advanced and new cladding materials such as ATF,…) and to the processes affecting the fuel and impacting rod response (fuel fragmentation and relocation, fission gas release and transport, …). The progressive improvement of models will participate to better predict the number of failed rods under LOCA conditions.

In addition, some prospects concern the current limitations of the DRACCAR approach which can be dealt independently from physical modelling improvement. One limitation of the proposed methodology concerns the core model which only represent a part of the core (8^{th} or 4^{th} of core assumed to represent the average response of the whole core to LOCA) instead of a full core model where all fuel assemblies would be modelled. Therefore, without a full 3D RPV model, the non-symmetric distribution of flow within the core (due to location of the break on one of the primary loops) is not represented whenever it could strongly impact the rod response. This limitation of the approach relates to the DRACCAR numerical performance which needs to be improved to allow LOCA simulation of the whole core in a reasonable CPU time. At the same time, improving computational performance of DRACCAR software should allow to propose 3D sub-channels simulation on extended domain. For instance, such extension of the domain could be useful to better study flow redistribution at fuel assembly boundaries or between fuel assemblies.

Another limitation is directly associated to the initial fission product inventory and release. Assessing the radiological consequences of LOCA requires the evaluation of the source term and then to compute the initial fission product inventory and the fission product release during LOCA. According to the proposed methodology which distinguishes the different fuel assemblies composing the core and predicts the eventual failure of their fuel rods, it seems relevant to gather fission products inventory and release particular to each fuel assembly. In the frame of DRACCAR application, it means managing multiple initial fission products inventories (at least one per fuel assembly) instead of the total core inventory. Moreover, the decay of fission products must be computed for each of these inventories (multiple ISODOP computations embedded in DRACCAR simulation instead of just one on the total core inventory). Concerning the fission products release, ELSA from ASTEC V2.2.0 severe accident integral code is used. One the prospects is to improve fuel modelling in the FUEL+ software platform to which the DRACCAR software belongs by coupling DRACCAR fuel rod model to new models describing the fission gas behaviour in fuel and its possible release under LOCA conditions.

Finally, the new DRACCAR core model approach which was developed in the frame of R2CA for the radiological consequences provides new insights on the LOCA simulations which must be deepened. With adaptation, this methodology could serve as the basis for creating a specific whole core methodology for PCT evaluation and coolability assessment. Development and software improvement are pursued to better model the physical phenomena affecting fuel rod response under LOCA conditions and to extend the DRACCAR software performance and capabilities with the idea of simulating the full RPV in 3D.

HZDR : New 3D core modelling approach with ATHLET-CD

An important goal to be reached in the framework of the R2CA project are new methodologies to estimate the number of burst rods during LOCA accidents. This is a necessary prerequisite for quantifying the source term, i.e., the amount of fission products released from the core into the containment (and further into the environment) during the accident.
According to German licensing guidelines for PWR, the emergency core cooling system has to be designed such that at maximum 10 % of the fuel rods burst during the LB-LOCA accident [103]. To estimate that number, a detailed core model is needed, which take a realistic power distribution and local thermal-hydraulic conditions (pressure, temperature, void, coolant mass flow rates) into account. The rod behavior with rod deformation, burst of rods and the feedback to thermal-hydraulic has to be included.
At the beginning of the project (Task 2.3), LOCA simulations have been performed with the system code ATHLET-CD, using a coarse core nodalization with 6 concentric rings. However, with that coarse model, no prediction could be made about the number of burst fuel rods.
Therefore, a new core modelling approach has been developed, which combines an already existing approach for the thermal-hydraulic modelling with the capabilities of ATHLET-CD (mechanical rod behavior model and rod burst models, calculation of product inventory, release and transport of fission products). The new approach provides a much more detailed modelling of the core compared to previous applications of ATHLET-CD.
The thermal-hydraulic model is described first (section 0), followed by the new ATHLET-CD core nodalization and necessary modifications of the code (section 0). The mechanical rod behavior model of ATHLET-CD is discussed in section 0 and the derivation of the 3D power distribution is shown in section 0. Limitations of the current model are summarized in section 0.
To show the capabilities of the new model, results of LOCA analyses performed for a generic German PWR are discussed in section 0.
There have been previous studies with assessment of the number of failed rods during a LB-LOCA performed for German PWR. Usually the reported fractions of failed rods are small:

- Siemens [104] reported a fraction of failed rods of 0.6 % obtained by deterministic (conservative) analyses for German PWR
- GRS reported a fraction of failed rods of 3.2 % for German PWR [104][105]
- Heins obtained in his analyses a fraction of failed rods of 1.8 % [105][106]

However, for conservative analysis the number of failed rods can be close to the 10% criterion, e.g. GRS reported 9.1% for a Konvoi analysis if the conservative NUREG-0630 failure criterion is applied [104]. Siemens reported a value of up to 16.6% for application of the same conservative failure criterion in combination with a conservative core census (distribution of fuel rods by maximum linear power and burn-up steps) [104].
Those studies included a thermal-hydraulic analysis of the LOCA by application of system codes like RELAP or ATHLET, but they did not include a 3D model of the RPV. Instead, a rather coarse scheme has been applied to determine the thermal-hydraulic boundary conditions, which were used afterwards by a transient fuel rod model, such as BETHY or the GRS code TESPA [104].

Description of new core modelling approach

Thermal hydraulic model of plant and reactor vessel

The reactor pressure vessel is modelled by a hydraulic multichannel approach, i.e. the thermal-hydraulic domain of the RPV is subdivided azimuthally into inter-connected parallel channels. These channels are represented in ATHLET by so called thermo-fluid-objects (TFOs) and each TFO is subdivided axially into a certain number of control volumes (CVs), sometimes also called nodes. Adjacent channels are interconnected by so-called cross-connection objects (CCOs), which provide flow paths between adjacent CVs.

The ability to solve the momentum equation in 3D-domains, such as RPVs, was introduced into ATHLET version 3.0A back in 2012 [107], with further improvements introduced in version 3.1A in 2016. Since that time, the 3D option has been applied for various light water reactor thermal hydraulic analyses. Diaz-Pescador et al. investigated the thermal-hydraulics of PWR Konvoi during a main steam line break [108] and the multidimensional fluid mixing during an asymmetric injection of cold water in the primary side of the same reactor type [109].
The validation of ATHLET's 3D capability was based on the recalculation of selected experiments. These include the recalculation of experiments from the ROCOM test facility, which was a mock-up of the 4-loop Konvoi PWR, scaled down by a factor of 5. Several of the ROCOM mixing tests were re-calculated with ATHLET [110]-[115]. Similar approaches have been developed for other system codes, such as RELAP or CATHARE [116].

The new model is based on an ATHLET sample input deck provided with the ATHLET code [117]. That input deck is a 3D model of generic German PWR including 17 core channels and was later extended by HZDR to a more detailed model with 193 core channels [118].
Figure 120 shows the nodalization scheme of the vessel, visualizing the described parallel channel approach.
In detail the new model comprises:

- the downcomer, subdivided into 16 parallel channels (Figure 120 shows two of the 16 downcomer channels);
- the lower plenum, which is subdivided into 1 central channel and 3 concentric rings, each ring subdivided into 16 parallel channels;
- the core region, which is described in more detail below;
- and the upper plenum, which is subdivided into a central channel and 3 concentric rings, each ring subdivided into 16 parallel channels.

All of the aforementioned parts of the vessel (except the core) are modelled by cylinder coordinates system. Furthermore, the upper head of the RPV is modelled by a single large CV, but with by-pass connections between the 16 downcomer sections and the upper head.

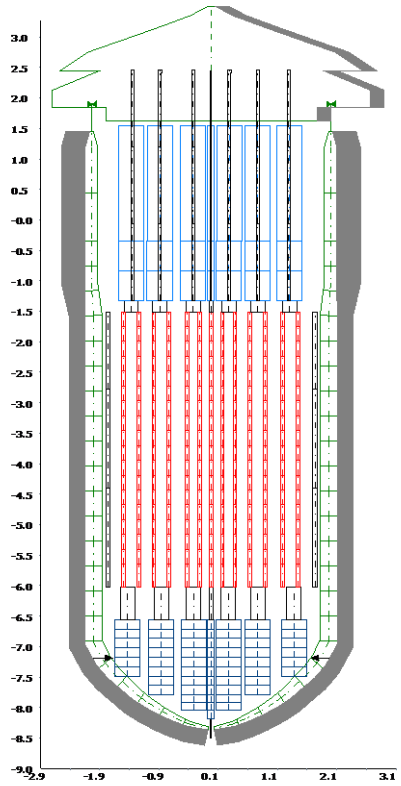

Figure 120: Nodalization scheme of RPV.

The core region of the Konvoi PWR consists of 193 fuel assemblies, arranged by a 15-by-15 matrix. For the new core model, it was decided to model each assembly separately with one TFO per assembly. This results in the scheme shown by Figure 80 with 193 TFOs to model the fuel assemblies. The fuel assembly indexing is arbitrary (mainly in the order from the center to periphery), but important for the reader to orientate within the results given later.

The 193 FA TFOs, which are modelled within a Cartesian coordinate system, have to be coupled to the lower and upper plenum TFOs which are modelled by the above described 3 concentric rings in cylinder coordinates (with 16 azimuthal nodes per ring). That is done by so called branches, which are single control volumes, to which multiple channels can be connected. Each of the lower plenum channels shown in Figure 79 is connected to one core inlet volume (branch object), from which four core channels branch off (only two shown in the figure).

The assignment of the fuel assemblies to the lower plenum topology is indicated by Figure 121 and Figure 122:

- 1 central assembly (#5, marked with orange in Figure 121) is connected to the central channel of the plena
- 64 assemblies of the central part of the core (marked with yellow in Figure 121) are connected to the 1st plena rings
- 64 assemblies marked with green in Figure 121 connected to the 2nd plena rings
- 64 assemblies marked with blue in Figure 121 connected to the 3rd plena rings

16 additional TFOs (marked in grey) represent the reflector channels.

0	0	0	0	204	204	204	204	205	205	205	205	206	0	0	0	0
0	0	203	203	203	160	161	165	166	167	173	174	206	206	206	0	0
0	202	203	154	157	158	159	162	163	164	171	172	179	180	207	207	0
0	202	152	153	155	156	63	64	68	69	169	170	177	178	187	207	0
202	202	149	150	151	58	59	62	67	73	74	168	175	176	186	207	208
201	145	146	147	148	56	57	61	66	71	72	78	79	183	184	185	208
201	142	143	144	53	54	55	60	65	70	75	76	77	84	181	182	208
201	140	141	49	50	51	52	7	8	9	80	81	82	83	192	193	208
201	138	139	45	46	47	48	4	5	6	85	86	87	88	190	191	209
200	136	137	41	42	43	44	1	2	3	12	13	14	89	188	189	209
200	134	135	40	37	38	39	34	29	24	19	10	11	94	95	96	209
200	131	132	133	35	36	32	33	28	23	17	18	90	91	92	93	209
200	199	129	130	128	122	30	31	27	22	15	16	100	101	102	194	194
0	199	125	126	127	120	121	25	26	20	21	108	109	98	99	194	0
0	199	199	123	124	118	119	113	114	115	105	106	107	97	195	194	0
0	0	198	198	198	116	117	110	111	112	103	104	195	195	195	0	0
0	0	0	0	198	197	197	197	197	196	196	196	196	0	0	0	0

Figure 121: Detailed core configuration (location of 193 fuel assemblies with assembly numbers and assignment to core rings)

0	0	0	0	REF11	REF11	REF11	REF11	REF12	REF12	REF12	REF12	REF13	0	0	0	0
0	0	REF10	REF10	REF10	113	113	123	123	123	123	133	REF13	REF13	REF13	0	0
0	REF9	REF10	103	113	113	112	112	122	122	132	133	133	143	REF14	REF14	0
0	REF9	103	103	103	102	112	112	122	122	132	132	133	143	143	REF14	0
REF9	REF9	93	93	102	102	101	101	111	121	121	132	142	143	153	REF14	REF15
REF8	93	93	92	92	102	101	101	111	121	121	142	142	142	153	153	REF15
REF8	83	92	92	91	91	91	91	111	131	131	131	131	152	152	153	REF15
REF8	83	82	82	81	81	81	81	111	141	141	141	141	152	152	163	REF15
REF8	83	82	82	71	71	71	71	C	151	151	151	151	162	162	163	REF16
REF7	83	72	72	61	61	61	61	31	161	161	161	161	162	162	163	REF16
REF7	73	72	72	51	51	51	51	31	11	11	11	11	12	12	163	REF16
REF7	73	73	62	62	62	41	41	31	21	21	22	12	12	13	13	REF16
REF7	REF6	73	63	62	52	41	41	31	21	21	22	22	13	13	REF1	REF1
0	REF6	63	63	53	52	52	42	42	32	32	22	23	23	23	REF1	0
0	REF6	REF6	63	53	53	52	42	42	32	32	33	33	23	REF2	REF1	0
0	0	REF5	REF5	REF5	53	43	43	43	43	33	33	REF2	REF2	REF2	0	0
0	0	0	0	REF5	REF4	REF4	REF4	REF4	REF3	REF3	REF3	REF3	0	0	0	0

Figure 122: Detailed core configuration (assignment of 193 core assemblies to 49 channels of lower/upper plenum)

It has to be emphasized, that a model limited to the core alone or the reactor pressure vessel is not sufficient to study the plant behavior during LOCA accident, as precise boundary conditions at the RPV inlet and outlets are not known à priori. There is interaction between the vessel and the loops and the emergency core cooling system (ECCS, e.g. its initiation of injection depends on how fast the pressure is reduced in the RPV). Furthermore, the reactor shows a strong asymmetric behavior during the LOCA transient:

- break of only 1 of 4 loops,
- asymmetric ECCS injection due to malfunction and outage of selected systems,
- influence of pressurizer, which is connected to only one of the loops.

Therefore, it was decided to develop the new core modelling approach within a full plant ATHLET model (including full primary and parts of the secondary circuits). Figure 123 shows the nodalization scheme of the complete model, including

- the RPV,
- 4 separate loops with hot leg, SG inlet and SG exit chamber, SG U-tubes, cold leg and main coolant pump (only 2 of the 4 loops are shown in Figure 123)
- 1 pressurizer with surge line connected to hot leg of loop #2
- 8 accumulators (4 connected to hot legs, 4 connected to cold legs)
- Further ECCS components (HPI and LPI)
- SG secondary sides with feedwater line, downcomer, riser, separator, steam dome, and main steam line (simplified as a single junction)

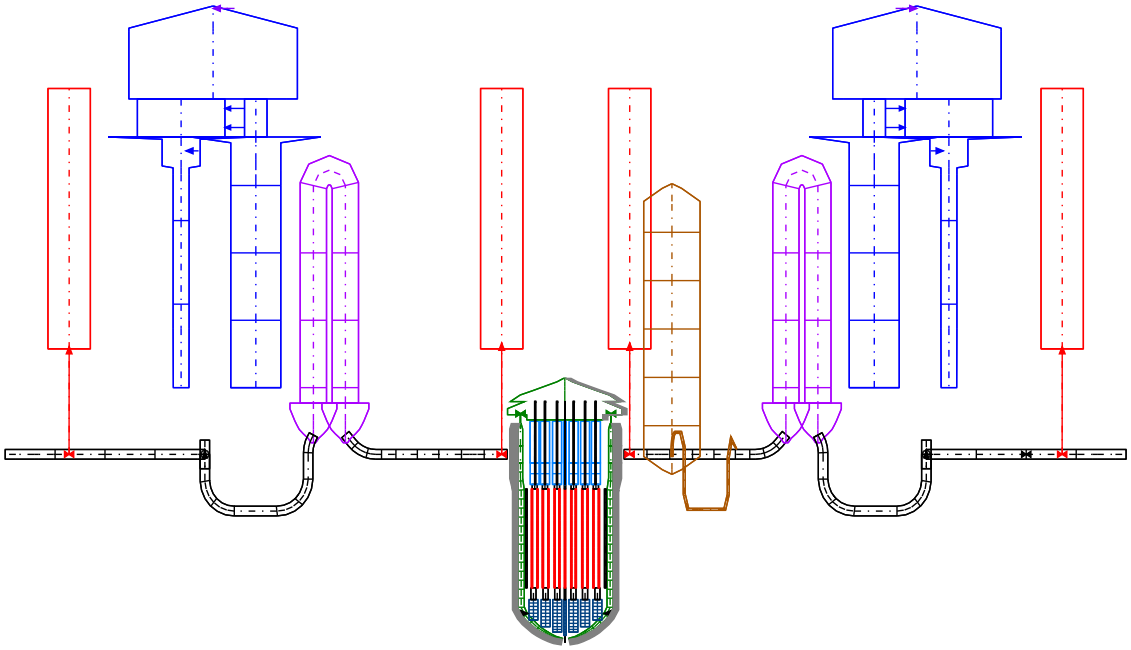

Figure 123: Nodalization scheme of primary and secondary side.

New type of custom nodalization in ATHLET-CD

The classical approach applied in severe accident codes such as ATHLET-CD is subdivision of the core into a certain number of concentric rings with the assumption of azimuthally symmetric behavior, especially symmetrical power distribution and symmetrical thermal-hydraulic boundary conditions. This approach was also applied in Task 2.3 of the R2CA project (first set of reactor calculations,[108]), with a sub-division into 6 concentric rings (see Figure.124). Each ring has been modelled by one TFO and one representative fuel rod and control rod. Usually, the power of those assemblies assigned to a ring is averaged [120]-[123]. However, with such coarse nodalization and average power factors, it is not possible to estimate the number of failed rods during the accident, as typically only a few percent of the hot rods burst, as reported by previous studies (see introduction above).
Therefore the detailed thermal hydraulic ATHLET model (described in section 0) needs to be coupled with a more detailed/flexible nodalization scheme of the core components which are modelled by ATHLET-CD (especially the rod behavior model which is not available in standalone ATHLET).

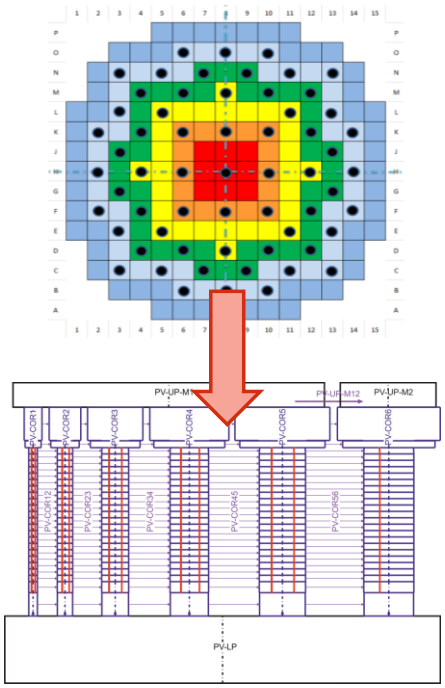

Figure.124: Top: reactor core with 193 assemblies. Bottom: ATHLET-CD nodalization scheme with 6 concentric-rings, the inner most ring is visualized on the left side of the scheme (PV-COR1), the outer-most ring on the right side (PV-COR6)

A more flexible nodalization scheme has been developed by GRS and has been implemented in the release version of ATHLET-CD 3.3. Two new options to create a more detailed reactor core model are available [124]:

- Subdivision of the concentric rings into azimuthal segments
- Free definition of rectangular shaped nodes (within a Cartesian coordinate system)

The first option has been developed to model local phenomena of a reactor core more adequately, see Figure 125 and has been applied to severe accident analyses with strongly asymmetrical characteristics [125][126].

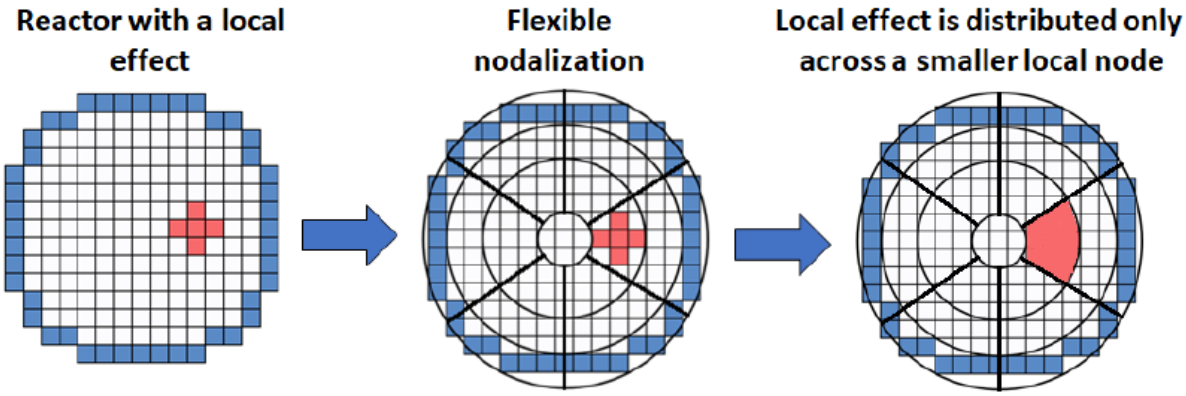

Figure 125: Local phenomenon using the new custom nodalization (azimuthal sub-division) [22]

The second option was originally developed to simulate the behavior of accident scenarios in spent fuel pools [124][127]. For such cases, the assemblies stored in the pool are grouped into areas with relatively uniform power levels, as shown by Figure 126. Basically analyses with relatively small configurations (e.g. subdivision into 2x3 sections) have been reported in [124][127].

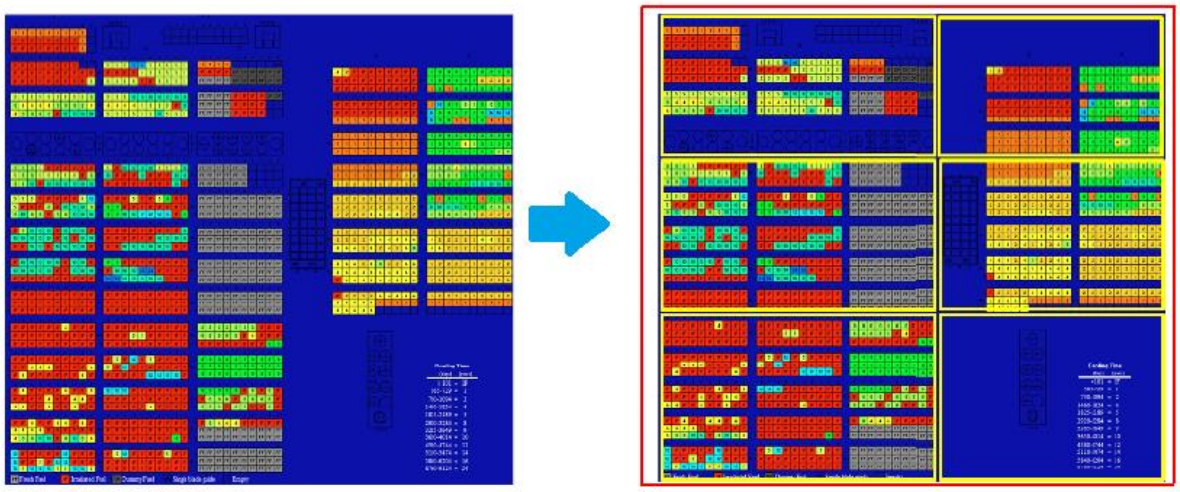

Figure 126: Example of spent fuel pool nodalization (2x3 sections) [22]

The second approach provides the necessary flexibility to model each assembly separately. The resulting matrix has a size of 15x15 sections (193 active sections and 32 dummy sections with zero power). Later it was decided to further subdivide each assembly into 4 sections to improve the accuracy of the calculations (see section 0). The resulting matrix has a size of 30x30 (772 active sections and 128 dummy sections). The official release of ATHLET-CD 3.3 had to be extended to handle such large core configuration. Therefore a developer version was provided by code developer GRS in July 2021 and the necessary code extensions of data arrays have been implemented by HZDR.

Major code modifications needed for the new nodalization scheme were the replacement of heat radiation model and the model simulating horizontal movement of molten material [124]. However, for the DBA and DEC-A cases, heat radiation and movement of molten material play a secondary role or no role at all, respectively. Furthermore, the new 3D heat radiation model involves the calculation of view factors between the surfaces of the formed core nodes. As the general case covered by ATHLET-CD takes relocation of material into account, the view factors are calculated not only between adjacent nodes, but between every single surface to all other surfaces from all nodes in the core. That leads to a huge calculation matrix for the full core geometry under consideration (too huge to be stored in memory of a typical PC) and extended calculation time. Therefore, the heat radiation model has been eliminated from the code for the analyses presented in this report. For the DBA case, cladding temperatures do not exceed 1200 °C and the space between fuel rods is usually filled with steam, liquid or two-phase mixture and heat transfer to the coolant is mainly driven by convection. Non-heated components of the fuel assemblies (such as control rods, guide tubes, spacers) are not taken into account by the newly developed ATHLET-CD input data sets[5], which means on the one hand a reduced heat capacity resulting in higher average assembly temperatures, and on the other hand radiation heat exchange to these component is not modelled, which also leads to higher fuel rod temperatures (conservative solution). Radiation heat transfer from the fuel rods to steam, described e.g. by [128], is not taken into account by the ATHLET-CD code.

Mechanical rod behavior model and rod burst criteria

The mechanical rod behavior module of ATHLET-CD calculates the thermal strains as well as the elastic and plastic deformations due to the difference between the rod internal pressure (RIP) and the system pressure. The RIP is calculated as a function of the mean gas gap temperature and the gas gap volume (including the fuel rod

[5] In general it is possible to include control rods and guide tubes, but for reasons of simplicity this has been neglected.

plenum volume) under consideration of the fuel porosity and the amount of gas substance (moles). The amount of gas is calculated from the initial gas gap volume, a given initial gas pressure and temperature, e.g. the fill gas pressure (which is 2.25 MPa for fresh Konvoi fuel [129]) at ambient temperature.
For fresh Konvoi fuel (low burn-up → 0.0), steady state RIP of the maximum power rods reaches values of 6 to 7 MPa, as indicated by Figure 127 (left side) and Figure, which is in agreement to values reported by [129]. These values are the lowest steady state values which can be observed for a fuel rod operated at that power level. With increasing operation time, i.e. increasing burn-up, the rods show higher RIP at the same power level because of the accumulation of fission gases in the gap. As the heat generation rate of high burn-up rods is usually lower than that for the fresh fuel (see e.g. Figure 94), the RIP increase is limited. However, the accumulation of fission gas during normal operation is not computed by ATHLET-CD. Furthermore, for the current code version, only one initial gas gap pressure value can be defined by the user, which is applied to all rods. Consequently, the burn-up dependency of the gas gap pressure (at the beginning of the LOCA transient) cannot be modelled in detail. As a work-around, the possible pressure range has been estimated. This range is bounded by 2.25 MPa cold state gas gap pressure (for fresh fuel) till highest possible burn-up of approx. 70 GWd/tHM (maximum rod-averaged burn-up value observed at EOC). For the latter, an initial cold state gas gap pressure of 3.6 MPa has been estimated with the resulting steady state distribution of rod internal pressure depicted by Figure 127 (right side). The simulation has been performed with both initial values. The first one returns a lower bound of failed rod number and the second one returns an upper bound.

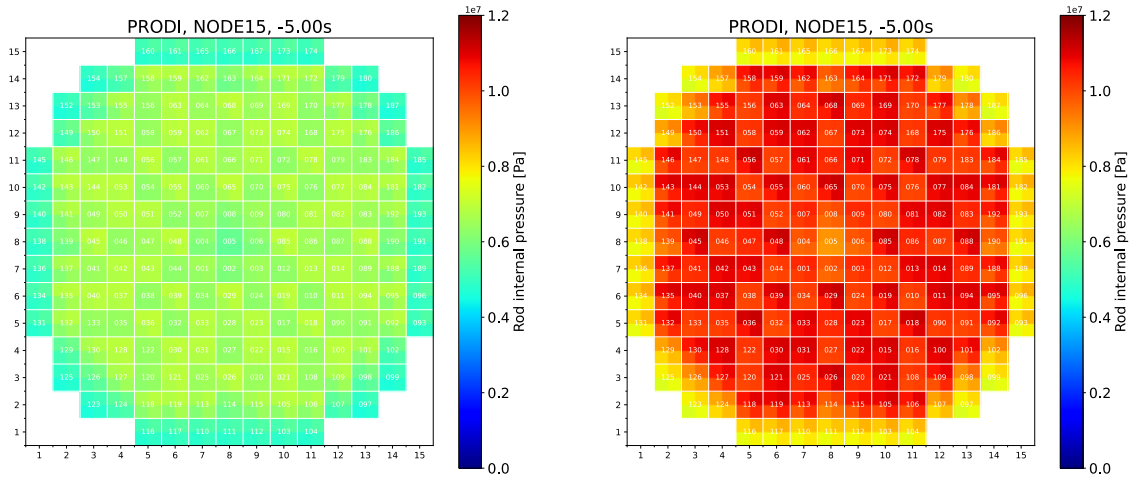

Figure 127: Distribution of rod internal pressure PRODI calculated by ATHLET-CD for two bounding cases. Left side: initial pressure value 2.25 MPa applied for all rods (fresh fuel). Right side: initial pressure value 3.6 MPa applied for all rods.

During the LB-LOCA transient, the system pressure drops within approx. 5 to 10 s from 158 bar initial pressure down to values, which leads to a positive value of

$$\Delta p = p_{\mathrm{rod,int.}} - p_{\mathrm{sys}} > 0 \qquad (1)$$

Afterwards, the system pressure is further reduced, while the rod internal pressure remains at a higher level for several seconds.
During the discharge phase of the LOCA transient, the peak cladding temperature (PCT) of those rods with highest heat generation rate reaches values of up to 1080°C within approx. 5 s, which is a similar time span as it takes the system pressure to fall below $p_{\mathrm{rod,int.}}$. The maximum heating rates can exceed 400 K/s between 1 s and 2 s, followed by a more moderate heating rate of up to 100 K/s. Usually, a slight drop of the PCT is observed afterwards

between 5 and approx. 10 s, followed by a second temperature rise to values above 1000 °C. This second peak or plateau lasts until the rods are quenched by the ECCS (several tens of seconds).
Consequently, from about 10 s on, a significantly large internal overpressure is observed (can reach values in the order of 2.0 MPa, as shown by Figure 128), while the cladding of those rods remains at high temperature.
Consequently, deformation of the rods takes place which is mainly caused by creep of the cladding material, which leads to ballooning and later to burst of rods. That process continues during the refilling and reflooding phases of the LB-LOCA as long as the rods are at elevated temperatures.
ATHLET-CD is able to model the cladding deformation due to creep. Therefore several models/correlations are implemented, which are based on similar assumptions to develop the models. It is assumed that the deformation process up to burst of internally pressurized Zircaloy claddings can be calculated from the steady-state (secondary) creep equation of the material [130]. The steady-state creep rate $\dot{\varepsilon}$ of a material at constant temperature and constant stress can be represented by a power law-Arrhenius equation (the so-called Norton equation) of the form:

$$\dot{\varepsilon} = \frac{d\varepsilon}{dt} = A\sigma^n \left(-\frac{Q_\alpha}{kT}\right) \quad (2)$$

σ is the applied hoop (azimuthal) stress in Pa, T is the cladding temperature given in K, and k is the universal gas constant = 8.314 J/mol·K^{-1}. The structure parameter A (unit MPa^{-n}·s^{-1}), the stress exponent n (dimensionless) and the activation energy Q_α (unit J/mol) are derived from experimental data.
All models assume symmetrical deformation of the rods. Therefore, the hoop stress for a tube under a differential pressure $\Delta p = p_{\mathrm{in}} - p_{\mathrm{ex}}$ is given by [131]:

$$\sigma_t = \Delta p \frac{R}{s} - \frac{p_{\mathrm{in}} + p_{\mathrm{ex}}}{2} \quad (3)$$

with R as the instantaneous mean tube radius and s the instantaneous tube wall thickness.
A typical evolution of the primary pressure and RIP for a high power rod is shown by Figure, with a maximum Δp after 15 s of approx. 2.0 MPa and average pressure $\frac{p_{\mathrm{in}}+p_{\mathrm{ex}}}{2} \approx 6$ MPa, which is reduced to 3 MPa later during the transient (at 23 s, short before rod failure). For Konvoi fuel the initial wall thickness is 0.64 mm and R = 4.43 mm. According to eq. (3), σ_t can be estimated as -72 MPa and 11 MPa at 0 s and 23 s, respectively. Due to deformation of the rod, the radius increases and the wall thickness decreases, which leads further increase of σ_t. The evolution of the hoop stress for the selected high power rod (the rod with earliest failure) is depicted by Figure 129, with maximum observed value of 20 MPa just before the rod failure. For other rods which burst later, maximum hoop stress of approx. 30 MPa is oberserved.

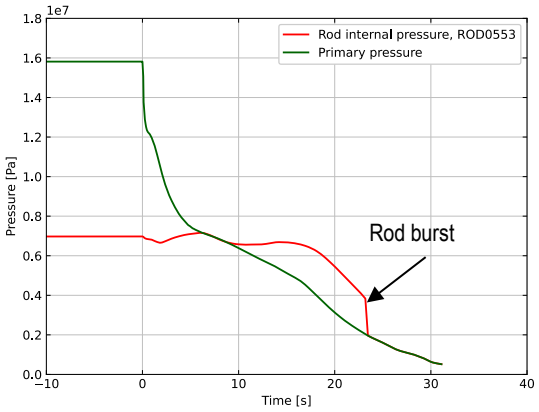

Figure 128: Typical evolution of the primary pressure and rod internal pressure of high power rod during the first 40 s of the LB-LOCA transient

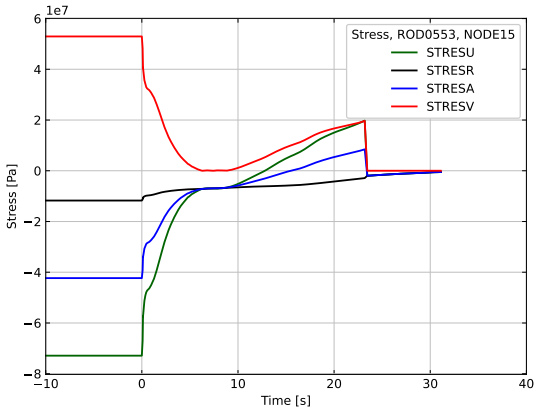

Figure 129: The different stresses computed by ATHLET-CD for the peak power location of high power rod (hoop stress STRESU, radial stress STRESR, axial stress STRESA, and equivalent stress STRESV)

The modelling of the rod deformation requires an accurate description of the material parameters. Zircaloy exists in two different phases with a phase transformation at temperatures around 800 °C and above [105] and therefore, different correlations are applied for both phases. For pure zirconium, the phase transition from hexagonal closed packed phase α to the body centred cubic β phase is observed at approximately 860 °C. For zirconium alloys the phase transition takes places within a temperature range, for as received Zircaloy-4 that range spans from 812 °C to 975 °C. The creep parameters of both phases differ significantly, with higher creep rates of the β phase. In the transition range the creep has to be described by a law of mixture. Furthermore, oxidation of the cladding can lead to significant strengthening of the cladding (lower creep rates) [94].

Four different correlations for creep computation are implemented in the ATHLET-CD code:

- Model based on Erbacher et al. [130](ATHLET-CD parameter ITESPA = 1);
- Model based on Rosinger et al. [132] (ITESPA = 2);
- Model of Burton [133] for α phase, but with a modified calculation procedure for the shear modulus G, as default and recommended option according to the ATHLET-CD manual [134], (ITESPA = 3). That correlation is called standard correlation of KESS (as it was used in the predecessor of ATHLET-CD, developed by IKE Stuttgart [135]);
- Original model of Burton [133] for α phase, (ITESPA = 4).

It has to be mentioned, that no correlations are implemented for the β phase Zircaloy for Burton's models[6].

For Erbacher and Rosinger correlations, the model parameters are given by Table 50. In case of the Erbacher correlation, the hoop stress is applied, while for the Rosinger correlation, the engineering stress is applied.

Model	Phase	n	A	Q_i
		-	$MPa^{-n} \cdot s^{-1}$	J/mol
Erbacher et al. [28]	α phase	5.89	1487.0	321000 + 24.69 (T – 923.15)
	β phase	3.78	3.9721	141919
Rosinger et al. [30]	α phase	5.32	2000.0	284600
	β phase	3.79	8.1	142300

Table 50: Creep correlation parameters applied in ATHLET-CD for Erbacher and Rosinger model

[6] Despite values for the beta-phase are given in the cited literature and can also be found in the ATHLET-CD source code, they are not used during the calculation, for an unknown reason.

The temperatures to describe both phases are implemented as:

$$\begin{aligned} T < T_\alpha = 1085.15\text{K} \qquad & \alpha\text{phase} \\ T_\alpha < T < T_\beta \qquad & \text{interpolation region} \\ T > T_\beta = 1248.15\text{K} \qquad & \beta\text{phase} \end{aligned} \tag{4}$$

The Burton model describes the creep rate $\dot{\varepsilon}$ by using a Harper-Dorn equation for the α phase of Zircaloy [133]:

$$\dot{\varepsilon} = A_1 \left(\frac{G}{T}\right)\left(\frac{\sigma}{G}\right)^n exp\left(\frac{-Q_\alpha}{kT}\right) \tag{5}$$

Beside the model parameters explained under equation (2), this approach also takes the shear modulus G into account. Burton et al. [133] derived the following model parameters from experimental creep data of Zircaloy-2: $A_1 = 1.82 \times 10^{19} \frac{\text{m}^2}{\text{N}} \frac{\text{K}}{\text{s}}$, $n = 5.36 \pm 0.11$, and $Q_\alpha = (290 \pm 15) \frac{\text{kJ}}{\text{mol}}$. The temperature-dependent shear modulus G is calculated by the following expression:

$$G = (40.87 - 0.0197T) \times 10^9 \frac{\text{N}}{\text{m}^2} \tag{6}$$

With creep model option 3, instead of eq. (6), the following equations are applied to compute the shear modulus:

$$G = \frac{1+\nu}{2} E \tag{7}$$

$$E = \begin{cases} 1.088 \cdot 10^{11}\text{Pa} - 5.475 \cdot 10^7 \frac{\text{Pa}}{\text{K}} \cdot T & T \leq 1090\text{K} \\ 4.912 \cdot 10^{10}\text{Pa} - 4.827 \cdot 10^7 \frac{\text{Pa}}{\text{K}} \cdot T & 1090\ \text{K} < T \leq 1090\text{K} \\ max\left(1 \cdot 10^{10}\text{Pa}, 9.21 \cdot 10^{10}\text{Pa} - 4.05 \cdot 10^7 \frac{\text{Pa}}{\text{K}} \cdot T\right) & T > 1090\ \text{K} \end{cases} \tag{8}$$

and

$$\nu = 0.3 \tag{9}$$

Despite the coefficients have been created for Zircaloy-2, the data might be also used to model Zircaloy-4, as experiments show good agreement between both types, especially for high temperatures [132].

The creep rates computed by the four different options are compared in Figure 89 for the temperature range between 600 °C and 1100 °C and a stress range between 1.0 MPa and 100 MPa. As discussed above, stress values up to 30 MPa are observed during the LOCA transient. Creep rates above 0.005/s have to occur to create large enough final strain of about 38 % (currently selected default burst criterion) within the duration of 80 s (maximum observed time for quenching). Furthermore, the code limits the strain rate to a maximum value of 0.3/s. This region of interest for the typical LOCA conditions is framed by the dashed lines in Figure 130. It is visible that the Rosinger correlation produces significantly larger creep rates than the Erbacher model (approx. by a factor of 2 larger for the high temperature range, approx. 1 order of magnitude larger for the low temperature range). The Burton model gives similar values for the low-temperature α phase as the Rosinger correlation. Due to missing correlation for β phase in the ATHLET-CD implementation of the Burton model, the calculated creep rates for the high-temperature range are significantly lower than those computed by Rosinger as well as those by Erbacher. As the current status of the code and new model is documented in this report, the results of the Burton models shown in Figure 89(c)-(d) are extended to whole temperature range (as it is done in the current version of the code).

The consequences of the four different creep models have been investigated for the rod with highest power (a case with top-peaked power profile has been taken for this analysis) with the evolution of the hoop strain depicted in Figure 131. It can be seen that the Rosinger model leads to fastest straining of the cladding. It is the only model that leads to significant negative creep rates during the first temperature peak (during discharge phase, 3-4 s after break opening), with creep-down of the cladding to pellet and consequently $\varepsilon < 0$. Following the positive Δp after 10 s, the Rosinger model also leads to earliest start of ballooning of the cladding. However, the burst criterion (in this case 38 % maximum strain has been defined) is reached at almost the same time for all four models (2 seconds

later for the Burton model compared to the Rosinger model). The evolution of the number of burst rods is shown by Figure 132. The Rosinger model results in a faster increase in the number of burst rods and also leads to a 20% higher number of total burst rods compared to the other three burst models.

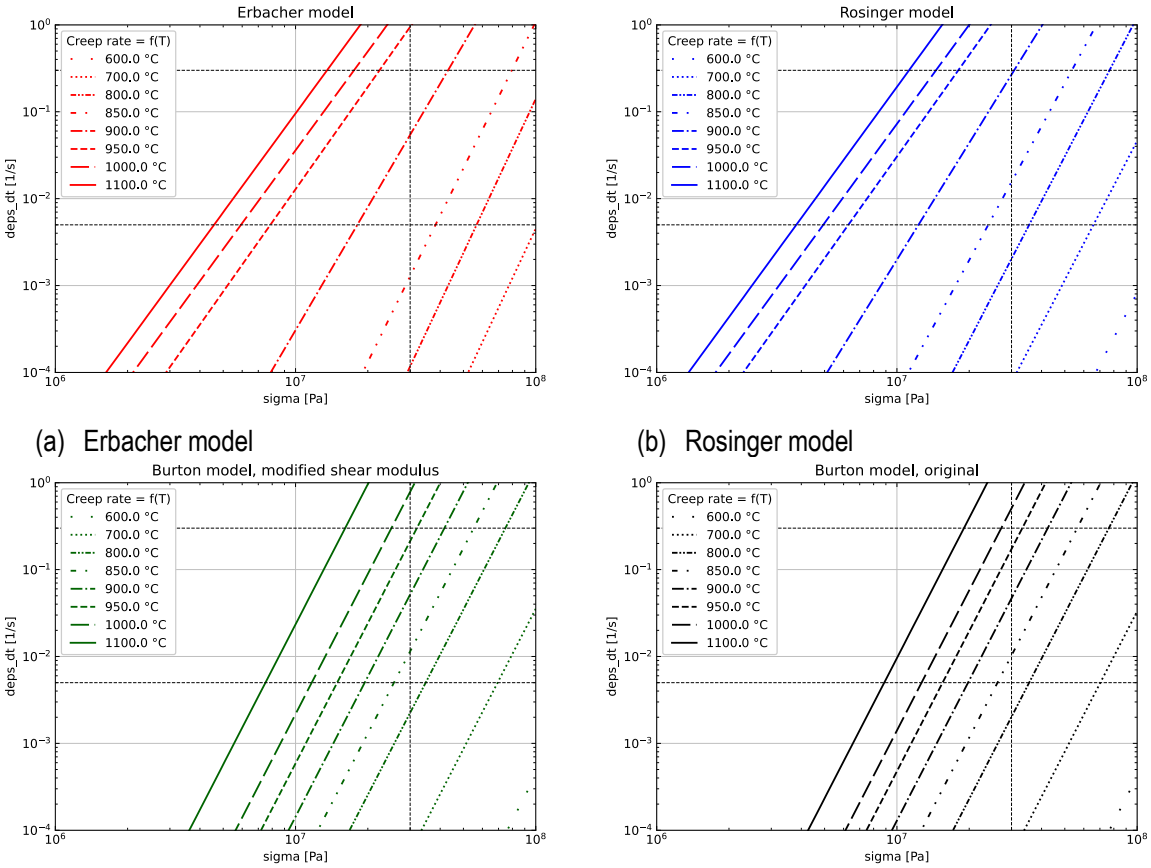

(a) Erbacher model

(b) Rosinger model

(c) Burton model (with modified shear modulus) as it is implemented in ATHLET-CD

(d) Burton model (original equations for shear modulus) as implemented in ATHLET-CD

Figure 130: Creep rates calculated by the four creep rate models implemented in ATHLET-CD

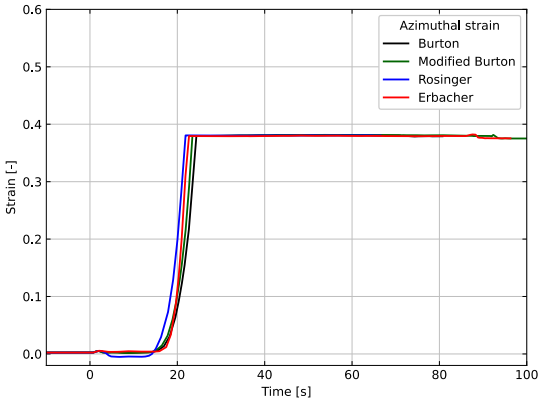

Figure 131: Comparison of four creep rate models implemented in ATHLET-CD. Evolution of the azimuthal (hoop) strain of selected high power rod during LBLOCA.

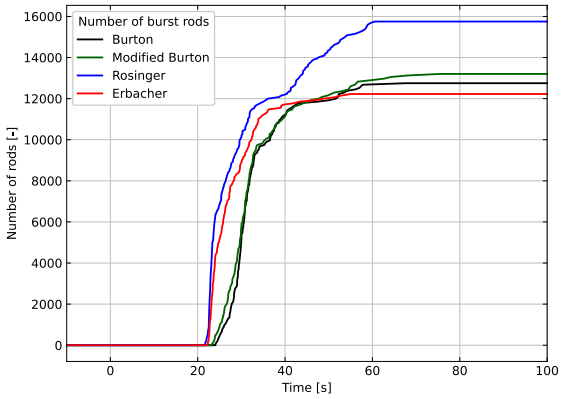

Figure 132: Comparison of four creep rate models implemented in ATHLET-CD. Number of burst rods computed for a LB-LOCA case with top-peaked power profile.

Both ATHLET-CD implementations of the Rosinger and the Erbacher model take the strengthening effect due to cladding oxidation into account. However, the model is implemented in a simplified way, by adjusting the phase transition temperatures T_α and T_β which are increased by 200 K per weight % oxygen in the cladding. The oxygen concentration is not calculated by the code. It has to be given by user-defined input parameter TSPOX0 and by default, TSPOX0 = 0.0 is selected. To study the strengthening effect, the simulation case with the Rosinger model has been repeated with 0.5 wt-%, 1.0 wt-%, 1.5 wt-% and 2.0 wt-% oxygen. The obtained results are depicted by Figure 133 and Figure 134. According to the obtained results, small amount of oxygen lead to a reduction of the creep rates and a delay of the first rod burst, and lower number of burst rods. If the cladding contains more or equal than 2.0 wt-% oxygen, the Rosinger correlation (as implemented in ATHLET-CD) predicts no burst of the cladding for the investigated scenario. A discussion among the project partners revealed, that this result seems to be questionable and the model will need further assessment.

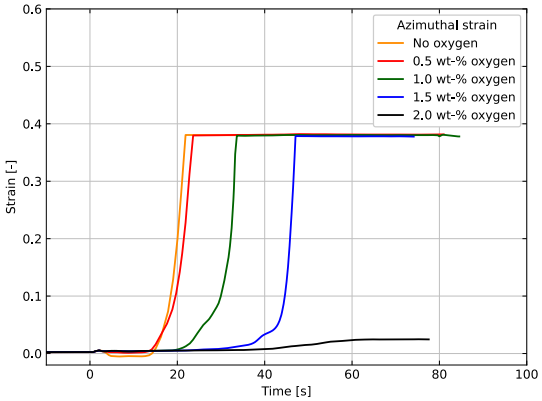

Figure 133: Study of strengthening effect due to oxygen. Evolution of the azimuthal (hoop) strain of first burst rod / selected high power rod during LB-LOCA (Rosinger creep rate correlation applied).

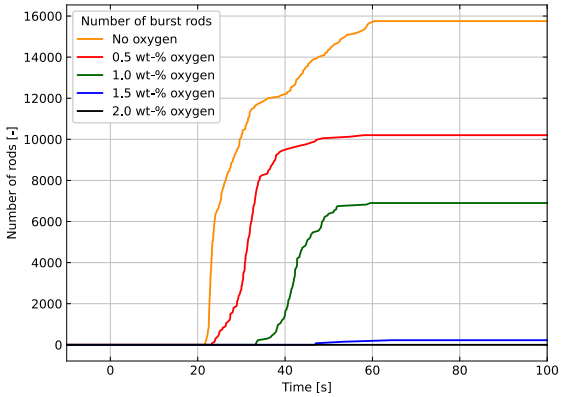

Figure 134: Study of strengthening effect due to oxygen. Number of burst rods computed for a LB-LOCA case with top-peaked power profile (Rosinger creep rate correlation applied).

For the remainder of the analyses presented in this report, the modified Burton model (ITESPA=3) has been applied (default model of ATHLET-CD) and the effect of oxygen has been neglected. The main reason for this selection is that the following analyses have been performed before the above discussed investigation of the

different creep rate equations has been done. Due to long calculation time (more than 1 month for each simulation), there is no time at the moment to repeat the simulations with alternative creep rate equations.

Another important model parameter is the implemented rod burst criterion. ATHLET-CD provides 4 different rod burst models, which are set by an input parameter(parameter IBLOW) [134]:

- Option 0: Maximum hoop strain criterion (38 %);
- Option 1: Stress criteria as function of heat-up rate (Chapman correlation);
- Option 2: Stress/strain criteria (Model of Hagrman);
- Option 3: Extended model based on the code TESPA-ROD.

Option 3 is mandatory, if the user wants to apply one of the above discussed creep-rate correlations (with parameter IBLOW < 3, only the KESS-standard-correlation for creep rate can be applied [134]). With option 3, there are further options to describe the burst criterion, which are defined by another input parameter (IBURST):

- Option 3-A: a fixed maximum hoop strain value of 38 % is applied (identical to option 0 concerning the burst prediction);
- Option 3-B: maximum hoop strain exceeds a user-defined value;
- Option 3-C: same as option 3-B or maximum strain rate exceeds a user-defined value.

Some details about the different burst options are given in the following. If option 0 is selected, the maximum hoop strain criterion is hard-coded as 38 %. According to the ATHLET-CD documentation [124], that criterion is mainly used to test the model. Option 1 is based on the Chapman correlation [125][126]:

$$\vartheta_R = 3960 - \frac{20.4\sigma'_v}{1+\alpha^*} - \frac{8.51\cdot 10^6\sigma'_v}{100(1+\alpha^*)+2790\sigma'_v} \tag{10}$$

with burst temperature ϑ_R in °C, the engineering hoop stress in ksi and the ratio of the heat-up rate α (given in °C/s) and a maximum heat-up rate of 28 °C/s:

$$\alpha^* = \frac{\alpha}{28°\mathrm{C/s}} \tag{11}$$

The scaling factor between ksi and Pa is:

$$1\mathrm{ksi} = 6{,}894{,}757\mathrm{Pa} = 6.894757\mathrm{MPa} \tag{12}$$

However, a review of the ATHLET-CD implementation revealed, that 689643.0 has been used as scaling factor instead of 6894757.0, which leads to very low calculated burst temperatures[7].

The third burst model option is based on the model of Hagrman [138][139]. The azimuthal burst stress is calculated as a function of the temperature [124]. The burst criterion is furthermore combined with a maximum strain criterion. However, the model has not been assessed in detail and no simulations have been performed with this model option due to lack of time / computational resources.

For most of the analyses presented in this report, the extended model based on the code TESPA-ROD (IBLOW=3) has been selected in combination with maximum hoop strain of 38 % selected as burst criterion (IBURST=0).

Calculation of initial power distribution and transient evolution of fission and decay power

Knowledge of the detailed and precise initial power distribution and burn-up is of particular importance for the evaluation of the fuel rod behavior during the LOCA accident and determining the number of failed fuel rods. The power distribution of the generic Konvoi has been taken from core simulator calculations, which have been performed for a typical cycle. Data has been provided for beginning of cycle (BOC), e.g. at 6 equivalent full power days (EFPD) and end of cycle (EOC), e.g. at 330 EFPD. The data has been prepared as local relative power factors vs. burn-up for all 57900 fuel rods and 32 layers per rod (in total 1.85 10^6 data points per core state). The highest local power factors are observed at BOC (at approx. 2.05, which corresponds to a linear heat generation

[7] The code additionally limits the calculated temperature to values not lower than 900°C.

rate (LHGR) of approx. 360 W/cm). For EOC, the local peak power factor is significantly lower, but maximum local burn-up of 75 GWd/tHM is observed. For the further analyses, it has been decided to focus on the BOC data, as this case shows the maximum power factors.

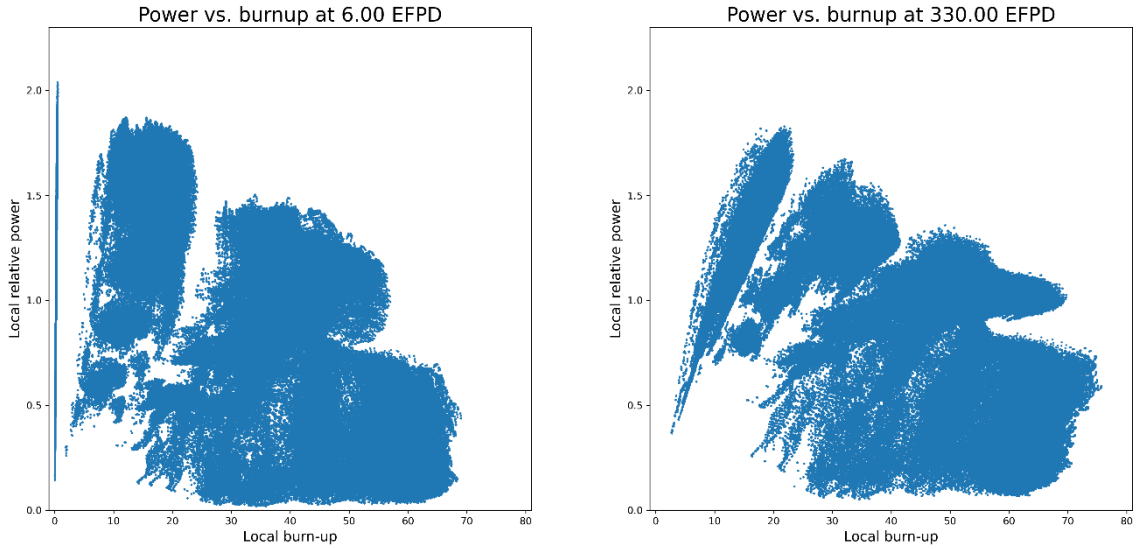

(a) BOC data (6.0 EFPD). (b) EOC data (330 EFPD)

Figure 135 Local relative power vs. local burn-up for all fuel rods (57900 rods at 32 axial layers).

The power distribution is shown exemplarily for a selected axial layer by Figure 136. From the power distribution, rod power factors (RPF, rod averaged value of the 32 axial layers) can be calculated. The location of those rods with RPF > 1.5 is shown by Figure 135. With the current version of ATHLET-CD, it is not possible to set-up a pin-by-pin (57900 fuel rods) core model, including separate fluid channels for each fuel rod. Instead, the core is modelled by a lower number of core channels and representative fuel rods. Appropriate average RPF and power profiles have to be derived from the detailed power distribution. One option is the computation of average RPF for each assembly, shown by Figure.138. The maximum RPF is 1.445 and the corresponding assembly averaged power profile is shown in Figure 139. Preliminary analyses performed with that configuration showed that no rods fail during the LOCA transient, as the PCT do not exceed 620 °C.

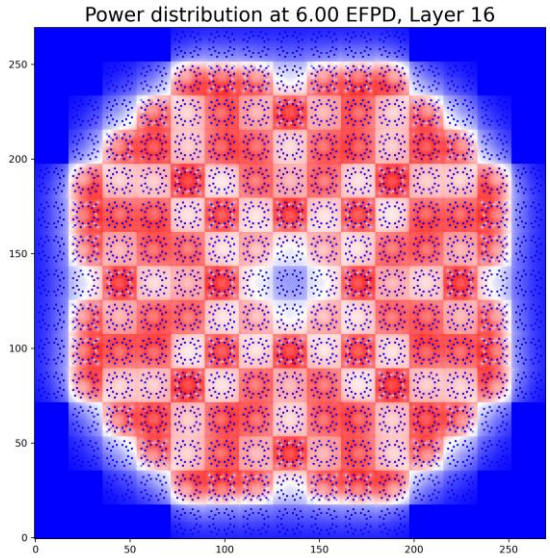

Figure 136: Power distribution

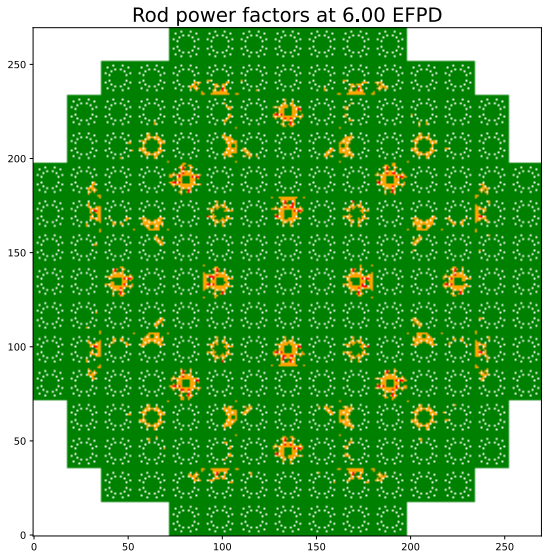

Figure 137: Rod power factors with indication of high power rods (red RPF ≥ 1.6, orange 1.5 ≤ RPF < 1.6, green RPF < 1.5)

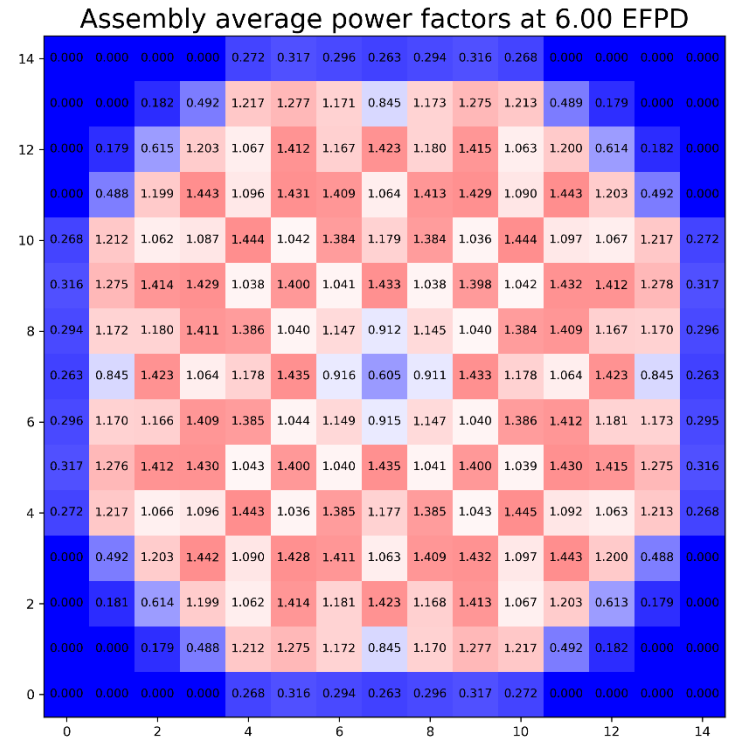

Figure.138: Assembly average rod power factors

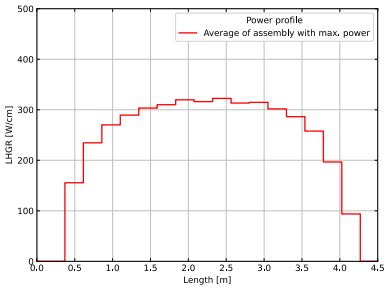

Figure 139: Assembly averaged rod power profile (assembly with maximum power)

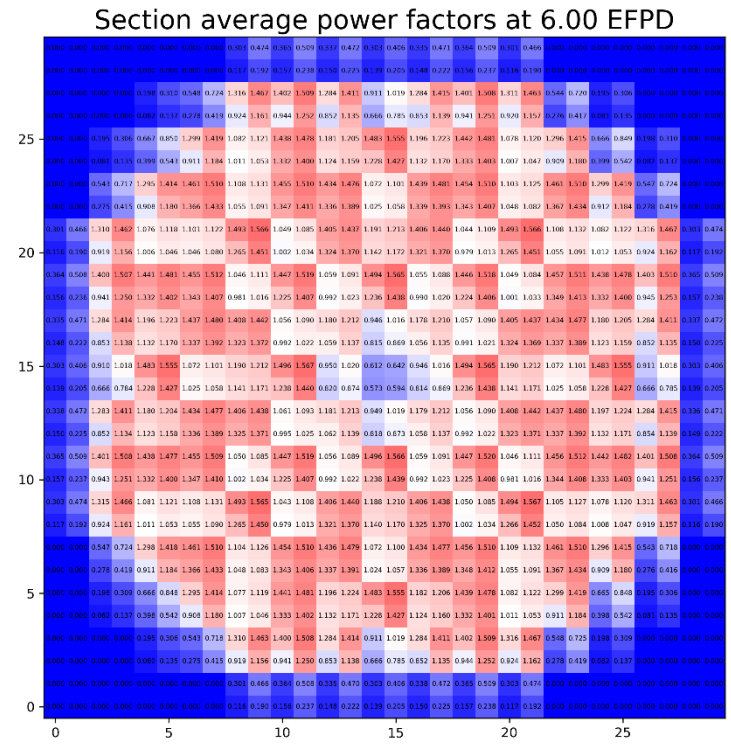

Figure 140: Average rod power factors for 4 rod sections per assembly

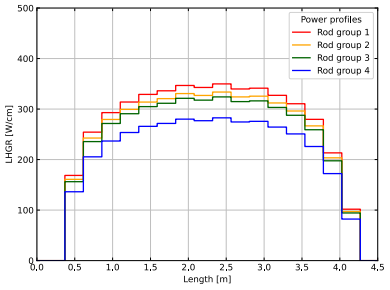

Figure 141: Four rod power profiles for assembly with maximum power

Therefore, a more detailed configuration has been investigated, with 4 representative rods per assembly, but retaining one thermal-hydraulic channel per assembly[8]. The fuel rods have been ordered according to their rod power and 4 groups have been created per assembly. The first group contains those 25 % of the rods of one assembly with maximum power, the second group those 25 % of the rods with second highest power and so on. The corresponding RPFs of the more detailed configuration are shown by Figure 99, with a maximum of 1.567. The corresponding realistic power profiles of the 4 rod groups forming the assembly with maximum power are shown by Figure 141, with a maximum LHGR of 350 W/cm.

According to [140], the most unfavorable conditions have to be selected for the loss-of-coolant accident analyses. Since first countermeasures by the reactor power limitation system takes place at a thermal reactor power of 103 %, that value determines the most unfavorable conditions. Furthermore, measurement uncertainties (3 %) have to be taken into account. Consequently, the total core power has been scaled to 106 % of the nominal power. Furthermore, the most unfavorable power density distribution has to be selected for the analyses [140] , which is a top-peaked power profile with a maximum LHGR of 485 W/cm (verification value for LHGR conservative LOCA analysis, [141]. To construct such a power distribution for the ATHLET-CD core sections, the RPFs derived from the core simulator results have been multiplied by a generic top-peaked power profile. However, for the top-peaked profile the maximum power has been limited to 455 W/cm (otherwise departure of nucleate boiling with unrealistic high cladding temperatures above 1000 °C has been observed during ATHLET-CD steady state). The final top-peaked power profiles applied in ATHLET-CD are exemplarily depicted by Figure 142 for the assembly with maximum power.

[8] Otherwise too large impact on the calculation time is expected.

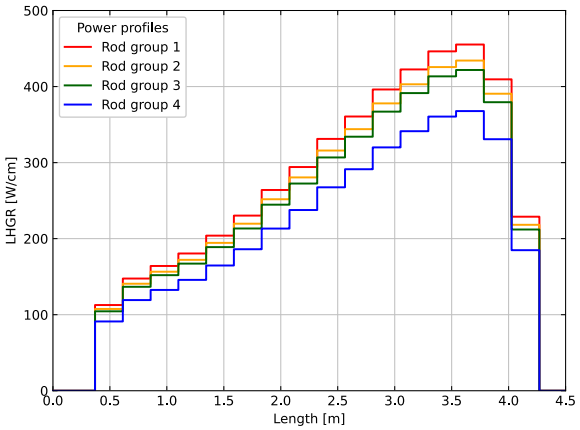

Figure 142: Four top-peaked rod power profiles constructed for the assembly with maximum power

As the axial power profile has significant effect on the fuel rod behavior during the LOCA accident, the analysis has been performed with both profiles (realistic profile directly derived from the core simulator and top-peaked power profile).
The new detailed ATHLET-CD core model contains in total 772 representative fuel rods, each represents 75 fuel rods of the total core (57900 rods), which means, that the fraction of failed rods could be estimated in steps of 0.13 %. Such configuration is a compromise between accuracy and calculation efforts.
The calculation of fission product inventory and decay heat is performed by the ATHLET-CD sub-programs OREST [142] and FIPISO [143]. The fission product inventory and decay heat is calculated separately for each of the 772 core sections (representative fuel rods) based on the power density and burn-up reached in the fuel rod.

Current limitations of the new model

The limitations of the current model are summarized as follows:

1. It is currently not possible to define the gas gap pressure for each fuel rod separately; only a single value can be given by the input data set at the corresponding temperature (e.g. fill gas pressure at room temperature) which is applied to all rods. The evolution of the RIP is calculated based on this initial value, the current gas gap temperature and changes of the gas gap volume. The burn-up dependent increase of RIP is not modelled. As a work-around two bounding cases are simulated (lowest and highest expected RIP values).
2. Heat transfer by radiation had to be neglected, due to practical reasons (too long running time and too large amount of memory needed), see discussion at the end of section 0.
3. The geometry of fuel assemblies is simplified. The fuel rods of each assembly are grouped into 4 groups of different power, their internal arrangement to each other is neglected. Therefore, also non-heated core structures such as control rods, guide tubes and spacers are not taken into account as it is currently not possible to model the arrangement of those structures to the different fuel rods. For each assembly only one thermal-hydraulic channel has been applied, instead of application of a separate thermal-hydraulic channel for each group of fuel rods.
4. Due to extremely long simulation times, the detailed model can only be applied to relatively short transients (such as the discharge and reflooding phase of a LB-LOCA which takes less than 200 s system time until all rods are quenched and no significant further changes are expected). As shown in the next section, approximately 1-2 months simulation time is needed to simulate the 200 s of the LOCA transient.

5. For each assembly, 4 groups of rods with ordered power are created (in total 75 rods per group) and rod power is averaged among the group. That leads to lower maximum power (e.g. for realistic power profile case, the max. LHGR applied in ATHLET-CD simulation is 350 W/cm, which is 3% lower than the peak LHGR observed in the real core). That issue can be resolved by creation of more rod groups per assembly.

First results obtained for generic German PWR (type Konvoi)

The analysis is performed for a German PWR of type Siemens-KWU (Konvoi design). However, the analysis is generic and no reference to any existing plant can be given. Therefore, input data and geometry has been simplified and is limited to data which is available to the public.

Short description of the assessed plant (components important for LOCA analyses)

The plant is a 4-loop plant, with nominal 3950 MW thermal power. For the current LOCA analyses, a conservatively high reactor power (106 % of nominal power) has been selected (see section 0). The reactor core consists of 193 fuel assemblies with 18x18-24 fuel rod grid (300 fuel rods per assembly). The control rods have been neglected in the current analyses.
The emergency core cooling system (ECCS) is designed with combined injection from cold leg and hot leg. The ECCS consists of [144][145]:

- 8 accumulators (1 connected to each hot leg and cold leg)
- High pressure injection system (HPIS), consisting of 4 high pressure safety injection pumps, injecting either to hot legs (default injection point) or to cold legs (automatic switch if break is located in hot leg)
- Low pressure injection system (LPIS), consisting of 4 low pressure (LP) residual heat removal (RHR) pumps, injecting 50 % of coolant to cold legs and 50 % of coolant to hot legs.

The hot leg ECC injection pipes are designed such that injection of borated water is directed to the upper plenum. This device is called “Hutze” and shown by Figure 143 [146][147]. Since the injection of sub-cooled liquid is parallel to the main flow in the hot leg (steam after the discharge phase during LOCA), no significant condensation is assumed to occur at the jet surface [148]. In cases, where the hot leg is filled with saturated water originating from the upper plenum, a thermal stratification will be established in the hot leg. ATHLET is able to model this behavior by application of the scoop injection model [148].

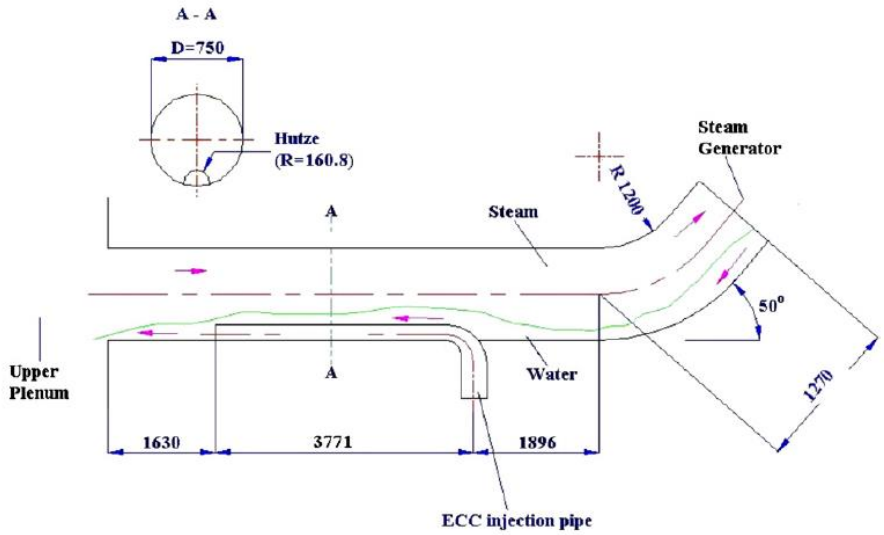

Figure 143: Hot leg ECC injection by application of a special injection pipe (Hutze) [136]

Short description of the investigated LB-LOCA scenario and assumptions for ECCS

The reactor is operated at full power. To cover uncertainties of reactor power [141], the power is set to 106 % of the nominal power in the current analysis (conservative value, 4187 MW).
The Large-break LOCA is initiated by a double-ended guillotine break of cold leg of loop 2 (loop connected to the pressurizer[9]), in combination with loss-of-offsite power (LOOP). The break is located close to the reactor pressure vessel. Diameter of the loop is 0.75 m; the break size is 2 x 4417 cm².
For DBA-LOCA, the assumptions for availability of the emergency core cooling systems (ECCS) are made according to RSK guidelines [140][103] [140] and are summarized in Table 51. The single failure (SF) criterion is applied, which means that one hot leg injection train is blocked. Furthermore, maintenance (MA) of one accumulator has to be assumed. The accumulator and low-pressure injection pumps connected to cold leg #2 inject directly to the break (and are therefore not efficient).
The active ECCS starts, when the emergency preparation signal is set. This signal is set, when two out of three of the following criteria are reached (activation by the reactor protection system):

- Pressure difference between containment and atmosphere > 30 mbar
- Primary pressure < 111 bar (absolute)
- Level in the pressurizer < 2.28 m

During LB-LOCA scenario, all three criteria are reached within a few seconds after the start of the accident.
After activation of ECCS preparation signal, the emergency diesel generators are started (start-up time 30 s is assumed) and borated water is injected into the reactor coolant system:

- HPIS: if primary pressure < 111 bar (absolute pressure)
- LPIS: if primary pressure < 10 bar (absolute pressure)

The active ECCS pumps inject until the borated water storage tanks are empty. From that moment on, injection is switched to injection from the containment sump.
The accumulators are a passive system and start to inject borated water, if primary pressure < 26 bar.

[9] The location of pressurizer has been varied during the study (additional simulations with pressurizer located in one of the intact loops).

Injection System	Loop 1		Loop 2		Loop 3		Loop 4	
	HL	CL	HL	CL	HL	CL	HL	CL
Safety injection pumps (high pressure pumps)	1	-	SF	-	1	-	1	-
Accumulators	1	1	SF	1*	MA	1	1	1
Residual heat removal pumps (low pressure pumps)	1	1	SF	1*	1	1	1	1

1 Injection system available
1* Injection system available, but injects to broken loop
SF Not available due to single failure
MA Not available due to maintenance

Table 51 : Assumptions for the ECCS applied in the DBA LOCA scenario.

Steady state solution obtained with new core model

The steady state results shown in this section have been obtained with an optimized input deck, which differs from the input decks applied for the preparation of the results for the current report (sections 0 – 0). The reason is that several issues have been observed during the preparation of the results, among others:

- Imbalanced power (core power was set to 106 %, but SG conditions were not adjusted properly);
- By default, the ATHLET-CD code tries to compensate the imbalanced power by adjusting the SG heat transfer surface → Different surface adjustment factors were calculated for each loop → Non-homogeneous temperature distribution in cold legs and at the core inlet (deviations of up to 4 K between the loops);
- No steady state core inlet temperature could be found;
- No constant primary pressure during zero transient (due to imbalanced power).

These issues have been resolved afterwards by adjusting the secondary side conditions and switching off the ATHLET SG surface adjustment option.
Furthermore several mistakes have been corrected in the input deck:

- Pump power has not be taken into account during steady state calculation;
- Initial values of accumulators corrected.

It is planned to repeat the simulations shown in the next sections with the optimized input data set. Due to the fact that the calculation time of one simulation is up to two months, those simulations have not been finished yet and will be presented in the framework of task 2.5 of the project.
ATHLET(-CD) first performs an initial steady state calculation, followed by a zero transient calculation (with constant reactor power). Due to long calculation time, the zero transient has been limited to 200 seconds. Selected parameters of the zero transient calculation are shown by Figure 144 and a comparison of the main figures to design values is given by Table 52. It has been possible to find a stable steady state solution and an acceptable agreement to design values. A main difference is due to the observed reduction of the loop mass flow rates just after the beginning of the simulation. While the given initial value is 4950 kg/s per loop (equal to the design value), the calculated steady state values are approx. 4550 kg/s per loop, which is approx. 8 % lower. This too low mass flow rate can partially explain the too high coolant temperature rise in the core observed in the ATHLET-CD simulation. The remaining deviation is to be explained by the increased core power (106 % while the design value is given for 100 % nominal power). The mass flow rate drop is still under investigation to further improve the

computed steady solution. It is not expected that the observed deviations affect the transient LOCA results significantly.
With the modifications mentioned above, it has been possible to obtain an almost uniform core inlet temperature distribution (Figure 144(e) and Figure 145).

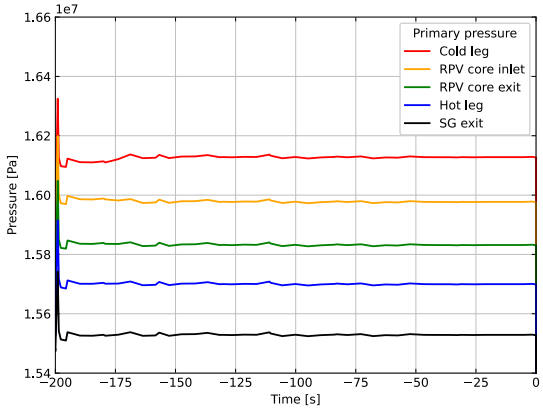

(a) Primary pressure

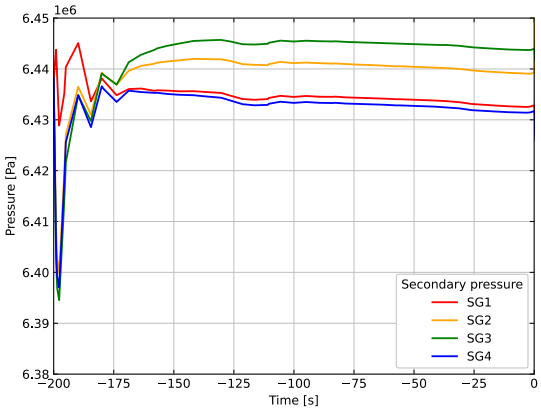

(b) SG pressure

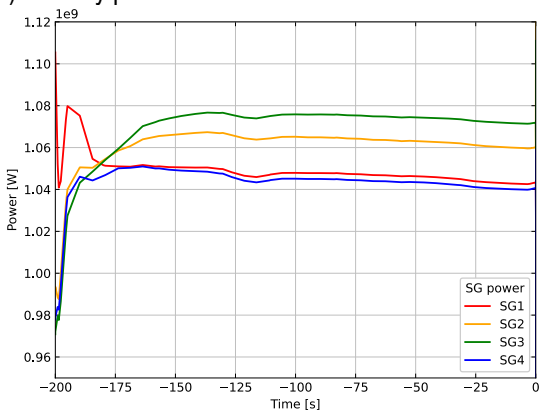

(c) Heat flow rate transferred in 4 SGs

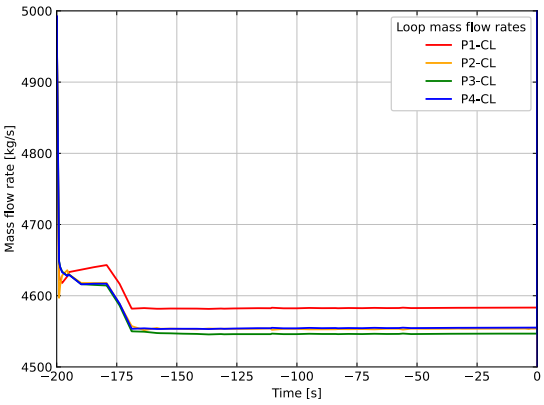

(d) Loop mass flow rates

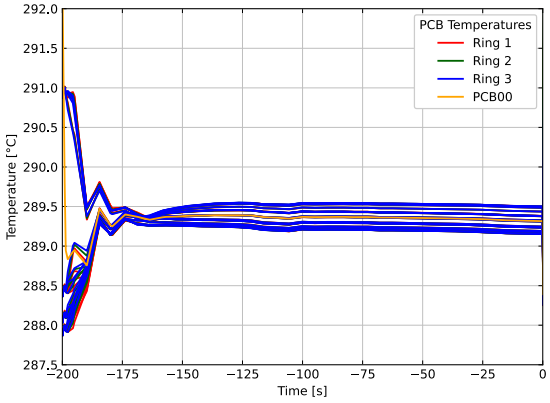

(e) Temperatures at the core inlet (49 inlet sections, arranged in 3 rings of 16 sections each and 1 central channel).

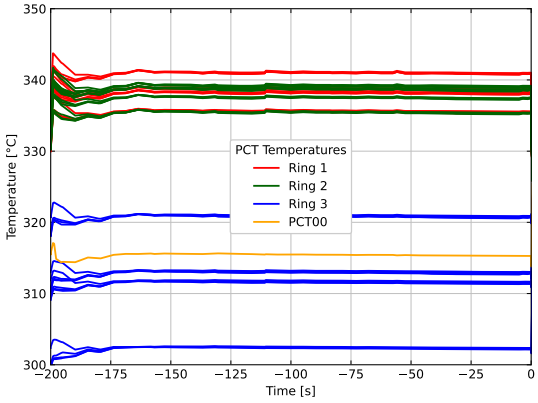

(f) Core outlet temperatures (upper plenum with 49 inlet sections, arranged in 3 rings of 16 sections each and 1 central channel).

Figure 144: Evolution of selected reactor parameters during the zero transient

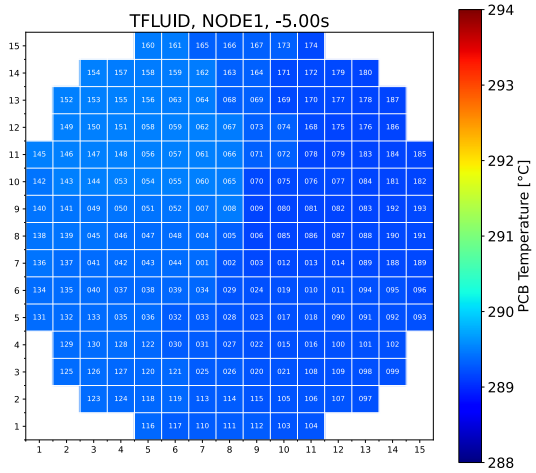

Figure 145: Steady state distribution of core inlet temperature

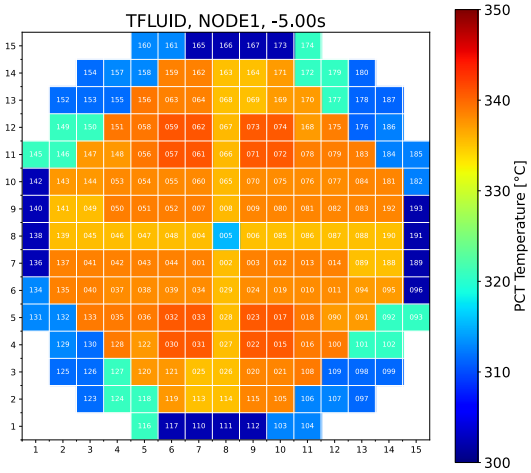

Figure 146: Steady state distribution of core outlet temperature (in upper plenum)

Plant parameter	Unit	Design value[10] [149]-[151]	ATHLET-CD	Deviation / %
Thermal core power (106 % of nominal value)	MW	4187	4187	0.0
Steam generator power	MW	4204	4213	+0.2
Pressure in hot leg	MPa	15.8	15.7	-0.06
SG pressure	MPa	6.5 MPa	6.44 MPa	-0.9
Total loop mass flow rate (sum of 4 loops)	kg/s	19787	18239	-7.8
RPV inlet temperature	°C	293.7	289.3	-1.5
RPV outlet temperature	°C	327.8	329.2	+0.4
Core ΔT	K	34.1	39.9	+17.0
Average coolant temperature (between SG inlet and outlet)	°C	310.6	309.3	-0.4
Feedwater mass flow rate	kg/s	2187.0	2280.0	+4.3
Steam mass flow rate	kg/s	2187.0	2295.9	+4.9

Table 52 : Comparison of selected steady state key parameters calculated by ATHLET-CD with design value

Results obtained for top-peaked power profile

The first analysis presented in the report is performed for a LB-LOCA case with break in CL of loop 2, but with pressurizer connected to loop 3. Results for a case with maximum initial RIP = 3.6 MPa are shown (resulting in the maximum steady state RIP of 11.2 MPa, see Figure 148). The maximum cladding temperatures of the 772 representative fuel rods are shown by Figure 147. During discharge phase a first temperature peak of 1020 °C (at 5 s) is observed, followed by a first temperature reduction. After 10 s, the temperature again starts to increase until about 18 s a plateau slightly above 1000 °C is reached. Afterwards, more and more rods are quenched until

[10] No publically available data has been found for the 106 % power case. Therefore, the nominal values are given for most parameters (except core power / SG power).

approx. at 75 s all rods have been quenched. Due to the elevated temperature and a drop of the primary pressure below rod internal pressure at approx. 2 s after the beginning of the LOCA (see Figure 148), the cladding of the first rods starts to balloon due to creep of the material (Figure 149). At 19 s the first rod reaches the activated burst criterion (38 % hoop strain). The progression of the number of burst rods is given by Figure 150, with a final number of 58 representative rods (eq. to 4350 real fuel rods, 7.5 % of all rods).

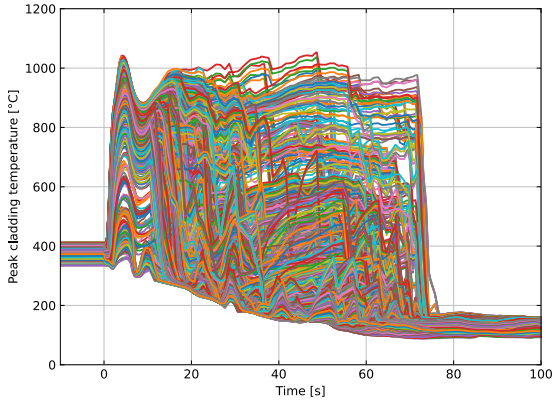

Figure 147: Simulation case #1. Maximum cladding temperature of the 772 representative rods.

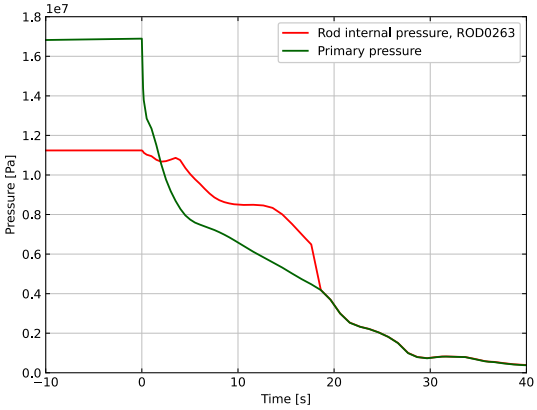

Figure 148: Simulation case #1. Primary pressure11 and RIP of the fuel rod which earliest burst.

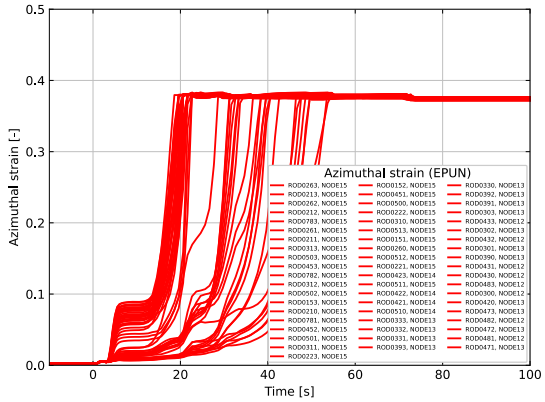

Figure 149: Simulation case #1. Hoop strain of those 58 representative rods that reach the burst criterion (38 % strain).

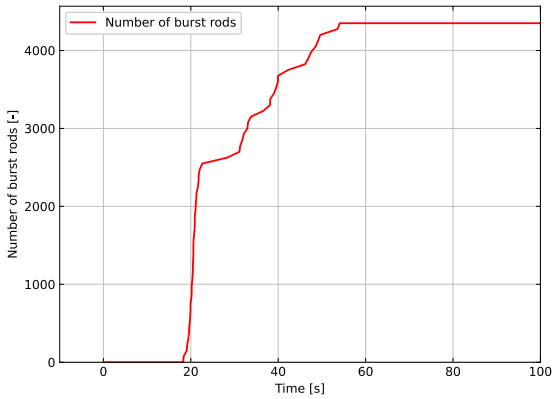

Figure 150: Simulation case #1. Progression of the number of burst rods.

In the following plots, the spatial distribution of selected output parameters is presented. Each of the plots shows values for the 193 assemblies (assembly numbers are given in the plots). For each assembly, 4 quadrants are depicted, each shows the result of one representative rod (the quadrant in the upper right corner of an assembly depicts the results of the representative rod with maximum power).

Figure 110 shows the cladding temperature of 6 different axial layers at 5 s after the break (first temperature peak). The temperature distribution is almost symmetrical and depends mainly on the energy stored in the fuel rods. Due to the top-peaked power profile with maximum power in layer 15, the highest temperatures are observed in that layer. At the top of the core (layer 17), the beginning of cold water injection from hot leg of loop 3 (due to coolant injection from the pressurizer) is observed, which leads to local reduction of the cladding temperatures (upper left corners of Figure Figure 151(d), (e) and (f)). Figure 152 shows the situation 15 s later with a strong asymmetric

[11] Due to imbalanced steady state solution, primary pressure in this simulation is higher than nominal value. This issue will be fixed for final simulations presented in Task 2.5. The deviation is not expected to have very large impact on the results.

temperature distribution due to asymmetric injection (before 20 s mainly from pressurizer, loop 3) and discharge to the break (loop 2). From the axial distribution the peak value has been computed for each rod and is shown by Figure 153(a) for t=5 s and by Figure 153(b) for t=20 s. The further progression of the radial distribution of PCT is indicated by Figure 153(c)-(f), showing that the region close to the loop 2 remains at elevated temperature for longer time.

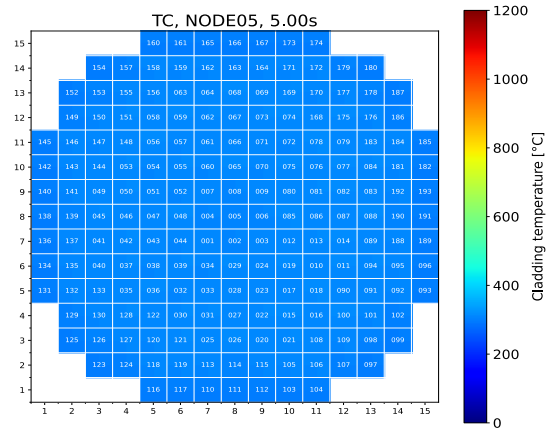

(a) Layer 5

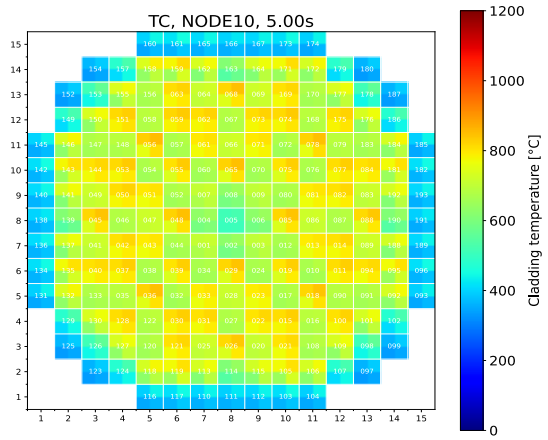

(b) Layer 10

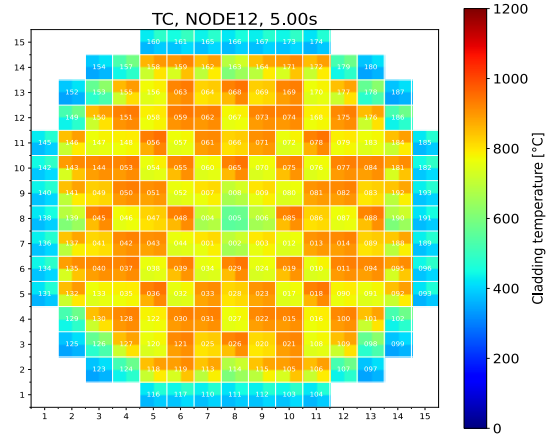

(c) Layer 12

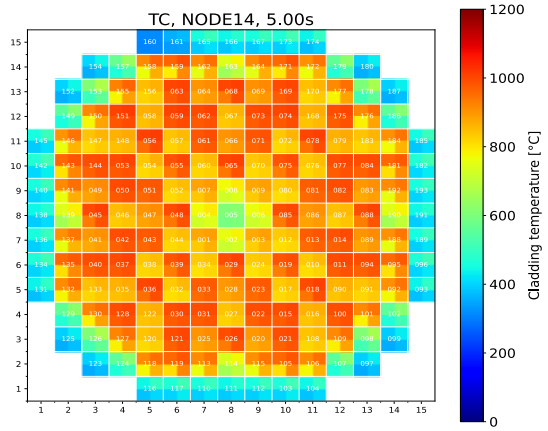

(d) Layer 14

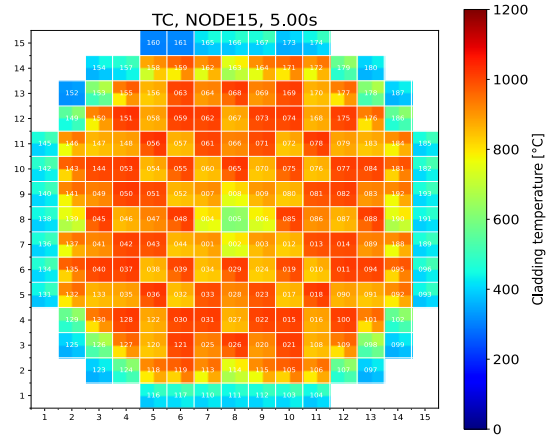

(e) Layer 15

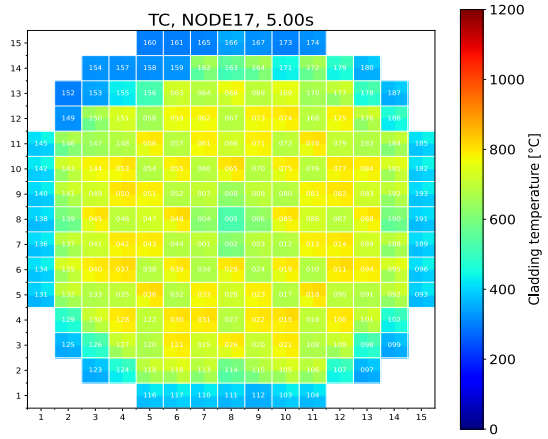

(f) Layer 17

Figure 151: Simulation case #1. Cladding temperature distribution at 6 different elevations 5 s after beginning of LOCA transient

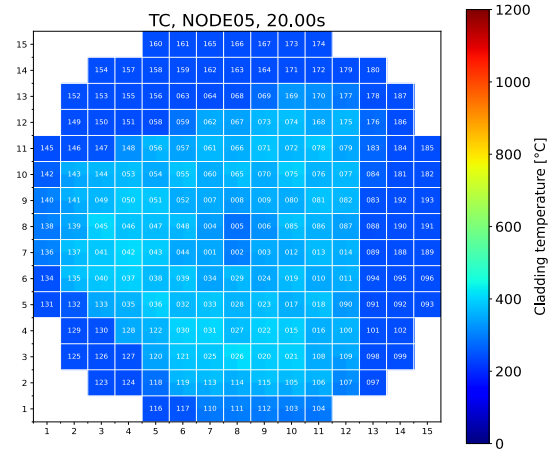

(a) Layer 5

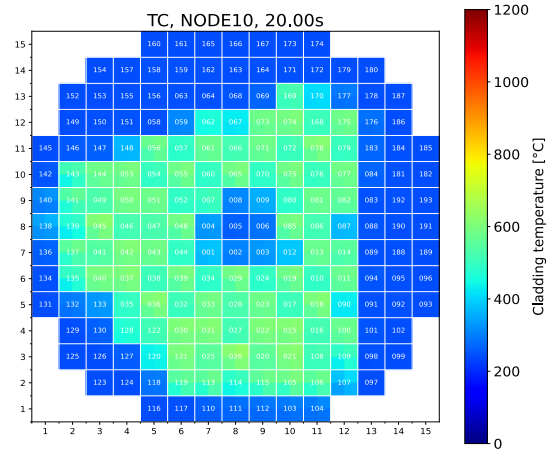

(b) Layer 10

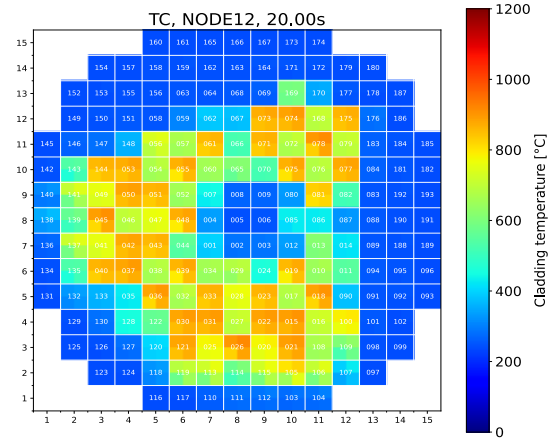

(c) Layer 12

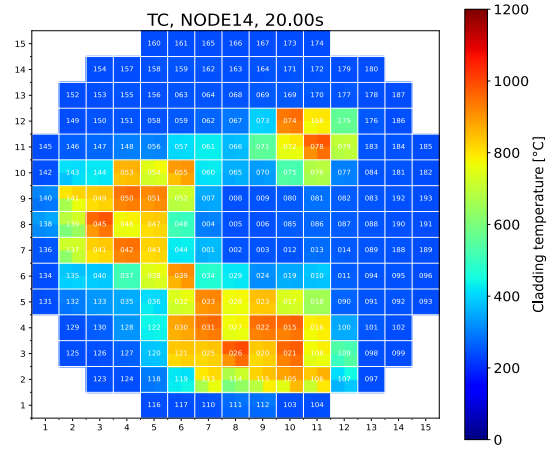

(d) Layer 14

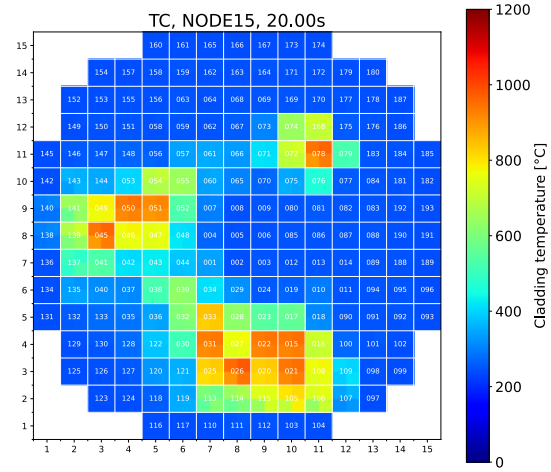

(a) Layer 15

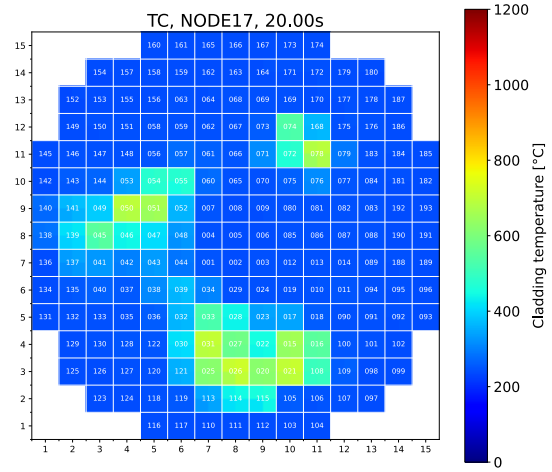

(a) Layer 17

Figure 152: Simulation case #1. Cladding temperature distribution at 6 different elevations 20 s after beginning of LOCA transient

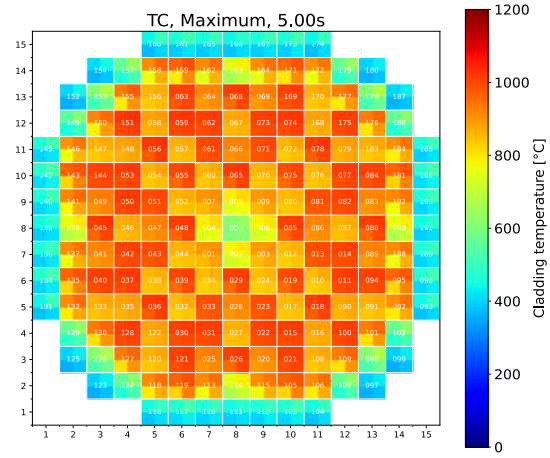

(a) t = 5 s

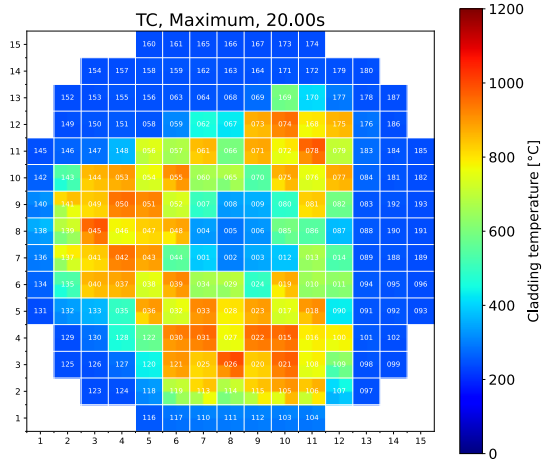

(b) t = 20 s

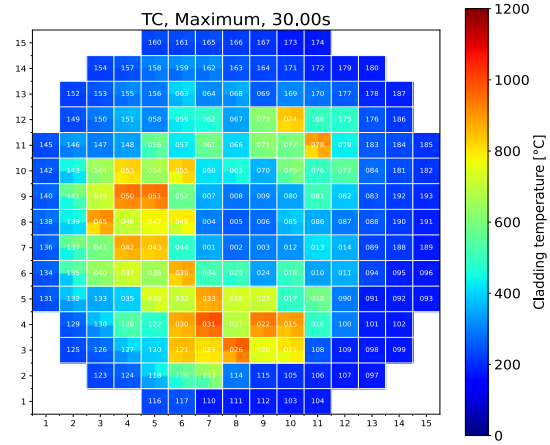

(c) t = 30 s

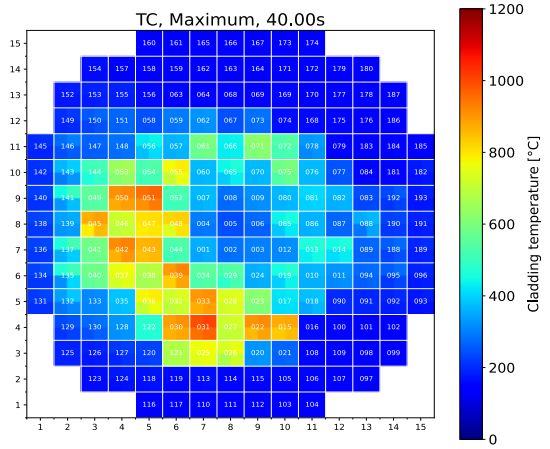

(d) t = 40 s

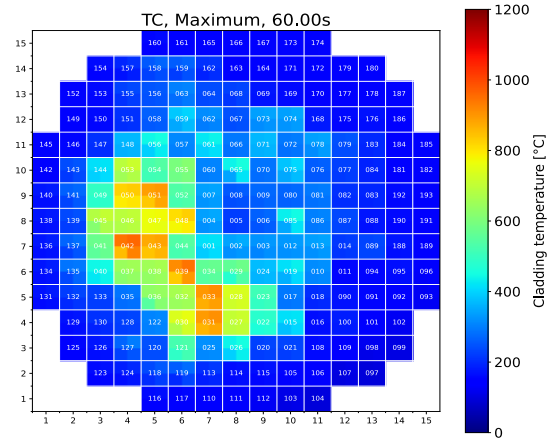

(e) t = 60 s

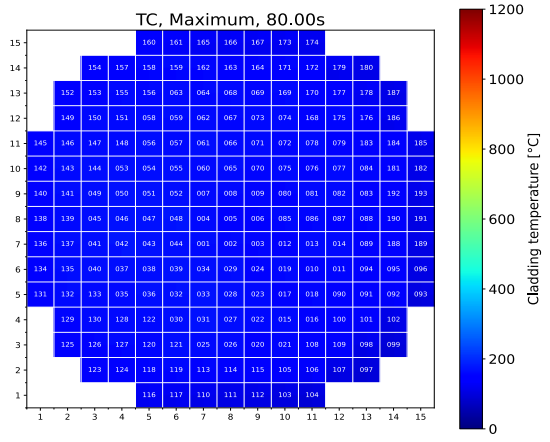

(a) t = 80 s

Figure 153 Simulation case #1. Maximum cladding temperature distribution (maximum cladding temperature of each of the 772 representative rods) at selected times

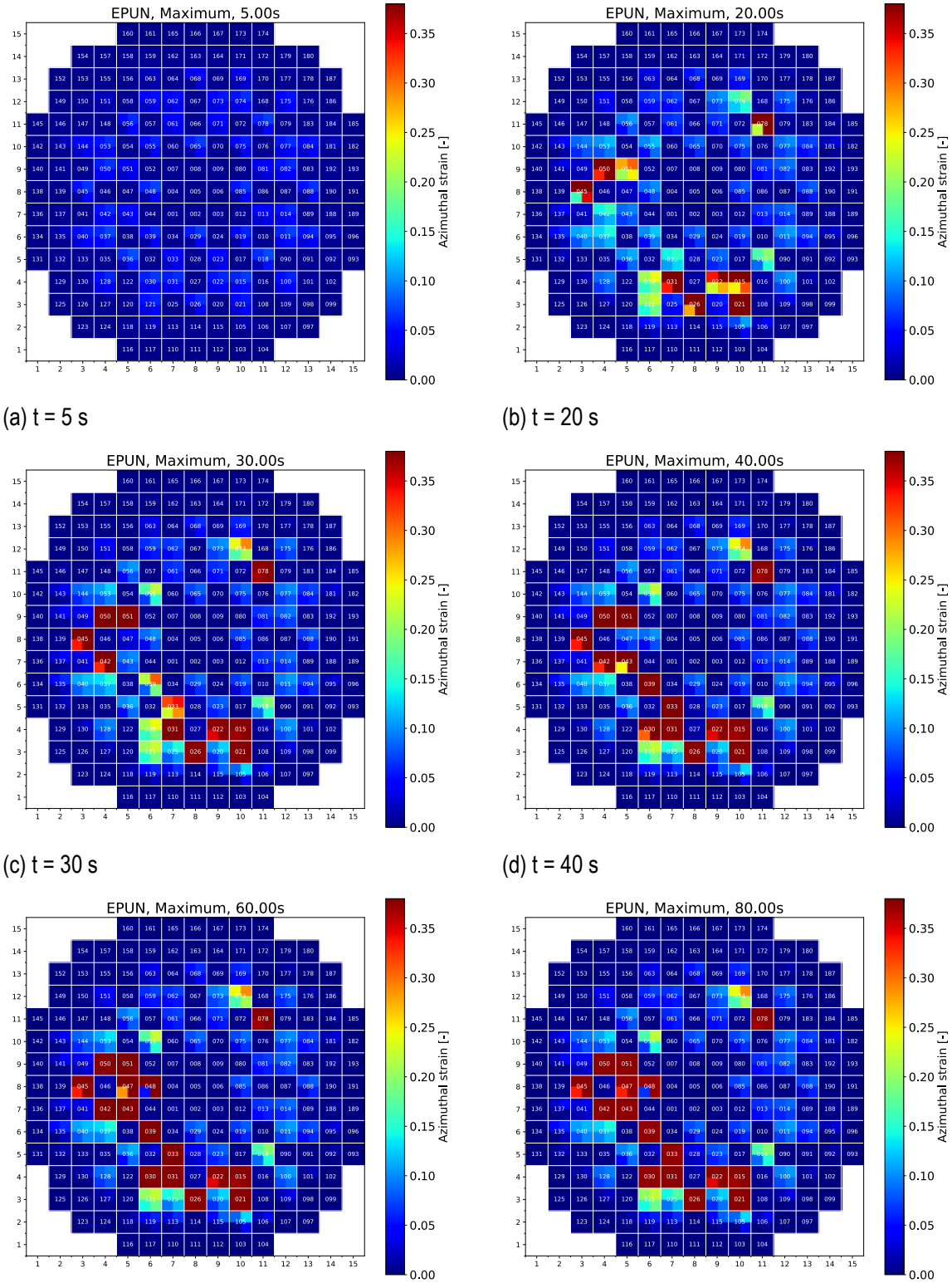

(a) t = 5 s (b) t = 20 s

(c) t = 30 s (d) t = 40 s

(e) t = 60 s (f) t = 80 s

Figure 154: Simulation case #1. Time course of the azimuthal strain distribution (maximum strain of each rod)

The simulation has been repeated with the minimum initial RIP value (2.25 MPa at 293 °C), equal to the fill gas pressure of fresh fuel, resulting in a significantly lower RIP during zero transient before the LOCA (7.0 MPa). Due to the lower RIP, no ballooning is observed before 20 s, and the creep rates of the cladding are lower. The first rod bursts at 36 s (approx. double the time observed for the high pressure case) and the total number of burst rods is 3 % of all rods. This number is the lower boundary for burst rods, compared to the previously determined upper boundary of 7.5 %. The spatial distribution of burst rods is similar to the previous variant with most of the burst rods located in the core quadrant connected to the broken loop (lower left corner of Figure 159).

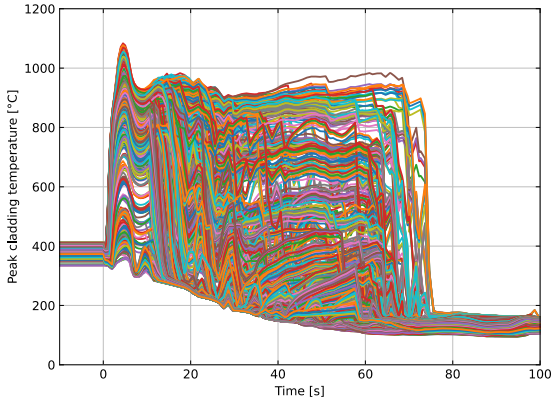

Figure 155 Simulation case #2. Maximum cladding temperature of the 772 representative rods.

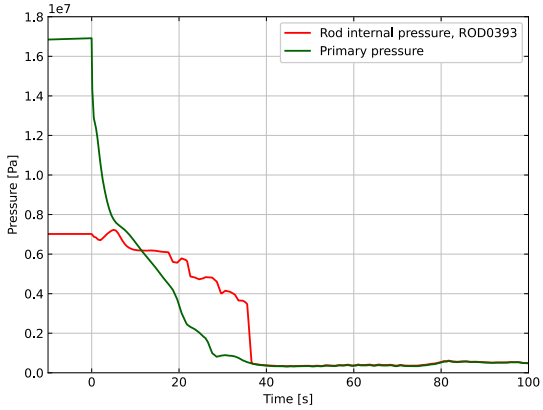

Figure 156 Simulation case #2. Primary pressure and RIP of the fuel rod which earliest burst.

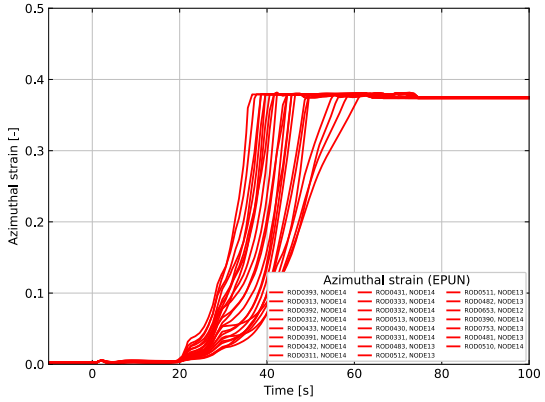

Figure 157: Simulation case #2. Hoop strain of those 58 representative rods that reach the burst criterion (38 % strain).

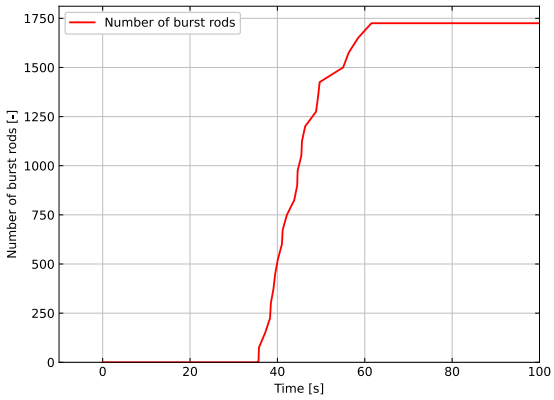

Figure 158: Simulation case #2. Progression of the number of burst rods.

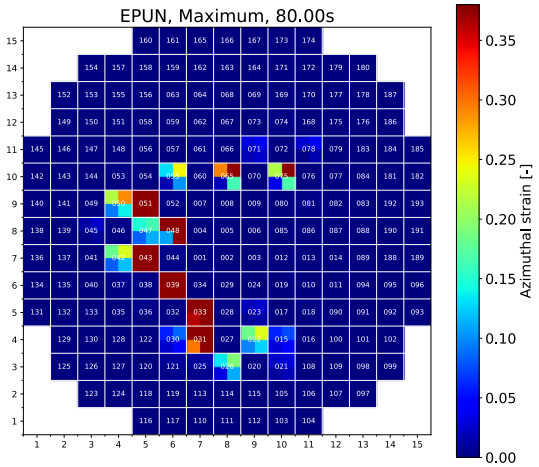

Figure 159: Simulation case #2. Distribution of maximum azimuthal strain at the end of LOCA

As described above, in both previous simulations the pressurizer has been connected to one of the intact loops and its inventory has been discharged into the RPV which leads to cooling of the hottest part of the core (top-peaked power profile) during the first 10 s of the transient. To study the influence of this effect, the simulation has been modified with pressurizer connected to the broken loop. Again two simulations with two bounding values of RIP have been carried out (case #3 with initial RIP = 3.6 MPa and case #4 with initial RIP = 2.25 MPa).
Figure 121 shows the cladding temperature distribution at the top of the core 5 s after beginning of the LOCA accident. A comparison of this figure to Figure 151(f) reveals that there is no water injection coming from pressurizer via hot leg of loop 3, which leads to less cooling of the hot core during the discharge phase and a higher PCT (Figure 160). In general a more homogenous distribution of the PCT is observed and larger parts of the core remain at elevated temperature (compare Figure 163 with Figure 153(b)). This leads to earlier burst of the rods and an increased number (13.6 % of all rods for the case with pressurizer connected to broken loop compared to 3 % if the pressurizer is connected to intact loop, see Figure 161). The burst rods are distributed more homogenously across the core than it has been observed for the cases with injection from pressurizer (compare Figure 164 with Figure 159 and Figure 165 with Figure 154(f)). For the upper boundary case (with initial RIP = 3.6 MPa), 18.9 % of all rods burst.

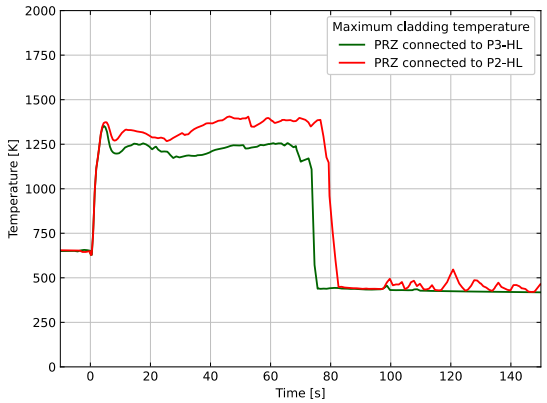

Figure 160: Evolution of PCT for two different scenarios (pressurizer connected to intact loop vs. pressurizer connected to broken loop).

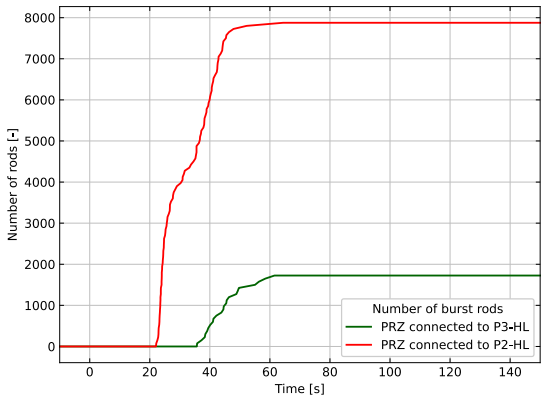

Figure 161: Evolution of number of burst rods for two different scenarios (pressurizer connected to intact loop vs. pressurizer connected to broken loop).

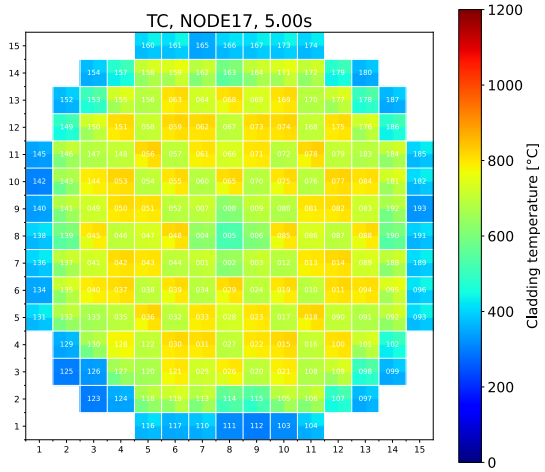

Figure 162: Simulation case #4 with pressurizer connected to broken loop and initial RIP = 2.25 MPa. Cladding temperature at top of the core (layer 17) 5 s after beginning of LOCA.

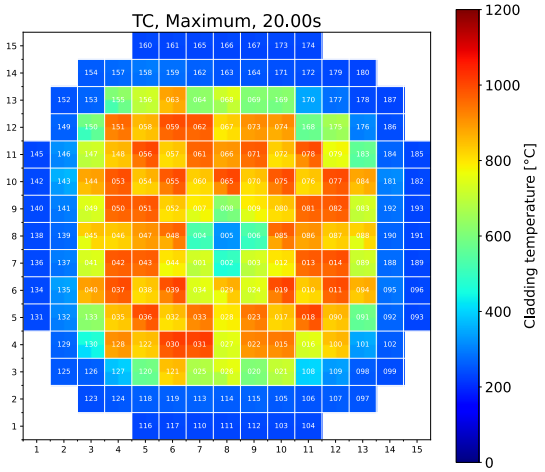

Figure 163: Simulation case #4 with pressurizer connected to broken loop and initial RIP = 2.25 MPa. Distribution of PCT at 20 s.

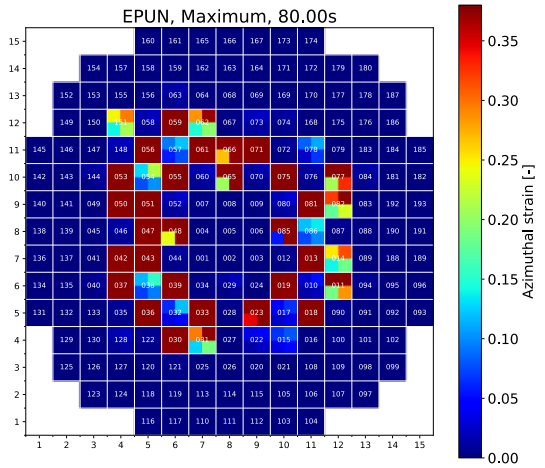

Figure 164: Simulation case #4 with pressurizer connected to broken loop and initial RIP = 2.25 MPa. Distribution of maximum azimuthal strain at the end of LOCA.

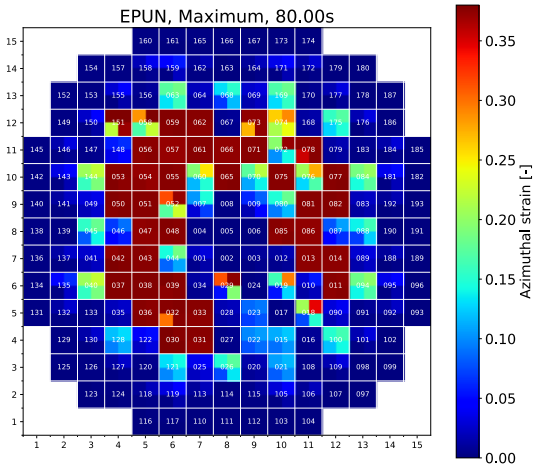

Figure 165: Simulation case #3 with pressurizer connected to broken loop and initial RIP = 3.6 MPa. Distribution of maximum azimuthal strain at the end of LOCA.

Results obtained for realistic power profile

The consequences of different core power profiles have been investigated. All 4 simulation cases discussed in the previous sections with top-peaked power profile have been repeated with realistic power profile taken directly from the core simulator results. One case (case #9 according to the enumeration in the summary Table 53) has been selected for comparison to a simulation case with top-peaked power profile. Apart from the different power-profiles, both simulations have been performed with almost identical initial and boundary conditions (e.g. 106 % of core

power, pressurizer located in the same loop as the break, low initial RIP = 2.25 MPa)[12]. The investigated simulation was suspended by code error shortly after 80 s. However, as no further significant increase of the rod deformation is expected later, the reached time span is enough to draw preliminary conclusions.
The PCTs of all 772 rods are shown for the top-peaked power profile and the realistic power profile by Figure 166 and Figure 167, respectively. As expected, in case of a top-peaked power profile higher temperatures are observed than for the case with realistic power profile. This trend is observed for the first peak (during discharge phase) and also for the second heat-up phase at around 50 s.

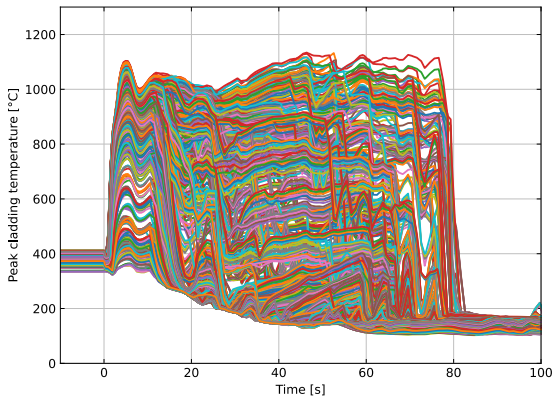

Figure 166: Simulation case #4 with top-peaked power profile. Evolution of PCTs.

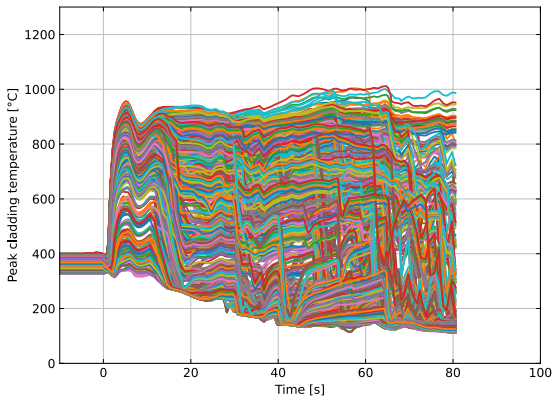

Figure 167: Simulation case #9 with realistic power profile. Evolution of PCTs.

For the top-peaked profile case, creep of rods starts earlier and higher creep rates are observed. A large number of rods reach 38 % hoop strain shortly after 20 s (defined burst criterion), whereas the code predicts first rod burst at 31 s for the realistic power profile case (see Figure 168 and Figure 169). With the assumptions made for the current analyses with a top-peaked profile, the proportion of rods that burst exceeds the 10% criterion at 13.7 %, while with a realistic performance profile only 5.2 % of the rods burst.

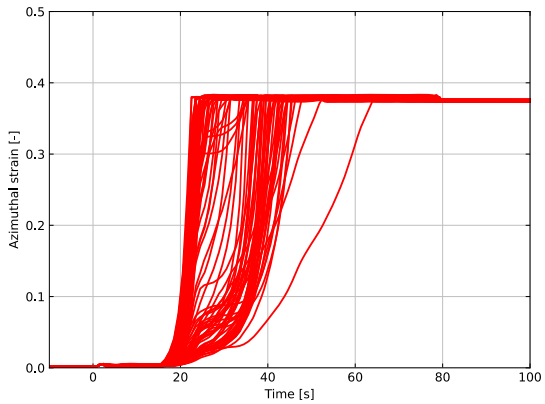

Figure 168: Simulation case #4 with top-peaked power profile. Evolution of hoop strain of those rods that reach burst criterion (38 % hoop strain, rod labels excluded due to too many burst rods).

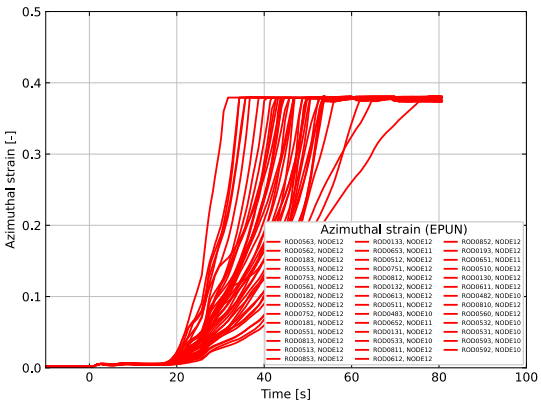

Figure 169: Simulation case #9 with realistic power profile. Evolution of hoop strain of those rods that reach burst criterion (38 % hoop strain).

[12] One exception is the too high initial pressure value set for the accumulators for case #4, which results in injection starting a few seconds too early. Due to too long run-times, that case could not be repeated up to now.

The distribution of the hoop-strain within the core at the end of the LOCA transient is shown by Figure 170 for different axial layers between layer 5 (bottom part of the core) and 16 (top-most layer). Dark red color indicates those rods which have reached 38 % hoop strain (burst criterion). For top-peaked profile, burst is observed from layer 12 to 14, whereas for realistic profile, burst is observed closer to the center of the core (layer 10 to 12).

Top-peaked power profile

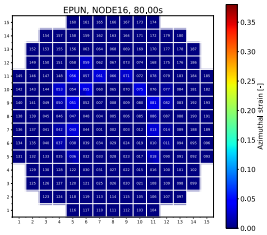

Layer 16

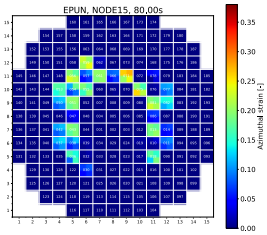

Layer 15

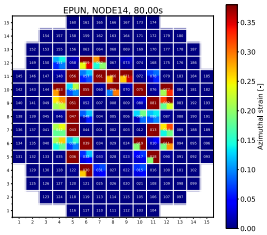

Layer 14

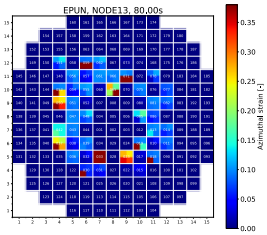

Layer 13

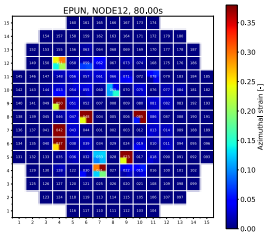

Layer 12

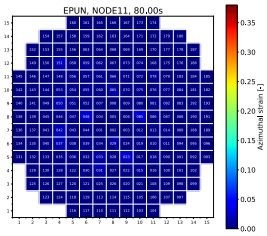

Layer 11

Realistic power profile

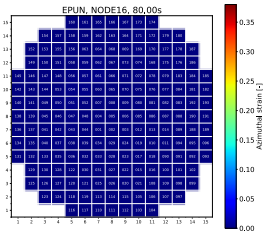

Layer 16

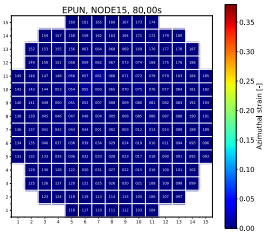

Layer 15

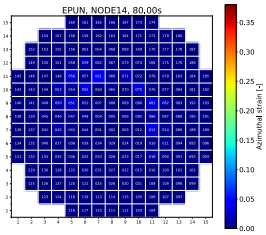

Layer 14

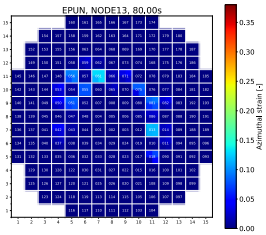

Layer 13

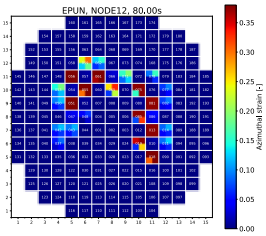

Layer 12

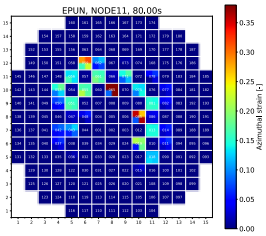

Layer 11

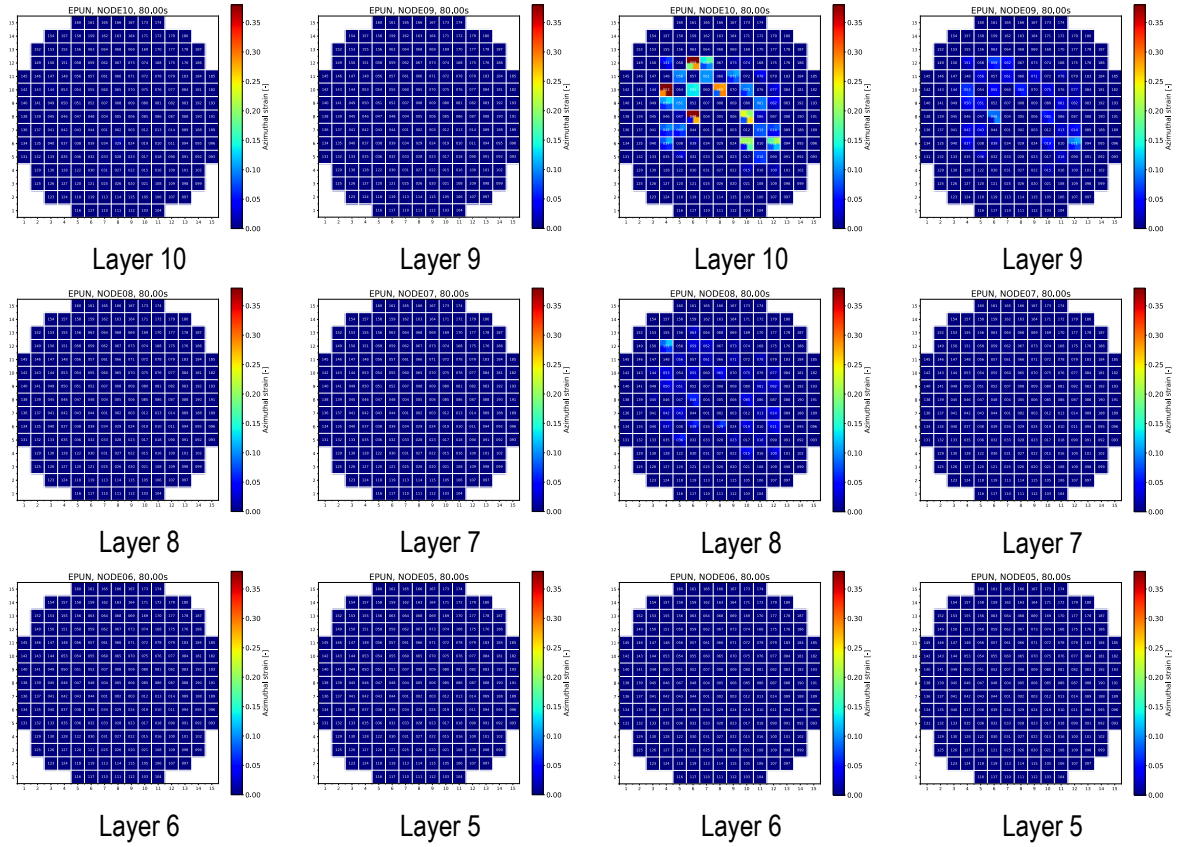

Figure 170: Distribution of azimuthal strain at t=80 s (top-peaked vs. realistic power profile).

Investigation of influence of core cross-connections

The newly developed core model contains connecting junctions (cross connections) between adjacent core channels. This feature enables coolant exchange in horizontal direction within the core and furthermore, pressure differences between neighboring control volumes are reduced. This is especially important for cases, where the flow cross-sectional area of a channel is reduced due to ballooning of fuel rods, or even is blocked due to neighboring fuel rods in contact. Without cross connections such a situation can lead to conditions, where the coolant flow vanishes completely and the affected region might heat-up until melting of the rods is reached. With cross-connections, flow can enter the affected region from neighboring channels and better cooling is expected.
To study the effect of the CCOs, one simulation has been performed where the core cross-connections have been removed. A case with realistic power distribution and minimum initial RIP (2.25 MPa) has been selected for comparison. Unfortunately, both simulations have been terminated at approx. 80 s due to an ATHLET-CD error, which is prior to complete quenching of the rods and the analysis has to be limited to that time.
An advantage of the model without cross-connections is the significantly shorter CPU time (approx. a factor of 2 faster, see Figure 171), due to the lower number of equations to be computed (reduced size of the Jacobi matrix). However, the results of the simplified model differ significantly from the results obtained by the model with CCOs. As in the model without CCOs the horizontal flows and the resulting cooling effects are neglected, the channels with high power rods heat up, the rods deform and block the channels, which leads to further heat-up of those channels later during the transient. This is depicted by Figure 134 with the maximum cladding temperature of each rod at approx. 80 s. While in the model with cross-connections most rods already have been quenched, in the model without CCOs large part of the core remains at high temperature. In contrast to the model with CCOs which

shows asymmetrical temperature distribution in the core due to asymmetrical boundary conditions, the model without CCOs shows a rather symmetrical temperature distribution. That leads also to a symmetrical distribution of the burst rods (Figure 176). That means that the asymmetric conditions observed at vessel boundaries almost vanish in the core if the simplified model is used.

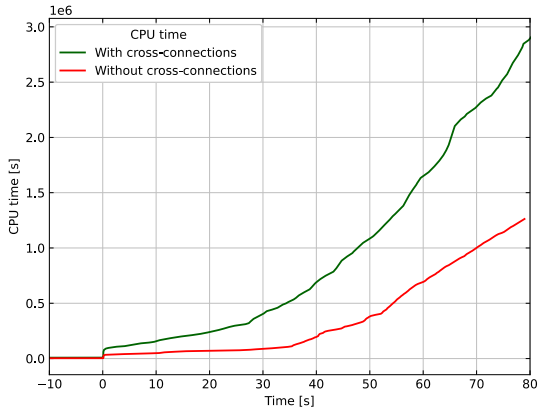

Figure 171: Core model with and without core cross-connections. Comparison of CPU time.

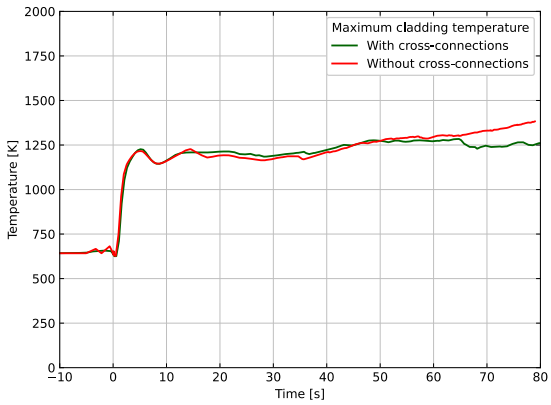

Figure 172: Core model with and without core cross-connections. Comparison of PCT

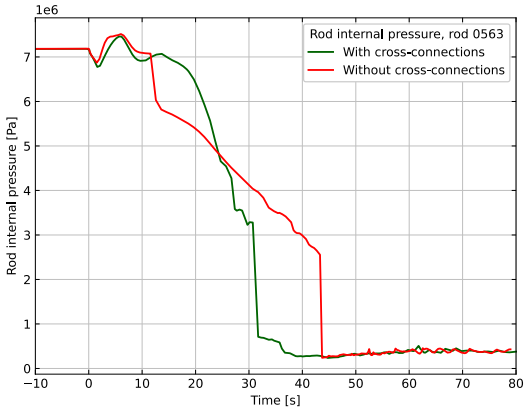

Figure 173: Core model with and without core cross-connections. Comparison of the rod internal pressure of selected fuel rod.

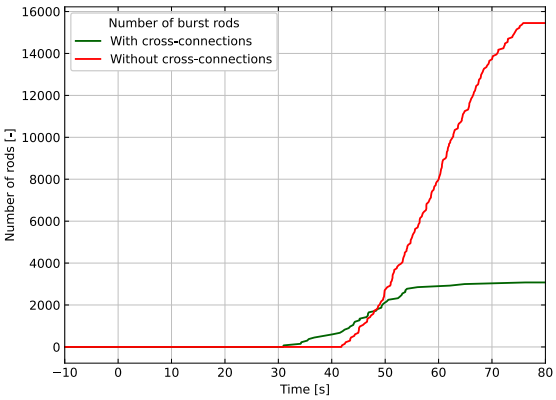

Figure 174: Core model with and without core cross-connections. Comparison of the number of burst rods.

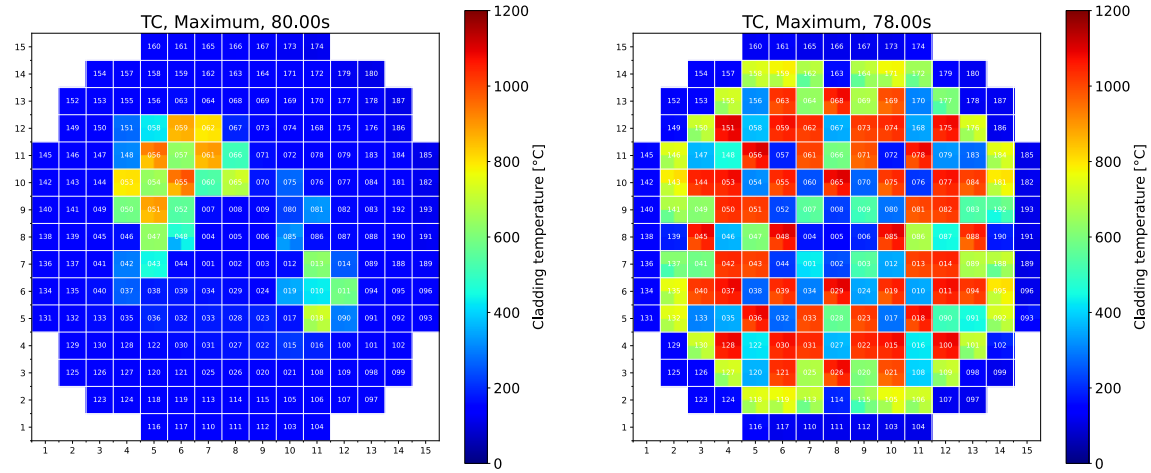

(a) with core cross-connections (b) without core cross-connections

Figure 175: Simulation with pressurizer connected to broken loop, initial RIP = 2.25 MPa, realistic power profile. Distribution of maximum cladding temperature at 80 s (end of simulation).

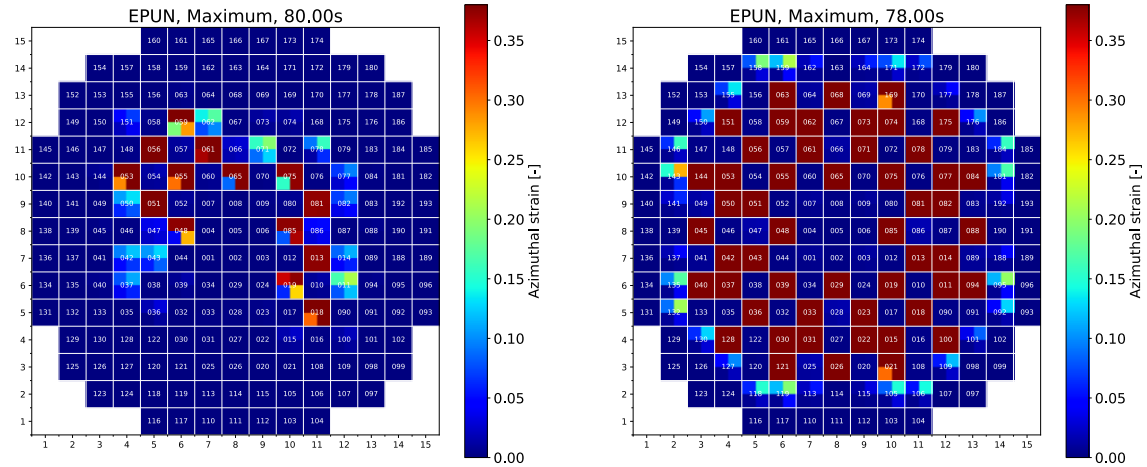

(a) with core cross-connections (b) without core cross-connections

Figure 176: Simulation with pressurizer connected to broken loop, initial RIP = 2.25 MPa, realistic power profile. Distribution of maximum azimuthal strain at 80 s (end of simulation).

Summary and outlook

A new core modelling approach has been developed which combines a 3D thermal hydraulic model of the PWR RPV and reactor core with the fuel rod model of ATHLET-CD (including mechanical rod behavior model, models for burst of cladding, calculation of fission product inventory and decay heat) and feedback from the fuel rod model back to thermal-hydraulic model (based on calculation of reduction of the flow cross sectional areas).
Despite the model still has several limitations and short-comings, it is (to the author's knowledge) the first time that the system code ATHLET-CD has been applied to model the degradation of fuel rods for a 3D configuration of PWR core. In contrast to the very coarse nodalization approach applied at the beginning of the project (subdivision of the core into 6 concentric rings, which is the typical approach applied in severe accident codes), the new approach enables to study the influence of local variations of the flow and cooling conditions to the behavior of the fuel rod. This is especially important for the analyses of a LB-LOCA with asymmetric boundary conditions due to break located in only 1 out 4 loops and asymmetric ECCS injection. With the new model the number of burst fuel rods during the LB-LOCA accident could be estimated, which was not possible with the previously used approach.
To investigate the performance and the capabilities of the new model, several LB-LOCA transients have been calculated for a generic German PWR of type Konvoi, with variation of the boundary conditions as well as model parameters and the number of failed rods has been calculated.
The results of the performed simulations are summarized in Table 53. For the cases investigated up to now, the break is located in cold leg of loop #2. The location of the pressurizer has been varied. In the first case, the pressurizer is connected to the hot leg of the affected loop (P2-HL), for other cases the pressurizer is connected to an intact loop (hot leg of loop #3). As explained in section 0, for each scenario, two boundary cases with low and high initial value of RIP have been calculated (RIP = 2.25 MPa vs. 3.60 MPa). Furthermore, two different power profiles have been investigated (top-peaked power profile vs. realistic power profile).
Depending on the investigated scenario, initial and boundary conditions, the fraction of failed rods varies between 3 % and 20 %. Even for cases with realistic power profile and lowest RIP values, the calculated number of failed rods exceeds the values reported in previous studies and higher numbers are expected if a realistic RIP distribution would be included into the current model. Furthermore, the analyses reported previously [93][94] show a symmetrical distribution of the burst rods, which is in contrast to the new results obtained by the 3D model.
The influence of the core blockage model (feedback from fuel rod behavior model to thermal-hydraulic model by reduction of flow cross sections due to rod deformation) has been studied. The comparison of simulation case #5 to case #4 shows that neglecting the cross flow reduction calculation leads to an underestimated failed rod number (underestimation by approx. 25% for the investigated case). Consequently, it is recommended to take the feedback from fuel rod behavior model to thermal-hydraulics into account for a best estimate study of LOCA.
One simulation case (#10) has been performed without cross-connections between the core channels. That means that the assemblies are isolated from each other and no horizontal flow is possible between adjacent channels, which is in contrast to the real configuration in a PWR core where cross flows are possible. Such assumptions lead to reduced cooling of the rods and a significantly increased number of burst rods (compare case #5 with case #10). That shows that modelling of cross-connections is essential for a realistic modelling approach.
The ATHLET-CD models for cladding creep and burst have been assessed and applied to the LOCA scenario. The code currently provides four different correlations for modelling of the creep of Zircaloy cladding. However, it was found out that some models are missing correlations for the beta-phase, which should be updated in the future. The implemented correlation according to Rosinger shows the highest creep rates and leads to the highest number of burst rods. Therefore, this correlation might be used in a conservative analysis, but no final conclusion could be drawn which correlation should be applied for a best estimate simulation of the LOCA transient.
The implemented burst criteria comprise simple criteria such as a user-defined maximum hoop strain or strain rate and more detailed criteria such as the Chapman correlation and the model according to Hagrman. For reason of simplicity, the maximum strain criterion has been applied in most analyses performed up to now with the new core modelling approach. Further assessment of the currently implemented models, literature research and possibly

also the implementation of more recently developed burst models has to be done until a recommendation for a best-estimate burst model can be given for the usage in ATHLET-CD and the assessed Konvoi reactor.

Case	Break location	Pressurizer	Initial RIP / MPa	Accumulator initial pressure / MPa	Power profile / additional modifications	Fraction of failed rods / %
#1	P2-CL	P3-HL	3.60	4.5**	Top-peaked	7.5
#2	P2-CL	P3-HL	2.25	4.5**	Top-peaked	3.0
#3	P2-CL	P2-HL	3.60	4.5**	Top-peaked	19.6
#4	P2-CL	P2-HL	2.25	4.5**	Top-peaked	13.7
#5	P2-CL	P2-HL	2.25	4.5**	Top-peaked / No feedback to thermal hydraulics[13]	10.2
#6	P2-CL	P3-HL	3.60	2.6	Realistic	10.4
#7	P2-CL	P3-HL	2.25	2.6	Realistic	4.7
#8	P2-CL	P2-HL	3.60	2.6	Realistic	18.7
#9	P2-CL	P2-HL	2.25	2.6	Realistic	5.2
#10	P2-CL	P2-HL	2.25	2.6	Realistic / No cross-connections between core channels	27.6
#11	P2-CL	P2-HL	2.25	2.6	Top-peaked / ***	17.4*
#12	P2-CL	P2-HL	2.25	2.6	Realistic / ***	5.4*

Table 53: Summary of results.

* Simulations still running (increase of number of failed rods expected).
** Due to mistake in the input deck, a too high initial accumulator pressure has been applied, which leads to too early start of injection.
*** Simulation with improved input deck (better steady state solution, corrected SG heat transfer surface)

[13] ATHLET-CD parameter ITFBK = 4.

Final conclusions

During the first period of the project, the methodologies used by some partners for the evaluation of radiological consequences in LOCA within DBA conditions were reviewed in WP2.1. In general, these methodologies use conservative deterministic assumptions mostly based on decoupled approaches. It was noticed that several different evaluation methodologies were employed among the R2CA partners without a shared agreement on the approach. These methodologies only share some assumptions and can differ significantly regarding isotopic inventory definition or fuel characteristics and state. In particular, the assumed rate of failed fuel rods for radiological consequence evaluations is also different among the participants, ranging from 10% to 100%. However, most of the methodologies agree on considering several different types of fuel assembly based on irradiation and core management in order to capture the respective behavior of fuel assemblies during LOCA.
This WP 3.2 aimed to develop specific models and methods to better predict the failed rod number during a LOCA scenario within DBA and DEC-A conditions. The work performed and achievements gained, will be used to build new (or refine) methodologies with regard to the core modeling and the simulation of the clad ruptures that will be used in WP 2.5 for improved and less conservative reactor calculations and better predictions of the radiological consequences of LOCA accidents within DBA and DEC-A conditions. Within the frame of the project several advances have been made, summarized below, regarding clad thermomechnical models, core modelling and LOCA calculation methodologies for prediction of the failed rod number.

Concerning clad thermomechanical models, clad burst database and criteria, the work that has been done, the main conclusions that can be drawn as well as the main achievement at the end of the project are :

- A very large database exists with significant scattering in terms of burst parameters (strain, stress, temperature …). IRSN collected about 1440 burst tests data from both litterature and internal documentation and EK reassessed about 30 additional burst tests performed on E110 clads by using very detailed post-test tomography measurements.
- No simple burst criterion was found to predict correctly both burst temperature and burst strain. Various enveloppes (minimum, mean, maximum, std) on true stress versus temperature were proposed by IRSN as well as an engineering stress limit versus temperature for as-received claddings. EK proposed a constant best-estimate strain limit of 0.35 and recommends to use 0.21 (-60%) to assess the number of failed rod.
- The impact of cladding hydrogen content on clad thermomechanical behaviour was also addressed but it was found that there is not enough data available to propose a specific model taking into account this effect, various correlations were compared.
- Creep laws and phase transformation models of Zr-based alloys were also updated or reassessed in two codes (FRAPTRAN, TRANSURANUS) and new laws for M5 alloy were implemented in some codes.
- Burst criteria were modified in FRAPTRAN-VTT and DRACCAR-IRSN codes and evaluations were performed on tests from code validation database.

Regarding LOCA calculation methologies, as the original methods were significantly different among R2CA partners, the resulting update brought in WP 3.2 for failed rod prediction is also heterogeneous. For each partner, the outcome on failed rod number prediction is generally associated to the improvement of the initial methodology and associated codes.

At the end of the project, the main achievements and conclusions are

- Several LOCA calculation methodologies were developed and/or updated using various simulation tools. Two main categories of methodologies were thus refined using a calculation chain approach sequentially

coupling a thermalhydraulic system code to a thermomechanical code (such as RELAP/TRANSURANUS or GENFLO/FRAPTRAN) or using an integral approach with a stronger coupling between thermalhydraulic and thermomechanical models within the same code (ASTEC, DRACCAR, ATHLET-CD)

- A particular effort has been made to the latter through a more detailed core modelling approach. New upcoming approaches with 3D multi-pin description were develooped such as a 3D core model (DRACCAR) or even a full 3D RPV model (ATHLET-CD). The 3D description evaluates transverse cross-flows between fuel assemblies and in the case of full RPV model can depict non-symetric distribution of flow in the reactor vessel that can occur during a LOCA transient. Several prospects are identified for these approaches which seems to propose many benefits compared to classical 2D or multi-1D models provided that thermalhydraulics and thermalmechanics phenomena are coupled. 3D approaches being CPU costly modelling the whole core very finely is still very challenging and often compromise must be reached between a 3D description of the whole core/vessel and CPU performance leading in some cases to restric the detailed 3D modelling to only a region of the core). Considering the outlooks on computational performance improvement, these 3D approaches will certainly become the standard for failed rod number prediction in a nearly future

Most of the methodologies aim to represent as best as possible the various characteristics of fuel assemblies before transient (according to the their initial composition, their power history and the core loading plan) provided by neutronic calculations (SCALE, DYN3D, VESTA,…) and fuel performance codes (TRANSURANUS, FRAPCON,…). Thus, they generally account for several type of rods/assemblies trying to depict as detailed as possible the respective characteristic of each fuel assemblies (or subdivision of fuel assemblies) in order to better predict the failed rod number in the core.
In parallel progress has been made for the statistical analysis method in TRANSURANUS by enhancing its build-in capabilities. In particular, the statistical post-processing program of the code was further improved in order to support the Best Estimate Plus Uncertainty (BEPU) analyses.

In addition, within the project, few sensitivity analyses using the Spearmann's correlations were performed with specific fuel codes on initial/operating parameters (i.e. relative power ratio, gap pressure, fuel pellet radius, cladding radii …) and on some model parameters in order to determine the most influential parameters for clad burst predictions. Uncertainties ranges and Pdf for some uncertain parameters were also taken into account in some cases. These analyses should be however still extended and generalized before drawing conclusions. Indeed whatever the methodologies chosen, further systematic sensitivity analysis to identify the most influential parameters among the wide range of parameters that can affect the rod failure will have to be performed. The results of these analyses will have then have to feed uncertainty analyses (deterministic bounding or BEPU) in order to better predict the range of failed rod number.

Finally, it has to be noted that the work performed within the project only addressed cladding materials in existing NPPs (Zr-4, E110 and M5). In the nearly future this research should be revisited for new materials such as those used in ATFs (Cr-coated Zr alloy…).

References

[1] Report on Fuel Fragmentation, Relocation and Dispersal, NEA/CSNI/R(2016)16, 2016

[2] Powers, D.A. and R.O. Meyer, Cladding Swelling and Rupture Models for LOCA Analysis, in NUREG-0630,1980, U.S. NRC

[3] Meyer, R.O. and W. Wiesenack, A critique of fuel behavior in LOCA safety analyses and a proposed alternative. Nucl. Eng. Design, 2022. 394.

[4] Nuclear Fuel Behaviour in Loss-of-Coolant Accident (LOCA) Conditions, NEA No. 6846, 2009, NEA.

[5] L. Yegorova et al.: Data Base on the Behavior of High Burnup Fuel Rods with Zr-1%Nb Cladding and U02 Fuel (VVER Type) under Reactivity Accident Conditions, NUREG/IA-0156 (1999)

[6] L. Yegorova et al.: Mechanical Properties of Unirradiated and Irradiated Zr-1% Nb Cladding, NUREG/IA-0199 (2001)

[7] F.J. Erbacher et al.: Temperaturtransiente Kriechberstversuche an Zirconium-Niob1-Hüllrohren – Vergleich zu Zircaloy-4 Hüllrohren, FZKA 5726 (1997)

[8] E. Perez-Feró et al.: Experimental Database of E110 Claddings under Accident Conditions, EK-FRL-2012-255-01/02 (2013)

[9] K.J. Geelhood, W.G. Lusher, J.M. Cuta, I.A. Porter: FRAPTRAN-2.0: A computer code for the transient analysis of oxide fuel rods, PNNL-19400, Vol.1 Rev2

[10] Cs. Győri et al.: Model development and code extensions, EXTRA PROJECT report, October 2003, EVOL-EXTRA-D-2 / FIKS-CT-2001-00173.

[11] A. Arkoma, M. Hänninen, K. Rantamäki, J. Kurki, and A. Hämäläinen, "Statistical analysis of fuel failures in large break loss-of-coolant accident (LBLOCA) in EPR type nuclear power plant," *Nuclear Engineering and Design*, vol. 285, pp. 1–14, Apr. 2015, doi: 10.1016/j.nucengdes.2014.12.023.

[12] L. J. Siefken, E. W. Coryell, E. A. Harvego, and J. K. Hohorst, "SCDAP/RELAP5/MOD 3.3 Code Manual MATPRO-A Library of Materials Properties for Light-Water-Reactor Accident Analysis," 2001.

[13] L. Yegorova *et al.*, "International Agreement Report Data Base on the Behavior of High Burnup Fuel Rods with Zr-1%Nb Cladding and U0 2 Fuel (VVER Type) under Reactivity Accident Conditions Description of Test Procedures and Analytical Methods Ministry of Science and Technologies of Russian Federation Published by U.S. Nuclear Regulatory Commission," 1999. [Online]. Available: http://www.nrc.gov

[14] K. J. Geelhood, W. G. Luscher, C. E. Beyer, J. M. Cuta, and M. E. Flanagan, "FRAPTRAN 1.4: A Computer Code for the Transient Analysis of Oxide Fuel Rods NUREG/CR-7023 Vol. 1," 2011.

[15] H. E. Rosinger, "A Model to predict the failure of Zircaloy-4 fuel sheating during postulated LOCA conditions," *Journal of Nuclear Materials*, vol. 120, p. 41, 1984, doi: 10.1016/0022-3115(84)90169-7.

[16] D. Kaddour, S. Frechinet, A. F. Gourgues, J. C. Brachet, L. Portier, and A. Pineau, "Experimental determination of creep properties of zirconium alloys together with phase transformation," *Scr Mater*, vol. 51, no. 6, pp. 515–519, 2004, doi: 10.1016/j.scriptamat.2004.05.046.

[17] G. Pastore *et al.*, "Analysis of fuel rod behavior during loss-of-coolant accidents using the BISON code: Cladding modeling developments and simulation of separate-effects experiments," *Journal of Nuclear Materials*, vol. 543, Jan. 2021, doi: 10.1016/j.jnucmat.2020.152537.

[18] H. J. Neitzel and H. E. Rosinger, "The Development of a Burst Criterion for Zircaloy Fuel Cladding under LOCA Conditions," 1980.

[19] A. R. Massih, "Transformation kinetics of zirconium alloys under non-isothermal conditions," *Journal of Nuclear Materials*, vol. 384, no. 3. pp. 330–335, Feb. 28, 2009. doi: 10.1016/j.jnucmat.2008.11.033.

[20] T. Taurines *et al.*, "Rod cladding failure during LOCA- Progress report on experimental database reassessment and model/code improvements," 2021.

[21] S. U. Lee, H. C. Kim, Y. S. Yang, and C. H. Shin, "STUDY ON THE LARGE DEFORMATION MODULE IN FRAPTRAN 2.0," 2018.

[22] D. L. Hagrman, “EGG-CDAP-5379, Fuel Behavior Model Development, Zircaloy Cladding Shape at Failure (BALON2).,” 1981.
[23] R. O. Meyer and W. Wiesenack, “A critique of fuel behavior in LOCA safety analyses and a proposed alternative,” *Nuclear Engineering and Design*, vol. 394, Aug. 2022, doi: 10.1016/j.nucengdes.2022.111816.
[24] L. O. Jernkvist and A. R. Massih, “Calibration of models for cladding tube high-temperature creep and rupture in the FRAPTRAN-QT-1.5 program 2021:04,” 2021. [Online]. Available: www.ssm.se
[25] [L. O. Jernkvist, “Assessment of data and criteria for cladding burst in loss-of-coolant accidents,” 2015. [Online]. Available: www.stralsakerhetsmyndigheten.se
[26] K. Lassmann, “TRANSURANUS: a fuel rod analysis code ready for use”, Journal of Nuclear Materials, 188, 1992, pp. 295-302.
[27] P. Van Uffelen, Cs. Győri, A. Schubert, J. van de Laar, Z. Hózer, G. Spykman, “Extending the application range of a fuel performance code from normal operating to design basis accident conditions”, Journal of Nuclear Materials, 383, 2008, pp. 137-143.
[28] V. Di Marcello, A. Schubert, J. van de Laar, P. Van Uffelen, “The TRANSURANUS mechanical model for large strain analysis”, Nuclear Engineering and Design, 276, 2014, pp. 19-29.
[29] Z. Hozer, Cs. Győri, M. Horváth, I. Nagy, L. Maroti, L. Matus, P. Windberg, J. Frecska, “Ballooning experiments with VVER cladding”, Nuclear Technology, 152, 2005, pp. 273-285.
[30] Cs. Győri, Z. Hózer, K. Lassmann, A. Schubert, J. van de Laar, M. Cvan, B. Hatala, “Extension of the TRANSURANUS code applicability with niobium containing cladding models (EXTRA)”, in: Proceedings of the FISA 2003: Symposium on EU Research in Reactor Safety, Luxembourg, 10–13 November 2003, pp. 589–594.
[31] B. Baurens, “IFA-650.15 LOCA TEST: In-pile results,” 2016.
[32] [A. Chaieb *et al.*, “Computational assessment of LOCA simulation tests on high burnup fuel rods in Halden And Studsvik using Cyrano3 code,” in *Topfuel 2021*, 2021.
[33] P. Magnusson *et al.*, “SCIP III-Subtask 1.1: Fuel fragmentation, relocation and dispersal Final summary report,” 2021.
[34] K. J. Geelhood, W. G. Luscher, C. E. Beyer, and M. E. Flanagan, “FRAPTRAN 1.4: Integral Assessment,” 2011.
[35] T. Taurines, S. Belon, T. Glantz, and F. Jacq, “NEW BURST CRITERIA, AXIAL FUEL RELOCATION AND FISSION GAS RELEASE MODELS IN THE DRACCAR CODE,” 2021.
[36] Cs. Győri, P. Van Uffelen, "The modifications required for the simulation of DBA by means of TRANSURANUS", International Workshop “Towards nuclear fuel modelling in the various reactor types across Europe”, Institute for Transuranium, Elements, Karlsruhe, 25-26 June, 2007.
[37] A. Kecek, K. Tuček, S. Holmström, P. Van Uffelen, “Development of M5 Cladding Material Correlations in the TRANSURANUS Code: Revision 1”, EUR 28366 EN, Publications Office of the European Union, Luxembourg, 2016.
[38] J.-C. Brachet, L. Portier, T. Forgeron, J. Hivroz, D. Hamon, T. Guilbert, T. Bredel, P. Yvon, J.-P. Mardon, P. Jacques, “Influence of hydrogen content on the α/β phase transformation temperatures and on the thermal-mechanical behavior of Zy-4, M4 (ZrSnFeV) and M5™ (ZrNbO) alloys during the first phase of LOCA transient”, Zirconium in the Nuclear Industry: 13th. International Symposium, June 10-14 2001, Annecy, France, ASTM STP 1423, American Society for Testing and Materials, West Conshohocken, PA, 2002, pp. 673-701.
[39] U. Dackermann, “Influence of Hydrogen on the Burst Behavior during Large Break Loss of Coolant Accidents of Zirconium Alloy Fuel Rod Claddings”, Master Thesis, Munich University, Munich, 2011.
[40] R. Calabrese, A. Schubert, P. Van Uffelen, “Review of M5™ Cladding Models Relevant for LOCA Simulation with the TRANSURANUS Code”, Proc. Int. Conf. Nuclear Energy New Europe 2021, Bled, Slovenia, September 6-9, Nuclear Society of Slovenia, 2021, paper 908.
[41] A.R. Massih, L.-O. Jernkvist, “Solid state phase transformation kinetics in Zr base alloys”, Scientific Reports, 2021, 11:7022.

[42] D. Kaddour, S. Frechinet, A.F. Gourgues, J.C. Brachet, L. Portier, A. Pineau, “Experimental determination of creep properties of zirconium alloys together with phase transformation”, Scripta Materialia, 51, 2004, pp. 515-519.
[43] A.R. Massih, “High-temperature creep and superplasticity in zirconium alloys”, Journal of Nuclear Science and Technology, 50, 2013, pp. 21-34.
[44] R. Calabrese, “Crystallographic Phase Transition of Zirconium Alloys: New Models for the TRANSURANUS Code”, Proc. Int. Conf. Nuclear Energy for New Europe, Portorož, Slovenia, September 12-15, Nuclear Society of Slovenia, 2022, paper 606.
[45] Z. Duan, H. Yang, Y. Satoh, K. Murakami, S. Kano, Z. Zhao, J. Shen, H. Abe, "Current status of materials development of nuclear fuel cladding tubes for light water reactors", Nuclear Engineering and Design, 316, 2017, pp. 131-150.
[46] T. Forgeron, J. Brachet, F. Barcelo, A. Castaing, J. Hivroz, J. Mardon, C. Bernaudat, "Experiment and Modeling of Advanced Fuel Rod Cladding Behavior Under LOCA Conditions: Alpha-Beta Phase Transformation Kinetics and EDGAR Methodology", in Zirconium in the Nuclear Industry: Twelfth International Symposium, ed. G. Sabol and G. Moan, West Conshohocken, PA: ASTM International, 2000, pp. 256-278.
[47] M.F. Ashby, R.A. Verrall, “Diffusion-accommodated flow and superplasticity”, Acta Metallica, 21, 1973, pp. 149–163.
[48] G. Trego, “Comportement en fluage à haute température dans le domaine biphasé (α + β) de l’alliage M5®”, Doctorat ParisTech Thèse, 2011.
[49] A.R. Massih, “Transformation kinetics of zirconium alloys under non-isothermal conditions”, Journal of Nuclear Materials, 384, 2009, pp. 330-335.
[50] C.-T. Nguyen, "Microstructure Changes during Fast β Cycles of Zirconium Alloys", PhD thesis, University of Manchester, UK, 2017.
[51] Accident Analysis for Nuclear Power Plants, INTERNATIONAL ATOMIC ENERGY AGENCY, Vienna, 2002.
[52] "Transients and Design Basis Accident Analyses", in: ETSON (Ed.), Technical Safety Assessment Guide, ETSON Secretariat - LEI, Kaunas, Lithuania, 2014, p. 18.
[53] K. Pettersson, H. Chung, M. Billone, T. Fuketa, C. Grandjean, G. Hache, L. Heins, Zoltan Hozer, J. In de Betou, S. Kelppe, Ralph Mayer, F. Nagase, J. Papin, H. Scott, H. Sonnenburg, S. Sunder, M. Valach, J. Voglewede, V. Vrtilkova, N. Waeckel, W. Wiesenack, M. Zimmermann, "Nuclear Fuel Behaviour in Loss-of-coolant Accident (LOCA) Conditions. State-of-the-art-report", in, OECD-NEA, Paris, France, 2009, p. 369.
[54] P. Van Uffelen, A. Schubert, Z. Soti, C. Gyori, S. Boneva, H. Hozer, L. Luzzi, P. Blair, M. Jonson, B. Hatala, J. Klouzal, M. Ieremenko, V. Peri, S. Bznuni, The application of the TRANSURANUS Fuel Performance Code to VVER fuel - An overview, in: 13th Int.Conf.on WWER Fuel Performance - Modelling and Experimental Support (INRNE, Nessebar, Bulgaria, 2019).
[55] Cs. Győri, Z. Hózer, K. Lassmann, A. Schubert, J. van de Laar, M. Cvan, B. Hatala, Extension of TRANSURANUS Code Applicability with Niobium Containing Cladding Models (EXTRA), in: EU Research in Reactor Safety, Conclusion Symposium on Shared-Cost and Concerted Actions (FISA-2003), Vol. EUR 21026 (EC, Luxembourg, 2003) 584.
[56] Cs. Győri, Z. Hózer, K. Lassmann, A. Schubert, J. van de Laar, B. Hatala, M. Cvan, "Extension of Transuranus code applicability with Niobium containing cladding models (EXTRA) ", in: Final EXTRA Project Report, EVOL-EXTRA-D5 / FIKS-CT2001-00173, 2004.
[57] P. Van Uffelen, Cs. Győri, A. Schubert, J. van de Laar, Z. Hozer, G. Spykman, Extending the application range of a fuel performance code from normal operating to design basis accident conditions, Journal of Nuclear Materials 383 (2008) 137.
[58] Cs. Győri, P. Van Uffelen, A. Schubert, J. van de Laar, E. Perez-Feró, E. Szabó, Z. Hózer, G. Spykman, "Model developments for the simulation of LOCA events by means of the TRANSURANUS Code ", Proceedings of 7th Int. Conf. on WWER Fuel Performance, Modelling and Experimental Support, Albena, Bulgaria, 17-21 September.

[59] C. Győri, H. Hozer, L. Matus, E. Perez-Fero, "Modelling of Hydrogen Absorption and Embrittlement of Zr1%Nb cladding under Postulated LOCA Conditions. ", in, Report for contract: 370037-2004-10 F1ED KAR HU, AEKI, 2007.
[60] G. Spykman, D. Maertens, Cladding behaviour in a LOCA fuel rod analysis with the transuranus TUEV LOCA extension, in: Enlarged Halden programme group meeting, Vol. HPR-364-V1 (Institutt for energiteknikk, OECD Halden Reactor Project, Lillehammer (Norway), 2005) 138.
[61] M. Seidl, L. Holt, P. Blair, A. Lindquist, "Realistic LB-LOCA core analysis with TRANSURANUS", D.A.e.V. KTG (Ed.), Proceedings of Annual meeting on nuclear technology 2010, Jahrestagung Kerntechnik 2010, Inforum Verlag, Germany, 4-6 May.
[62] B. Hatala, Evaluation of fuel rod cladding failure, in: Water Reactor Fuel Performance Meeting (JNS, Kyoto, Japan, 2005) 827.
[63] S. Stefanova, G. Passage, I. Mandev, M. Georgieva, A. Ivanova, K. Kamenov, "Additional computational analysis of the WWER-1000 fuel rod thermomechanical characteristics at DB LOCA with extended conservatism of the initial and boundary conditions", Proceedings of 10 International conference on WWER fuel performance, modelling and experimental support, Sandanski, Bulgaria, 8-14 September 2013.
[64] M. Adorni, A. Del Nevo, F. D'Auria, O. Mazzantini, A Procedure to Address the Fuel Rod Failures during LB-LOCA Transient in Atucha-2 NPP, Science and Technology of Nuclear Installations 2011 (2010) 11.
[65] Cs. Győri, "Westinghouse-specific material properties and models in the TRANSURANUS code", in: ESSANUF project, NucleoCon, 2016.
[66] C. Győri, M. Jonson, G. Robertson, P. Blair, A. Schubert, P. Van Uffelen, Extension and validation of the TRANSURANUS code in the course of the ESSANUF project (Paper 3.10), in: 12th International conference on WWER fuel performance, modelling and experimental support (INRNE, Nessebar, Bulgaria, 2017).
[67] O. Hyvönen, TRANSURANUS analyses in LOCA conditions and normal operation for the Loviisa NPP, in: JRC (Ed.), International Workshop “Towards nuclear fuel modelling in the various reactor types across Europe” (Karlsruhe, Germany, 2019).
[68] M. Seidl, L. Holt, P. Blair, A. Lindquist, "Cycle specific hot channel analysis with TRANSURANUS", D.A.e.V. KTG (Ed.), Proceedings of Annual meeting on nuclear technology 2010, Jahrestagung Kerntechnik 2010, Inforum Verlag, Germany, 4-6 May.
[69] M. García, R. Tuominen, A. Gommlich, D. Ferraro, V. Valtavirta, U. Imke, P. Van Uffelen, L. Mercatali, V. Sanchez-Espinoza, J. Leppänen, S. Kliem, A Serpent2-SUBCHANFLOW-TRANSURANUS coupling for pin-by-pin depletion calculations in Light Water Reactors, Annals of Nuclear Energy 139 (2020) 107213.
[70] J. Basualdo, V. H. Sanchez-Espinoza, Multi-physics Coupling of Neutronics/Thermo-hydraulic/Thermo-mechanics codes for improved LWR core simulation, in: Towards nuclear fuel modelling in the various reactor types across Europe (European Commission, JRC, Lappeenranta, Finland, 2017).
[71] Z. Soti, The new graphical interface for the uncertainty and sensitivity analysis, in: International Workshop “Towards Nuclear Fuel Modelling in the Various Reactor Types Across Europe” (JRC, online, 2021).
[72] Z. Soti, A. Schubert, P. Van Uffelen, Extending the application of TRANSURANUS to coupled code calculations and statistical analyses, in: TOPFUEL 2021 (ENS, Santander, Spain, 2021).
[73] U. Dackermann, Influence of Hydrogen on the Burst Behavior during Large Break Loss of Coolant Accidents of Zirconium Alloy Fuel Rod Claddings, Master thesis, Lehrstuhl für Nukleartechnik, Technische Universtät München, 2011.
[74] A. R. Massih, Transformation kinetics of zirconium alloys under non-isothermal conditions, Journal of Nuclear Materials 384 (2009) 330.
[75] G. Pastore, R. L. Williamson, R. J. Gardner, S. R. Novascone, J. B. Tompkins, K. A. Gamble, J. D. Hales, Analysis of fuel rod behavior during loss-of-coolant accidents using the BISON code: Cladding modeling developments and simulation of separate-effects experiments, Journal of Nuclear Materials 543 (2021) 152537.
[76] T. Forgeron, J. C. Brachet, F. Barcelo, A. Castaing, J. Hivroz, J. P. Mardon, C. Bernaudat, Experiment and Modelling of Advanced Fuel Rod Cladding Behaviour under LOCA Conditions: Alpha-Beta Phase

Transformation Kinetics and EDGAR Methodology, in: 12th. Int. Symposium: Zirconium in the Nuclear Industry, Vol. ASTM STP 1354 (American Society for Testing and Materials, Toronto, Canada, 1998) 256.
[77] U. Dackermann, M. Seidl, P. Blair, "Adaptation of TRANSURANUS for the description of the creep and burst behavior of hydrogen loaded Zr-4 cladding tubes", D.A.e.V. KTG (Ed.), Proceedings of Annual meeting on nuclear technology 2011, Jahrestagung Kerntechnik 2011, Inforum Verlag, Germany, May.
[78] R. Calabrese, A. Schubert, P. Van Uffelen, "Review of M5™ Cladding Models Relevant for LOCA Simulation with the TRANSURANUS Code", Proceedings of 30th International Conference Nuclear Energy for New Europe 2021, Bled, Slovenia, 6-9 September 2021.
[79] A. Kecek.: Summary report on VVER 1000 /V320 LOCA calculations, D 2.5 of the R2CA project
[80] TRANSURANUS: a fuel rod analysis code ready for use, Journal of Nuclear Materials 188 (1992) 295-302
[81] J. Klouzal, V. Matocha: Doplnění a změny modelů kódu TRANSURANUS pro provádění BHK a BA, rev 6, UJV Z-4652, 2022 (UJV internal report)
[82] T. Lötsch, V. Khalimonchuk, A. Kuchin: Proposal of a benchmark for core burnup calculations for a VVER-1000 reactor core, Proceedings of the 19th AER Symposium on VVER Reactor Physics and Reactor Safety, St. St. Constantine and Elena resort, Bulgaria, Sept. 21–25, 2009, p.53.
[83] Fuel Modelling in Accident Conditions (FUMAC). Final Report of a Coordinated Research Project. IAEA-TECDOC-1889. INTERNATIONAL ATOMIC ENERGY AGENCY. VIENNA, 2019. http://www-pub.iaea.org/MTCD/Publications/PDF/TE-1889web.pdf
[84] M.Ieremenko, I.Ovdiienko. QUALIFICATION OF TRANSURANUS MODELS FOR MIXED CORE FUEL BASED ON THE FUMAC OUTCOME. Proceedings of a technical meeting Modelling of Fuel Behaviour in Design Basis Accidents and Design Extension Conditions, IAEA-TECDOC-1913, pp. 50-58. https://www-pub.iaea.org/MTCD/Publications/PDF/TE-1913_web.pdf
[85] Fuel Modelling in Accident Conditions (FUMAC). Final Report of a Coordinated Research Project. IAEA-TECDOC-1889. INTERNATIONAL ATOMIC ENERGY AGENCY. VIENNA, 2019. http://www-pub.iaea.org/MTCD/Publications/PDF/TE-1889web.pdf
[86] M.Ieremenko, I.Ovdiienko. QUALIFICATION OF TRANSURANUS MODELS FOR MIXED CORE FUEL BASED ON THE FUMAC OUTCOME. Proceedings of a technical meeting Modelling of Fuel Behaviour in Design Basis Accidents and Design Extension Conditions, IAEA-TECDOC-1913, pp. 50-58. https://www-pub.iaea.org/MTCD/Publications/PDF/TE-1913_web.pdf
[87] Ghasabian, M., Mofidnakhaei, F. and Talebi, S.. "Effect of gap design pressure on the LWR fuel rods lifetime" Kerntechnik, vol. 86, no. 3, 2021, pp. 202-209. https://doi.org/10.1515/kern-2021-0004
[88] S. Belon, L. Carenini, P. Chatelard, O. Coindreau, V. Topin, “Draft Manual for ASTEC V2.1: ICARE Module”, IRSN report PSN-RES/SAG/2016-00421, 2016.
[89] O. Coindreau, “ASTEC V2.2: Physical modelling of the ICARE module”, IRSN report IRSN/2016-00422, 2020.
[90] D.A. Powers and R.O. Meyer, “Cladding swelling and rupture models for LOCA analysis”, Technical Report NUREG-630, IRSN, 1980.
[91] R.H. Chapman, “Multi-rod Burst Test”, Program Progress report April-June 1979 USNRC report – ORNL/NUREG/CR-1023, Oak Ridge National Laboratory, 1979.
[92] „TRANSURANUS HANDBOOK“ European Commission, Joint Research Centre, 2019 (V1M2J19).
[93] Keisuke OKUMURA, Kensuke KOJIMA, Tsutomu OKAMOTO, Hiroyuki HAGURA, Kenya SUYAM, “Nuclear Data for Severe Accident Analysis and Decommissioning of Nuclear Power Plant”, Proceedings of the 2012 Symposium on Nuclear Data, November 15-16, 2012, Research Reactor Institute, Kyoto University, Kumatori, Japan.
[94] Kaliatka T., Jusevičiūtė A., Uškuras E. Adaptation of FEMAXI-6 Code for Fuel Rods of RBMKk-1500 and Employment of Uncertainty and Sensitivity Analysis In: Proceedings of the 17th International Conference on Nuclear Engineering (ICONE17), July 12-16, 2009, Brussels, Belgium.
[95] Marao A., Kaliatka T., Kaliatka A., Uškuras E. Adaptation of the FEMAXI-6 code and RBMK fuel rods model testing employing the best estimate approach In: Kerntechnik. 2013, Vol. 75, Iss. 3, p. 72-80. ISSN 0932-3902.

[96] Kaliatka T., Kaliatka A., Vileiniškis V. Application of Best Estimate Approach for Modelling of QUENCH-03 and QUENCH-06 Experiments In: Nuclear Engineering and Technology, Elsevier, 2016, Vol. 48, p. 419-433. ISSN 1738-5733.

[97] Soti Z., Schubert A., Van Uffelen P., Uncertainty and sensitivity analysis of nuclear fuel performance during aLOCA test case on the basis of the TRANSURANUS code, ANS Best Estimate Plus Uncertainty International Conference (BEPU 2018), Real Collegio, Lucca, Italy, May 13-19, 2018.

[98] T. Glantz, T. Taurines, O. de Luze, S. Belon, G. Guillard, et al. - DRACCAR A multi-physics code for computational analysis of multi-rod ballooning and fuel relocation during LOCA transients Part one General modeling description. *Nuclear Engineering and Design*, Elsevier, 2018, 339, pp.269-285. ⟨10.1016/j.nucengdes.2018.06.022⟩. ⟨hal-02881798⟩

[99] P. Chatelard, N. Reinke, S. Arndt, S. Belon, L. Cantrel, L. Carenini, K. Chevalier-Jabet, F. Cousin, J. Eckel, F. Jacq, C. Marchetto, C. Mun, L. Piar - ASTEC V2 severe accident integral code main features, current V2.0

modelling status, perspectives, Nuclear Engineering and Design, Volume 272, 2014, Pages 119-135, https://doi.org/10.1016/j.nucengdes.2013.06.040

[100] K.J. Geelhood, W.G. Luscher, P.A. Raynaud, I.E. Porter - FRAPCON-4.0: A Computer Code for the Calculation of Steady-State, Thermal-Mechanical Behavior of Oxide Fuel Rods for High Burnup. (nrc.gov) , September 2015, Pacific Northwest National Laboratory – US NRC - PNNL-19418, Vol.1 Rev.2

[101] A. Magni, A. Del Nevo, L. Luzzi, D. Rozzia, M. Adorni, A. Schubert, P. Van Uffelen, Chapter 8 - The TRANSURANUS fuel performance code, Editor(s): Jun Wang, Xin Li, Chris Allison, Judy Hohorst, In Woodhead Publishing Series in Energy, Nuclear Power Plant Design and Analysis Codes, Woodhead Publishing, 2021, Pages 161-205, ISBN 9780128181904, https://doi.org/10.1016/B978-0-12-818190-4.00008-5

[102] W. Haeck, B. Dechenaux, 2017, VESTA User's Manual – Version 2.2.0, IRSN Report PSN-EXP/SNC/2017-00251, Google Scholar

[103] RSK, RSK guidelines for pressurized water reactors, 3rd edition of October 14th, 1981 with modifications. 1998.

[104] Reactor Safety Working Group and Nuclear Regulators Working Group, Fuel Cladding Failure Criteria, in Nuclear Safety and the Environment. 1999, European Commission.

[105] Pettersson, K., Chung, H., Billone, M., Fuketa, T., Nagase, F., Grandjean, C., Hache, G., Papin, J., Heins, L., and Hozer, Z., Nuclear Fuel Behaviour in Loss-of-coolant Accident (LOCA) Conditions. 2009, Organisation for Economic Co-Operation and Development.

[106] Heins, L., Core Damage Extent Analysis to Fulfill an Additional LOCA Criterion, in SEG FSM Topical Meeting on LOCA Issues. 2004: Argonne National Laboratory.

[107] Schöffel, P., Entwicklung eines ATHLET-internen 2D/3D-Moduls. 2011, Gesellschaft für Anlagen- und Reaktorsicherheit (GRS) mbH.

[108] Diaz-Pescador, E., Schafer, E., and Kliem, S., Thermal-hydraulic insights during a main steam line break in a generic PWR KONVOI reactor with ATHLET 3.1A. Kerntechnik, 2019. 84(5): p. 367-374.

[109] Diaz-Pescador, E., Schäfer, F., and Kliem, S. Multidimensional fluid mixing study during an asymmetric injection of cold water in the primary side of a generic PWR KONVOI with ATHLET 3.1 A. in 50th Annual Meeting on Nuclear Technology (AMNT). 2019. Berlin.

[110] Diaz-Pescador, E., Grahn, A., Kliem, S., Schafer, F., and Hohne, T., Advanced modelling of complex boron dilution transients in PWRs - Validation of ATHLET 3D-Module against the experiment ROCOM E2.3. Nuclear Engineering and Design, 2020. 367.

[111] Diaz-Pescador, E., Schafer, F., and Kliem, S., Modelling of multidimensional effects in thermal-hydraulic system codes under asymmetric flow conditions-Simulation of ROCOM tests 1.1 and 2.1 with ATHLET 3D-Module. Nuclear Engineering and Technology, 2021. 53(10): p. 3182-3195.
[112] Pandazis, P., Ceuca, S.C., Schöffel, P., and Hristov, H.V., Investigation of Multidimensional flow mixing phenomena in the reactor pressure vessel with the system code ATHLET, in Nureth-16. 2015. p. 3378-3391.
[113] Hristov, H.V., Numerical analyses of the ROCOM Tests 1.1 and 1.2 with 1D and 3D ATHLET models. 2012, Gesellschaft für Anlagen- und Reaktorsicherheit (GRS) mbH.
[114] Hristov, H.V., Numerical analyses of the ROCOM Test 1.3 with 1D and 3D ATHLET models. 2012, Gesellschaft für Anlagen- und Reaktorsicherheit (GRS) mbH.
[115] Ceuca, S.C. and Pandazis, P., Nachrechnung der ROCOM-Versuche 2.1 und 2.2 mit ATHLET unter Anwendung des 2D/3D-Moduls im Ringraum und unteren Plenum. 2015, Gesellschaft für Anlagen- und Reaktorsicherheit (GRS) mbH.
[116] Salah, A.B. and Vlassenbroeck, J., Assessment of the CATHARE 3D capabilities in predicting the temperature mixing under asymmetric buoyant driven flow conditions. Nuclear Engineering and Design, 2013. 265: p. 469-483.
[117] GRS, Generic PWR Input Deck for ATHLET 3.2, 3D-RPV with 8 sectors, 17 core channels. 2021, Gesellschaft fuer Anlagen-und Reaktorsicherheit (GRS) gGmbH.
[118] Diaz-Pescador, E., Thesis (On-going work). 2022.
[119] Jobst, M., LB-LOCA analysis of Konvoi PWR (DBA and DEC-A). Annex to Deliverable D2.5 of project "Reduction of Radiological Consequences of design basis and design extension Accidents". 2021, Helmholtz-Zentrum Dresden-Rossendorf.
[120] Wilhelm, P., Jobst, M., Kozmenkov, Y., Schafer, F., and Kliem, S., Severe accident management measures for a generic German PWR. Part I: Station blackout. Annals of Nuclear Energy, 2018. 122: p. 217-228.
[121] Jobst, M., Wilhelm, P., Kozmenkov, Y., and Kliem, S., Severe accident management measures for a generic German PWR. Part II: Small-break loss-of-coolant accident. Annals of Nuclear Energy, 2018. 122: p. 280-296.
[122] Tusheva, P., Schäfer, F., Kozmenkov, Y., Kliem, S., Hollands, T., Trometer, A., and Buck, M., WASA-BOSS: ATHLET-CD Model for Severe Accident Analysis for a Generic KONVOI Reactor. atw - International Journal for Nuclear Power, 2015. 60(7): p. 442–447.
[123] Jobst, M., Kliem, S., Kozmenkov, Y., and Wilhelm, P., Verbundprojekt WASA-BOSS: Weiterentwicklung und Anwendung von Severe Accident Codes – Bewertung und Optimierung von Störfallmaßnahmen; Teilprojekt B: Druckwasserreaktor-Störfallanalysen unter Verwendung des Severe-Accident-Code ATHLET-CD, in Wissenschaftlich-Technische Berichte. 2017, Helmholtz-Zentrum Dresden-Rossendorf (HZDR) e.V.
[124] Lovász, L., Bals, C., D'Alessandro, C., Hollands, T., Köllein, C., Austregesilo, H., Pandazis, P., Tiborcz, L., and Weber, S., ATHLET-CD Mod 3.3 Models and Methods. 2021, Gesellschaft für Anlagen- und Reaktorsicherheit (GRS) gGmbH.
[125] Lovasz, L., Simulation of asymmetric severe accidents using the code system AC2, in 49th Annual Meeting on Nuclear Technology. 2018: Berlin.
[126] Lovasz, L., Weber, S., and Koch, M.K., Comparison of a Hypothetical Strongly Asymmetrical Severe Accident Using the Standard and the New Nodalization Method with the Code System AC, in 27th International Conference Nucelar Energy for New Europe (NENE). 2018: Portoroz.
[127] Lovasz, L., Weber, S., and Koch, M.K., New Approach for Severe Accident Simulations in Spent Fuel Pools Using the Code System AC2, in 12th International Topical Meeting on Nuclear Reactor Thermal-Hydraulics, Operation and Safety (NUTHOS-12). 2018: Qingdao.

[128] Sun, K.H., Gonzalez-Santalo, J.M., and Tien, C.L., Calculations of Combined Radiation and Convection Heat-Transfer in Rod Bundles under Emergency Cooling Conditions. Journal of Heat Transfer-Transactions of the Asme, 1976. 98(3): p. 414-420.
[129] Wunderlich, F., Eberle, R., Gärtner, M., and Groß, H., Brennstäbe von Leichtwasserreaktoren. KTG-Seminar, ed. Kerntechnische Gesellschaft e.V. 1990, Köln: Verlag TÜV Rheinland.
[130] Erbacher, F.J., Neitzel, H.J., Rosinger, H.E., Schmidt, H., and Wiehr, K., Burst criterion of Zircaloy Fuel Claddings in a Loss-of-Coolant Accident, in Zirconium in the Nuclear Industry; Fifth Conference, ASTM STP 754, D.G. Franklin, Editor. 1982, American Society for Testing and Materials. p. 271-283.
[131] Rill, G., Technische Mechanik II, Lecture notes, O.T.H. Regensburg, Editor. 2017.
[132] Rosinger, H.E., Bera, P.C., and Clendening, W.R., Steady-State Creep of Zircaloy-4 Fuel Cladding from 940-K to 1873-K. Journal of Nuclear Materials, 1979. 82(2): p. 286-297.
[133] Burton, B., Donaldson, A.T., and Reynolds, G.L., Interaction of oxidation and creep in Zircaloy-2, in Zirconium in the Nuclear Industry. Proceedings of the 4th International Conference. 1978, ASTM International.
[134] Lovasz, L., Austregesilo, H., Bals, C., Hollands, T., Köllein, C., Luther, W., Pandazis, P., Schubert, J.D., Tiborcz, L., Weber, S., and Wielenberg, A., ATHLET-CD 3.3 User's Manual. 2021, Ges. für Anlagen- und Reaktorsicherheit (GRS).
[135] Schatz, A. and Hocke, K.D., Kess - a Modular Program System to Simulate and Analyze Core Melt Accidents in Light-Water Reactors. Nuclear Engineering and Design, 1995. 157(1-2): p. 269-280.
[136] Chapman, R.H., Multirod burst test program. Progress report April-June 1979. 1979, Oak Ridge National Laboratory (ORNL).
[137] Rashid, Y.R., Transient Failure of Zircaloy Cladding. Nuclear Engineering and Design, 1987. 101(3): p. 305-313.
[138] Hohorst, J.K., Buccafurni, A., Carlson, E.R., Chambers, R., and Chmielewski, S.V., SCDAP/RELAP/MOD2 Code Manual Volume 4, MATPRO: A Library of Materials Properties for Light-Water-Reactor Accident Analysis. 1990, Idaho National Engineering and Environmental Laboratory (INL).
[139] Siefken, L.J., Coryell, E.W., Harvego, E.A., and Hohorst, J.K., SCDAP/RELAP5/MOD 3.3 code manual: MATPRO–a library of materials properties for light-water-reactor accident analysis. 2001, Idaho National Engineering and Environmental Laboratory.
[140] RSK, RSK-Empfehlung, Anforderungen an die Nachweisführung bei Kühlmittelverluststörfall-Analysen. 2005.
[141] Pointer, W., Berner, N., Kloos, M., and Wenzel, S., Statistische LOCA-Analysen. 2018, Gesellschaft für Anlagen- und Reaktorsicherheit (GRS) gGmbH.
[142] Hesse, U., Denk, W., and Deitenbeck, H., OREST - Eine direkte Kopplung von HAMMER und ORIGEN zur Abbrandsimulation von LWR- Brennstoffen. 1986.
[143] Hesse, U., FIPISO-98, ein Rechenmodell zum Nuklidverhalten in einem Raumzellensystem nach einem Reaktorstörfall. 1998, Gesellschaft für Anlagen- und Reaktorsicherheit (GRS) mbH.
[144] Kosowski, K. and Seidl, M., External Hazard Coinciding with Small Break Loca Thermohydraulic Calculation with System Code Athlet. Proceedings of the 26th International Conference on Nuclear Engineering, 2018, Vol 6b, 2018.
[145] Kozmenkov, Y., Jobst, M., Kliem, S., Kosowski, K., Schaefer, F., and Wilhelm, P., The efficiency of sequential accident management measures for a German PWR under prolonged SBO conditions. Nuclear Engineering and Design, 2020. 363.
[146] Wang, M.J. and Mayinger, F., Simulation and Analysis of Thermal-Hydraulic Phenomena in a PWR Hot Leg Related to SBLOCA. Nuclear Engineering and Design, 1995. 155(3): p. 643-652.

[147] Deendarlianto, Hohne, T., Lucas, D., and Vierow, K., Gas-liquid countercurrent two-phase flow in a PWR hot leg: A comprehensive research review. Nuclear Engineering and Design, 2012. 243: p. 214-233.
[148] Austregesilo, H., Lee, J., Schöffel, P., Skorek, T., von der Cron, D., Weyermann, F., and Wong, K.W., ATHLET 3.3 Models and Methods. 2021, Gesellschaft fuer Anlagen-und Reaktorsicherheit (GRS) gGmbH.
[149] E.ON, Kernkraftwerk Isar 2. Abschlussbericht für den Europäischen Stresstest. 2011.
[150] EnBW Kernkraft GmbH, Sicherheitsüberprüfung europäischer Kernkraftwerke vor dem Hintergrund des schweren Erdbebens und Tsunamis in Japan am 11. März 2011: Standortbericht des Betreibers für den Standort Neckarwestheim [GKN] - Abschlussbericht. 2011.
[151] von Linden, J., Löffler, H., Müller-Ecker, D., Verstegen, C., and Köberlein, K., Bewertung des Unfallrisikos fortschrittlicher Druckwasserreaktoren in Deutschland - Methoden und Ergebnisse einer umfassenden Probabilistischen Sicherheitsanalyse (PSA). 2001, Gesellschaft für Anlagen- und Reaktorsicherheit (GRS) gGmbH.

Appendixes

1. VTT contribution appendixes

Appendix A Validation cases results:

Table 54 Validation cases results with FRAPTRAN original plastic deformation model

	FRAPTRAN original plastic strain results					
Burst criterion / Test	**FRAPTRAN original burst criteria (stress +strain)**	**IRSN BE**	**IRSN min**	**IRSN max**	**T limit**	**Measured value**
IFA 650.5						
Time (s)	**169**	**168**	**155**	**169**	**166**	**179**
Temperature (K)	1005	1001	954	1005	994	1023
Max strain (%)	30	23.00	5.00	32.00	11.00	16.00
Pressure (Mpa)	10.2	10.60	10.60	10.20	10.80	
IFA 650.6						
Time (s)	**423**	**419**	**359**	**425**	**419**	**525**
Temperature (K)	1069	1067	1020	1071	1067	1103
Max strain (%)	38.0	29.0	5.0	40.0	29.0	36.0
Pressure (Mpa)	8.3	8.60	8.40	8.30	8.60	
IFA 650.7						
Time (s)	**152**	**152**	**145**	**152**	**152**	**247**
Temperature (K)	1221	1221.0	1197.2	1221.0	1221.0	1373
Max strain (%)	36.0	35.7	5.0	35.7	36.0	24.0
Pressure (Mpa)	1.98		2.10		1.98	
Treat rod 16 and 17						
Time (s)	**26.4**	**26.4**	**26.3**	**26.4**	**26.5**	**30.3–37.5**
Temperature (K)	1263.5	1263.5	1263.5	1263.5	1260.8	1533.5
Max strain (%)	68.6	117.0	9.6	248.0	248.0	58 and 33
Pressure (Mpa)	0.97	1.0	1.0	1.0	1.0	
LOC-11C rod 3	No Failure	No Failure	No Failure	No Failure	No failure	No Failure
Max strain (%)	13.7	13.7	13.7	13.7	13.7	1.6
LOC-11C rod 2						
Time (s)	14.4	14.4	10.8	14.4	14.4	No Failure
Temperature (K)	1017.7	1017.7	973.4	1017.7	1017.7	
Max strain (%)	90.4	38.2	5.0	1954.0	1960.9	2.5
Pressure (MPa)	8.4	8.40	11.30	8.40	8.40	

LOC-11C rod 1 and 4	No Failure	No Failure	No Failure	No Failure	No failure	No Failure
Max strain (%)	0.02	0.02	0.02	0.02	0.02	-0.96 and -0.84
IFA 650.15						
Time (s)	**191**	**188**	**166**	**191**	**189**	**245**
Temperature (K)	1021.7	1015.5	970.57	1021.7	1017.6	1073.2
Max strain %	69.83	24.35	5.00	69.83	29.05	50

Table 55 Validation cases results with Kaddour et al. 2004 high temperature creep deformation

	Kaddour et al. 2004 results					
Burst criterion / Test	**FRAPTRAN original (stress +strain)**	**IRSN BE**	**IRSN min**	**IRSN max**	**T limit**	**Measured value**
IFA 650.5						
Time (s)	**184**	**182**	**155**	**184**	**167**	**179**
Temperature (K)	1054.0	1047.4	953.7	1054.0	997.7	1023
Max strain (%)	31.46	23.01	5.01	31.46	6.09	16
IFA 650.6						
Time (s)	**453**	**453**	**359**	**454**	**431**	**525**
Temperature (K)	1086.5	1086.5	1020.0	1087.3	1074.4	1103
Max strain (%)	32.47	31.70	5.00	39.53	15.62	36
IFA 650.7						
Time (s)	**152**	**151**	**145**	**152**	**152**	**247**
Temperature (K)	1221.0	1216.7	1197.2	1221.0	1221.0	1373
Max strain (%)	35.44	35.44	5.00	35.44	35.44	24
Treat rod 16 and 17						
Time (s)	**28.50**	**28.50**	**27.00**	**28.50**	**28.50**	**30.3–37.5**
Temperature (K)	1348	1348	1285.1	1348	1348	1534
Max strain (%)	95.63	70.82	5.57	156.64	95.63	58 and 33
Pressure						
LOC-11C rod 3	No failure	No failure	No failure	No failure	No Failure	No Failure
Max strain (%)	5.66	5.66	5.66	5.66	5.66	1.6
LOC-11C rod 2						
Time (s)	No failure	No failure	**10.8**	No failure	No failure	No Failure
Temperature (K)			973.44			
Max strain (%)	25.16	25.16	5.00	25.16	25.16	2.5
LOC-11C rod 1 and 4	No failure	No failure	No failure	No failure	No failure	No Failure
Max strain %	0.02	0.02	0.02	0.02	0.02	-0.96 and -0.84
IFA 650.15						
Time (s)	**222**	**209**	**166**	**222**	**201**	**245**
Temperature (K)	1054.3	1040.9	970.6	1054.3	1033.2	1073.15
Max strain (%)	82.19	22.26	5.00	83.60	15.31	50

Table 56 Validation cases results with Rosinger 1984 high temperature creep deformation

	Rosinger 1984 results						
Burst criterion / Test	**FRAPTRAN original (stress +strain)**	**IRSN BE**	**IRSN min**	**IRSN max**	**Rosinger BE SSM 2021**	**T limit**	**Measured value**
IFA 650.5							
Time (s)	**220**	**192**	**155**	**220**	**203**	**167**	**179**
Temperature (K)	1153.7	1077.7	953.7	1153.7	1110.0	997.7	1023
Max strain (%)	31.50	5.27	5.01	31.50	6.61	5.10	16.00
IFA 650.6	N/A	N/A	N/A	N/A	N/A	N/A	N/A
IFA 650.7							
Time (s)	**257**	**234**	**145**	**256**	**175**	**160**	**247**
Temperature (K)	1509.8	1368.8	1197.2	856.8	1299.0	1248.2	1373
Max strain (%)	9.18	7.52	5.00	9.05	5.51	5.34	24.00
Treat rod 16 and 17							
Time (s)	No failure	**32.50**	**27.00**	**34.50**	No failure	**30.00**	**30.3–37.5**
Temperature (K)		1516.6	1285.1	1600.4		1411.6	1533.5
Max strain (%)		5.94	5.29	5.35		5.32	-0.96 and -0.84
LOC-11C rod 3	No failure	No failure	No failure	No failure	No failure	No Failure	No Failure
Max strain (%)	5.52	5.52	5.52	5.52	5.52	5.52	1.6
LOC-11C rod 2							
Time	No failure	No failure	**10.8**	No failure	No failure	**15.1**	No Failure
Temperature			973.44			1025.3	
Max strain %	5.5	5.5	5.0	5.5	5.5	5.5	2.5
LOC-11C rod 1 and 4	No failure	No failure	No failure	No failure	No failure	No failure	No Failure
Max strain %	0.02	0.02	0.02	0.02	0.02	0.02	-0.9

Appendix B Error calculations

Absolute mean error for the creep model:

First, the average error for each test is calculated separately:

- For the burst time and burst temperature, the mean error is given with

$$\text{Test ME} = \frac{1}{n}\sum_{i=1}^{n}\left|\frac{x_i - \boldsymbol{x_{experiment}}}{\boldsymbol{x_{experiment}}}\right|$$

x is the considered parameter, i denotes the burst criterion used and n is the number of burst criteria used with each validation test.

- For the strain value, since it is already a percentage, the average error is calculated as follow:

$$\text{Test ME} = \frac{1}{n}\sum_{i=1}^{n}\left|x_i - \boldsymbol{x_{experiment}}\right|$$

Once the absolute mean error for each test is obtained, then the overall average error of the plastic deformation model used, is calculated by taking the global average of each parameter (time, temperature and strain) considering all tests:

$$\text{Creep model ME} = \frac{1}{m}\sum_{j=1}^{m}\left|Test\ ME_j\right|$$

Where j denotes the validation case test and m is the total number of validation cases calculated.

Absolute mean error for the burst criterion:

The absolute mean error for each burst criterion is calculated with a more straightforward approach

For the burst time and burst temperature, the average error is

$$\text{Burst criterion ME} = \frac{1}{n}\sum_{i=1}^{n}\left|\frac{x_i - \boldsymbol{x_{experiment}}}{\boldsymbol{x_{experiment}}}\right|$$

i in this case denotes the number of calculations using the same burst criterion across all creep models and n is the number

For the strain value, since it is already a percentage, the average error is calculated as follow:

$$\text{Burst criterion ME} = \frac{1}{n}\sum_{i=1}^{n}\left|x_i - \boldsymbol{x_{experiment}}\right|$$

Table 57 Absolute mean error of employed high temperature creep deformation model

	Absolute mean error		
Ballooning deformation / Parameter	**FRAPTRAN original model**	**Kaddour et al. 2004**	**Rosinger et al. 1984**
Burst time	23.07 %	19.25 %	12.18 %
Burst temperature	8.41 %	6.96 %	6.92 %
Max strain	27.81 %	18.86 %	6.21 %

Table 58 Absolute mean error of employed burst criterion

	Absolute mean error				
Burst criterion / Parameter	**FRAPTRAN original (stress +strain)**	**IRSN BE**	**IRSN min**	**IRSN max**	**Temperature limit (Meyer & Wiesenack 2022)**
Burst Time	16.53 %	15.12 %	25.35 %	15.41 %	18.64 %
Burst Temperature	6.96 %	5.47 %	10.21 %	6.61 %	4.00 %
Max Strain	17.83 %	20.42 %	27.54 %	38.45 %	18.13 %

Appendix C Code modifications

Input instructions for modified high temperature creep model and burst criteria:
Three different input variables have been introduced in the modified FRAPTRAN 1.4 version. These NAMELIST variables should be specified in the input file within the ***$model*** data block to select the relevant model or criteria. Default values can be changed in the *modinp.f* source code file.

Variable	Description	Default
bcrtr	Option to select the burst criterion limit to predict failure `bcrtr = 1 FRAPTRAN original stress limit criterion` `bcrtr = 2 IRSN Best Estimate stress correlation` `bcrtr = 3 IRSN minimum stress limit correlation` `bcrtr = 4 IRSN max correlation for stress limit` `bcrtr = 5 Rosinger BE SSM 2021 correlation Zy-4` `bcrtr = 6 Forgeron et al. SSM 2015 correlation M5` `bcrtr = 7 Temperature limit`	*bcrtr = 1*
crpmod	Option to determine which plastic deformation model to be used in the BALON2 `crpmod = 1 Kaddour et al 2004 creep model` `crpmod = 2 Rosinger 1984 creep model` `crpmod = 3 FRAPTRAN original plastic strain model`	*crpmod= 1*
brstrn	Option to disable the strain limit `brstrn = 0 disable the strain limit` `brstrn > 0 enter a value to enable the strain limit` `e.g brstrn = 1`	*brstrn =1*

Appendix D: IFA-650.15 rod pressure results

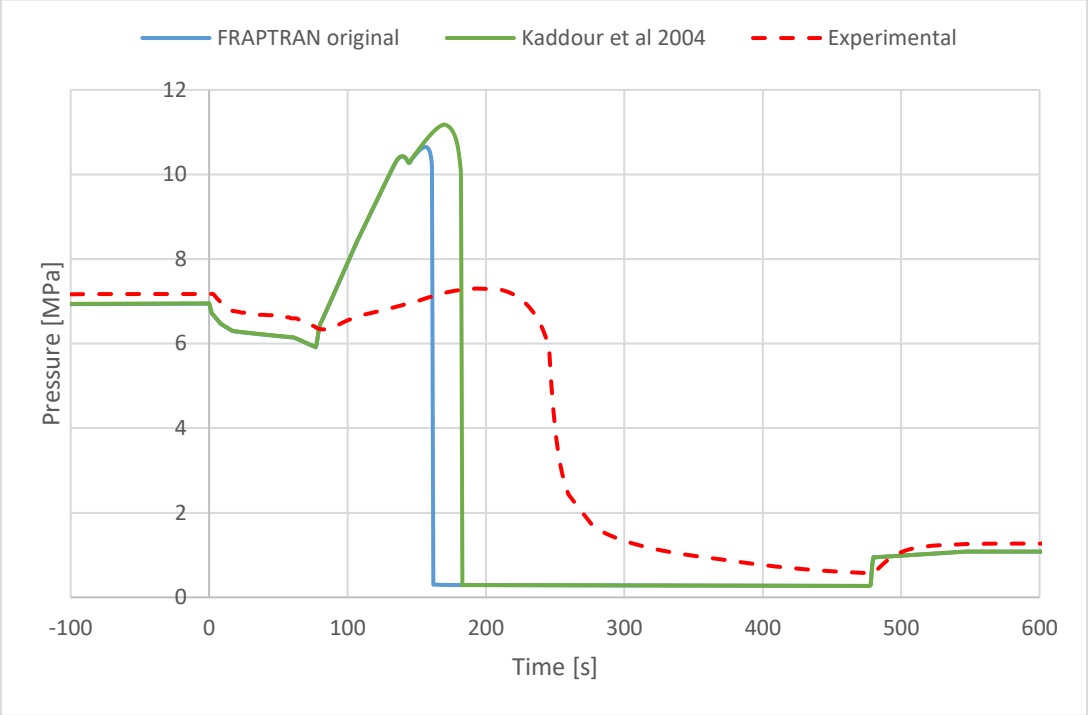

Figure D.1 FRAPTRAN predicted and measured rod internal pressure for IFA-650.15

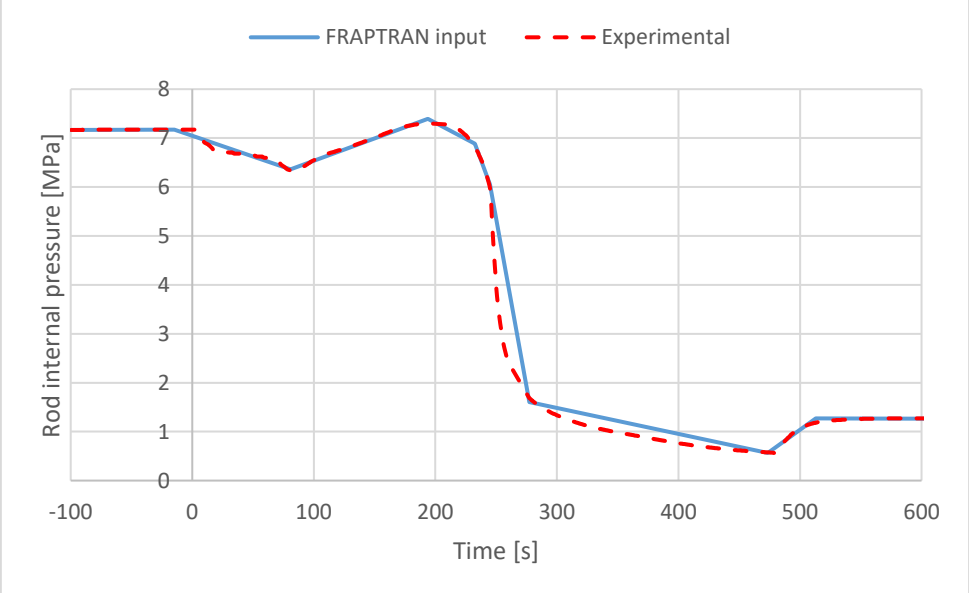

Figure D.2 FRAPTRAN input and measured rod internal pressure for IFA-650.15

2. SSTC codes used for full core modelling and developments

HELIOS

HELIOS-2 ([1], [2], [3]) is a generalized-geometry lattice physics code capable of analyzing nuclear fuel designs for hexagonal VVER reactors, non-LWR lattices (CANDU, PHWR, Magnox, RBMK), and for experimental reactor designs (like MTR and TRIGA).
The new Method of Characteristics solver allows larger models to be calculated with speed and accuracy.
High-resolution, 177-group neutron library for enhanced accuracy and resonance treatments.
HELIOS-2 includes an interactive geometry rendering module to ensure your model is built correctly.
HELIOS-2 includes an all-new Method of Characteristics solver, which allows larger models, such as multiple fuel bundles and fractional cores, to be calculated with fewer required computing resources. The same robust calculation method that powers CASMO is now native to HELIOS-2, providing increased speed and accuracy for solutions to even the most complicated geometric problems.
Users have the option to use the traditional collision probabilities solver for transport calculations when appropriate for the problem being solved. Resonance self-shielding is calculated via the subgroup method with a transport-based Dancoff calculation. The predictor-corrector method is used for depletion, and the depletion path allows arbitrary state changes, generalized decay capabilities, and branch-off calculations at any point in the solution path.
HELIOS-2 has been extensively validated against measured critical experiments, continuous-energy Monte Carlo calculations, and international isotopic benchmarks - delivering exceptional accuracy for traditional, non-traditional, and experimental fuel designs.
Lattice physics calculations are only as good as the underlying cross-section data, and HELIOS-2 has been updated with the latest available neutron and gamma data, fine-tuned to provide the most accurate solutions possible. Using the most recent ENDF/B-VII nuclear data available, Studsvik has developed a high-resolution, 177-group neutron library for use with HELIOS-2.
This extensive update from the previous HELIOS library improves accuracy and enhances resonance treatments.
HELIOS-2 also includes an updated 48-group gamma library for gamma transport and smearing calculations.
Cross-section data is available for over 350 nuclides and materials, including more than 175 fission products, 40 heavy nuclides, and expanded depletion chains.
HELIOS-2 is built on a centralized database system with advanced input and output processors. A flexible graphical geometry display assists in developing input for even the most complicated fuel designs. Users can view geometry, material, temperature assignments, and edit areas of both the full problem and individual structures before beginning the calculationsto be sure the model is correct.
The HELIOS-2 input processor allows datasets to be stored in the database and be accessed in the main input - allowing fixed or common data to be centrally available and accessible without the need to re-enter input data.
HELIOS-2 allows the stacking of multiple cases in a single input, which can be simultaneously analyzed and compared. With appropriate input, calculations can be stopped and restarted, allowing the user to perform mid-calculation geometry alteration.
The output processing module allows manipulation of flux, reaction rate, current edits, B1 calculations for subsets of the defined calculation geometry, and comparison of results from multiple calculation paths. Data may be displayed in tables or two-dimensional data maps; options also exist to write data to the database or to formatted external text files. HELIOS-2 can even create “data banks”• of previously burned fuel bundles for spent fuel pool analysis, shuffling and core management, or reinsertion into the core.

DYN3D

DYN3D is developed for investigations of transients in cores of thermal power reactors with hexagonal or quadratic fuel elements [4],[5], [6], [7], [8], [9].

The 3-dimensional neutron kinetics models of the code are based on a nodal expansion method for solving the two-group neutron diffusion equation in hex-z or rectangular x,y,z- geometry. This code was extended to an arbitrary number of energy groups recently. Further, a simplified transport (SP3) approximation for the flux calculation was implemented for fuel assemblies with the quadratic cross-section [10]. At present, the multi-group and the SP3- version are part of a special DYN3D-version. It is foreseen to combine both versions shortly.
The thermal-hydraulic part consists of a two-phase flow model describing coolant behavior and a fuel rod model. The fuel elements are simulated by separate coolant channels. Additionally, some hot channels with power peaking factors belonging to chosen fuel elements can be considered. Several safety parameters, such as temperatures, DNBR and fuel enthalpy are evaluated. The stationary state and transient behavior can be analyzed. Different libraries of macroscopic cross sections are linked to the code to meet the conditions of the different users several. DYN3D was validated by numerous benchmarks and experiments for thermal reactors with hexagonal and quadratic fuel assemblies. The kinetic benchmarks defined by the Working Group D "VVER Safety Analysis" of Atomic Energy Research (AER) were calculated for reactors with hexagonal fuel elements.

This code was verified using the NEACRP Benchmarks on control rod ejections in PWRs and the NEA-NSC Benchmarks on withdrawal of control rods at hot zero power for quadratic fuel assemblies.
The code has been coupled with the thermal-hydraulic plant model ATHLET developed by GRS [11]. The coupled code was validated with the help of the AER benchmark for a main steam line break (MSLB) in a VVER-440 (hexagonal) and the OECB-MSLB benchmark for the TMI-1 reactor, which is a western type pressurized water reactor (PWR) with quadratic fuel assemblies. The boiling water reactor (BWR) turbine trip (TT) benchmark organized by the OECD and the American Nuclear Regulatory Commission (NRC) is based on the turbine trip test 2 of the BWR Peach Bottom 2. The experimental results and the results of the other participants at the benchmark were used for validation of DYN3D and the coupled version DYN3D/ATHLET. Concerning VVER reactors DYN3D and DYN3D coupled with system codes have been validated in the frame of the project VALCO of the European Union with the help of measured data at the nuclear power plant Bohunice (VVER-440) in the Slovak Republic and the VVER-1000 power plant Kosloduj (Bulgaria). The measurements at the W1000 test facility of the Russian Research Center “Kurtchatov Institute” have been used for the validation of the neutron kinetics of DYN3D.

RELAP

The RELAP5 code [12], [13], [14] was developed at Idaho National Engineering Laboratory for the US Nuclear Regulatory Commission for the best-estimate simulation of light water reactor coolant systems during postulated transients and accidents without severe nuclear fuel damage. The RELAP5/MOD3.3 code is based on a nonhomogeneous and non-equilibrium model for the two-phase system that is solved by a fast, partially implicit numerical scheme.
The modelled system is simulated by a user with a set of one-dimensional control volumes that are connected with junctions. The code provides a variety of other components (pumps, valves, pipes, accumulators, heat structures, reactor point kinetics, etc.) that can be used. Complex geometries can be represented (in a simplified manner) by parallel 1-D channels that may be connected with cross-connections.
The code consists of several modules including time step control, the modules for calculating hydrodynamics, heat transfer, reactor kinetics, trip state, control variables, and state of the fluid in time-dependent volumes.
The thermal-hydraulic model of the code solves eight field equations (two phasic continuity, two phasic momentum, and two phasic energy equations, non-condensable and boron mass conservation equations) for eight variables: pressure, phasic specific internal energies, vapour volume fraction (void fraction), phasic velocities, non-condensable quality, and boron density. The constitutive relations include models for defining flow regimes and flow-regime-related models for interphase drag and shear, the coefficient of virtual mass, wall friction, wall heat transfer, interphase heat and mass transfer, and direct (sensible) heat transfer.

Four flow regime maps are implemented in the code: a horizontal map for flow in pipes; a vertical map for flow in pipes, annuli, and bundles; a high mixing map for flow in pumps; and an ECC mixer map for flow in the horizontal pipe near the ECC injection port.
A boiling curve is used in RELAP5 to govern the selection of the wall heat transfer correlations when the wall surface temperature is above the saturation temperature. These correlations are based mainly on internal flow in pipes. Additional geometries considered in the logic are vertical parallel plates, vertical and horizontal tube bundles, and horizontal flat plates. A table lookup method is used for predicting the critical heat flux developed by Groeneveld, Cheng, and Doan. Heat structures provided in RELAP5 permit the calculation of the heat transferred across solid boundaries of hydrodynamic volumes. Heat structures are assumed to be represented by one-dimensional heat conduction in rectangular, cylindrical, or spherical geometry. Surface multipliers are used to convert the unit surface of the one-dimensional calculation to the actual surface of the heat structure. Temperature-dependent thermal conductivities and volumetric heat capacities are provided in the tabular or functional form either from built-in or user-supplied data.
In the reflood model, a two-dimensional conduction scheme for cylindrical or rectangular heat structures is used. At the initiation of this model, each heat structure is subdivided into two axial intervals. Thereafter, the number of axial intervals is controlled by the code to efficiently use the two-dimensional conduction solution.
The dynamic gap conductance model is implemented in RELAP5 based on a simplified deformation model to define effective gas gap conductivity. The model allows to account for thermal expansion of fuel pellet and cladding, radial fuel swelling and cladding creep, and cladding elastic deformation. The latter depends on a difference between coolant pressure and internal gas pressure in the gap, which is calculated with an ideal gas approximation. The gas composition and radial displacement values for fuel swelling and cladding creep shall be provided via user input. Material thermal expansion and elastic deformation are calculated from correspondent UO_2 and zircaloy data defined within the code.
Cladding oxidation in steam is calculated using the Cathcart-Pawel correlation, and the reaction heat is added to the total heat source term for the heat structure. The metal-water reaction model is coupled with the fuel rod deformation model so that if the rod ruptures, then the inside of the cladding can react. The model doesn't account for potential steam starvation and doesn't alter the thermal-physical properties of the cladding as the oxide layers develop. Although the model calculates the amount of hydrogen generated, this hydrogen does not get included in the RELAP5 hydraulic equations, nor does the steam being consumed by the metal-water reaction get withdrawn from the hydraulic equations.
To account for the plastic deformation of the cladding in the calculation of fuel rod's cladding temperature during LOCA simulations an empirical cladding deformation model has been incorporated into RELAP5. The model may be invoked only in conjunction with the dynamic gap conductance model.
The logical statements can be defined by the user, and are evaluated in RELAP5 by the trip system. The control systems typically used in hydrodynamic systems are simulated by various control system components implemented in the code, such as arithmetic, integration and differentiation control components, and others.
The power behaviour in a nuclear reactor is calculated using the point reactor kinetics model that accounts an immediate fission power and the power from the decay of fission products. The user can select the decay power model based on either the American Nuclear Society Proposed Standard ANS 5.1, Decay Energy Release Rates Following Shutdown of Uranium-Fueled Thermal Reactors, revised October 1973, or the American National Standard for Decay Heat Power in Light Water Reactors, ANSI/ANS-5.1-1979.

TRANSURANUS

TRANSURANUS is a computer programme written in FORTRAN95 for the thermal and mechanical analysis of fuel rods in nuclear reactors that is owned by the Joint Research Centre of the European Commission. TRANSURANUS has been used by research centers, nuclear safety authorities, universities and industrial partners (see Refs [15]-[29]).

TRANSURANUS is generally referred to as a fuel performance code meaning that it solves the equations for the radial heat transfer, the radial displacement along with the stress distribution in both the fuel and its surrounding cladding, and the release of fission product and its behaviour as a function of time. In general, the equations, for fuel performance prediction, embody the following phenomena:

- thermal performance: heat conduction, radiation and convection;
- mechanical performance: creeps (radiation and high temperature), densification, thermal expansion, pellet cracking and relocation, solid and gaseous swelling;
- actinide behaviour: depletion and build-up of main Th, U, Np, Pu, Am and Cm nuclides, impact on the radial power profile;
- fuel restructuring: Pu and Am redistribution, grain growth (normal and columnar), central void formation;
- fission product behaviour: creation in the fuel matrix, diffusion to grain boundaries, release to free rod volume after saturation of grain boundaries, a thermal release, recoil, formation of High Burnup Structure (HBS, which is depleted and contains porosity).

The heat transfer in the fuel-to-cladding gap is simulated by means of a combination of heat conduction, radiation and convection (URGAP model [30]). Main assumptions and equations for mechanical performance are provided in Ref. [16].
Main assumptions and equations for actinide concentrations can be found in Refs [28], [29].
In the TUBRNP model the calculation of the radial power profiles is split into (a) the approximation of the neutron flux through thermal diffusion theory, and (b) the computation of the local concentrations of the relevant actinide isotopes with simplified depletion equations. The most recent extension covers the nuclides 232Th, 233-236,238U, 237Np, 238–242Pu, 241Am, 243Am, 242–245Cm. More details are given in Ref [31].
The TRANSURANUS code consists of a well-defined mechanical and mathematical framework, which additional physical models can easily be incorporated. The code has comprehensive material data files for oxide, mixed oxide, carbide, nitride fuel types, Zircaloy and steel claddings and several different coolants (water, sodium, potassium, lead, bismuth). TRANSURANUS can be used as a single code system for simulating both long-term irradiations under normal operating conditions as well as transient tests. The 'restart' mode allows simulating re-fabricated (recycled) fuel rods, where the fill gas has been completely changed as an example.
The code can be employed in two different approaches: as a deterministic or a statistical code. The restart may be used to perform a statistical analysis employing the Monte Carlo technique. This option may be helpful for the analysis of long base irradiation, then followed by a transient.
Besides its flexibility for fuel rod design, the TRANSURANUS code can deal with a wide range of different situations, as demonstrated in experiments, under normal, off-normal and accident conditions, although some models specific to RIA (e.g. plenum temperature) are still under development. Furthermore, the code is being used for BWRs, PWRs, and VVERs. The time scale of the problems to be treated may range from milliseconds to years. Hence complex irradiation experiments can be simulated including re-fabricated instrumented fuel rods and changing operating conditions.

SCALE

The SCALE Code System ([32], [33]) is a widely-used modelling and simulation suite for nuclear safety analysis and design that is developed, maintained, tested, and managed by the Reactor and Nuclear Systems Division (RNSD) of Oak Ridge National Laboratory (ORNL). SCALE provides a comprehensive, verified and validated, a user-friendly toolset for criticality safety, reactor and lattice physics, radiation shielding, spent fuel and radioactive source term characterization, and sensitivity and uncertainty analysis. Regulators, licensees, and research institutions around the world have used SCALE for safety analysis and design since 1980. SCALE provides an integrated framework with dozens of computational modules, including three deterministic and three Monte Carlo radiation transport solvers that are selected based on the desired solution strategy. SCALE includes current nuclear data libraries and problem-dependent processing tools for continuous-energy (CE) and multigroup (MG) neutronics, and coupled neutron-gamma calculations, as well as activation, depletion, and decay calculations.

SCALE includes unique capabilities for automated variance reduction for shielding calculations, as well as sensitivity and uncertainty analysis. SCALE's graphical user interfaces assist with accurate system modelling, visualization of nuclear data, and convenient access to desired results.
SCALE 6.2 provides many new capabilities and significant improvements of existing features.
New capabilities include:

- ENDF/B-VII.1 nuclear data libraries CE and MG with enhanced group structures;
- neutron covariance data based on ENDF/B-VII.1 and supplemented with ORNL data,
- covariance data for fission product yields and decay constants;
- stochastic uncertainty and correlation quantification for any SCALE sequence with Sampler;
- parallel calculations with KENO;
- problem-dependent temperature corrections for CE calculations;
- CE shielding and criticality accident alarm system analysis with MAVRIC;
- CE depletion with TRITON (T5-DEPL/T6-DEPL);
- CE sensitivity/uncertainty analysis with TSUNAMI-3D;
- simplified and efficient LWR lattice physics with Polaris;
- large scale detailed spent fuel characterization with ORIGAMI and ORIGAMI Automator;
- advanced fission source convergence acceleration capabilities with Sourcerer;
- nuclear data library generation with AMPX;
- integrated user interface with Fulcrum.

Enhanced capabilities include:

- accurate and efficient CE Monte Carlo methods for eigenvalue and fixed source calculations;
- improved MG resonance self-shielding methodologies and data;
- resonance self-shielding with modernized and efficient XSProc integrated into most sequences;
- accelerated calculations with TRITON/NEWT (generally 4x faster than SCALE 6.1);
- spent fuel characterization with 1470 new reactor-specific libraries for ORIGEN;
- modernization of ORIGEN (Chebyshev Rational Approximation Method [CRAM] solver, API for high-performance depletion, new keyword input format);
- extension of the maximum mixture number to values well beyond the previous limit of 2147 to ~2 billion;
- nuclear data formats enabling the use of more than 999 energy groups;
- updated standard composition library to provide more accurate use of natural abundances;
- numerous other enhancements for improved usability and stability.

The user documentation for SCALE also has been substantially updated and reorganized. The appropriate citation to use when referencing SCALE is as follows [33].

Code developments during R2CA project:

"Special module for preparing input files for TRANSURANUS code, running of the code, selecting the necessary reference calculation results, and saving files to libraries
Main features of the module:
• formation of an input file for various types of fuel rods;
• formation of fuel rods load history before the LOCA. All cycles of operation of the fuel assemblies are taken into account, its movement in the core during refueling, power reduction schedules during shutdowns, and power increase at the startup of the cycle;
• formation of fuel rod power history and boundary conditions during LOCA based on the libraries of T/H boundary conditions and fuel rods power at the beginning of LOCA;

• adjustment (if necessary) of the fuel rod power Kr in the form of Kr□Keng separately for each fuel cycle;
• execution of the calculation for the full core, symmetry sector and individual assemblies;
• reading from the output files of the necessary reference calculation results;
• determination of the number of failed fuel rods during the LOCA;
• assessment of the activity release to the primary circuit from failed fuel rods;
• saving all input and output files for the possibility of performing additional calculations of individual fuel rods.

Appendix References

[1] Casal J J, Stamm'ler R J J, Villarino E A and Ferri A A, HELIOS: Geometric capabilities of a new fuel-assembly program, Intl. Topical Meeting on Advances in Mathematics, Computations, and Reactor Physics, Pittsburgh, Pennsylvania, USA, April 28-May 2, 1991, Vol. 2, p. 10.2.1 1-13.

[2] Wemple C A, H-N.M. Gheorghiu, R.J.J. Stamm'ler, E.A. Villarino (2008) "Recent Advances in the HELIOS-2 Lattice Physics code," International Conference on the Physics of Reactors (PHYSOR-2008), Interlaken, Switzerland.

[3] https://www.studsvik.com/testing-new-web/start2/our-solutions/products/helios-2/

[4] Rohde, U.: The modelling of fuel rod behaviour under RIA conditions in the code DYN3D. Annals of Nucl. Energy 28 (2001) 1343–1363, DOI:10.1016/S0306-4549(00)00128-6.

[5] Kliem, S.; et al.: The reactor dynamics codeDYN3D. Kerntechnik 81 (2016) 170–172, DOI:10.3139/124.110692.

[6] Rohde, U. et al.: The reactor dynamics code DYN3D – Models, validation and applications. Progress in Nuclear Energy 89 (2016) 170–90, DOI:10.1016/j.pnucene.2016.02.013.

[7] U. Grundmann, U. Rohde, S. Mittag, S. Kliem. DYN3D Version 3.2. Code for Calculation of Transients in Light Water Reactors (LWR).with Hexagonal or Quadratic Fuel Elements. Description of Models and Methods. Institute of Safety Resarci, 2005.

[8] U. Grundmann, U. Rohde, S. Mittag und S. Kliem, „DYN3D Version 3.2 - Code for Calculation of Transients in Light Water Reactors (LWR) with Hexagonal or Quadratic Fuel Elements - Description of Models and Methods," Report FZR 434, Rossendorf, 2005.

[9] U. Grundmann, U. Rohde und S. Mittag, „DYN3D - Three-Dimensional Core Model for Steady-State and Transient Analysis of Thermal Reactors", Proc. of Int. To- pl. Mtg. on Advances in Reactor Physics and Mathematics and Computation into the Next Millennium," in PHYSOR2000, Pittsburgh (USA), 2000.

[10] C. Beckert und U. Grundmann, „Development and verification of a nodal approach for solving the multigroup SP3 equations," Annals of Nuclear Energy 35/1, pp. 75-86, 2008.

[11] U. Grundmann, D. Lucas, S. Mittag und U. Rohde, „Weiterentwicklung und Verifikation eines dreidimensionalen Kernmodells für Reaktoren vom Typ WWER und seine Ankopplung an den Störfallcode ATHLET," Report FZR-84, Rossendorf, 1995.

[12] RELAP5/MOD3.3 Code Manual Volume I: Code Structure, System Models, And Solution Methods. Nuclear Safety Analysis Division. Information Systems Laboratories, Inc. Rockville, Maryland, Idaho Falls, Idaho. December 2001

[13] RELAP5/MOD3.3 Code Manual: Volume II: User's Guide And Input Requirements. Nuclear Safety Analysis Division. Information Systems Laboratories, Inc. Rockville, Maryland, Idaho Falls, Idaho. December 2001

[14] RELAP5/MOD3.3 Code Manual: Volume IV: Models And Correlations. Nuclear Safety Analysis Division. Information Systems Laboratories, Inc. Rockville, Maryland, Idaho Falls, Idaho. December 2001

[15] K. LASSMANN, URANUS -- A computer programme for the thermal and mechanical analysis of the fuel rods in a nuclear reactor, Nucl. Eng. Des. 45 (1978) 325.

[16] K. Lassmann, H.Blank, Modelling of Fuel Rod Behaviour and Recent Advances of the TRANSURANUS Code, Nucl. Eng. Design, 106 (1988), 291-313.

[17] K. LASSMANN, TRANSURANUS: a fuel rod analysis code ready for use, J. Nucl. Mater. 188 (1992) 295. DOI:10.1016/0022-3115(92)90487-6

[18] K. LASSMANN, C. RONCHI, G. J. SMALL, The development of fuel performance models at the European institute for transuranium elements, J. Nucl. Mater. 166 (1989) 112.

[19] K. LASSMANN, C. O'CARROL, J. VAN DE LAAR, C. T. WALKER, The radial distribution of plutonium in high burnup UO2 fuels, J. Nucl. Mater. 208 (1994) 223.

[20] K. LASSMANN, C. T. WALKER, J. VAN DE LAAR, F. LINDSTRÖM, Modelling the high burnup UO2 structure in LWR fuel, J. Nucl. Mater. 226 (1995) 1.

[21] K. LASSMANN, J. VAN DE LAAR, "The Transient TRANSURANUS version", Proceedings of IAEA

RER/4/019, Licensing Fuel and Fuel Modelling Codes for WWER Reactors, Seminar " Implementation of the WWER version of the TRANSURANUS code and its application to safety criteria", Sofia, Bulgaria, 7–11 December 1998.
[22] K. Lassmann, The TRANSURANUS Code – Past, Present and Future, Review Article, ITU Annual Report 2001, EUR 20252
[23] P. VAN UFFELEN, Cs. GYORI, A. SCHUBERT, J. VAN DE LAAR, Z. HOZER, G. SPYKMAN, Extending the application range of a fuel performance code from normal operating to design basis accident conditions, J. Nucl. Mater. 383 (2008) 137.
[24] Cs. GYORI, Z. Hózer, K. Lassmann, A. SCHUBERT, J. VAN DE LAAR, B. HATALA, M. CVAN, "Extension of Transuranus code applicability with Niobium containing cladding models (EXTRA) ", Final Report, EVOL-EXTRA-D5 / FIKS-CT2001-00173, 2004.
[25] G. SPYKMAN, D. MÄRTENS, D. BOUR, P. KOCK, K. LASSMANN, A. SCHUBERT, J. VAN DE LAAR, "Implementation of a Cladding Failure Model for a Loss of Coolant Accident (LOCA)-Analysis in Transuranus", Proceedings of Enlarged Halden Programme Group Meeting on High Burn-up Fuel Performance, Safety and Reliability, Sandefjord, Norway, 9–14 May 2004.
[26] V. DI MARCELLO, A. SCHUBERT, J. VAN DE LAAR, P. VAN UFFELEN, The TRANSURANUS mechanical model for large strain analysis, Nucl. Eng. Des. 276 (2014) 19.
[27] G. PASTORE, L. Luzzi, V. Di Marcello, VAN UFFELEN, Physics-based modelling of fission gas swelling and release in UO2 applied to integral fuel rod analysis, Nucl. Eng. Des. 256 (2013) 75.
[28] V. DI MARCELLO, V. RONDINELLO, A. SCHUBERT, J. VAN DE LAAR, P. VAN UFFELEN, Modelling actinide redistribution in mixed oxide fuel for sodium fast reactors, Progress in Nuclear Energy 72 (2014) 83.
[29] V. DI MARCELLO, A. SCHUBERT, J. VAN DE LAAR, P. VAN UFFELEN, Extension of the TRANSURANUS plutonium redistribution model for fast reactor performance analysis, Nucl. Eng. Des. 248 (2012) 149.
[30] K. LASSMANN, F. HOHLEFELD, The revised URGAP model to describe the gap conductance between fuel and cladding, Nucl. Eng. Des. 103 (1987) 215.
[31] A. SCHUBERT, P. VAN UFFELEN, J. VAN DE LAAR, C. T. Walker, W. HAECK, Extension of the TRANSURANUS burn-up model, J. Nucl. Mater. 376 (2008) 1.
[32] https://www.ornl.gov/scale
[33] B. T. Rearden and M. A. Jessee, Eds., SCALE Code System, ORNL/TM-2005/39, Version 6.2.3, Oak Ridge National Laboratory, Oak Ridge, Tennessee (2018). Available from Radiation Safety Information Computational Center as CCC-834.